UILU-ENG-76-2022

CIVIL ENGINEERING STUDIES

STRUCTURAL RESEARCH SERIES NO. 429

ORNL/Sub/4164-1
Dist. Category UC-77

SHEAR STRENGTH OF END SLABS OF PRESTRESSED CONCRETE NUCLEAR REACTOR VESSELS

By
J. D. REINS, J. L. QUIROS, JR.
W. C. SCHNOBRICH and M. A. SOZEN

A Report on an Investigation Carried Out as Part of the Prestressed Concrete Reactor Vessel Program of the Oak Ridge National Laboratory Operated by the Union Carbide Corporation for the Energy Research and Development Administration

UNIVERSITY OF ILLINOIS
at URBANA-CHAMPAIGN
URBANA, ILLINOIS
JULY 1976

Printed in the United States of America. Available from

National Technical Information Service

U.S. Department of Commerce

5285 Port Royal Road, Springfield, Virginia 22161

Price: Printed Copy $7.00 Microfiche $4.00

CONTENTS

SHEAR STRENGTH OF END SLABS OF PRESTRESSED CONCRETE NUCLEAR REACTOR VESSELS

LIST OF FIGURES

LIST OF FIGURES (cont'd)

LIST OF FIGURES (cont'd)

LIST OF FIGURES (cont'd)

LIST OF FIGURES (cont'd)

LIST OF FIGURES (cont'd)

LIST OF FIGURES (cont'd)

LIST OF FIGURES (cont'd)

LIST OF TABLES

BLANK PAGE

1. INTRODUCTION

1.1 Object and Scope

An investigation of the strength of prestressed concrete nuclear reactor vessels is currently in progress at the Structural Research Laboratory of the Civil Engineering Department, University of Illinois. The project is part of the Prestressed Concrete Reactor Vessel Program of the Oak Ridge National Laboratory sponsored by the Energy Research and Development Administration. This report records the progress in various phases of the project.

The objective of the current studies is to determine the effect of penetrations in the end slab on the strength and behavior of flat end slabs of prestressed concrete nuclear reactor vessels. A previous study by Karlsson (1971) indicated that the shear strength of the end slab was rather insensitive to size and arrangement of penetrations. Karlsson rationalized this observation by demonstrating that, for the particular failure mechanisms observed in the vessels tested (Fig. 1.1), the stress conditions in the concrete were not critical in the immediate vicinity of the penetrations. The same hypothesis would suggest that the end-slab shear strength would become sensitive to the presence of penetrations if the stress combinations acting on the concrete near the penetrations exceeded the strength limit. The current study was initiated in order to investigate this limit experimentally and analytically so that a reasonably general design (or safety analysis) procedure could be developed.

Analytical and experimental activities on the project are complementary and are directed toward the development of an analytical model to simulate the response of the end slab. The model is intended to reproduce the entire range of response, automatically differentiating between different failure mechanisms, under increasing internal pressure. To develop and substantiate such a model, the experimental work is designed specifically to investigate (a) the strains leading to internal inclined cracking, (b) stresses in the vicinity of the end-slab penetrations, and (c) stress redistributions in the fully cracked end slab. The series of end-slab tests have been planned with emphasis on span-depth ratios and penetration arrangements which reflect the geometry of slabs covering the main cavity for the current generation of vessel designs.

The experimental program includes three series. The results of the first two series, comprising eight test vessels, are reported here. The outline of the experimental program is given in Chapter 2 along with a brief description of the test vessels and procedures. Detailed information on fabrication and testing is provided in Appendices A and B. Chapter 3 is devoted primarily to comparisons of the results from analyses using axisymmetric models with those from three-dimensional analyses in the linear range. Chapters 4 and 5 describe salient features of the test results.

1.2 Acknowledgments

The reported work was carried out at the Structural Research Laboratory of the Civil Engineering Department, University of Illinois, Urbana, as part of the Prestressed Concrete Reactor Vessel Program of the Oak Ridge

National Laboratory sponsored by the Energy Research and Development Administration. The program is coordinated by Dr. J. P. Callahan of the Oak Ridge National Laboratory.

Several graduate students in Civil Engineering who were part-time research assistants contributed to the project. The experimental work was initiated by B. Oland, K. Clapp, and A. C. Stepneski and continued by J. Reins. Data reduction and analysis were performed by J. L. Quiros. H. O. Abdulrahman developed ISA, the axisymmetric-analysis program used in studies of the test results. E. Chen aided in the analysis of the end slabs.

Special acknowledgment is due Professor L. Lopez for making FINITE, a general-purpose computer program for structural mechanics problems, available to the project and giving unstintingly of his own time.

R. D. Metz, Laboratory Technician, was instrumental in developing the prestressing equipment and the liner for the vessel. Without his dedication and resourcefulness, the work would have been much delayed.

The success of the instrumentation is due to the careful work of G. H. Lafenhagen, J. H. Sterner, and D. C. Hines. The experimental work was supported by the staff of the Civil Engineering Machine and Electrical Shops under the direction of Professor V. J. McDonald and Mr. O. H. Ray.

All computational work was carried out on the DEC-10 and IBM 360/75 systems of the Digital Computer Laboratory of the University of Illinois, Urbana.

The project is directed by W. C. Schnobrich and M. A. Sozen.

2. OUTLINE OF THE INVESTIGATION

The test specimens were small-scale cylindrical pressure vessels designed to investigate the influence of penetrations in the end slab on strength and behavior of the vessel. The overall dimensions of the eight test vessels described in this report were 40 by 40 in. round (1.02 by 1.02m) as shown in Fig. 2.1. The cavity, closed at one end by the test slab and at the other by a 4 in. (0.10m) steel plate, had a diameter of 25 in. (0.64m).

Circumferential prestressing was provided by five bands, each containing approximately 290 wraps of 0.08-in. (2mm) high strength wire at an effective prestress at time of test of approximately 120 ksi (830 MPa). Sixty Stressteel rods, uniformly distributed around the perimeter in two rows, were used to develop a total effective longitudinal prestress force of approximately 2700 kips (12×10^6 N).

The target concrete compressive strength was 5500 psi (37 MPa). No reinforcing bars were used in the end slab. The bars in the skirt were placed to maintain integrity of the specimen during circumferential prestressing.

A composite liner made up of thin sheets of steel, copper, and neoprene was used for all specimens.

The two main variables in the experimental program were (1) the thickness of the end slab which was either 10 or 12.5 in (0.25 or 0.32m) and (2) the size and arrangement of the penetrations (Fig. 2.1). The eight test vessels were distributed as indicated below with respect to the two variables.

	Clear Span/Nominal Depth of Slab	
	2.5	2.0
Solid slab	PV26	PV28
Six penetrations, 5-in.	PV27	PV32,PV33
Thirty-seven penetrations, 2 in.	PV29	PV30,PV31

The five-in. (0.13m) penetrations (PV27, PV32, PV33) were arranged uniformly on an 8-in. (0.20m) radius. Locations of the two-in. (0.05m) penetrations (PV29, PV30, PV31), spaced at 3 in. (0.075m) center-to-center to each other, are shown in Fig. 2.1. No reinforcing sleeves were used in the penetrations which were closed by steel plates on the pressurized surface of the slab.

The test vessels were first prestressed circumferentially. After installation of the liner, a 4-in. (0.10m) steel plate was placed at the open end and the longitudinal prestressing was applied. The vessel was then placed in the testing room and pressurized internally, using oil after the cavity was filled with water, to failure over a period of approximately three hours. In addition to the pressure, measurements included deflections of the end slab and the side wall, and strains in the concrete and the longitudinal rods, with the majority of the strain gages concentrated on the walls of the penetrations if any.

The analyses in the first phase of the project were aimed primarily at the interpretation of the experimental data which required a large number of solutions with the critical factors varied parametrically. This required the development of an interactive computer program (Abdulrahman, 1976) which is suitable for linear axisymmetric and plane-stress or plane-strain problems. Three-dimensional effects in the solid and cracked end slab were studied using FINITE, a three-dimensional analysis program developed by Lopez (1975).

3. COMPUTER ANALYSIS OF END SLABS

3.1 Introduction

In order to analytically determine the stress and strain distribution in the heads of the test vessels, linear three dimensional finite element analyses were performed on a segment of the full head of the vessel. Three dimensional analyses are extremely expensive to obtain. The number of equations and the bandwidth of those equations are of necessity very large. The result of these factors is to destroy the solution efficiency of most equation solvers. Therefore, because of the expense normally involved in obtaining each 3D solution, one of the major objectives of the 3D solutions was to provide a basis for confirmation of an approximate axisymmetric solution which could be quickly and inexpensively run. This approximate axisymmetric procedure can then be run to investigate the influence of various parameter changes without the costs and time delays associated with 3D procedures.

3.2 Linear Three Dimensional Analysis

Because of the high relative computational efficiency of the isoparametric element over other three dimensional elements, tetrahedrons etc., the twenty node isoparametric element programmed in the FINITE system (Lopez, 1975) was selected for use in this investigation. This element has several advantages over lower order elements. The twenty node element, having three node points along each edge of each element, has the capacity to properly model with a curved surface the region

around the circular holes that penetrate the slab. The element more readily accommodates sharp strain gradients than would lower order elements. The price paid for these is an increased bandwidth.

The element layout used in the analysis is shown in Fig. 3.1. Advantage was taken of the symmetry of the problem. Even taking full advantage of symmetry, eight hundred plus node points were needed. Each node point has three translational displacement degrees of freedom. This involves then twenty four hundred plus equations. When considered with the wide bandwidth common to three dimensional analysis (in this case 160 nodes or 480 degrees of freedom) this represents a sizeable computational effort.

The FINITE program was selected over other general purposes (i.e., SAP and NASTRAN) and even special purpose 3D programs because of FINITE's data generator capability and the options available for output. A major disadvantage of most general purpose programs when applied to three dimensional problems is the amount of pre and post processing necessary to get the results into a reference frame convenient to the user rather than that convenient to the programmer. Output from most programs results in a simple global system. Although three dimensional analysis was necessary, the flow of stress in the end slab is still basically polar rather than cartesian.

One further reason behind using FINITE is its ability to reuse the stiffness matrix of an element. The twenty node element does require a significant computational effort to form the stiffness matrix. It is more economical to store and retrieve the matrix each time it is needed than to recompute it each time. FINITE has a coordinate transformation so it is possible to generate one stiffness matrix then for

example use it for all twelve elements near the center of the slab.

To include elements to model the side wall (skirt) as well as over the head was beyond the current capacity of FINITE (833 nodes). It was therefore necessary to replace the side wall by a system of springs and a set of applied nodal loads to represent the interaction of the wall with the head as load is applied.

Two spring systems were employed. A set of longitudinal springs provide the axial stiffness and moment stiffness equivalent of the skirt. To model the shear transfer or hoop effect, radial springs were also connected to each node located on the outside bottom face of the slab. The value of the spring stiffnesses were selected to match the stiffness coefficients for a circular cylindrical shell with a shear and bending moment applied to one end.

$$\begin{Bmatrix} M_i \\ Q_i \end{Bmatrix} = \left[\begin{array}{c|c} \dfrac{0.2194\ Et^3/\sqrt{rt}}{\text{Sym.}} & \dfrac{0.2887\ Et^2/r}{0.7598\ E\sqrt{(\frac{t}{r})^3}} \end{array}\right] \begin{Bmatrix} \theta_i \\ w_i \end{Bmatrix}$$

To model the loading, the solution for a cylindrical shell fixed to the base slab was used. For the dimensions of the test specimen the values are:

$$M_o = 35.185\ \Delta P \qquad \text{in.-lbs/in.}$$

$$Q_o = 8.388\ \Delta P \qquad \text{lbs/in.}$$

This effect must be superimposed on top of the prestress. One thousand psi was selected as the pressure for which the comparisons would be made between 3D, 2D and experimental results. At that pressure there is a near balance between internal pressure and external prestress effects on the cylinder. Therefore, the net interactive forces are negligible

for this reference pressure. Displacement and stress plots for the 3D solutions are shown with zero unbalanced interactive forces.

Grid Layout. Because of the mentioned limit of slightly more than eight hundred nodes presently existing in the program, it was possible to use only three rays of elements over that section of the head (30^0 segment) taken out for analysis (Fig. 3.1). The stresses near the center of the segment were expected to be reasonably constant or uniform with respect to changes in the radial coordinate. Therefore the grid was not continued all the way in to the exact center of the head. Allowing this small artificial hole to exist at the center eliminated the need to coalesce several nodes into one in the process of reducing the 20 node element to one with a triangular plan form.

In the vicinity of the real holes or penetrations in the slab, the grid layout selected was a compromise between the grid giving the best stress resolution around the hole and that gridded in a regular pattern thereby minimizing data input, within the constraints of the size limitations set down by the program. The resulting pattern (Fig. 3.1) contains only one regular ray of elements for the cross section at the radius of the holes. Any other grid arrangement would have meant either a totally irregular grid or highly distorted element geometries in some locations. Neither of these alternatives was acceptable. Also it was felt essential that the elements framing the hole should not degrade to triangular elements at the side of the hole. Thus the layout shown was selected.

Four layers of elements are used through the thickness of the slab. This provides ample points of stress definition to accommodate all but very sharp stress gradients through the thickness. The finite program

allows stress output at either the points of integration or at the node points. In order to have the values printed for nodes in the hole area so that a comparison could be made with experimentally obtained strains, nodal values were optioned. This was done recognizing that corner node points represent the locations of poorest stress definition for an element procedure. Simple arithmetric averaging was used (i.e., no weighting on basis of tributary areas, etc.) in determining the nodal stresses from the element values.

Boundary Conditions. Within the context of a displacement or stiffness form of finite element analysis conditions can only be specified on the displacements. The segment of the slab that was analyzed is shown in Fig. 3.2 on which the boundary conditions are also indicated. Symmetry lines of $\theta=0$ and $\theta=30^{o}$ require that the displacements normal to the symmetry surface be specified as zero. However, within the element method no restriction can be placed upon the shear stress on those faces. The inner surface, radius equal one inch has zero radial and circumferential displacements but allows normal (or in other words vertical) displacements. The previous section discussed the interaction problem at the junction of the slab with the cylindrical wall. As noted vertical and radial springs replace the interactive stiffness with the cylinder.

The magnitude of the interactive forces was approximated based on thin shell solutions of a fixed ended cylinder. The interactive bending moment was split into statically equivalent vertical nodal forces. The shear force was applied as radial nodal loads for those nodes along the contact surface between the cylinder and the slab.

The pressure to the steel closure covering the five inch openings was applied to the finite element model as a line load around the circumference of the opening. Such a loading is a realistic model of the actual force transfer. However, no account was taken of the stiffening effect of the steel insert used as a seat for the closure plug. The pressure loads were converted to consistent loads in all cases.

3.3 Two Dimensional Axisymmetric Model

Two dimensional solutions for the test vessel were obtained using the ISA program. The test specimen is modeled by an axisymmetric element system as shown in Fig. 3.3 . A four node quadrilateral shaped torus element is the basic ingredient. Because of the inherent excess stiffness of this element to strain gradients over the depth or in other words flexural type actions, nonconforming modes are used. These soften the element thereby improving the quality of the results. Because only rectangular element configurations are used, questions raised concerning the convergence of elements utilizing nonconforming modes are not of consequence.

Modeling the vessel with penetrations as an axisymmetric structure is accomplished by assuming that reducing the Young's Modulus in the appropriate directions has the same effect as the softening introduced by the presence of the holes. An orthotropic material property matrix is used therefore in the computation of the element stiffness matrix. With a symmetric array of holes as with the five inch diameter penetrations, the hoop direction was assumed ineffective so that modulus was taken as zero. The values of the radial and vertical moduli used in

the matrix were selected based on the ratio of the perimeter of material remaining in the real vessel at the radius of the penetrations versus the perimeter of a solid vessel. For the two inch holes this means the moduli are reduced to

$$(2\pi 8 - 30)/2\pi 8 = 0.4$$

of the original value. The reduced orthotropic values apply to elements 61 to 75 of Fig. 3.3a while the rest of the elements (1 to 60) retain the original isotropic values. For the vessels with the two inch penetrations, the grid of holes is such that the properties are rectangular rather than polar. Therefore an isotropic material matrix with modulii reduced based on actual plan area to gross plan area was used. The Poisson ratio was set to zero however to account for the lack of interaction between the radial and hoop directions. From this reasoning elements 1 to 20 used in the ISA solution had the modulus reduced to 3/8 of the modulus for the normal concrete. (Fig. 3.3b)

For the ISA program it was only necessary to specify symmetry boundary conditions on the vessel center line and fixity at the base of the skirt wall. With the use of nonconforming modes, however, the boundary conditions are satisfied only at the node points, not between.

3.4 Results

The ten inch and the twelve and one half inch thick specimens (PV27 and PV32) were both investigated by a linear three dimensional solution with the FINITE program. The internal pressure used for each analysis was the failure pressure for the appropriate vessel (2400 psi for PV27 and 3075 psi for PV32). Solutions for internal pressure,

longitudinal prestress and hoop prestress were obtained by multiple back passes of the various load vectors over the triangularized version of the stiffness matrix. Because the analysis is linear, these pressure values along with the elastic moduli can be scaled to any value desired for purposes of making comparisons. The strains at the levels of the gages placed in the penetrations and those at the lower level of the vessel provide a test comparison with values from the experimental and the orthotropic axisymmetric solutions from ISA. Such comparisons are made in a subsequent chapter of this report.

Figure 3.4 compares the vertical deflections as measured during the experiment and those calculated by the two dimensional ISA program and by the three dimensional FINITE programs. The comparisons are quite good. The 3D system appears to be overly stiff near the center line. This is in part the result of shifting out one inch from the center of the slab in order to avoid the use of elements with a triangular shaped plan form.

Figures 3.5 to 3.6 show the stresses as computed from the axisymmetric program and those from the 3D program. The stresses were calculated for an internal pressure of 1000 psi and no prestress. The load condition was selected to represent the test condition of the already prestressed vessel. That is the vessel being subjected to an internal pressure of 1000 psi, the prestressed vessel being the zero or base of reference.

The radial stresses for the two solutions follow the same patterns. Near the center line both sets of stresses show strong flexure with some axial tension. The flexure diminishes as the hole area is approached

while the axial tension force builds. Then as the wall is approached the reverse sign moment develops. The sharp increase near the reentrant corner shows in both solutions.

Shear stresses in both solutions are low near the center region. Then as the hole area is traversed there is a rapid increase. This is the result of the vertical load being funneled through the rib area. On the back side of the hole the shear stresses computed by both the 3D and the axisymmetric solutions show a distribution departing from the parabolic shape normally associated with flexure to a shape biased to the bottom or inside surface. The latter effect must also be a manifestation of the reentrant corner. Elements are trying to adapt to the stress gradient partly by shear.

The hoop stresses also model well between the 3D and the 2D solutions. However, once in the hole area, the 2D solution reduces to a zero hoop force because of the assumed zero hoop modulus. The 3D solution on the other hand does show a flow of stress around the hole with the consequent low but not insigificant values.

For further conformation the stresses at select locations are compared directly in Fig. 3.7.

The comparisons between the 3D and the axisymmetric solutions support the assumption that the actual vessel can be adequately analyzed by a properly materialed axisymmetric structure.

3.5 Stress State in Cryptodome Head

Using the reconstructed shapes of the cryptodome for specimen PV27, a three dimensional stress analysis was run using the FINITE program. For each vessel the loading applied was the failure pressure, however,

elastic material properties were assumed. One modification was made for PV27 where a reduced modulus was used for some of the highly stressed elements in the vicinity of the hole.

The shape of the cryptodome and the boundary conditions used are shown in Fig. 3.8. It is assumed that horizontal cracking has progressed through the skirt wall-end slab connection. It is therefore admissible to model only the structure shown in the figure. The vertical movement (rigid body motion) was constrained out of the system by a roller support placed around the outer edge. Vertical forces simulate the longitudinal prestress. The presence of the circular steel seating plate at the base of each penetration was neglected in the solution as was the rigidity of the anchor ring for the longitudinal prestress. Although the FINITE program contains the ability to provide for relative constraints, that is interrelate the displacements at a number of node points, that option was not used because of its severe effect on the bandwidth and consequent sizeable increase in equation solving time.

The loading used in the 3-D analysis is from a consistent formulation that is a work equivalent rather than a static equivalent. The pressure applied to the plate covering the penetrations is applied as a uniform line load around the perimeter of the holes.

The general pattern of the stress picture calculated by the three dimensional analysis showed no great surprises (Fig. 3.9). Near the center of the head the stresses convert from basically flexural for the solid head to a strong membrane field after the dome has formed. The calculated stress resultants for a section 1.5 in. from the center of PV27 for example translate into radial axial compression force of

23 kips/in. while the corresponding moment is 3 in.-kips/in. In the hoop direction the axial force is 14 kips/in. compression and a moment of 2 in.-kips/in. At a section through the hole area the radial normal force has increased to 35.5 kips/in. which sums to a total force of 60 kips. The corresponding forces for PV32 are 27 kips/in. axial, 3.8 in.-kips/in. moment in the radial direction. The vertical shear stress on the hole section is shown in Fig. 3.9c. The shear is seen to remain relatively constant over the depth. The summation of the shear over the cross section sums to 40 kips for PV27. This total shear is in agreement with the total vertical load. The non-vanishing of the shear on the top surface, which might at first thought appear to be in error, is the result of the free surface being inclined to the plane of reference about which the stresses are being defined. The boundary condition of stress normal to the free surface is adequately satisfied, adequate meaning within the tolerances that are usually found with finite element solutions. For example, along the top surface at a section through the 8-in. perimeter line, the stress normal to the surface is in the sixty to eighty psi range versus principal compressive forces parallel to the faces of magnitudes seven to ten thousand psi.

Principal stresses calculated for PV27 on a section through the vessel at the eight inches radius are listed on Fig. 3.10. A sizeable percentage of this cross section is at a high (10,000 psi) stress level.

4. OVERALL RESPONSE AND FAILURE MECHANISMS

The measured relationships between deflection at center of slab and internal pressure for all eight vessels are shown in Fig. 4.1 and 4.2. The entire set of recorded pressure-deflection relationships are included in Appendix A. The deflections reported are the total deflections with respect to the initial position of the slab and include the small but finite extension of the side wall. In comparing the pressure-deflection curves, it must be considered that these refer to second-loadings for PV26, 28, 31, and 33. As recorded in Appendix B, the liner in some of the vessels leaked during initial pressurization at various levels (PV26, 800 psi; PV28, 3200 psi; PV31, 1200 psi; PV33, 1700 psi). These vessels were relined and reloaded. The curves in Fig. 4.1 and 4.2 refer to the tests in which structural failure was achieved.

All curves show two typical ranges of response: an initial linear and a following nonlinear range. As would be expected, the initial linear range extends to higher pressures for the vessels with the thicker slabs. Although a certain amount of "ductility" may be read into the curves, this is a moot question considering that the maximum deflection at failure was less than 0.4 percent of the clear span or one percent of the slab thickness for all test vessels. It should also be pointed out that, had the only available sensor been the deflection at midspan of the slab, structural distress would have been anticipated simply from comparing the change in measured deflection over a short time with that based on a linear analysis of the structure and that warning would have been registered well in advance of failure in

terms of pressure although possibly not in terms of time.

Slab deflection distributions calculated using the axisymmetric model, with the penetrations simulated by softened portions as described in Chapter 3, are compared with the measured values in Fig. 4.3 through 4.5. Slab deflections are plotted relative to the center of the side wall and as rates (in./psi) which refer to the initial slope of the pressure-deflection record. Two data points are shown for the two tests of PV28. Considering the possible scatter because of the rather small magnitude of the data, the comparisons indicate that the axisymmetric model is satisfactory for determining slab deflections in the linear range for slabs with penetrations. As described in Appendix A deflection dials had direct contact with the end slab only for vessel PV26. Because all dials measuring slab deflections were destroyed at the end of the test of PV26, dials in following tests were located at some distance from the surface of the slab with the connection provided by pretensioned piano wire.

Shear failure of the end slab limited the structural strength of all eight vessels tested. However, the mechanism of the failure differed depending on the thickness of the end slab and the presence of penetrations.

Despite the use of a hydraulic system for internal pressurization, failure occurred explosively in every case. Chunks of slab concrete were thrown about the testing room. This is attributable primarily to trapped gas in the pressurizing fluid.

Cross sections and photographs of the failed end slabs are shown in Fig. 4.6 through 4.13. The pressures registered at failure are listed in Table 4.1 along with data on the geometry of the vessel, index

values for the circumferential and longitudinal prestresses, and the compressive strength of the concrete in the end slab. (The index value for the circumferential prestress is determined as the internal pressure required to balance the force, at time of test, in prestressing bands 1 and 2 located on and next to the end slab.)

Conditions of the end slab after testing indicated that final collapse occurred always through failure of the concrete in a complex state of stress but that the failures could be classified in two types depending on the location of final distress in the concrete.

One type of failure is illustrated in Fig. 4.6 and 4.9 which refer to solid slabs. As in the tests reported by Karlsson (1971), a three-dimensional inclined crack carves out from the end slab the kernel shown in the lower photograph leaving behind a "cryptodome" to resist the internal pressure. Collapse occurs as a result of failure of the concrete in the cryptodome near the center of the slab. Viewed in two dimensions (in the vertical plane), this mode of failure has characteristics similar to the shear-compression failure observed in reinforced concrete beams.

The "shear-proper" or "punching" failure is illustrated best by the state of the failed end slab of vessel PV30 (Fig. 4.10) having a 12.5-in. end slab with two-in. penetrations. After initiation of inclined cracking within the slab, concrete in the reduced area between the openings fails allowing the central portion of the slab to extrude along a nearly cylindrical failure surface.

The failure modes for each vessel are identified as SD (cryptodome) and SP (shear-proper) in Table 4.1. Not every failure could be classified

as belonging clearly to one category or the other. The failed end slab of vessel PV29 (Fig. 4.8), in addition to a well developed dome had a vertical failure plane through the outermost line of penetrations.

Table 4.2 lists the nominal shear stresses, based on measured dimensions of the end slabs, for all test vessels. Failure pressures and maximum shear stresses normalized with respect to the square root of the compressive strength of concrete (in psi) are plotted against the slab thickness in Fig. 4.14.

Both modes of failure involve complex internal stress conditions. As hypothesized by Karlsson (1971), maximum pressure for failure in the cryptodome mode is a function of the overall geometry and concrete strength with the influence of the prestressing forces affecting the pressure through their influence on the initiation and trajectory of the three-dimensional inclined crack. The shear-proper failure occurs on a plane through the penetrations and close to the boundary, both of which conditions complicate the stress distribution. Strain measurements discussed in the next chapter imply that failure occurs after appreciable redistribution of internal stresses. To generalize the results of the tests must await the conclusion of the numerical studies some of which are briefly discussed in Chapter 3. However, certain trends discernible in Fig. 4.14 are of interest.

Consider Fig. 4.14a which shows the raw test results. As in the series of tests by Karlsson (1971), the difference between the measured strengths of the 10-in. end slabs with and without openings was quite small. The perforated slabs had 92% of the strength of the solid slab. The difference, if considered significant, is plausible. As long as the final collapse is by material failure in the cryptodome near the

center of the slab, the penetrations, which are removed from this zone, should have little negative influence on the strength of the slab.

For the 12.5-in. slabs, there was a meaningful difference in maximum pressures measured for the solid and the perforated slabs, consistently with the observation that the perforated slabs failed in the section through the openings.

Figure 4.14b shows the maximum nominal shear stress for the perforated slabs as a function of the square root of the compressive strength of the concrete. The first cautious conclusion which may be drawn from this plot is that the data for the slabs with 5- and 2-in. penetrations must be considered separately. Assuming then that the parameter used may be applied simultaneously to slabs with 10- and 12.5-in. thicknesses, it may be concluded that, for the test specimens, the nominal unit shear strength is approximately $39\sqrt{f'_c}$ and $33\sqrt{f'_c}$ for the slabs with 2- and 5-in. penetrations, respectively. Taking the results of the 12.5-in. slab as hard evidence, the insensitivity of the end-slab strengths to size of penetrations in the results of the 10-in. slabs reported here and by Karlsson (1971) become plausible.

Evidently, the applicability of a statement of the shear strength of the end slab in terms of a single nominal stress must be limited to end slabs having geometries and loading conditions similar to those for the test specimens. Studies toward the generalization of these observations are in progress.

5. STRAINS MEASURED ON WALLS OF PENETRATIONS

5.1 Introductory Remarks

Strains were measured at three levels on the walls of several penetrations of five test vessels with perforated slabs. Because these measurements provide information on changes in the load-resisting mechanisms of the end slabs, all pressure-strain plots for two vessels (PV30 with 2-in. and PV32 with 5-in. penetrations) are presented in this chapter along with mean values of strains measured in the linear range of response in all tests of vessels with perforated slabs. The mean values are compared with those calculated using linear axisymmetric models of the test vessels.

The locations of the 45^0 strain rosettes (3/4-in. gage length, 9/64-in. gage width) on penetration walls of vessels PV30 and PV32 are shown in Fig. 5.1 and 5.31. Walls of five penetrations in PV30 and two in PV32 were instrumented at levels of 2.25, 6.25, and 10.25-in. from the pressurized surface of the slab. The locations of gages around the circumference of the penetration walls of vessels PV32 (Fig. 5.31) are designated by reference to the face of a clock viewed from the center of the slab. In vessel PV30, rosettes were used at two diametrically opposite locations (Fig. 5.1) around the circumference of five penetrations. In vessel PV32, rosettes were attached at four circumferential locations (Fig. 5.32) on the walls of two penetrations.

Designations of all gages are identified in Fig. 5.1 and 5.31. Figures 5.2 through 5.30 contain the pressure-strain plots for PV30 and

Fig. 5.32 through 5.52 contain the plots for PV32. In reading and comparing these plots it must be recognized that (1) horizontal (strain) scales are not all the same, (2) minus sign in the horizontal axis indicates tensile strain, (3) where the stress in the direction of the gage is low, observed strain may be influenced appreciably by stresses in orthogonal directions, and (4) gages at 45-deg. to the horizontal read compressive or tensile strains depending on their orientations.

Strain data were reduced and plotted using the DEC-10 and IBM 360/75 computer systems. Each measured concrete strain increment was corrected by the corresponding mean increment indicated by a set of check gages, gages mounted on blocks of concrete located near the test specimen. The maximum total strain correction was less than 1×10^{-5}, or less than the limit of reliability of the strain measuring system.

Data from gages designated 4, 10, 17, 18, 34, and 70 in vessel PV30 are not reported because of malfunctioning of those gages.

5.2 Strains Measured in End Slab of Vessel PV30

All strains recorded by strain rosettes installed at three levels within five penetrations in the end slab of vessel PV30 are shown plotted against the internal pressure in Fig. 5.2 through 5.30. Readings of all strain gages indicate that the end slab responded reasonably linearly to an internal pressure of 1000 psi. The first definite indication of nonlinear response was given by the horizontal gages at level 1 in the central penetration (Fig. 5.15). The calculated radial compressive prestrain at this level is approximately 1×10^{-4}. Thus, a tensile strain increment of 4×10^{-4} is an indication of the onset of local cracking. Therefore, the readings of gages 20 and 29 are assumed to

indicate initiation of flexural cracks at the outside face of the end slab at a pressure of 1000 psi. Larger strains indicated by the gages suggest that the gages continued to function even after the development of the cracks, measuring not strain but average total deformation over their gage lengths of 0.75 in. Oriented radially, the cracks indicated by these gages must be the flexural cracks initiating on the outer surface of the slab. The penetration of these cracks into the slab appears to be limited. Horizontal gages 23 and 32 (Fig. 5.15) continue to indicate a reasonably steady increase in tension up to over a pressure of 2000 psi.

The next critical event is signalled by the diagonal gages at level 2 of penetrations 1 and 3 (Fig. 5.8 and 5.9). Both the compressive (Fig. 5.8) and tensile-strain (Fig. 5.9) readings indicate definite nonlinear response at an internal pressure of approximately 1500 psi. The tensile-strain readings are more significant in that, compared with a calculated compressive prestrain of 2×10^{-4} in the direction and at the location of the gages, a tensile strain increment of 5×10^{-4} is a strong indication of cracking. The readings of gages 42 and 15 are complementary, with the inference that gage 42 was straddling a crack while gage 15 was not. The increase in strain rate of the gages reading compressive strain (Fig. 5.8) also suggests a rearrangement of the paths through which pressure is transmitted from the slab to the vessel wall. The compressive-strain increment at which nonlinear response was initiated (approximately 5×10^{-4}) is too small to justify ascribing the observed phenomenon to inherent inelastic action of the material (6300-psi concrete). An increase in the ratio of compressive stress to internal

pressure must also have contributed to the increase in the observed strain rate.

It would appear from the data in Fig. 5.8 and 5.9 that internal inclined cracking was initiated in the end slab within 3.5 in. of the inside face of the side wall at a pressure of approximately 1500 psi, less than half the maximum pressure of 3210 psi.

The magnitude of the measured compressive strains at level 2 in penetrations 1 and 3 is also of interest. The final readings indicated a compressive-strain increment of virtually 0.005 (Fig. 5.8). The diagonal compressive-strains recorded at level 3 of the same penetrations (Fig. 5.12) were of comparable magnitude though not quite as large. Furthermore, strains measured in similar heights and directions in penetrations 4 and 5, which are located closer to the center of the slab span, were perceptibly smaller (Fig. 5.25 and 5.29). (As would be expected, corresponding measurements in the walls of the central penetration 2 are very small. See Fig. 5.16 and 5.17). The measured diagonal compressive strains, then, did indicate the location of the failure. They may also be used as evidence to provide an insight into the mechanism of failure which is suggested to be, in one radial plane, first a development of compressive struts followed by a primary compression failure of the struts.

The sudden change in the response of the horizontal gages at level 3 of penetrations 1 and 3 (Fig. 5.11) is likely to have been related to the development of cracking at the reentrant corner between the slab and the side wall. Accordingly that event must have taken place at an internal pressure of over 2000 psi.

Measurements of vertical strain, which are affected most critically by "background noise" because of their typically low magnitude, do confirm the changes in the load-carrying mechanism inferred from other measurements. Consider the measurements of vertical strain in the central penetration 2. At level 3, closest to the pressurized surface, the increase in compressive strain is, relative to vertical strains at other levels, large and steady with a slight increase in its rate at high pressures (Fig. 5.17). At levels 1 and 2 (Fig. 5.14) the increase in compressive strain stopped at approximately 1800 psi, indicating that the pressure was being transmitted to the supports through compressive dome action. Generally similar conclusions may be drawn from readings of vertical gages on the walls of penetrations 4 and 5.

5.3 Strains Measured in the End Slab of Vessel PV32

Strains measured on the walls of two diametrically opposite penetrations in the end slab of vessel PV32 are shown in Fig. 5.32 through 5.52. Because the penetrations in the end slab of vessel PV32 were limited to a single radial location, the information from the strain gages is not of as wide a scope as that from the gages in PV30.

Strain measurements indicate changes in response at internal stresses of approximately 1250 and 2000 psi. Horizontal gages 20 and 56 at level 1 (Fig. 5.34) signal the reaching of radial cracks to the "6 o'clock" sides of the penetrations at approximately 1250 psi. Indications of inclined cracking are provided by the measurements of gages 15 and 51 (Fig. 5.44), located at level 2 and "3 o'clock," at an internal pressure of 2000 psi. The increased compressive strain rate, at 2000 psi, shown in Fig. 5.45, attributable to a change in the internal load-carrying mechanism, confirms the opening of inclined cracks at an internal pressure

of approximately 2000 psi. It would appear from the measurement of the rosettes at mid-height (level 2) that permanent internal damage occurred at a pressure of 65 percent of the ultimate.

The compressive strains at levels 2 and 3, projected to the failure pressure of 3075 psi, are all less than 0.04. Given the observation that the material failed on a circular plane passing through the axes of the penetrations, the indicated strains appear low for confined concrete.

It is interesting to note that most gages on the 6 and 12 o'clock locations indicated negligible shearing strains, which suggests that the gages were functioning properly.

5.4 Comparison of Measured and Calculated Strains

Figures 5.53 through 5.61 contain a series of comparisons of measured and calculated strains in the range of linear response. The plots show the variation of strain per 1000 psi internal pressure over the thickness of the slab.

Measured values represent the mean initial slope of the pressure-strain plots obtained from gages attached to the walls of the penetrations. Each datum point represents the average of all available data for that location. The scatter range was as large as 60% for mean values less than 1×10^{-4} and less than 20% for mean values equal to or greater than 1×10^{-4}. Readings from initial and second loadings of test vessels which had to be loaded twice because of leakage in the first test were treated as independent values.

Strains were calculated using the linear axisymmetric models described in Chapter 3 with modifications to represent the effect of the penetrations. It should be noted that the calculated strains refer

to an ideal radial plane without strain variations in the circumferential direction while the strains were measured on the surfaces of the penetrations. A better experimental check for the results of the modified axisymmetric models would be at the radial plane bisecting the angle between two penetrations.

The comparisons are, in general, favorable indicating that the axisymmetric model may be used to investigate strain conditions around the penetrations in the linear range of response.

6. SUMMARY

This report summarizes the experimental and part of the analytical work carried out in connection with an investigation of the structural strength of prestressed concrete reactor vessels. The project is part of the Prestressed Concrete Reactor Vessel Program of the Oak Ridge National Laboratory sponsored by ERDA. The objective of the current phase of the work is to develop procedures to determine the shear strength of flat end slabs of reactor vessels with penetrations.

6.1 Analytical Studies

The assimilation and generalization of the experimental observations demand two different levels of analytical capability. The necessity for a large number of parametric studies to determine sensitivity to variations in physical properties for design as well as data interpretation requires a computer program which is easily accessible and which produces solutions at moderate cost. On the other hand, the necessity for simulating the three-dimensional nonlinear discontinuous phenomena in order to study local forces and deformations in the end slab requires a rather large computer program.

To satisfy the first requirement, an interactive computer program, ISA, based on a linear axisymmetric model was developed. ISA is also suitable for problems of plane stress or strain and has been designed to be developed further to include options for nonlinear analysis as well as analysis of crack development within the end slab. The current version

of ISA is described by Abdulrahman (1976).

Linear three-dimensional analyses of the end slab, in intact and cracked conditions, have been made with the use of FINITE (Lopez, 1975). These studies have confirmed the feasibility of using modified axisymmetric models to determine strains around the penetrations in the linear range of response.

6.2 Experimental Studies

The dimensions and properties of the eight cylindrical flat-ended test vessels are described in Fig. 2.1 and Table 4.1. The main experimental variables in the tests reported were the thickness of the end slab and the size and arrangement of end-slab penetrations. No reinforcing steel was placed within the end slab. The penetrations, which had no sleeves or liners, were closed by steel plates at the pressurized surface of the slab. Prestressing was provided by 60 Stressteel rods longitudinally and 5 bands of 0.08-in. (2-mm) high-strength wire circumferentially, each band containing approximately 290 wraps of wire. Prestress forces are tabulated in Tables 4.1 and 4.2.

The liner for the internal cavity comprised sheets of steel, copper, and Neoprene. Each vessel was pressurized hydraulically to failure over a period of approximately three hours. Maximum pressures ranged from 2400 psi (16.6 MPa) to 3765 psi (26.0 MPa). Despite the use of fluid as the loading medium, the structural failures were violent.

All end slabs failed in shear, but in different modes (Fig. 4.6 through 4.13). As listed in Table 4.1, all three vessels with 10-in. (0.25m) slabs and the vessel with a solid 12.5-in. (0.32m) slab failed

after the formation of a "cryptodome", as observed by Karlsson (1971), within the end slab. The location of concrete failure was near the center of the slab and away from the section of maximum shear stress. For this mode of failure, the shear strength of the end slab was insensitive to the presence of the penetrations.

The shear failures of 12.5-in. (0.32m) end slabs having penetrations were characterized by failure of the concrete on an almost vertical plane through the section of maximum shear stress and were designated as "shear-proper" or "punching" failures. In this case, the strength of the end slab was affected by the penetrations. Measured nominal shear stresses are listed in Table 4.2.

Measured strains on the walls of the penetrations indicated the initiation of the failure process (development of inclined cracks within the end slab) and permanent internal damage at pressures less than half the ultimate pressure for the test vessels with 2-in. (0.05m) openings and 12.5-in. (0.32m) slabs.

7. REFERENCES

1. Abdulrahman, H. O., "ISA, Interactive Stress Analysis, A Program for Plane Stress, Plane Strain and Axisymmetric Analysis in Structural Continua," Civil Engineering Studies, Structural Research Series No. 428, University of Illinois, Urbana, July 1976.

2. Karlsson, B. I. and M. A. Sozen, "Shear Strength of End Slabs with and Without Penetrations in Prestressed Concrete Reactor Vessels," Civil Engineering Studies, Structural Research Series No. 380, July 1971.

3. Lopez, L., "FINITE, A POLO II Subsystem for Structural Mechanics," Civil Engineering Systems Laboratory, University of Illinois, Urbana, June 1975.

TABLE 4.1

Maximum Internal Pressure at Failure

Mark	Nominal Slab Thickness in. (mm)	Concrete Comp Strength psi (MPa)	Penetrations No.	Penetrations Dia. in. (mm)	Prestress Index Long.[a] psi (MPa)	Prestress Index Circum.[b] psi (MPa)	Failure Pressure psi (MPa)	Failure Mode[c]
PV26	10 (254)	6710 (46.3)	-	-	5010 (34.5)	1560 (10.8)	2610 (18.0)	SD
PV27	10 (254)	6845 (47.2)	6	5 (127)	5340 (36.8)	1560 (10.8)	2400 (16.6)	SD
PV29	10 (254)	5480 (37.8)	37	2 (50.8)	5330 (36.8)	1710 (11.8)	2400 (16.6)	SD
PV28	12.5 (317.5)	6420 (44.3)	-	-	5760 (39.7)	1700 (11.7)	3765 (26.0)	SD
PV30	12.5 (317.5)	6300 (43.4)	37	2 (50.8)	5340 (36.8)	1690 (11.7)	3210 (22.1)	SP
PV31	12.5 (317.5)	4970 (34.3)	37	2 (50.8)	5500 (37.9)	1680 (11.6)	2800 (19.3)	SP
PV32	12.5 (317.5)	5720 (39.4)	6	5 (127)	5540 (38.2)	1780 (12.3)	3075 (21.2)	SP
PV33	12.5 (317.5)	4875 (33.6)	6	5 (127)	5400 (37.2)	1780 (12.3)	3100 (21.4)	SP

[a]Total effective prestress force divided by horizontal cross-sectional area of cavity.

[b]Mean effective prestress force in prestressing bands 1 and 2 divided by vertical tributary area of cavity.

[c]SD = Shear failure after complete formation of cryptodome. SP = Shear failure by punching.

TABLE 4.2

Nominal Shear Stresses in End Slab

Mark	Meas. Slab Thickness in.	Penetrations No. x Size in.	Maximum Pressure psi	Shear Stress at Slab Edge[a]		Maximum Shear Stress[b]	
				v psi	$v/\sqrt{f'_c}$	v_m psi	$v_m/\sqrt{f'_c}$
PV26	9.81	-	2610	1660	20.3	-	-
PV27	10.06	6 x 5	2400	1490	18.0	2370	28.8
PV29	9.94	37 x 2	2400	1510	20.4	2820	38.1
PV28	12.38	-	3765	1900	23.7	-	-
PV30	12.22	37 x 2	3210	1640	20.7	3070	38.7
PV31	12.02	37 x 2	2800	1460	20.7	2720	38.6
PV32	12.30	6 x 5	3075	1560	20.7	2490	33.0
PV33	12.45	6 x 5	3100	1560	22.3	2480	35.6

[a]Nominal shear stress at the slab-wall interface.

[b]Nominal shear stress at the net section through the penetrations.

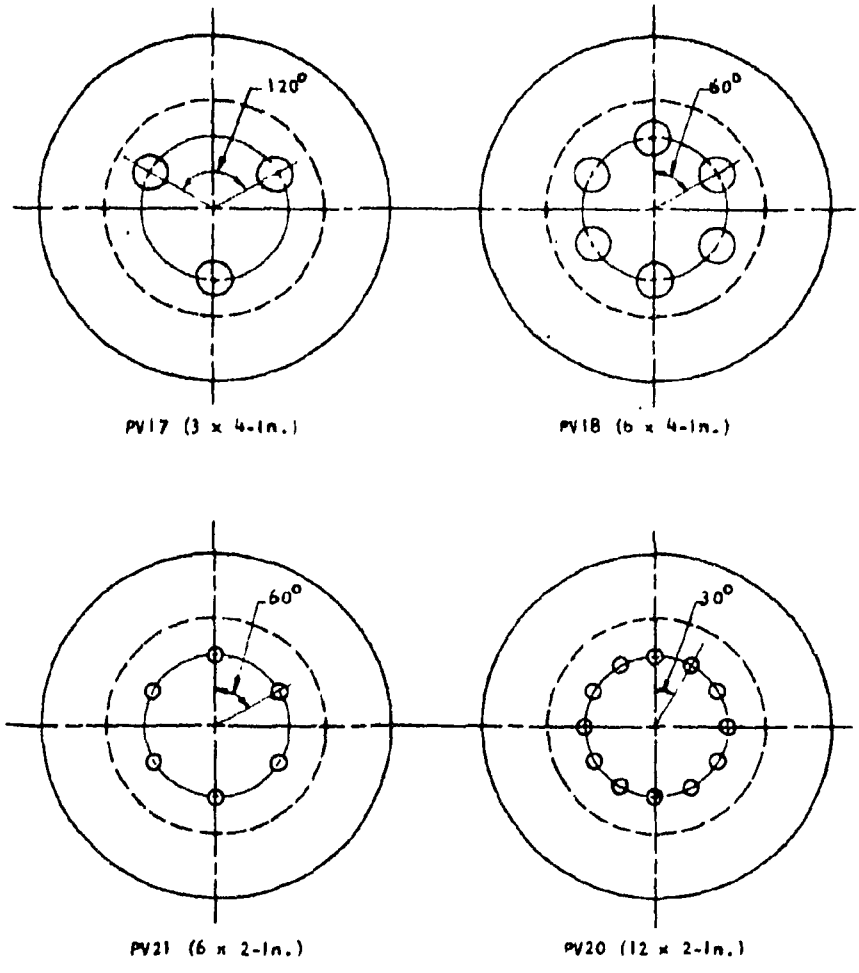

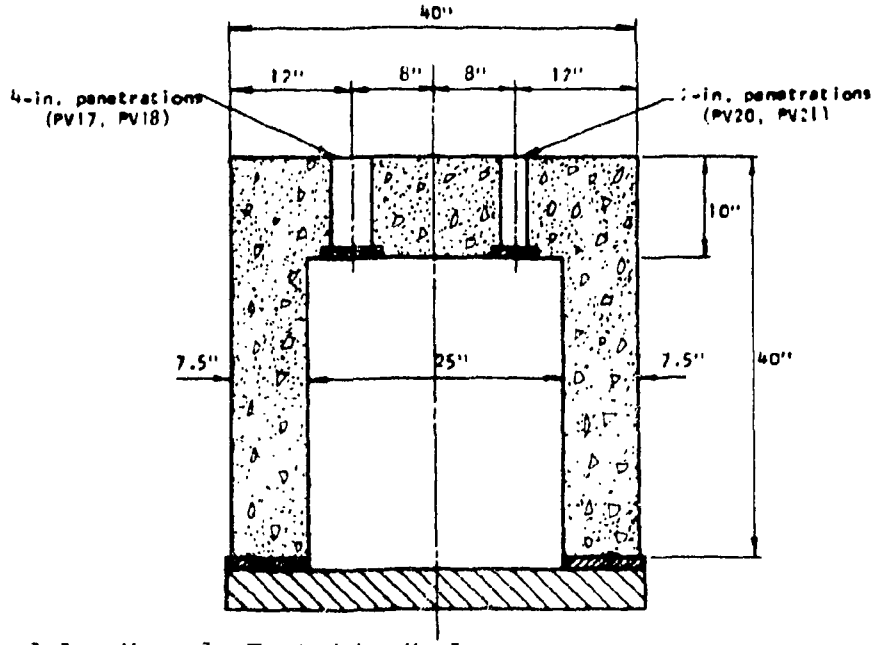

Fig. 1.1a Vessels Tested by Karlsson

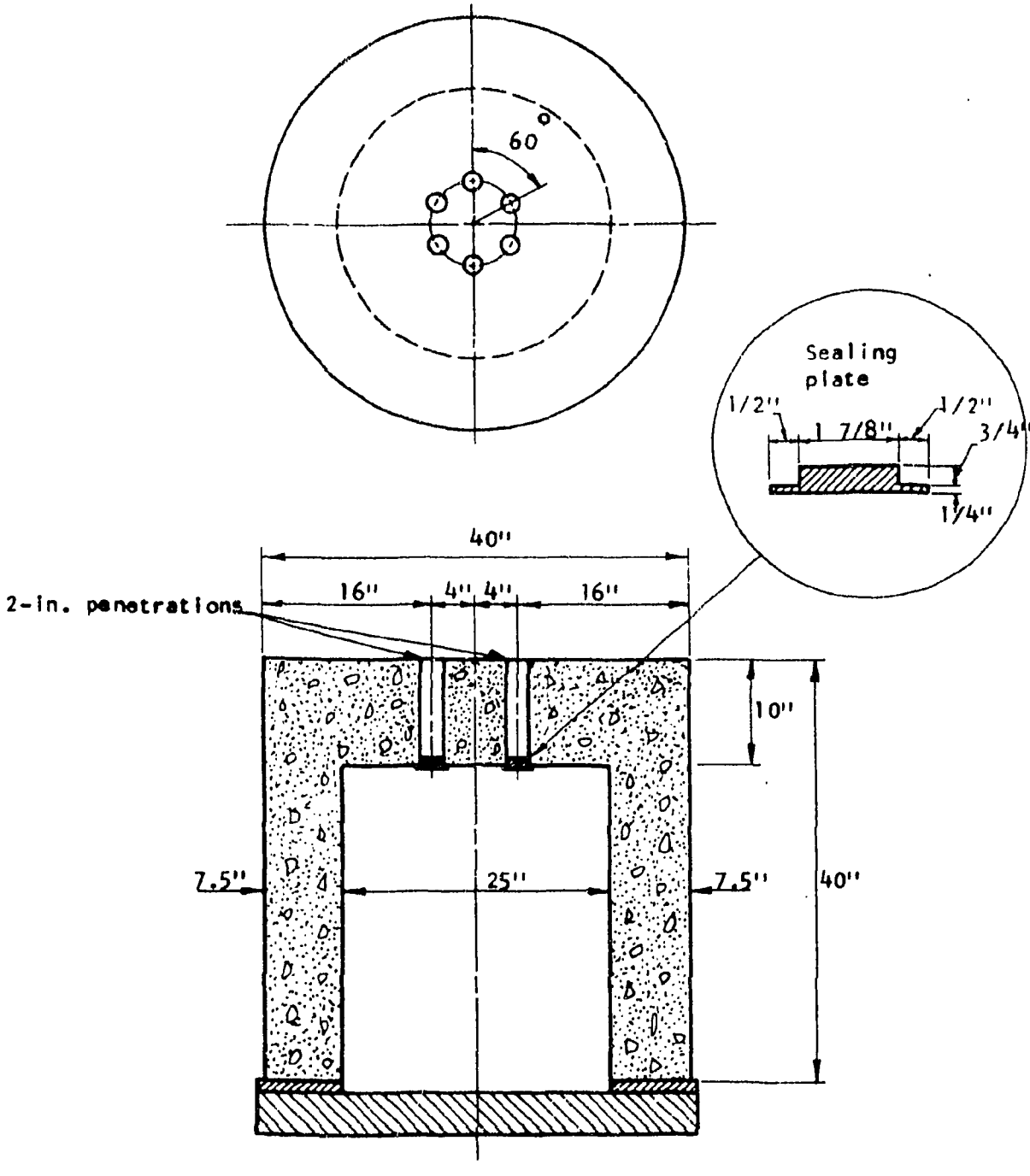

Fig. 1.1b Vessels Tested by Karlsson

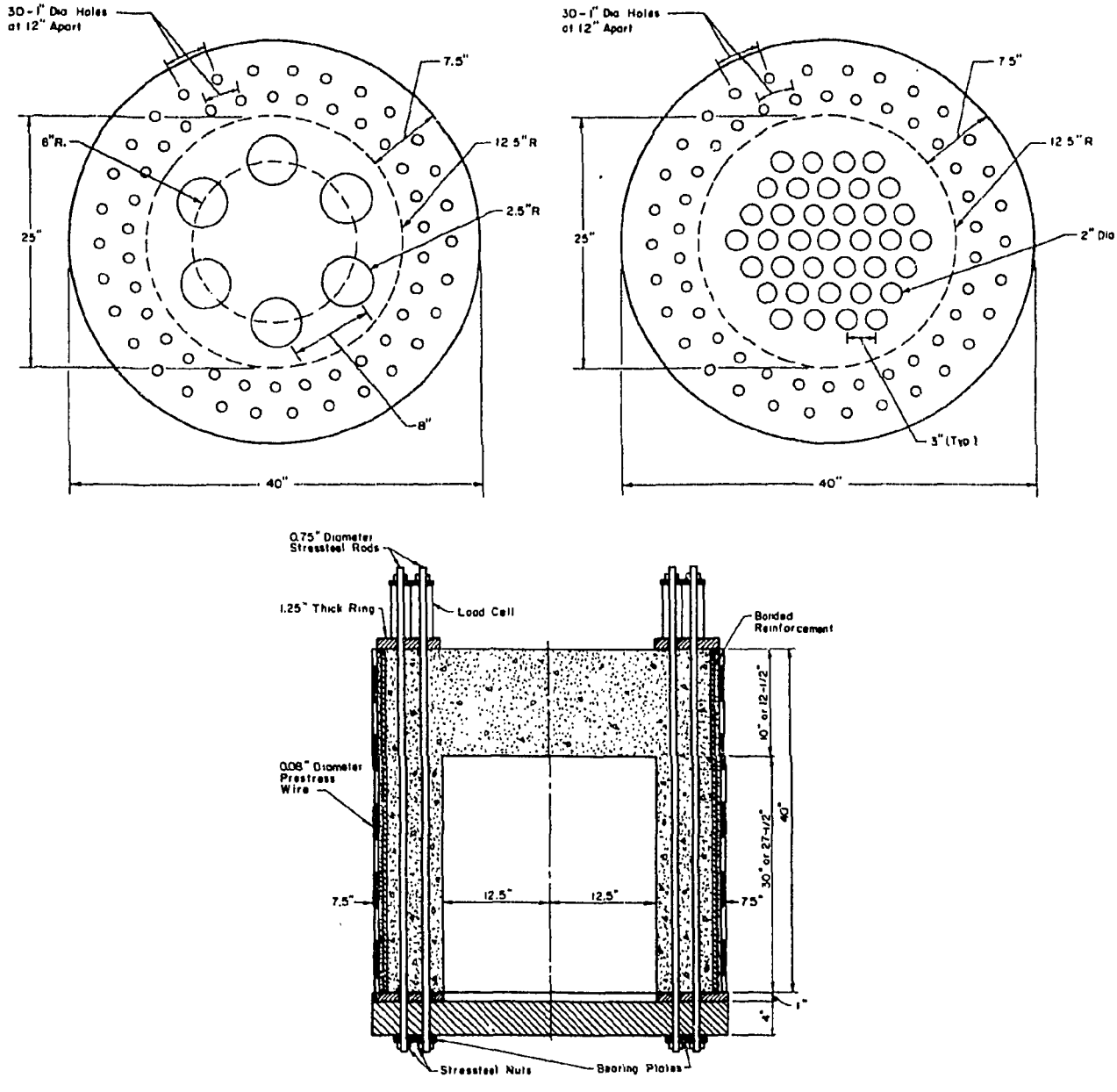

Fig. 2.1 Penetration Patterns and Cross-section of Vessel

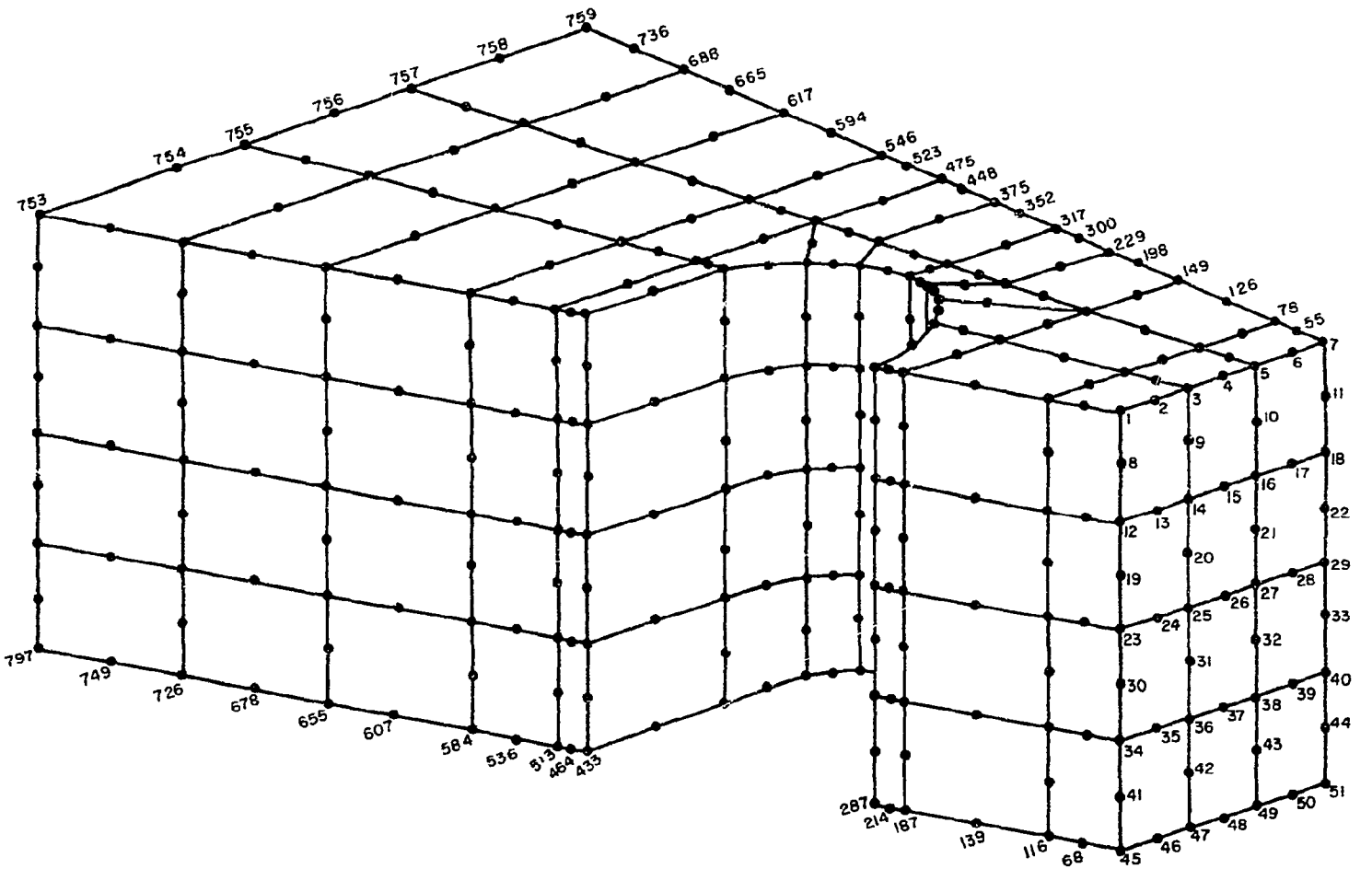

Fig. 3.1 Finite Element Grid Used in Three Dimensional Analysis

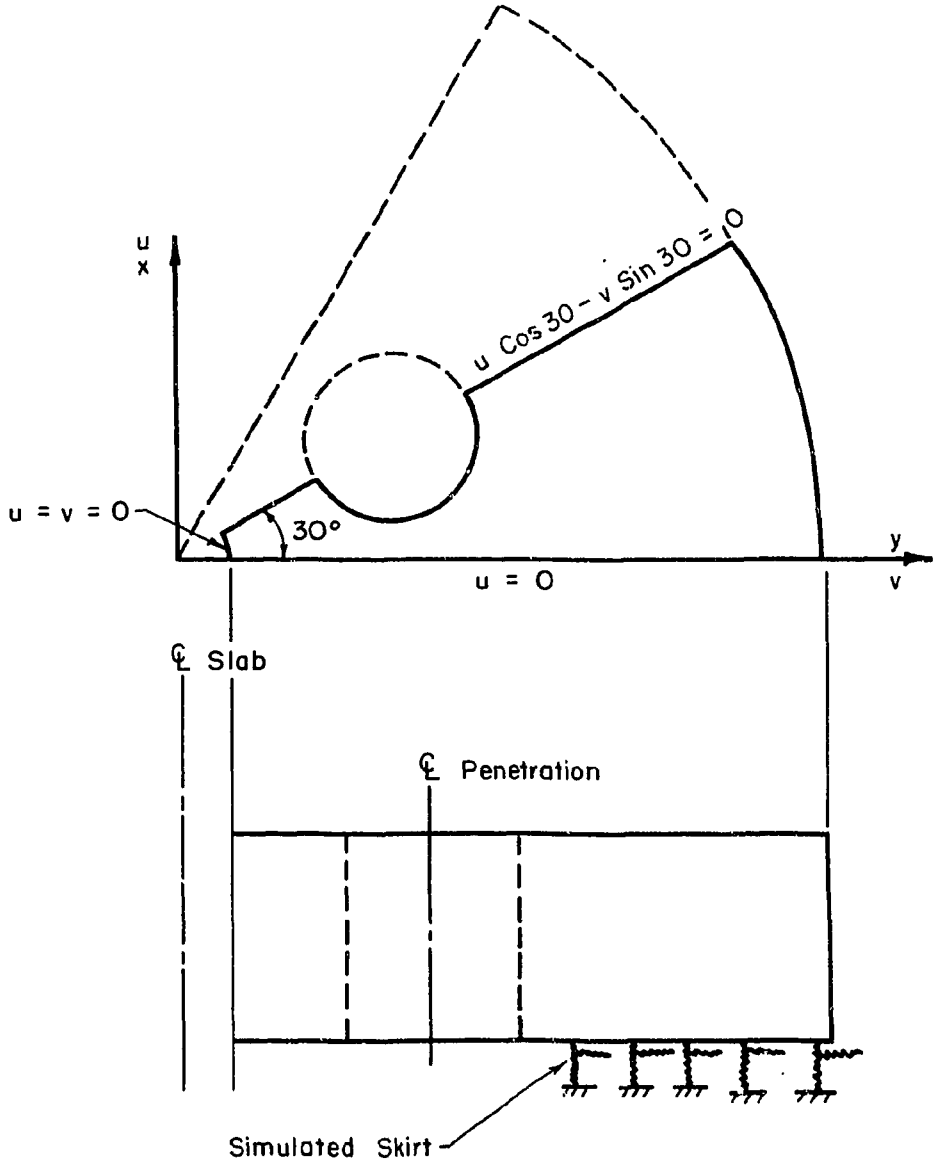

Fig. 3.2 Boundary Conditions Used in Three Dimensional Analysis

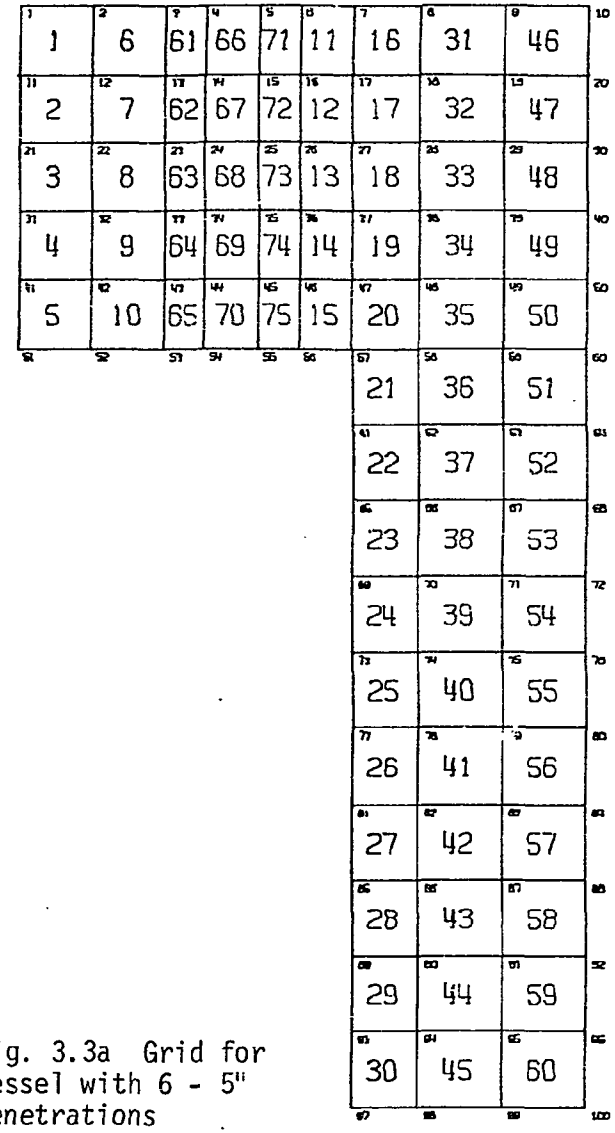

Fig. 3.3a Grid for vessel with 6 - 5" penetrations

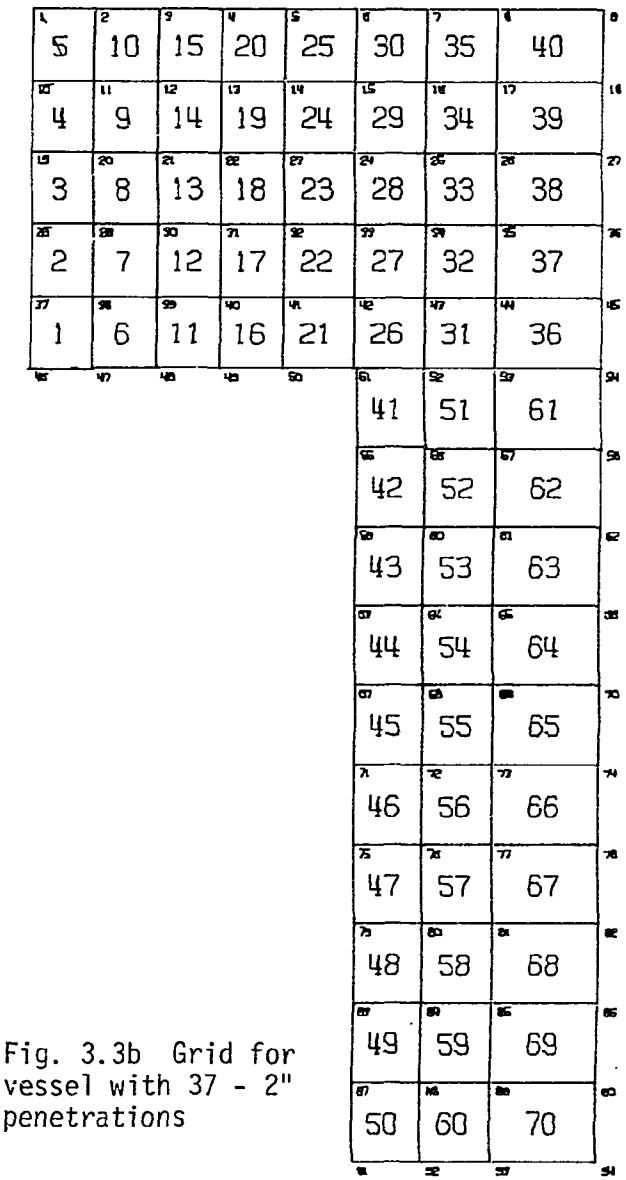

Fig. 3.3b Grid for vessel with 37 - 2" penetrations

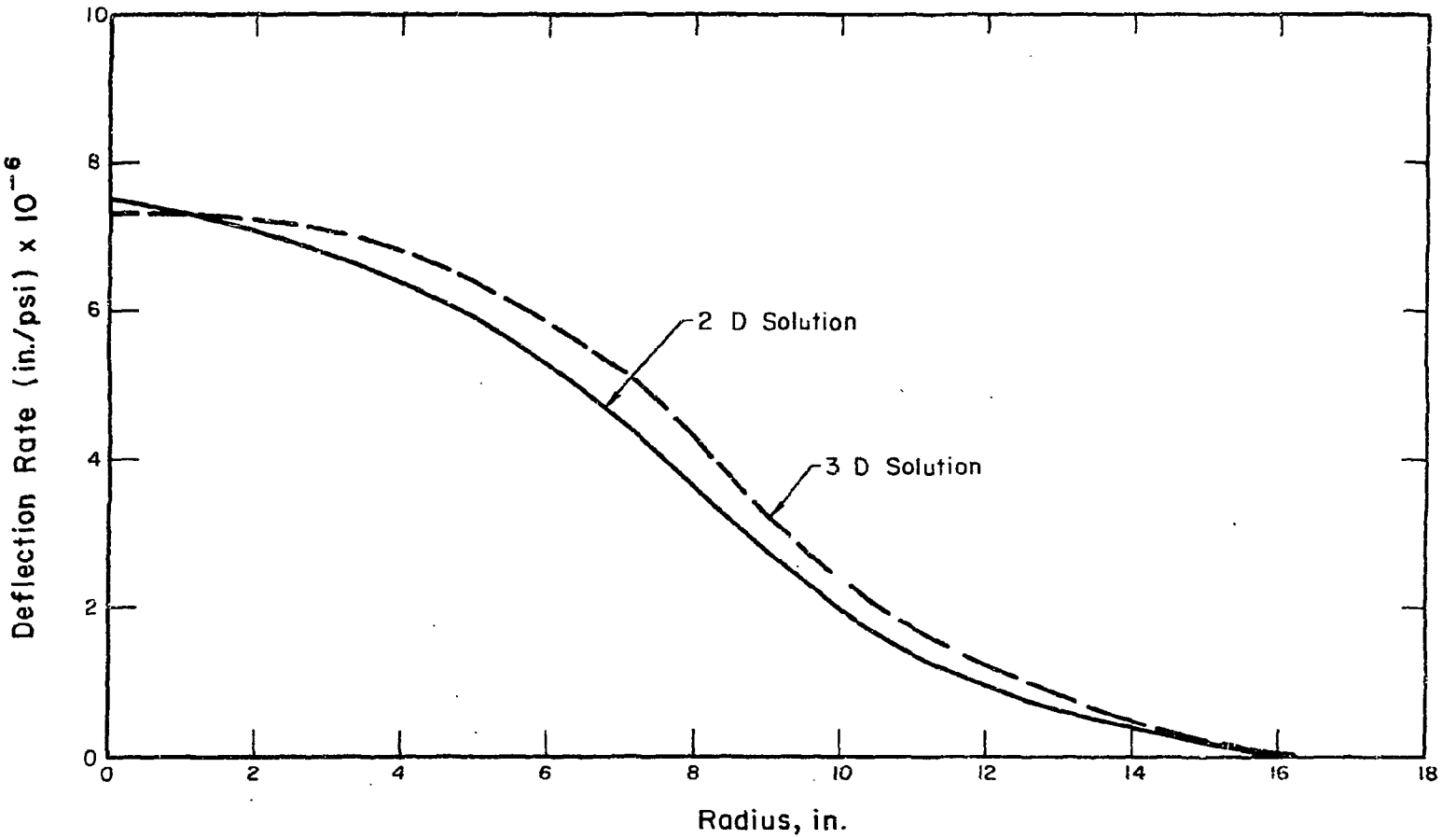

Fig. 3.4a Vertical Deflections of 10-in. Slab

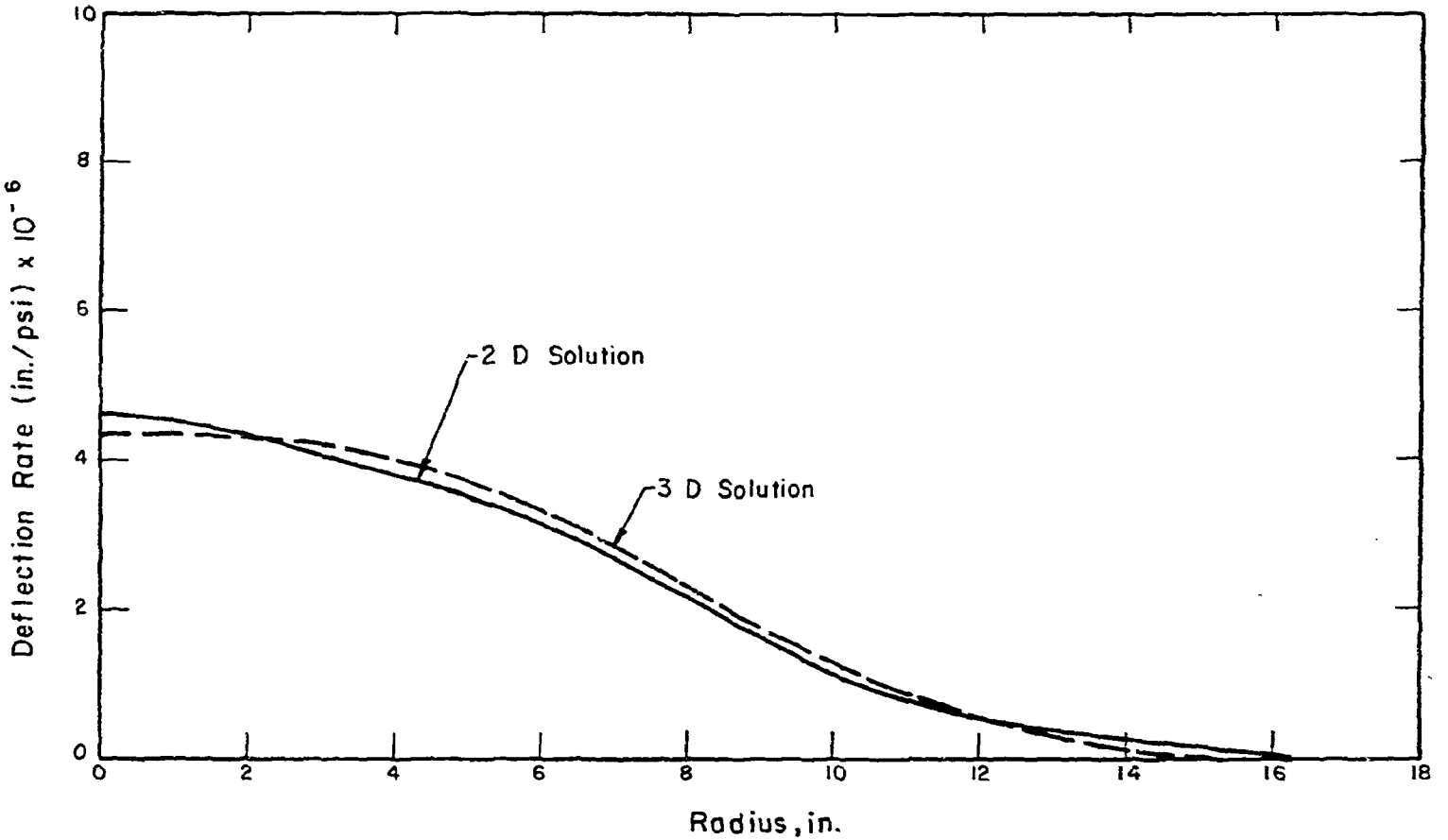

Fig. 3.4b Vertical Deflections of 12.5-in. Slab

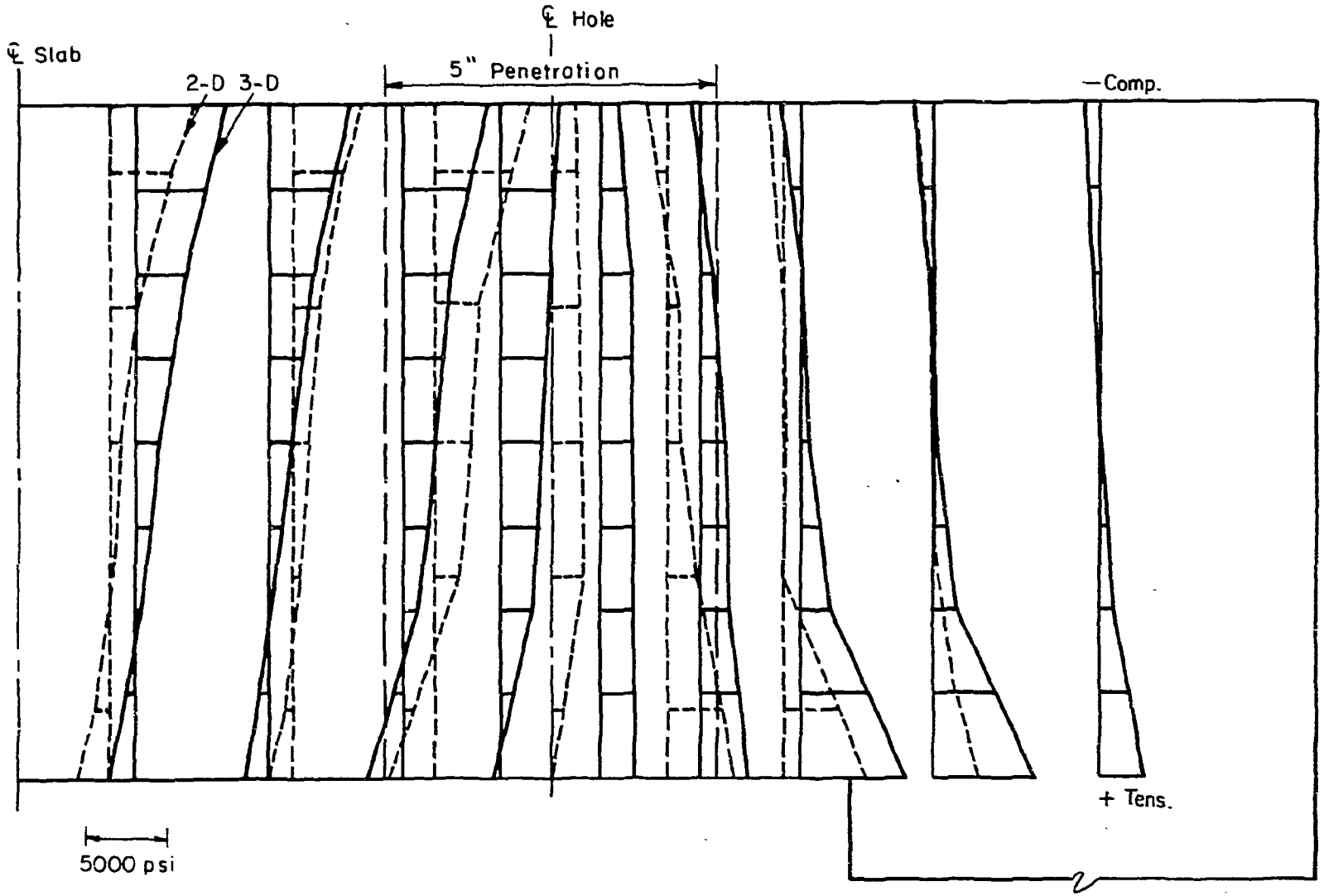

Fig. 3.5a Radial Stress in 10-in. Slab with 5-in. Diameter Penetrations

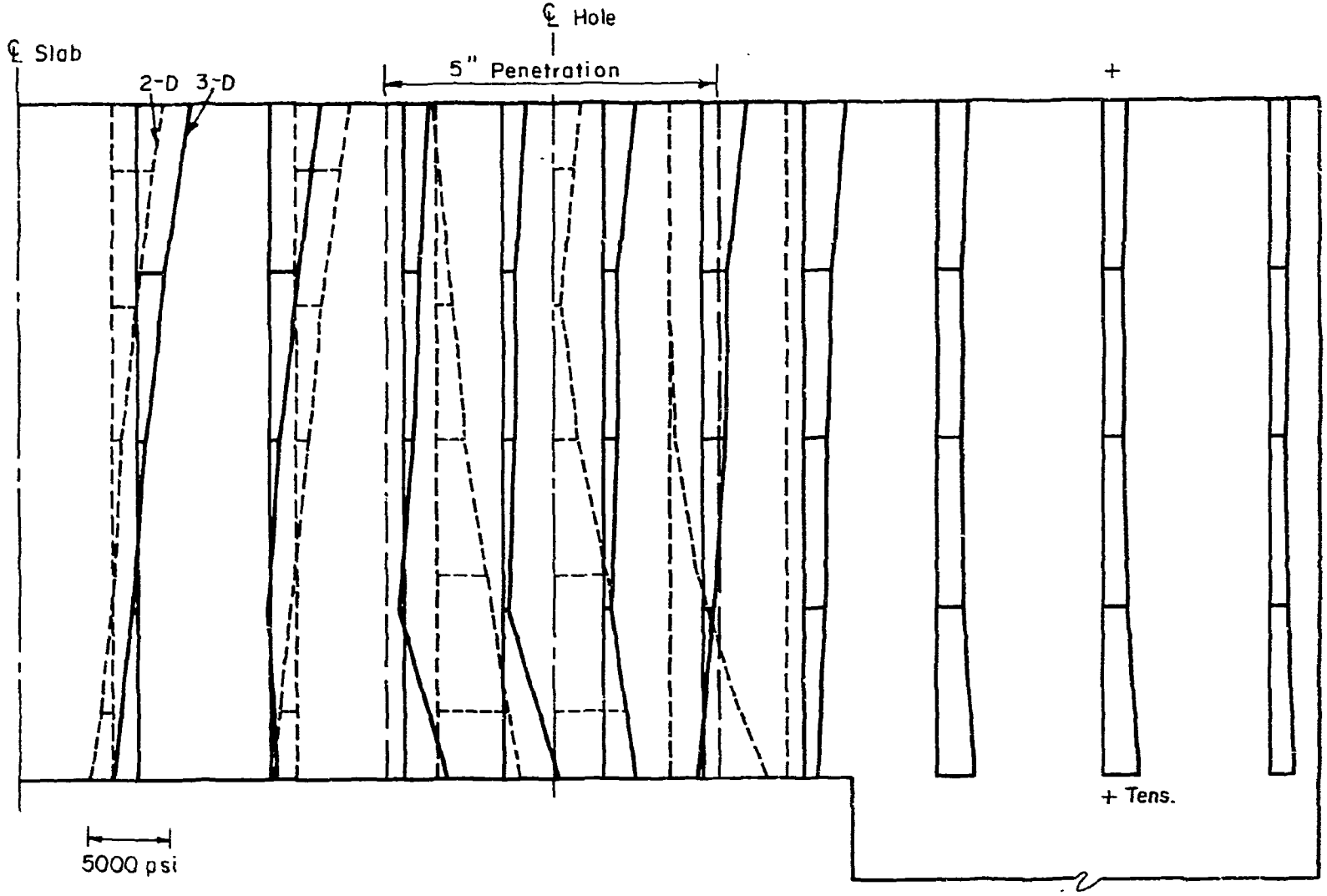

Fig. 3.5b Hoop Stress in 10-in. Slab with 5-in. Diameter Penetrations

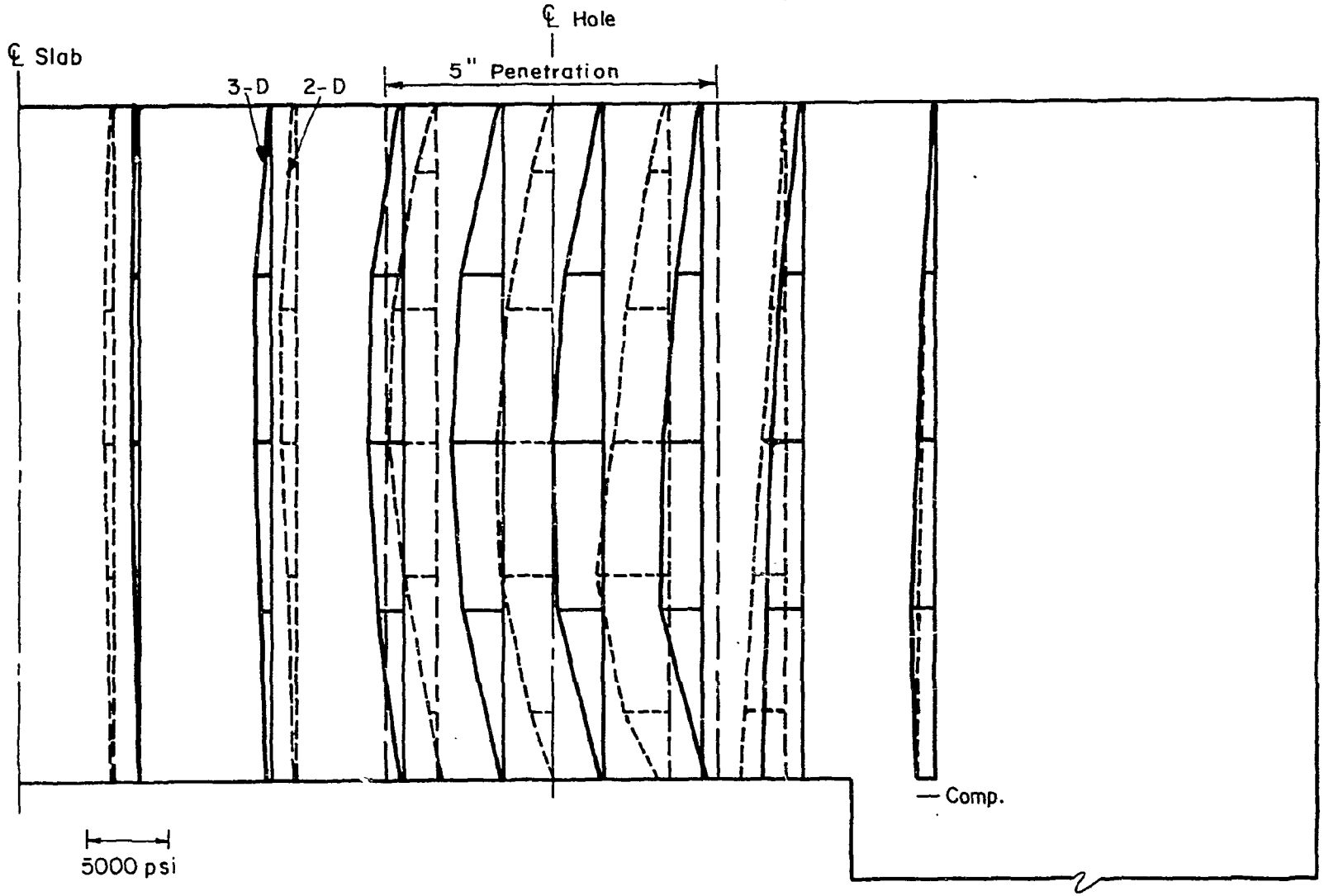

Fig. 3.5c Shear Stress in 10-in. Slab with 5-in. Diameter Penetrations

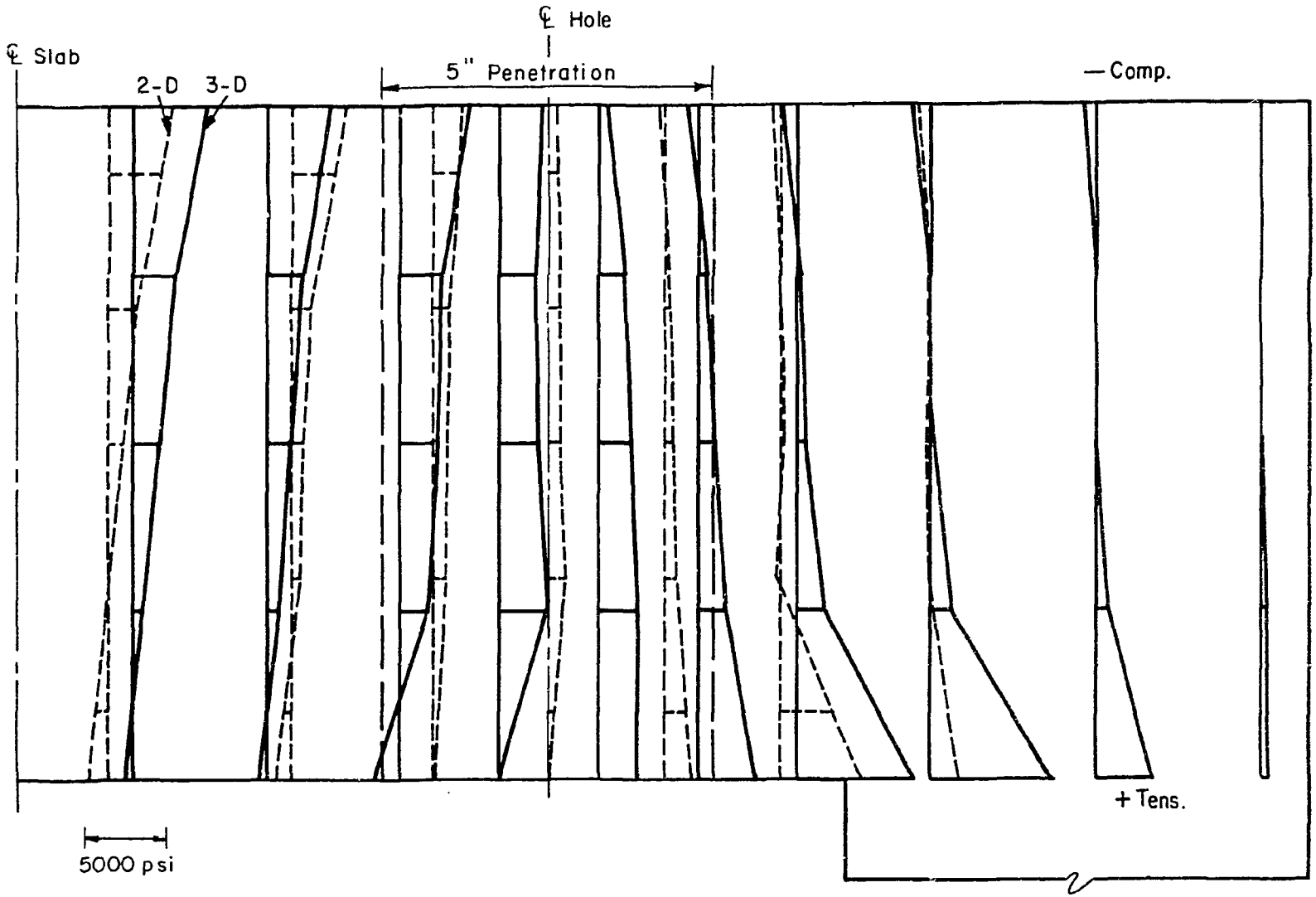

Fig. 3.6a Radial Stress in 12.5-in Slab with 5-in. Diameter Penetrations

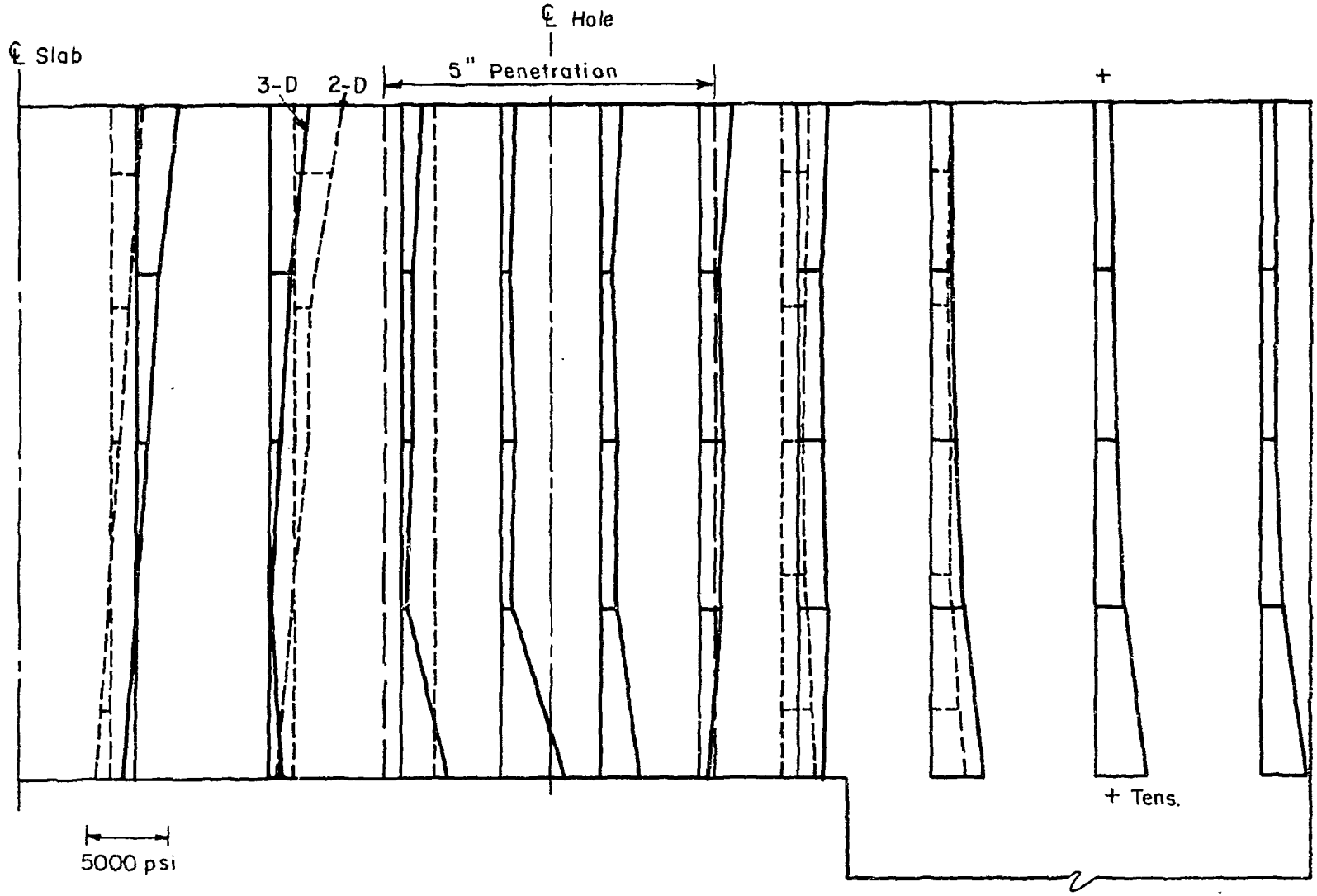

Fig. 3.6b Hoop Stress in 12.5-in. Slab with 5-in. Diameter Penetrations

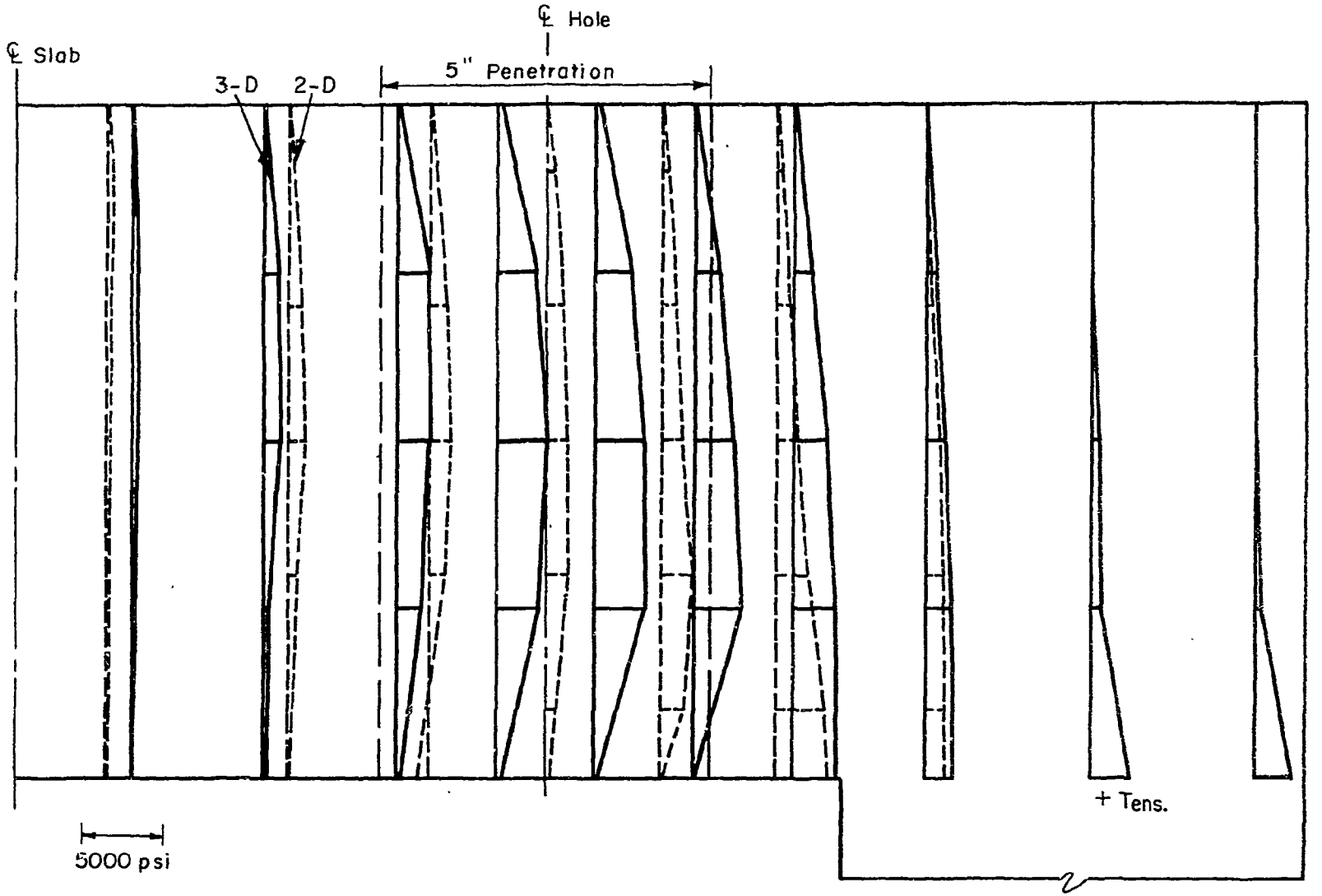

Fig. 3.6c Shear Stress in 12.5 in. Slab with 5-in. Diameter Penetrations

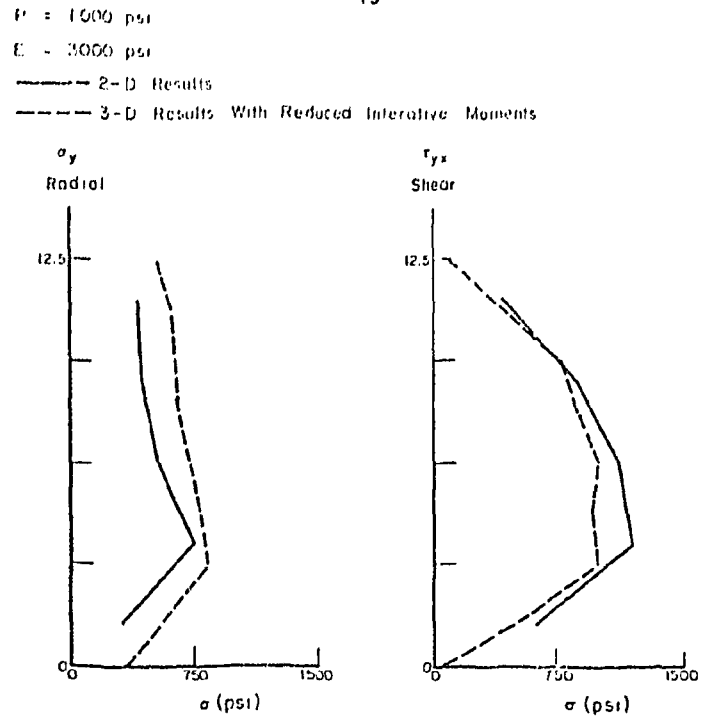

3.7a Stresses at R = 8 inches

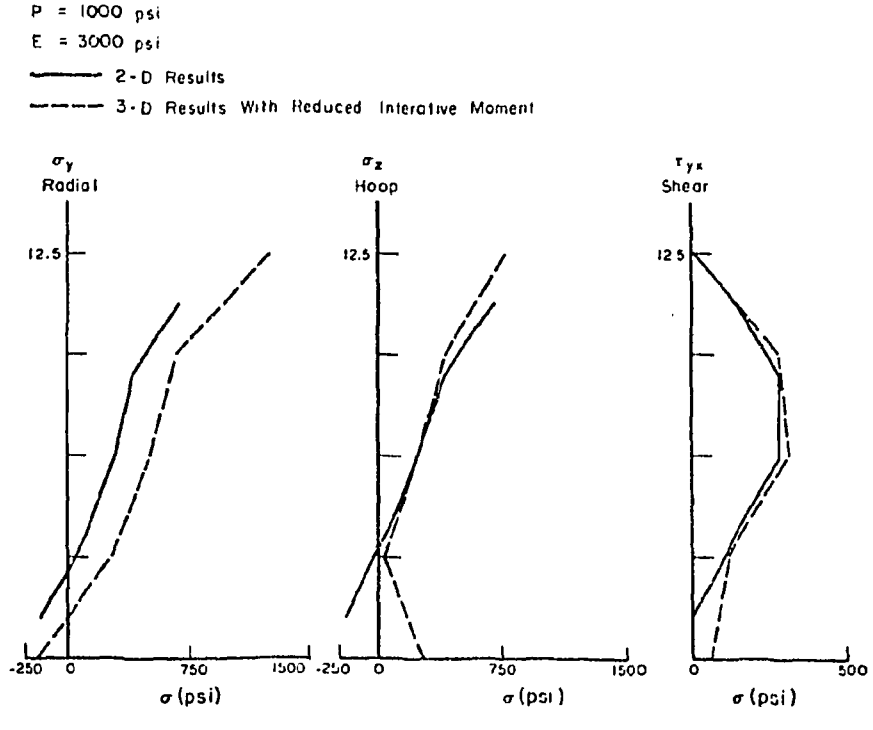

3.7b Stresses at R = 3.75 inches

Fig. 3.7 Comparison of Stresses Calculated by Axisymmetric and by Three Dimensional Analyses for 12.5-in. Thick Head

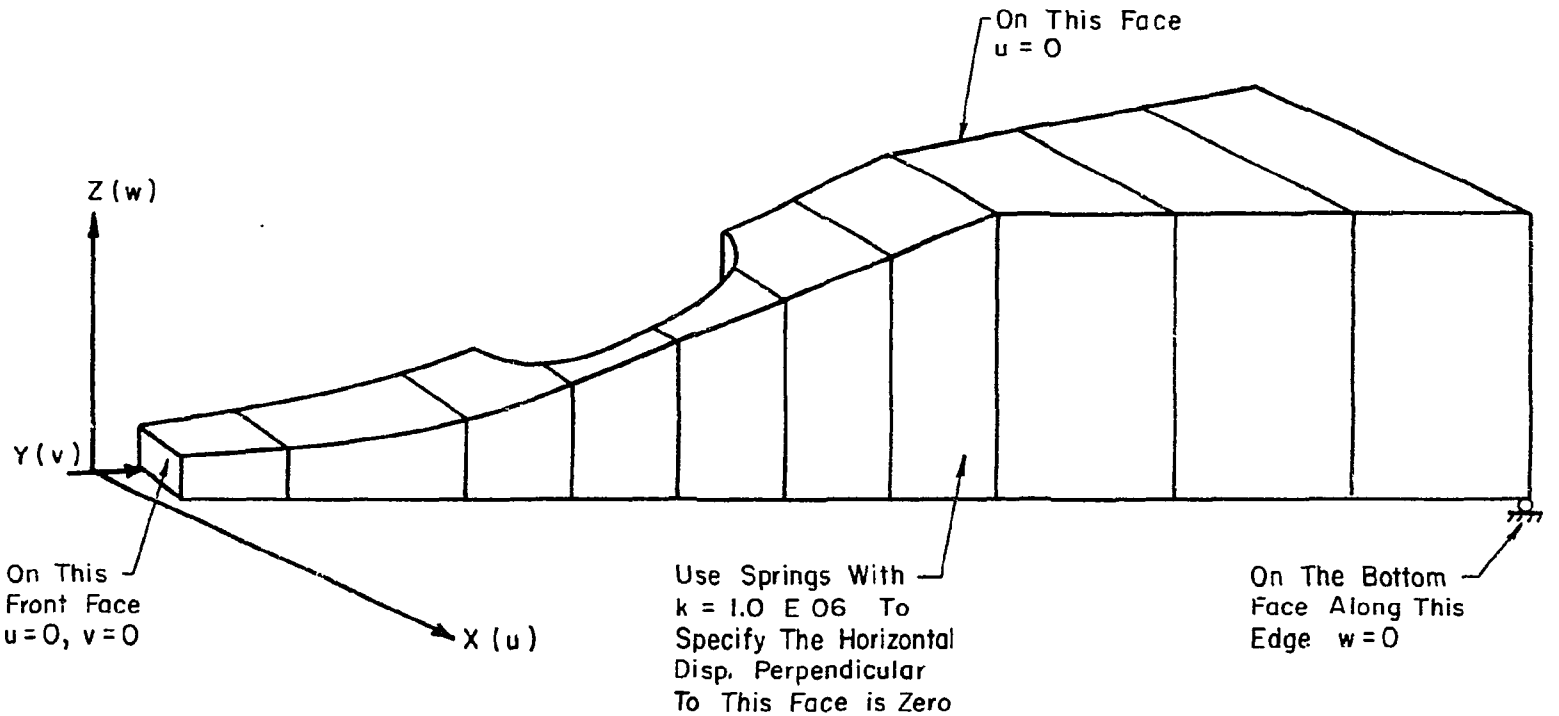

Fig. 3.8 Boundary Conditions Used in Cryptodome Analysis

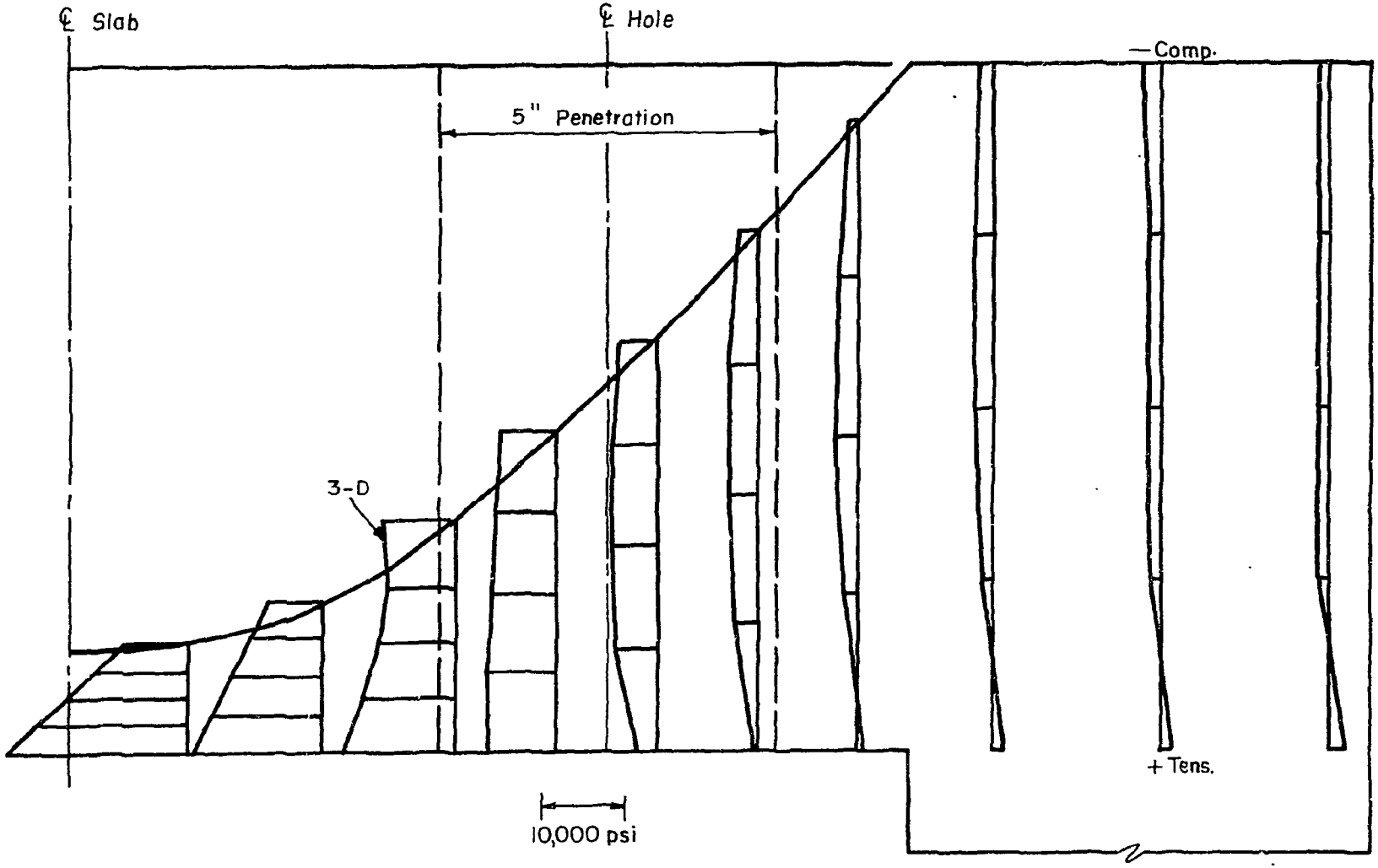

Fig. 3.9a Radial Stresses in Cryptodome Shaped from 10-in. Slab

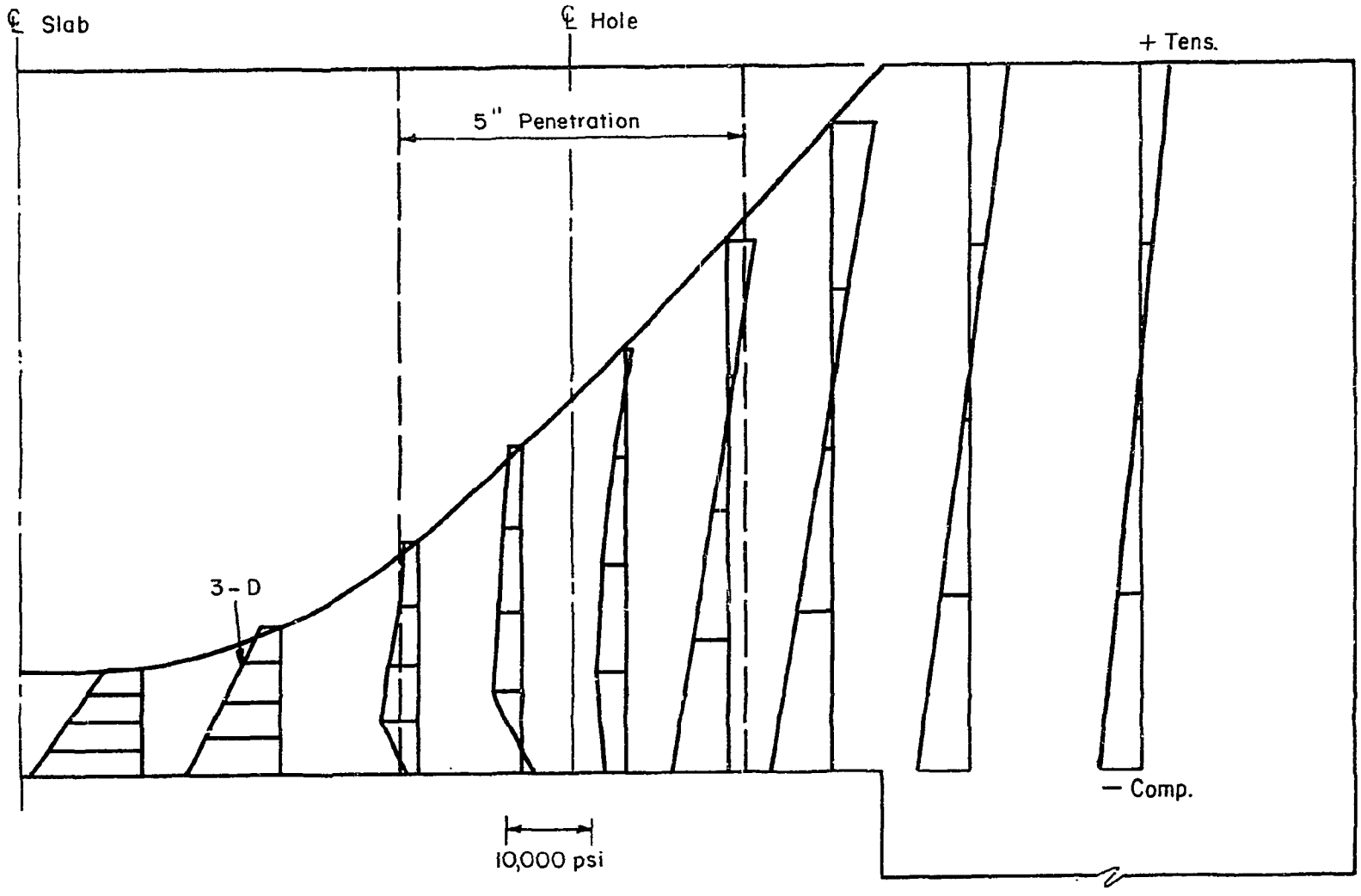

Fig. 3.9b Hoop Stresses in Cryptodome Shaped from 10-in. Slab

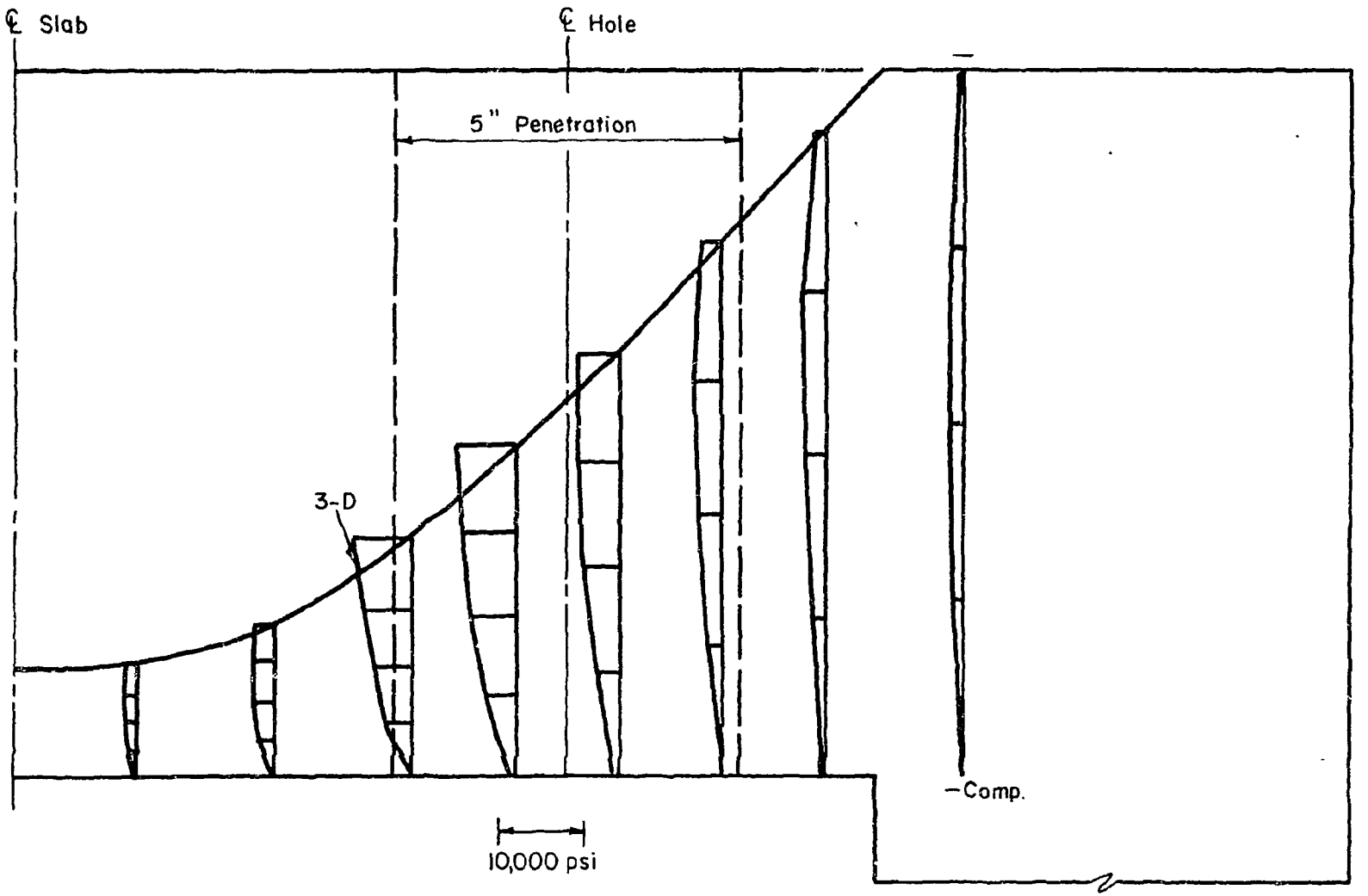

Fig. 3.9c Shear Stresses in Cryptodome Shaped from 10-in. Slab

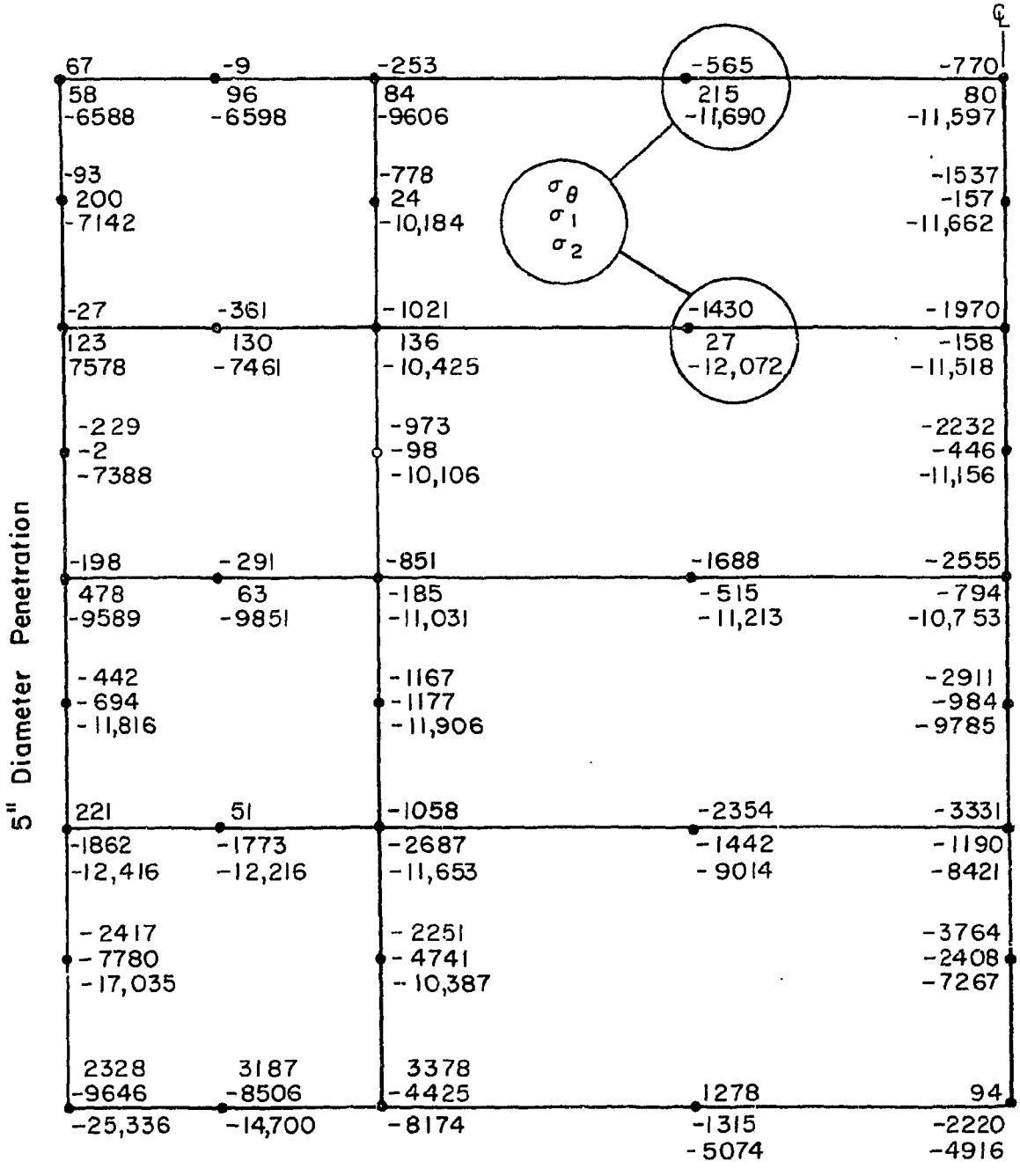

Fig. 3.10 Principal Stresses on a Section Adjacent to Penetration Through 10-in. Head

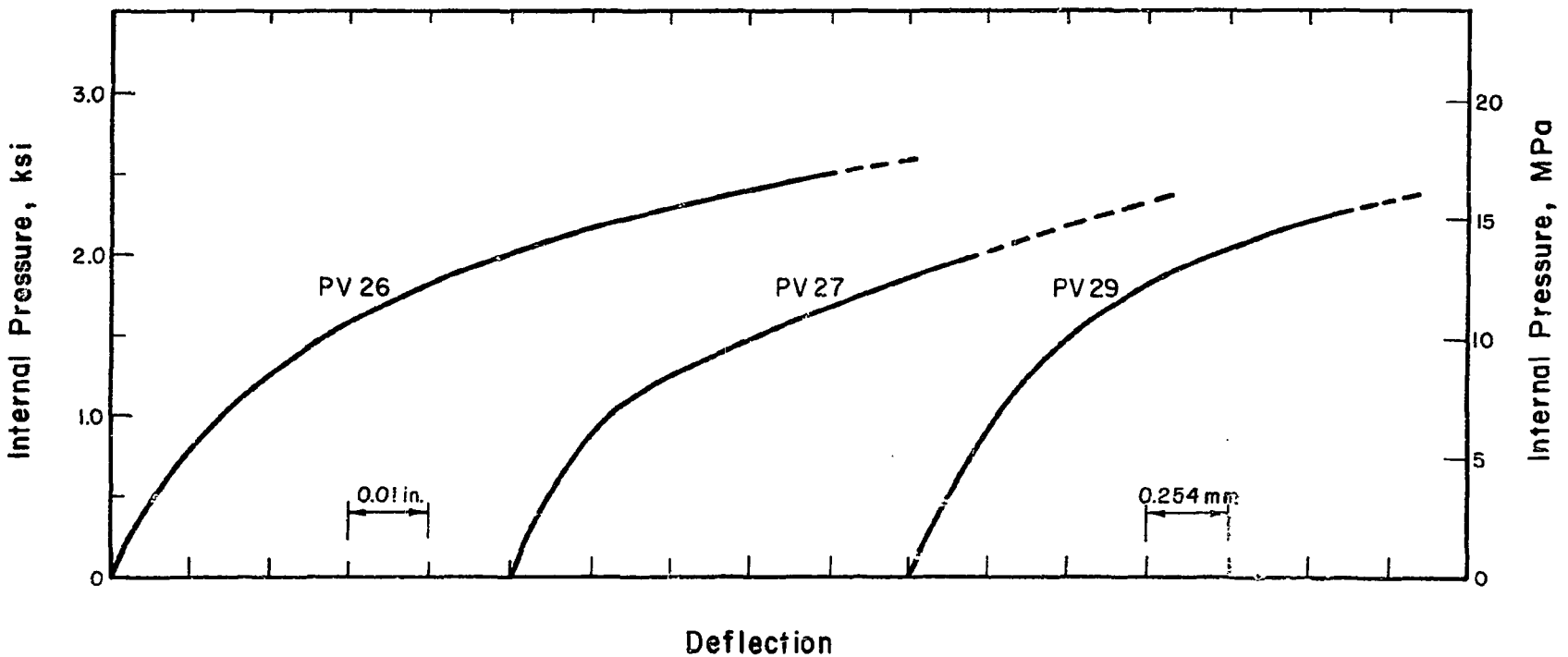

Fig. 4.1 Measured Relationships Between Internal Pressure and Total Deflection at Midspan of End Slab for Test Vessels with 10-in. End Slabs

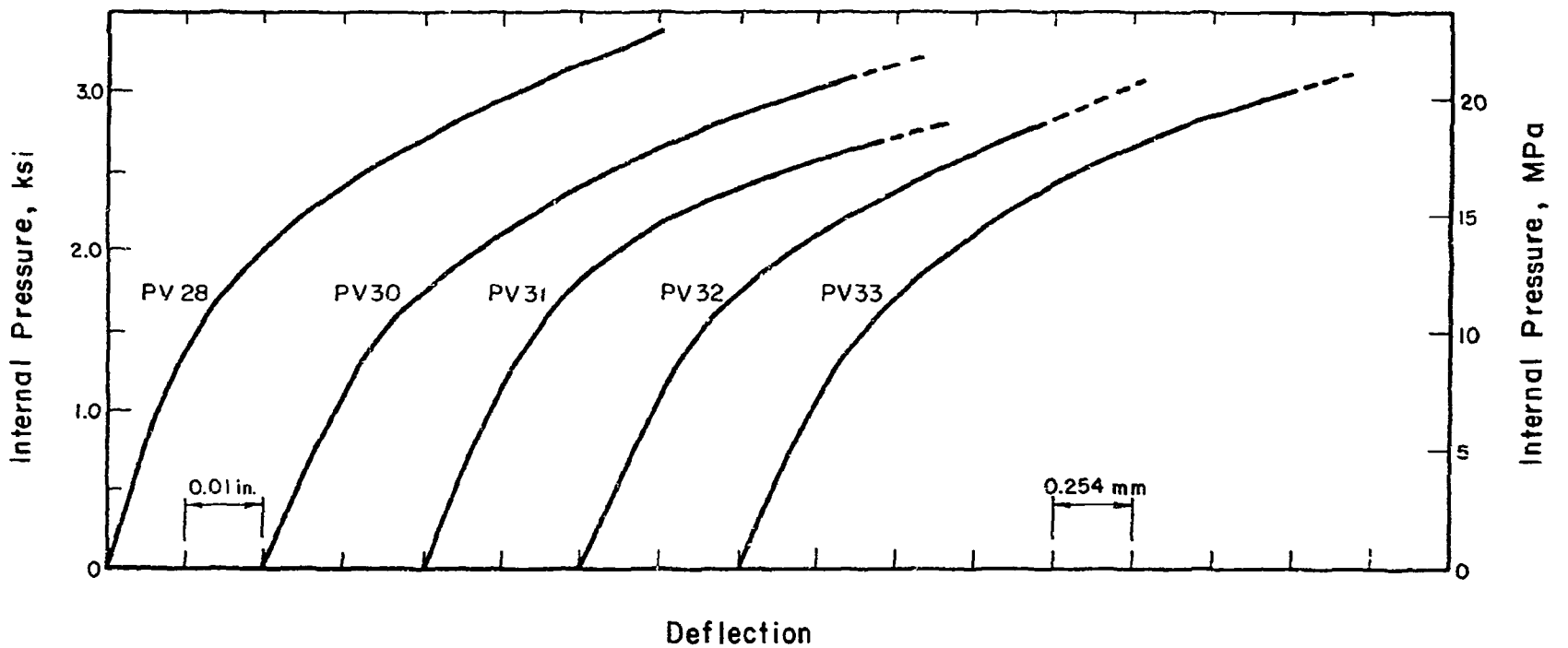

Fig. 4.2 Measured Relationships Between Internal Pressure and Total Deflection at Midspan of End Slab for Test Vessels with 12.5 in. End Slabs

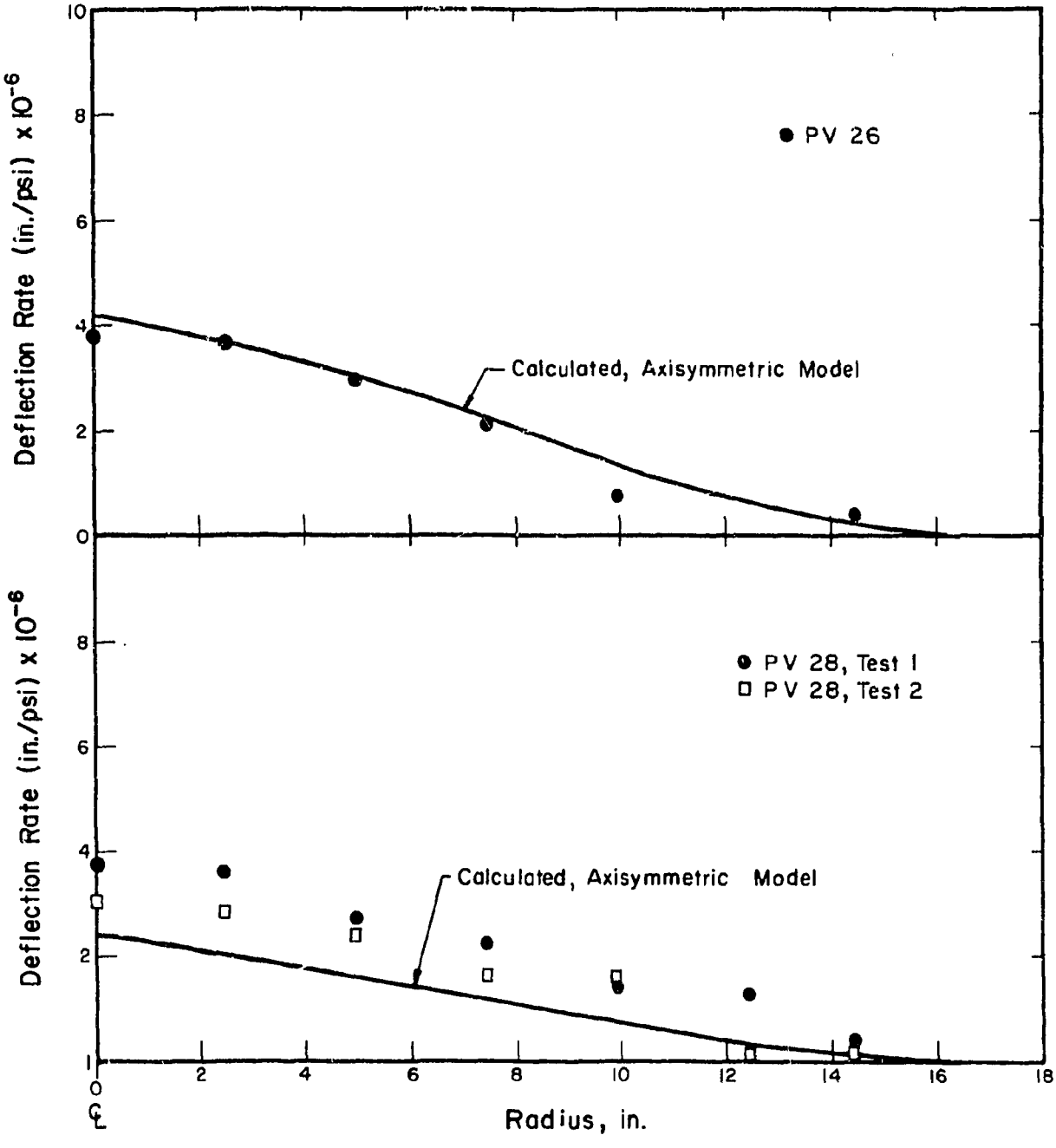

Fig. 4.3 Deflected Shape of End Slab for Vessels with Solid Heads

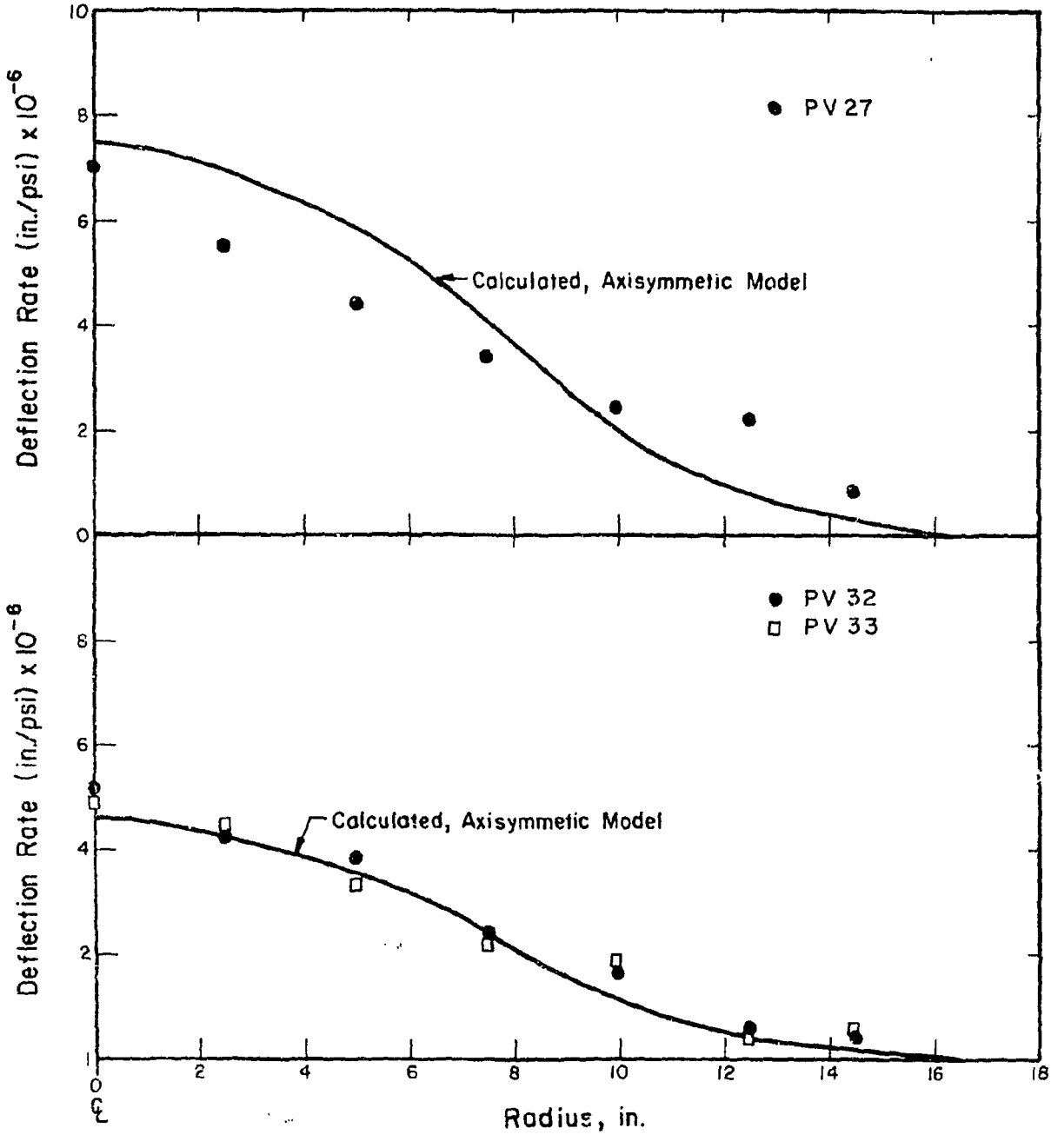

Fig. 4.4 Deflected Shape of End Slab for Vessels with 5-in. Penetrations

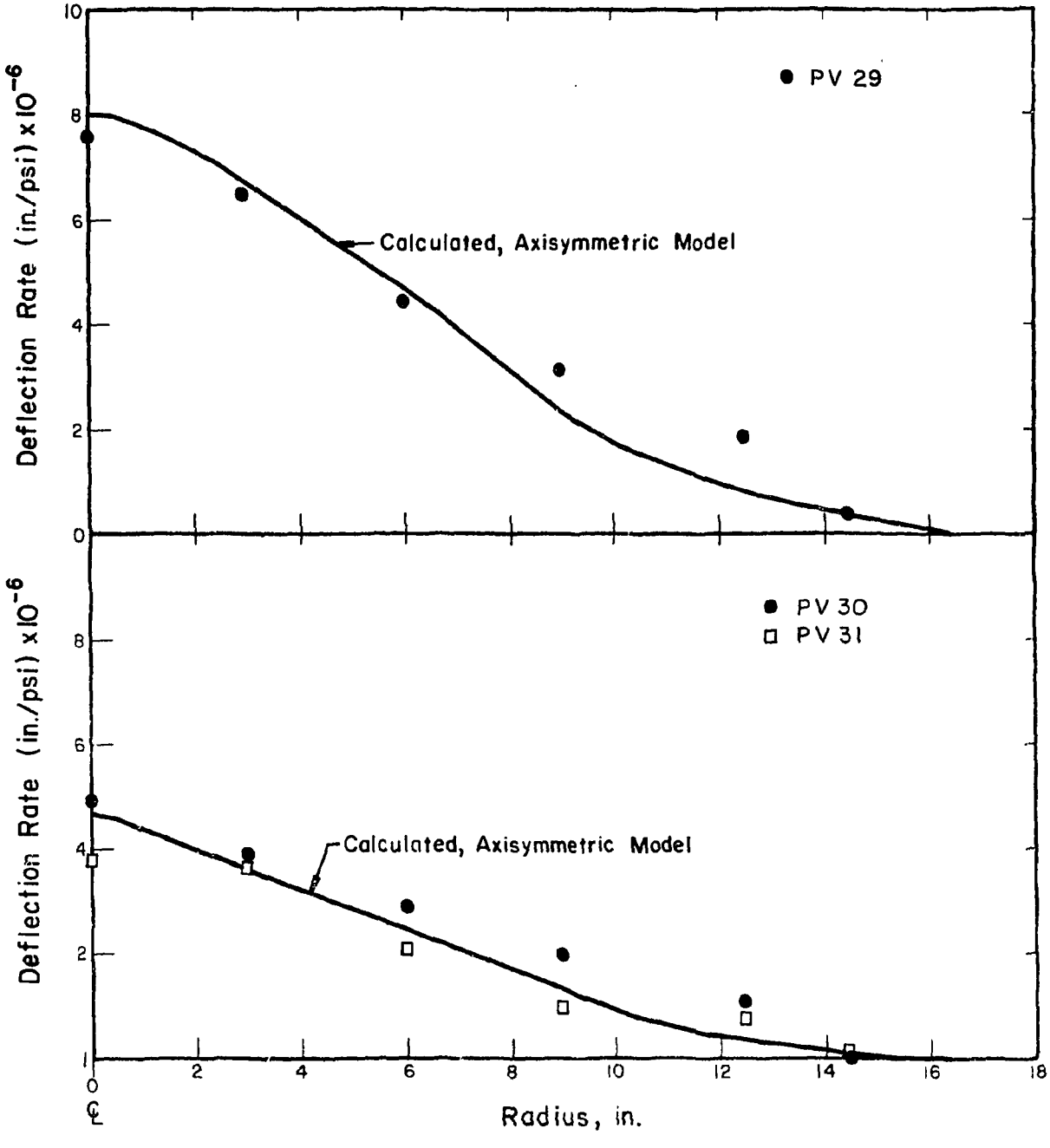

Fig. 4.5 Deflected Shape of End Slab for Vessels with 2-in. Penetrations

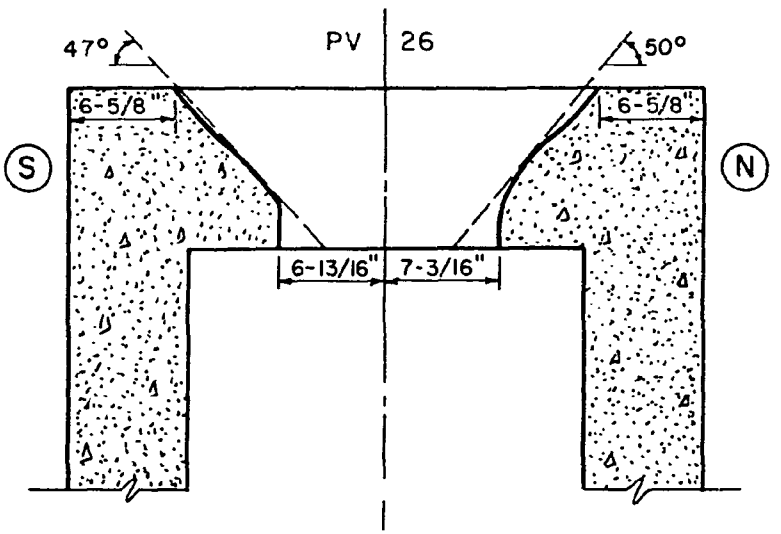

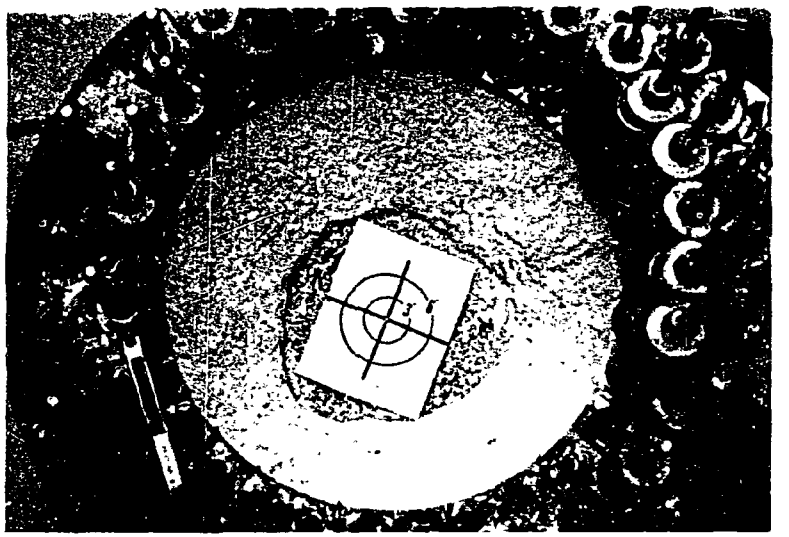

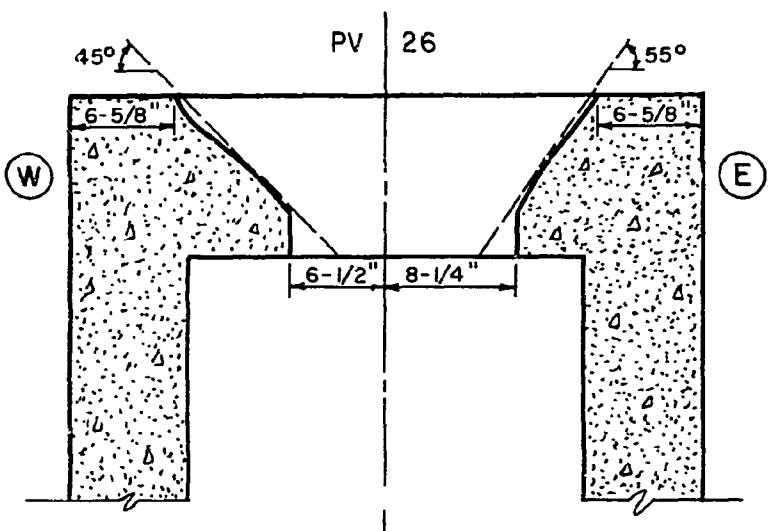

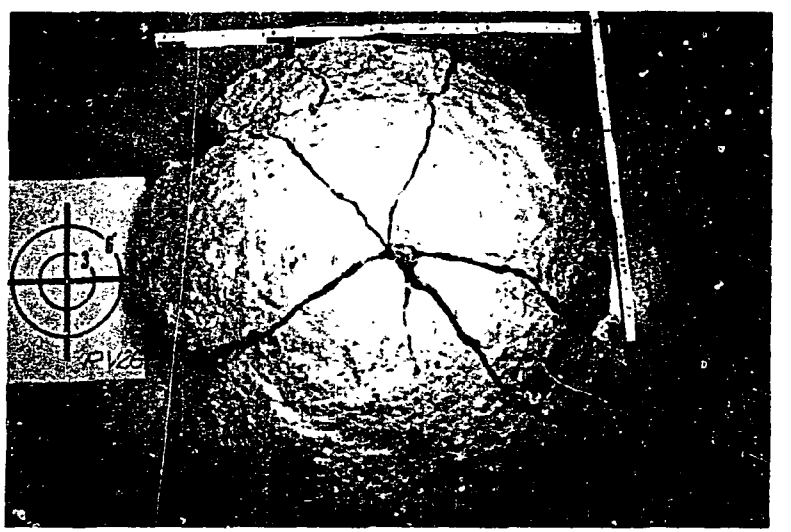

Fig. 4.6 End Slab after Test, PV26

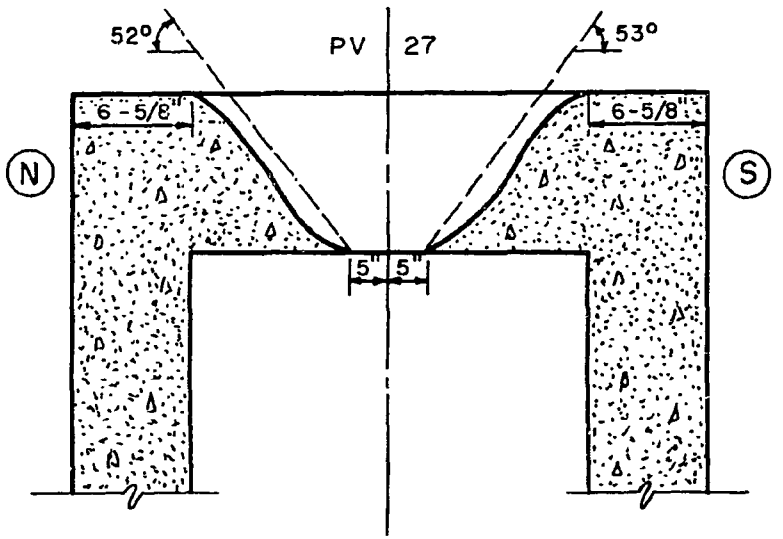

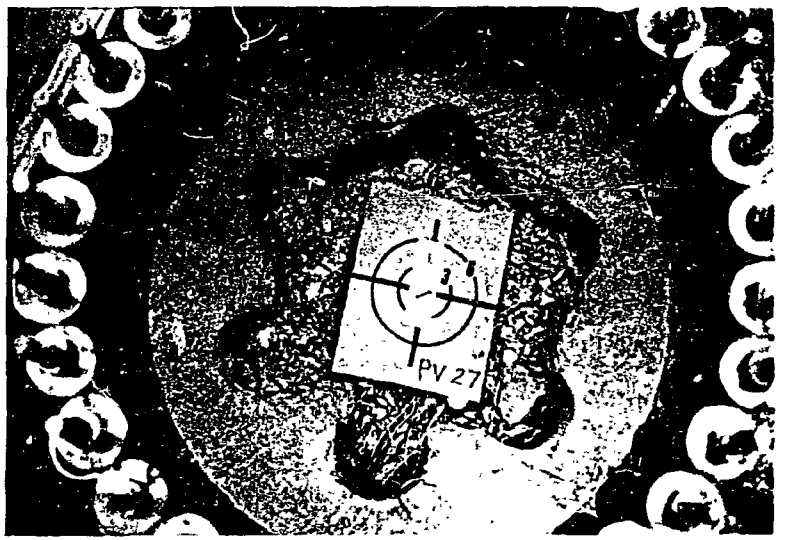

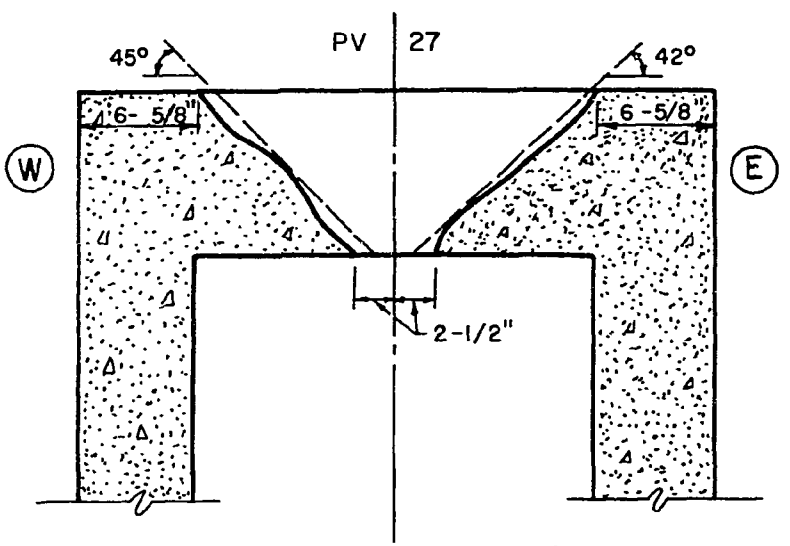

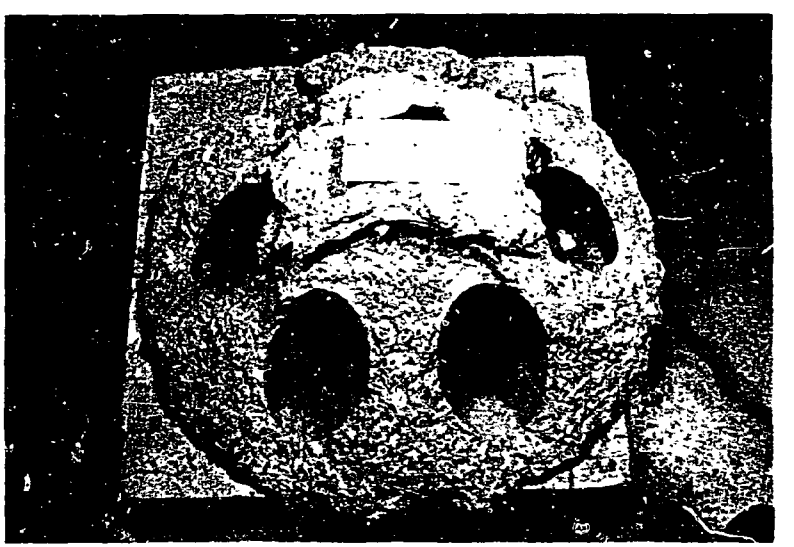

Fig. 4.7 End Slab after Test, PV27

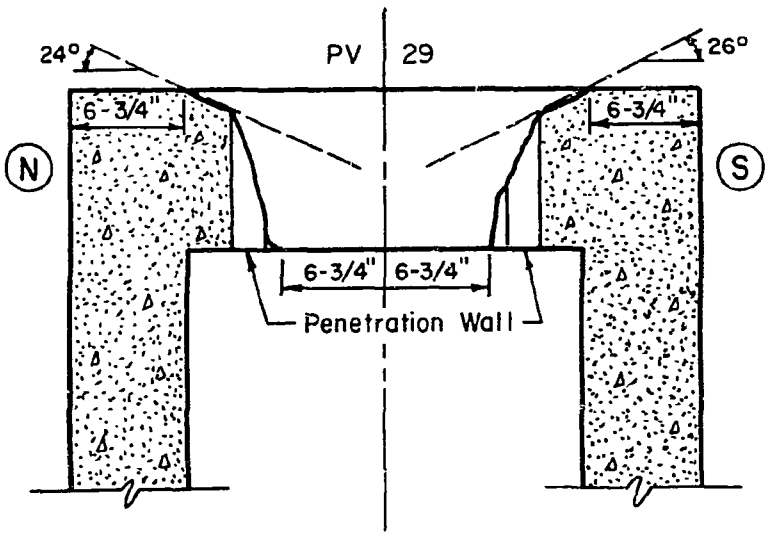

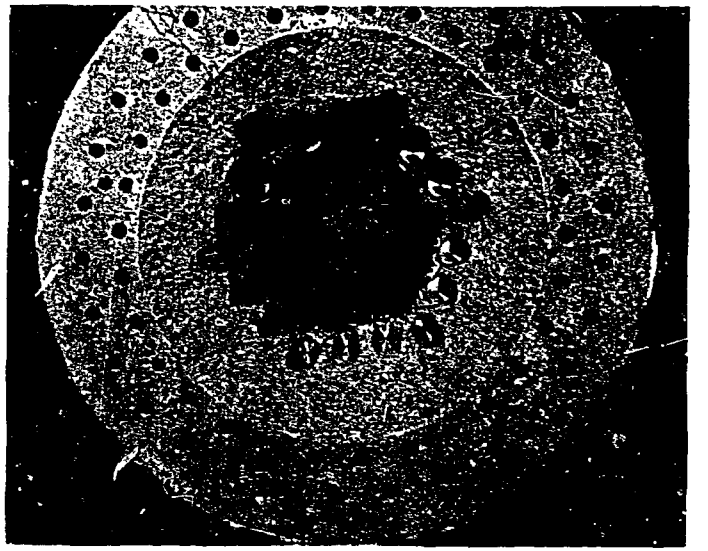

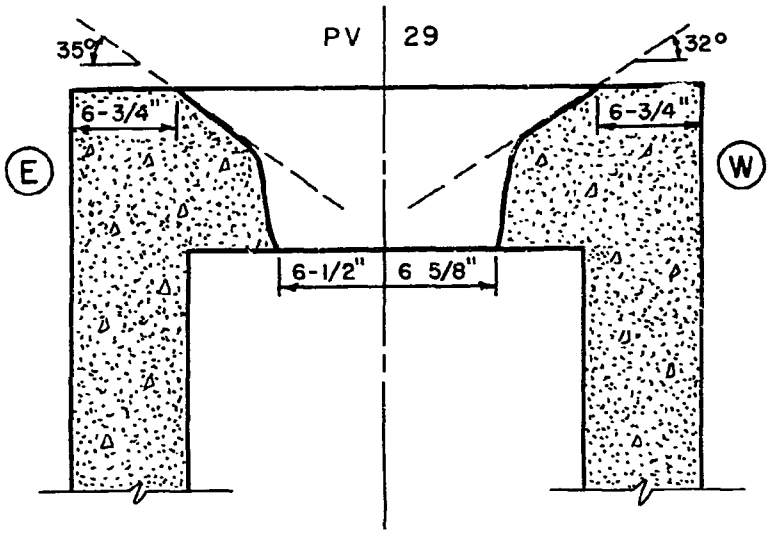

Fig. 4.8 End Slab after Test PV29

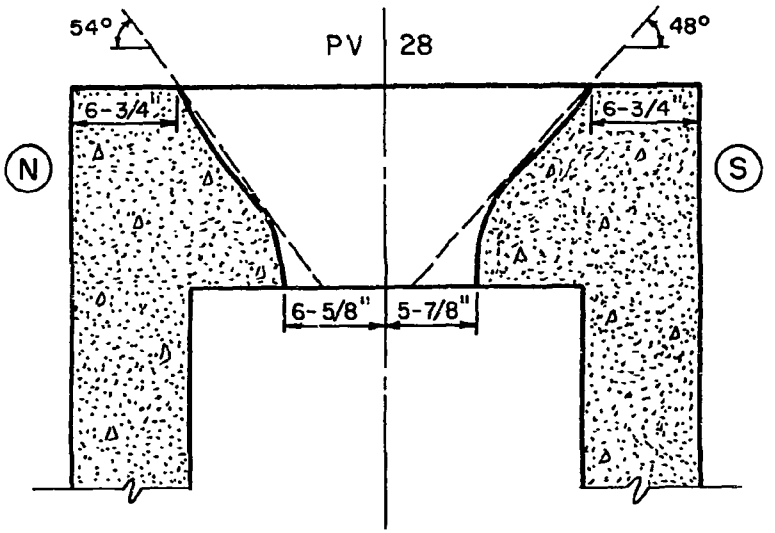

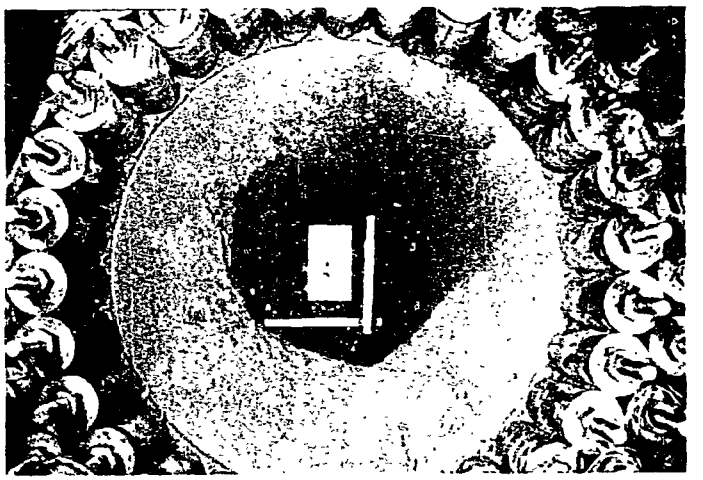

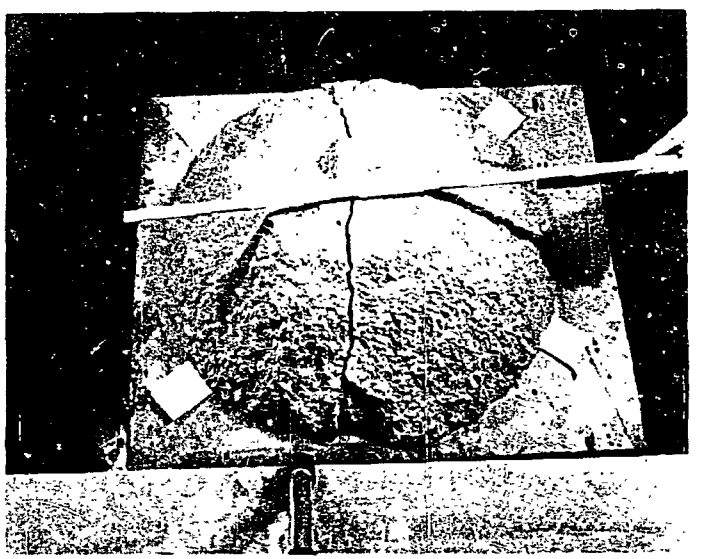

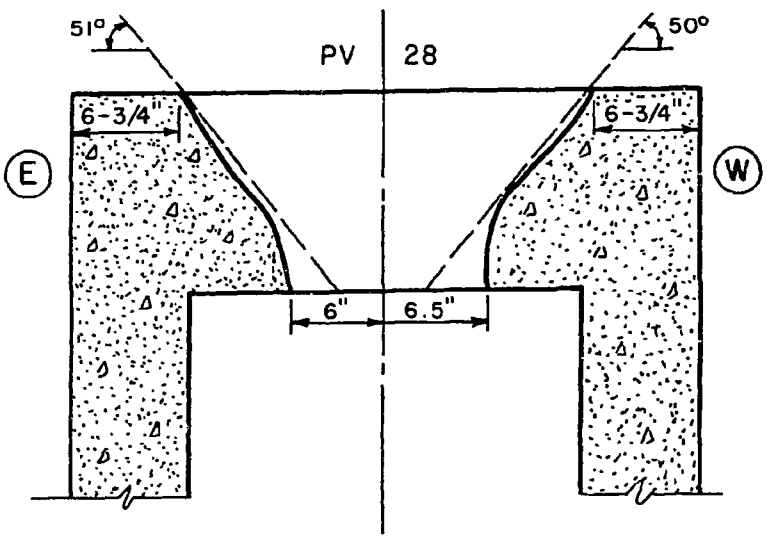

Fig. 4.9 End Slab after Test PV28

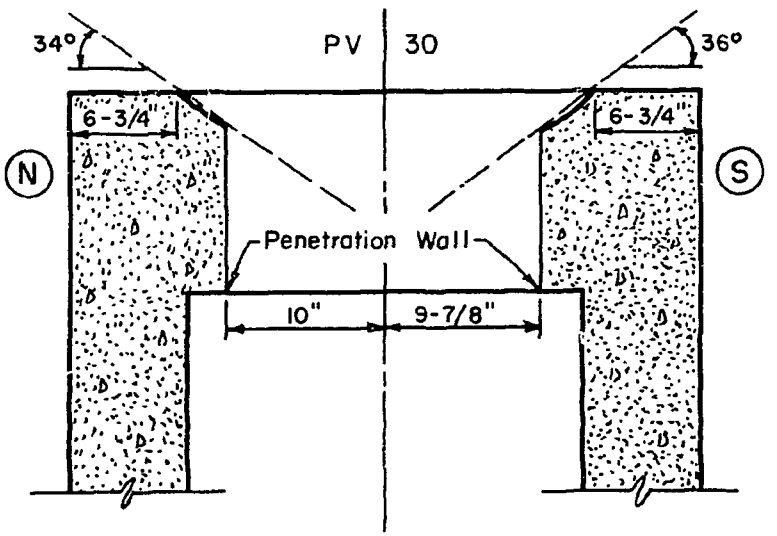

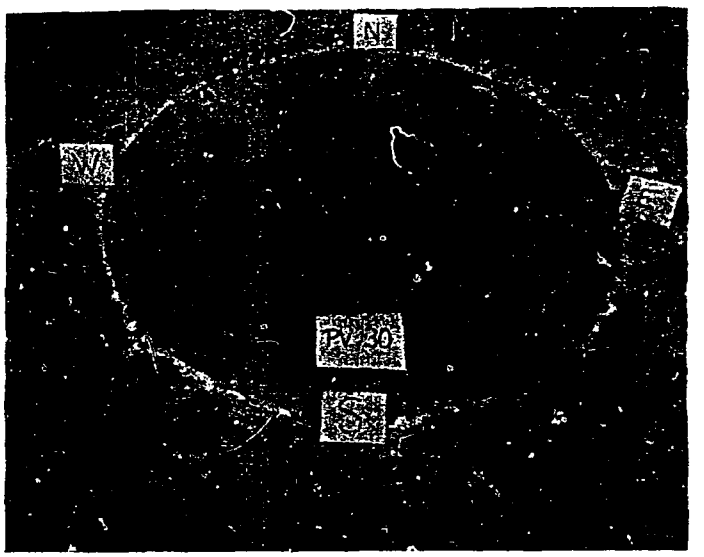

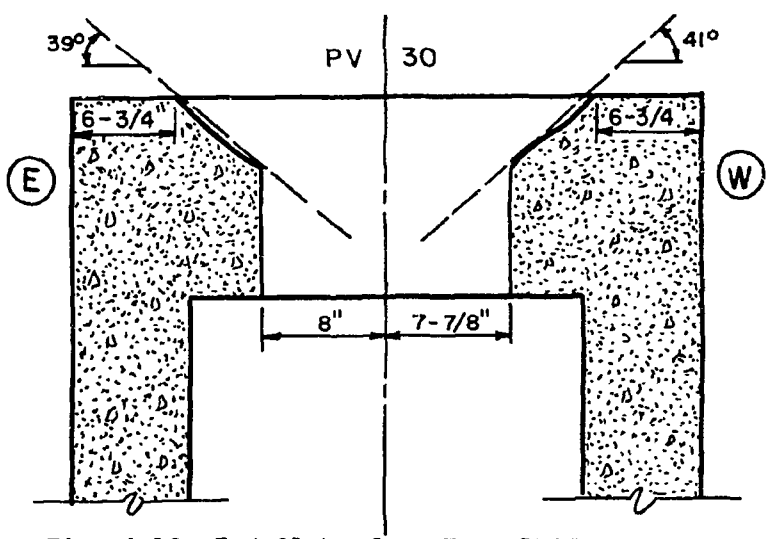

Fig. 4.10 End Slab after Test PV30

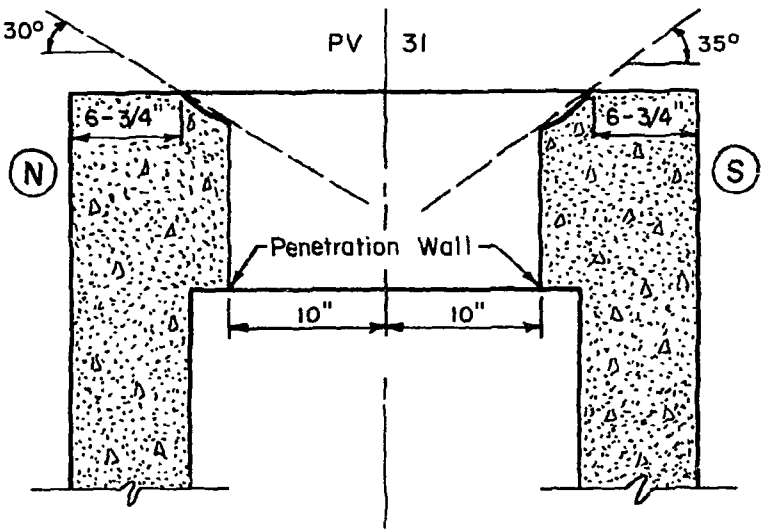

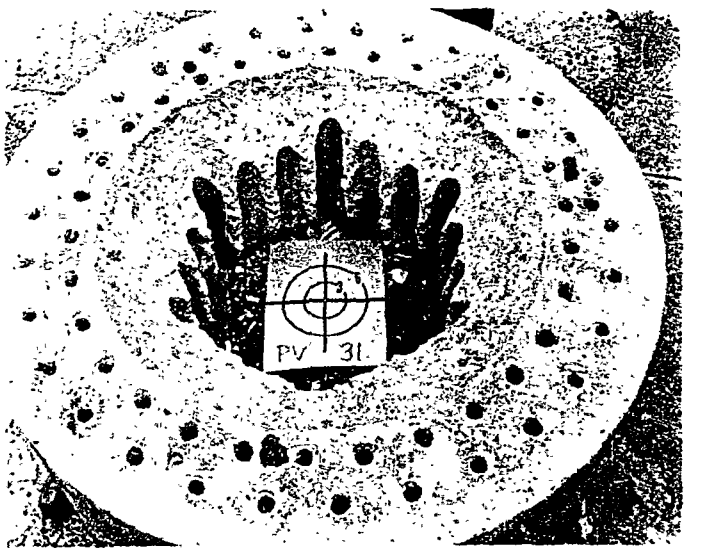

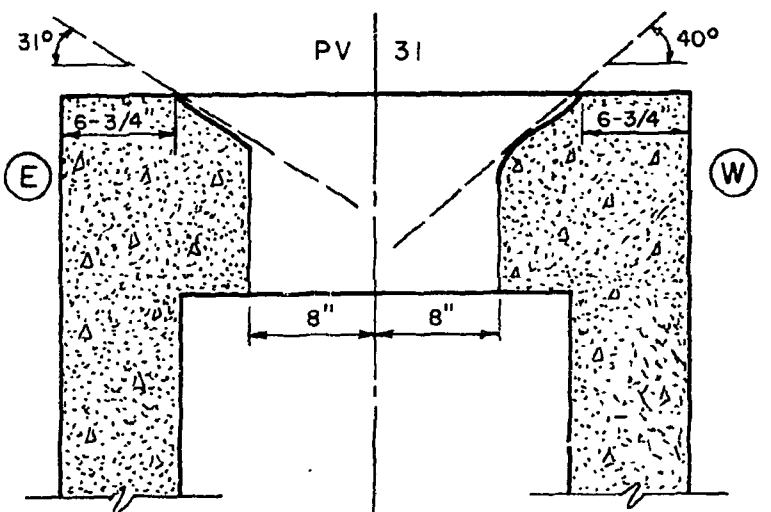

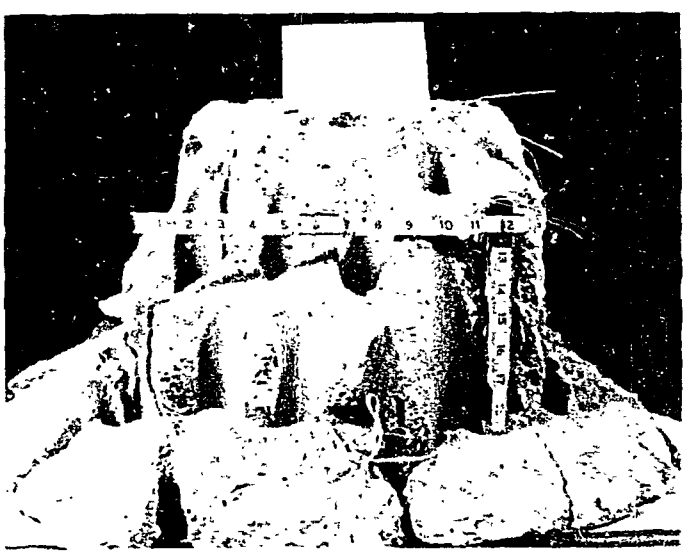

Fig. 4.11 End Slab after Test PV31

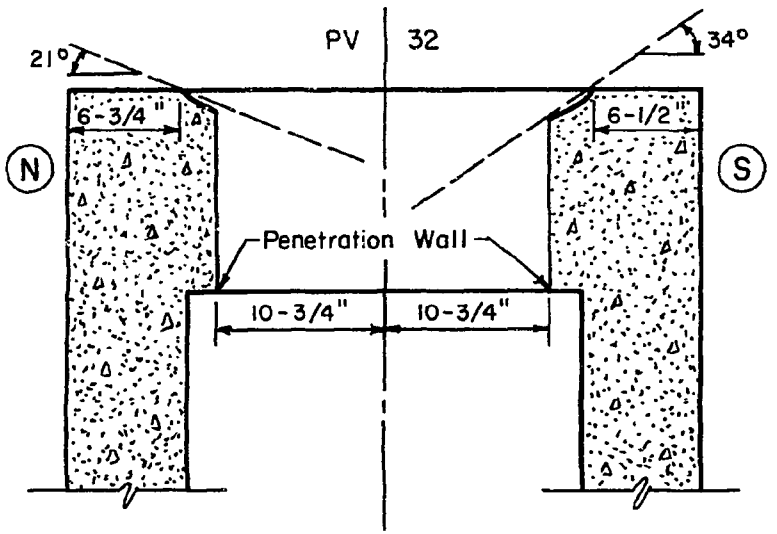

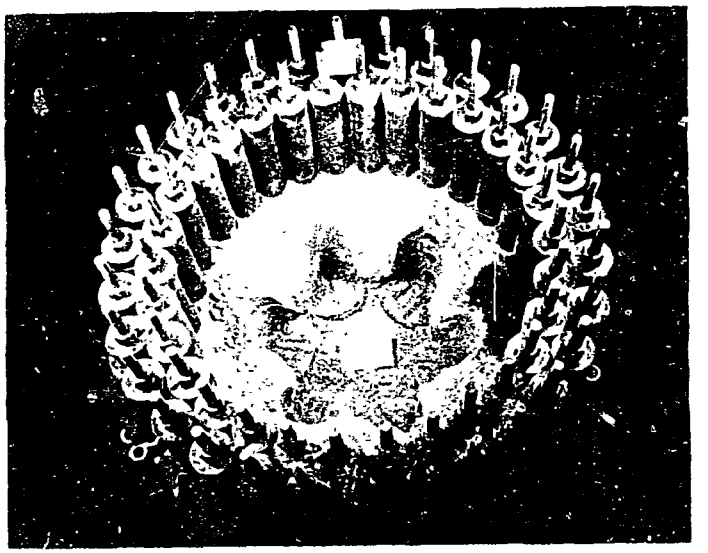

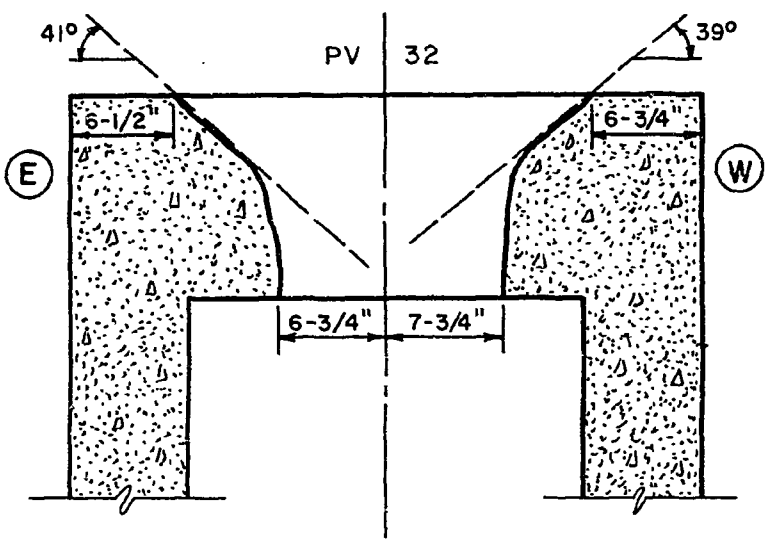

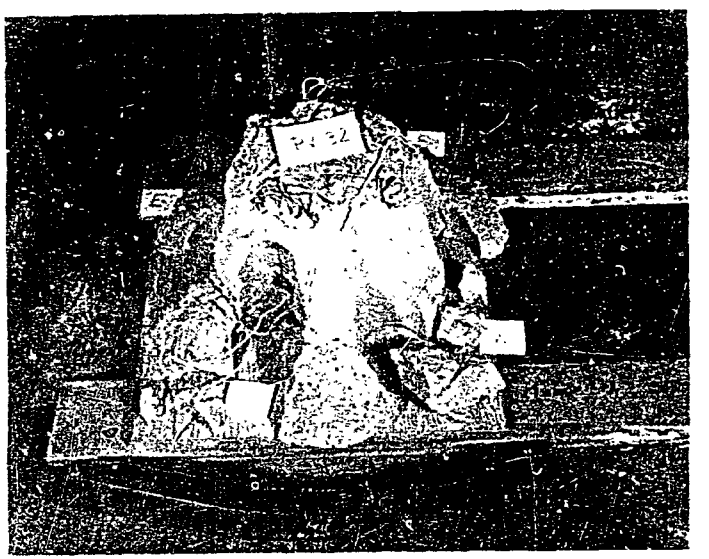

Fig. 4.12 End Slab after Test PV32

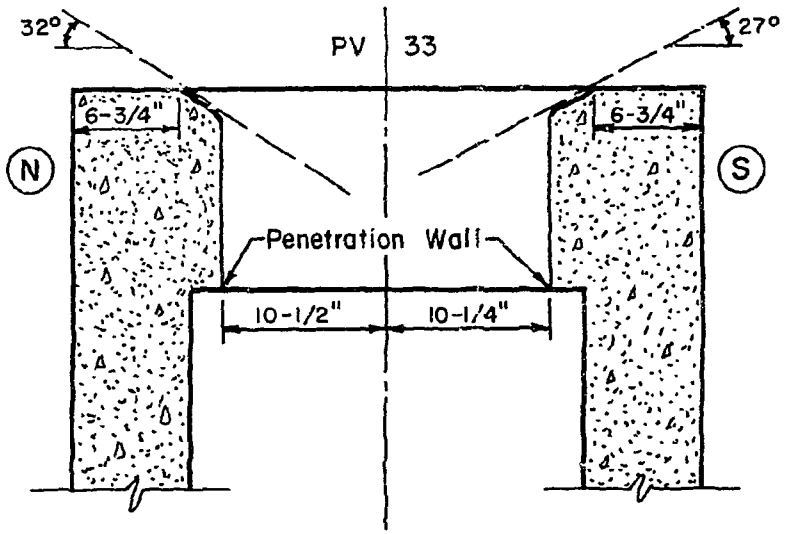

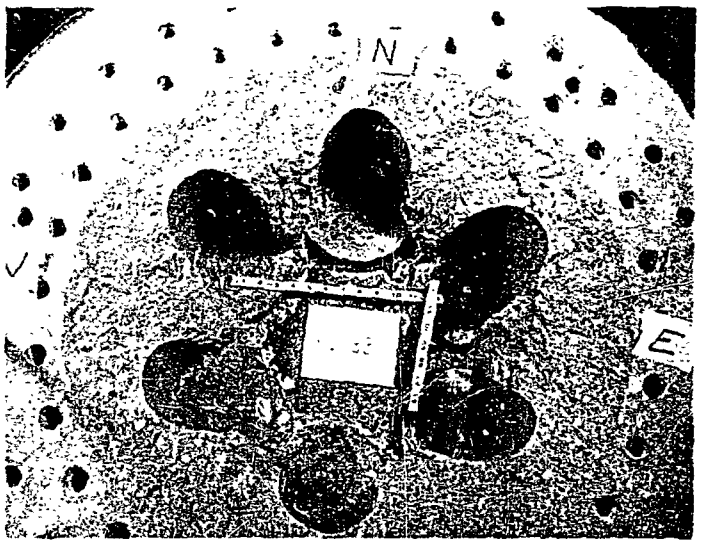

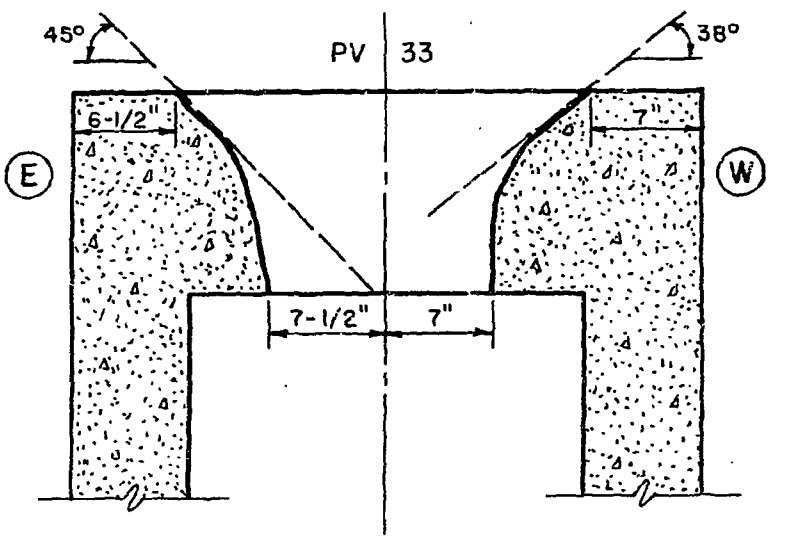

Fig. 4.13 End Slab after Test PV33

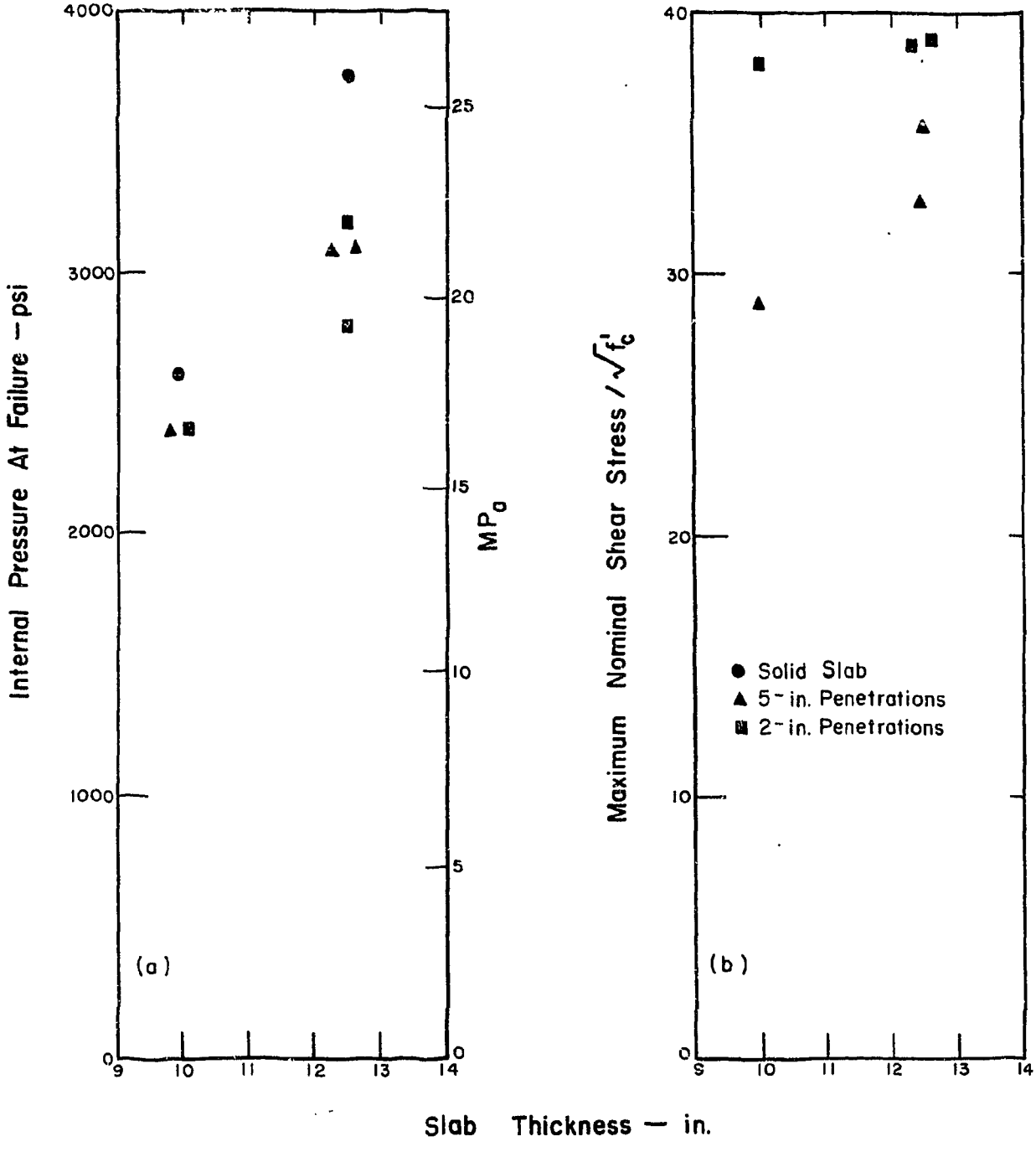

Fig. 4.14 Failure Prestress and Maximum Nominal Shear Stresses

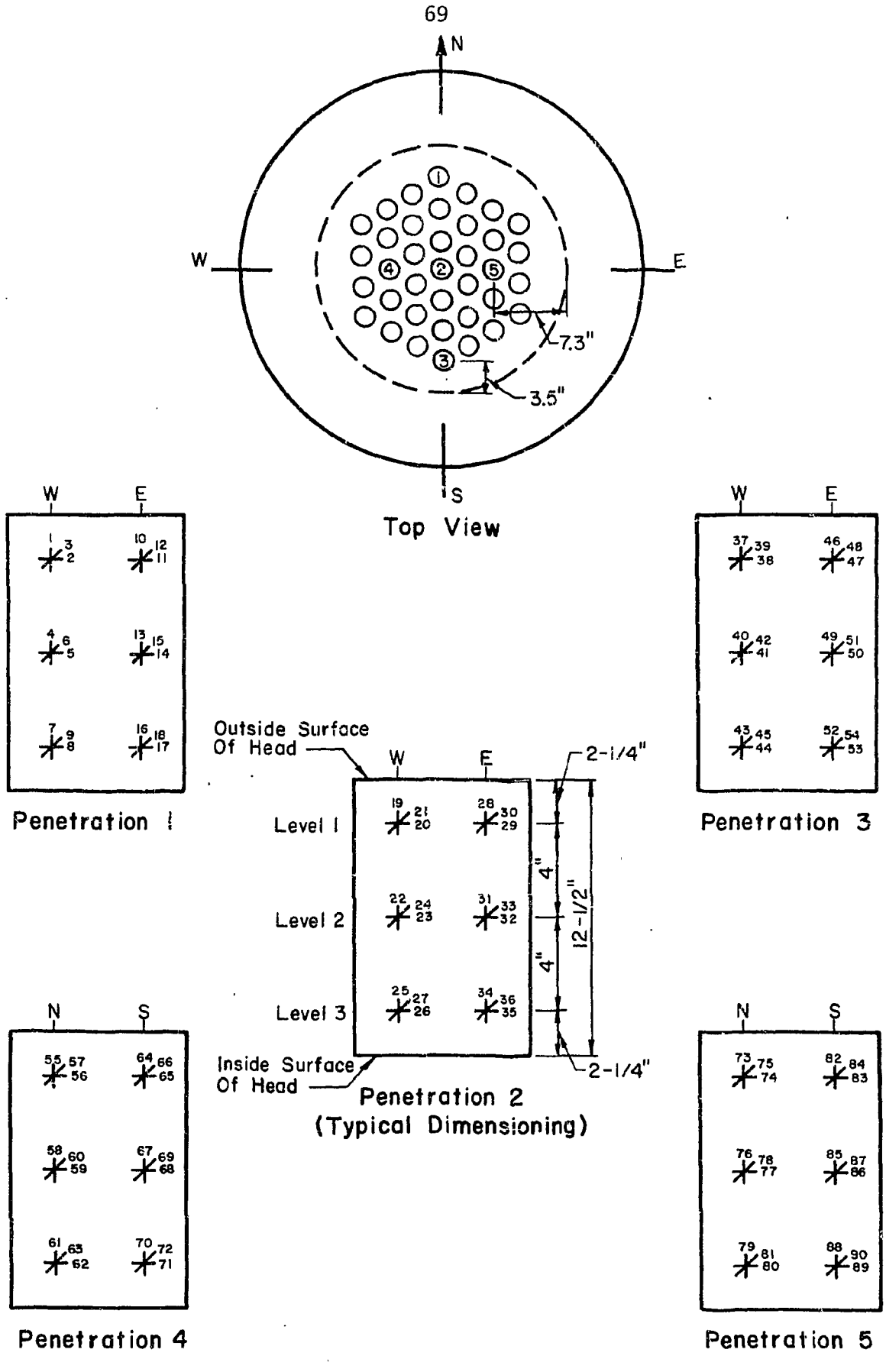

Fig. 5.1a Location of Strain Gages in End Slab with 2-in. Penetrations

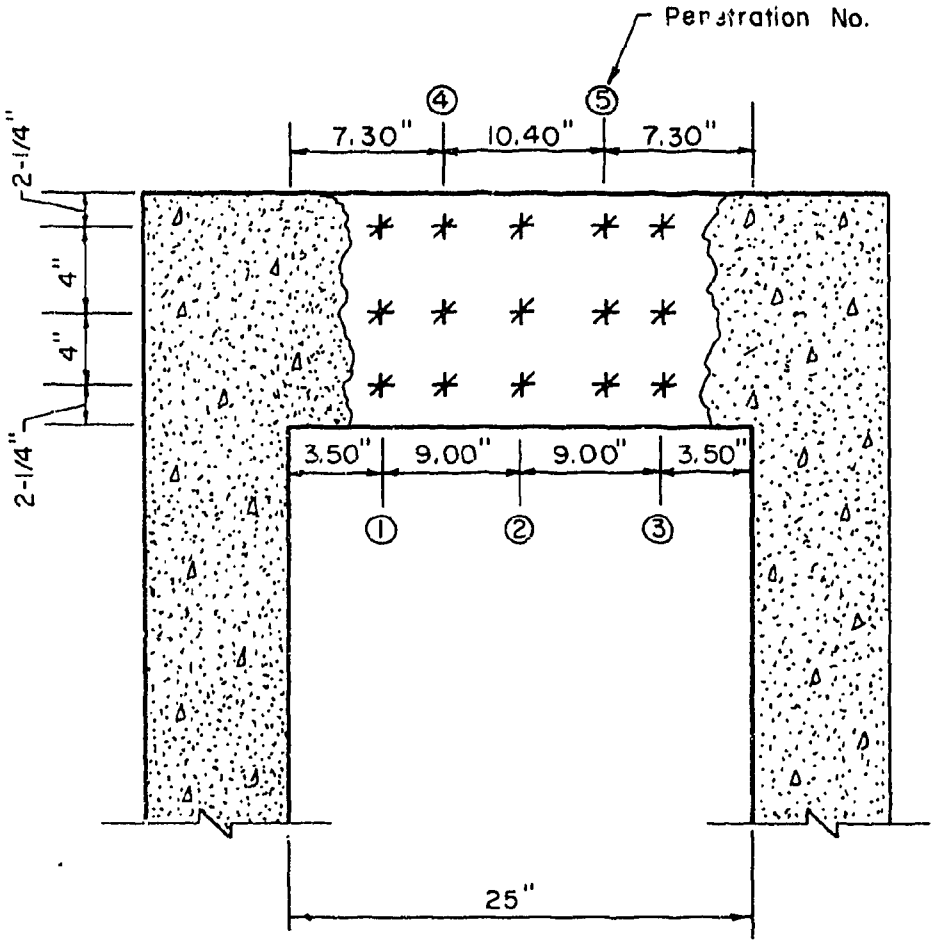

Fig. 5.1b Location of Strain Rosettes in the Vertical Plane
(See Fig. 5.1a for location of penetrations in plan).

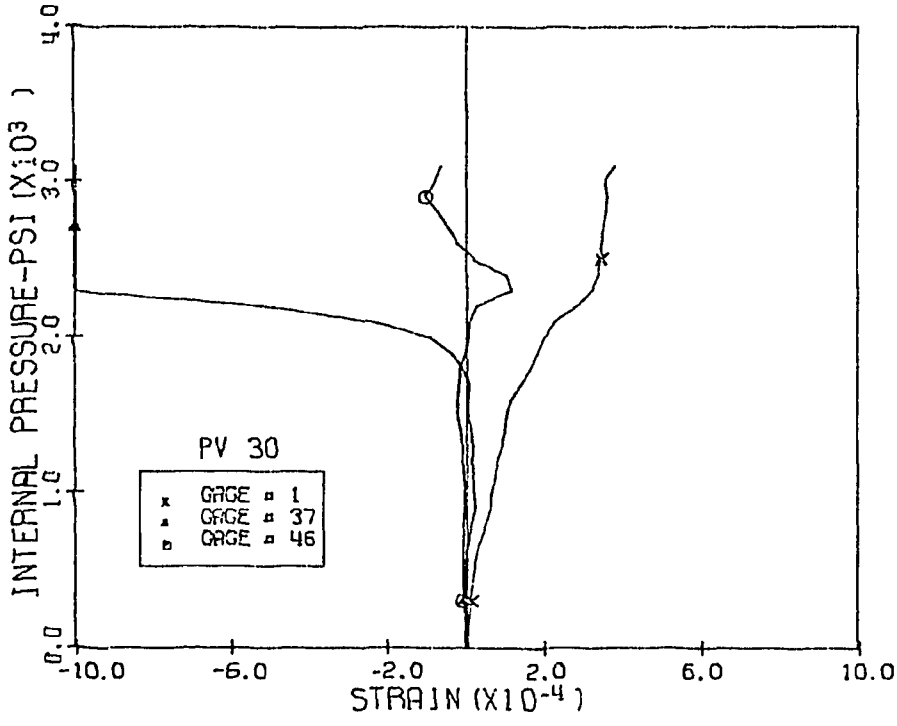

Fig. 5.2 Measured Vertical Strains, Level 1 Penetrations 1 and 3, PV30

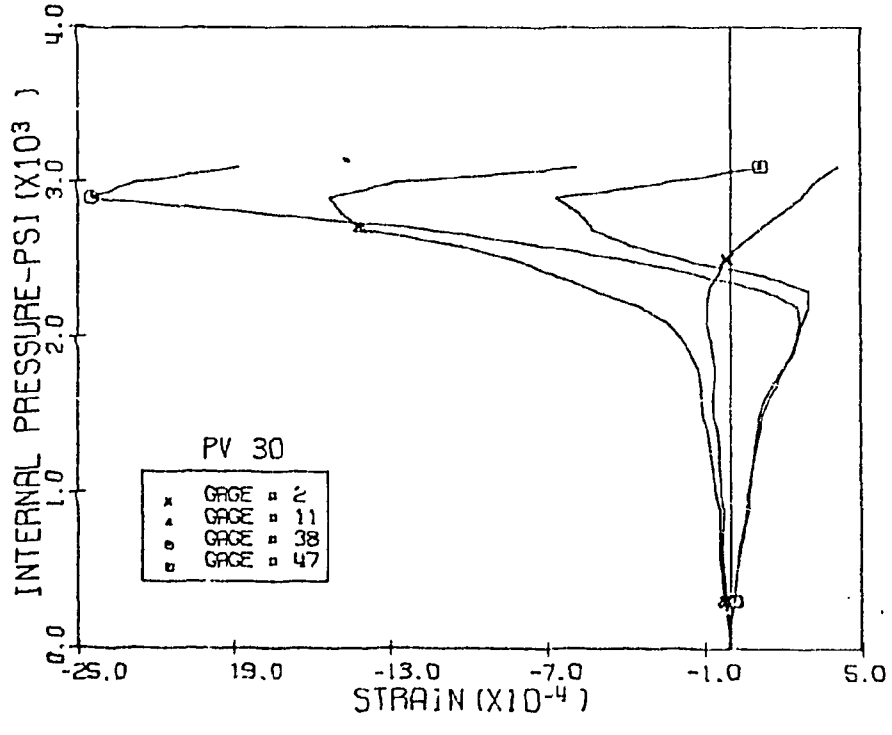

Fig. ... easured Horizontal Strains, Level 1 Penetrations 1 and 3, PV30

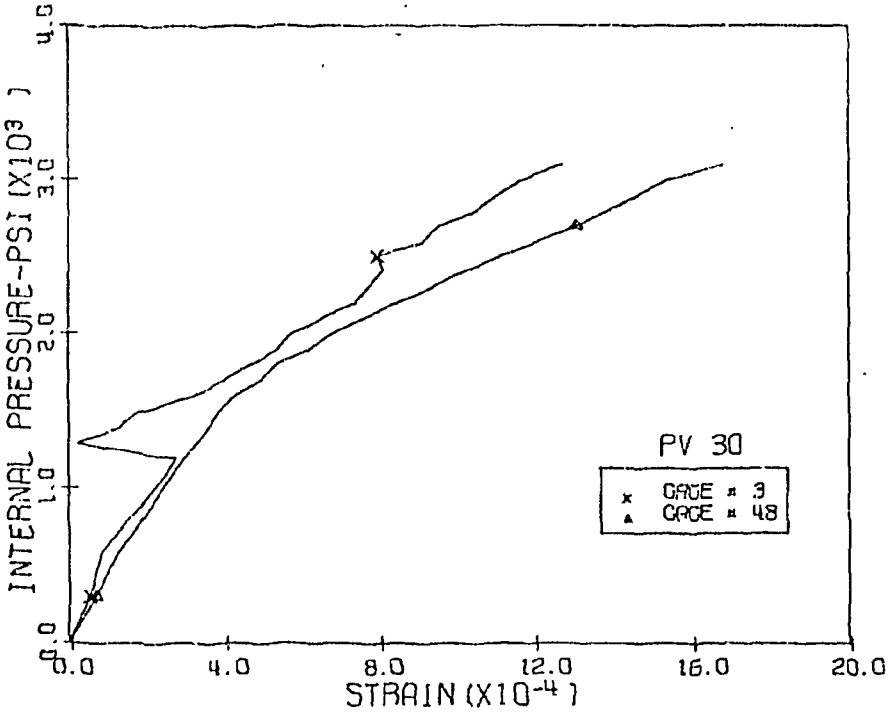

Fig. 5.4 Measured Compression Diagonal Strains, Level 1 Penetrations 1 and 3 PV30

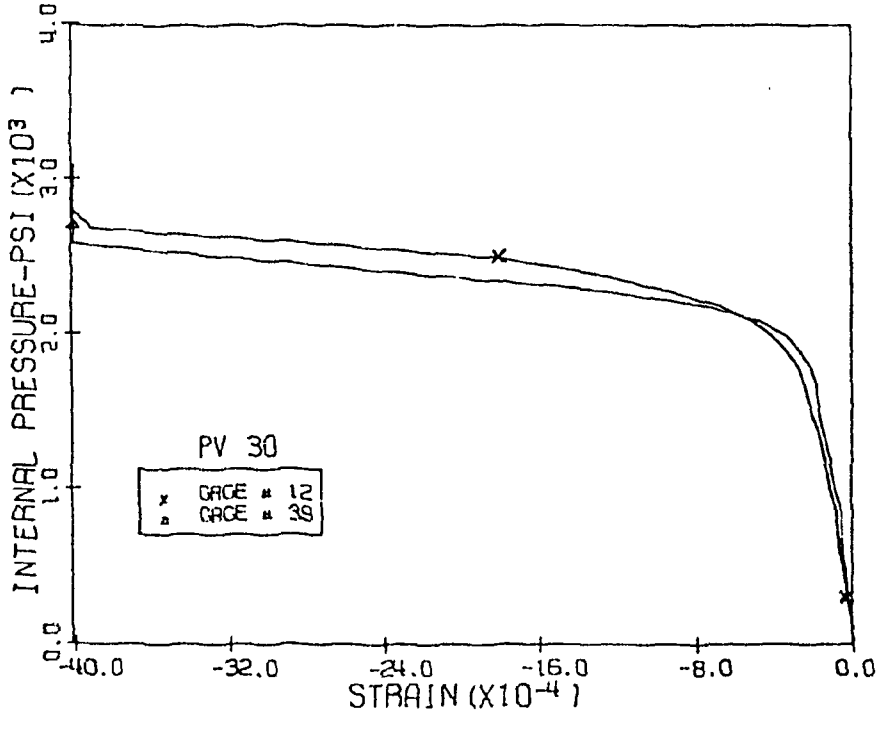

Fig. 5.5 Measured Tension Diagonal Strains, Level 1 Penetrations 1 and 3 PV30

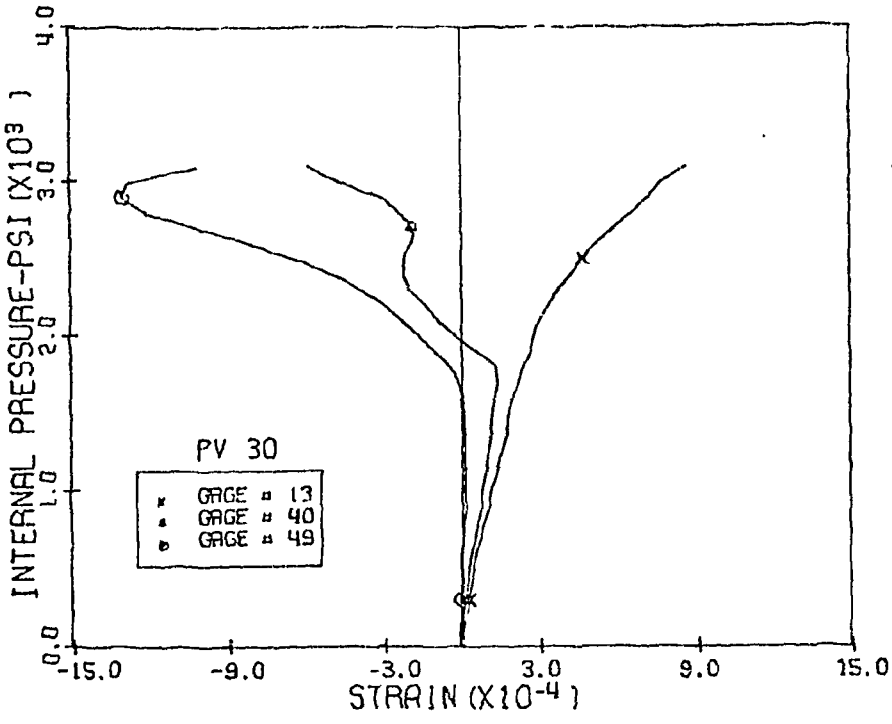

Fig. 5.6 Measured Vertical Strains, Level 2 Penetrations 1 and 3, PV30

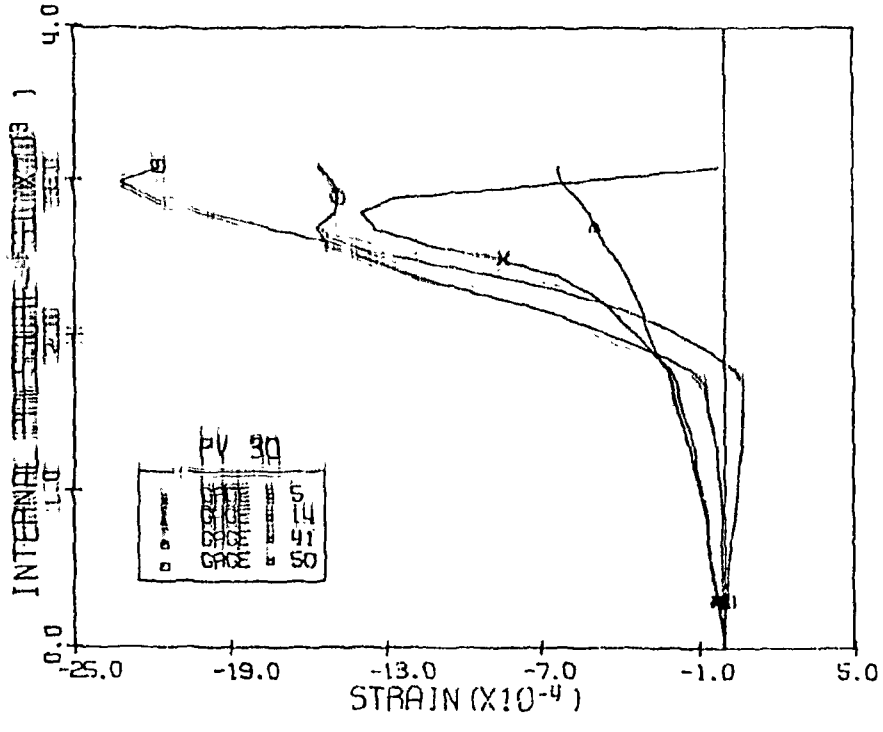

Fig. 5.7 Measured Horizontal Strains, Level 2 Penetrations 1 and 3, PV30

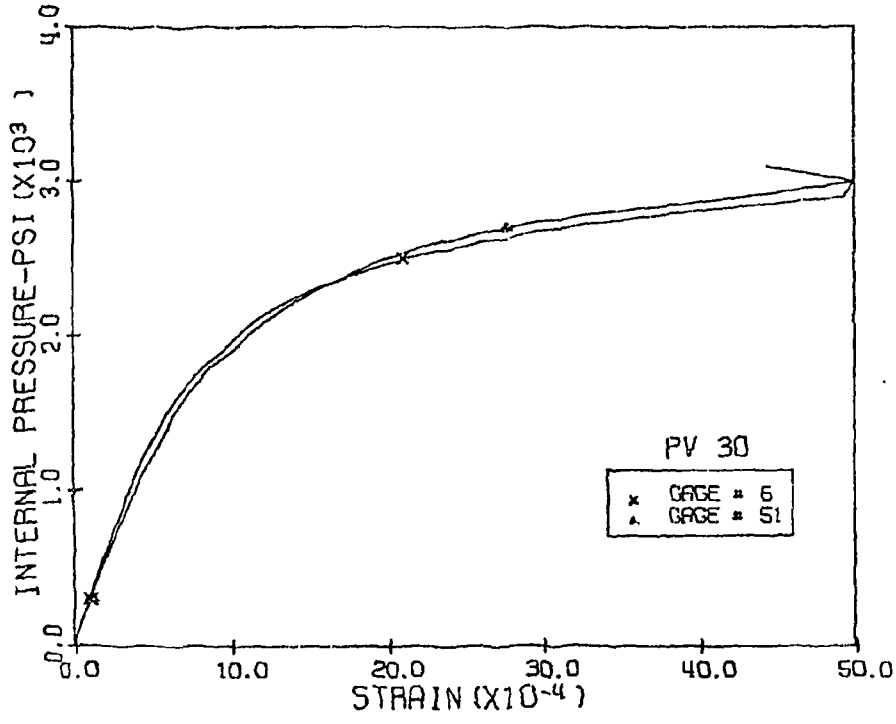

Fig. 5.8 Measured Compression Diagonal Strains, Level 2 Penetrations 1 and 3, PV30

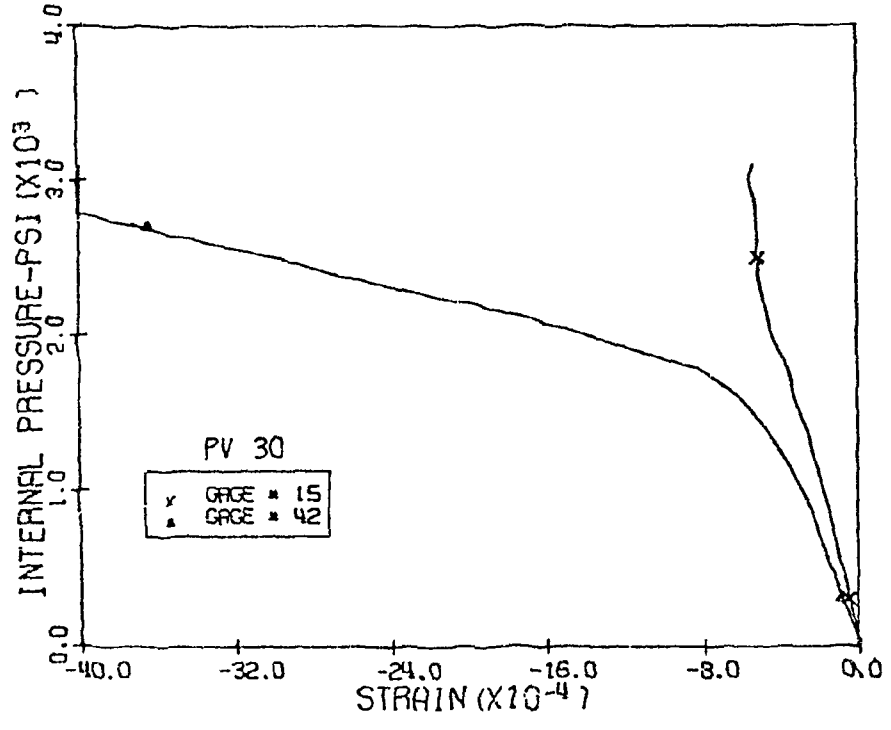

Fig. 5.9 Measured Tension Diagonal Strains, Level 2 Penetrations 1 and 3, PV30

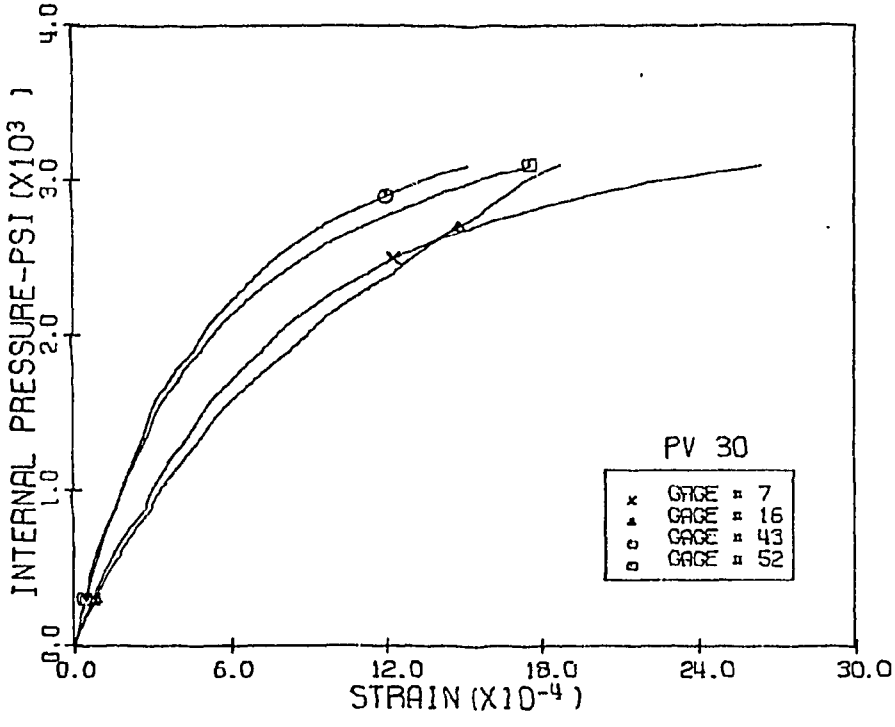

Fig. 5.10 Measured Vertical Strains, Level 3 Penetrations 1 and 3, PV30

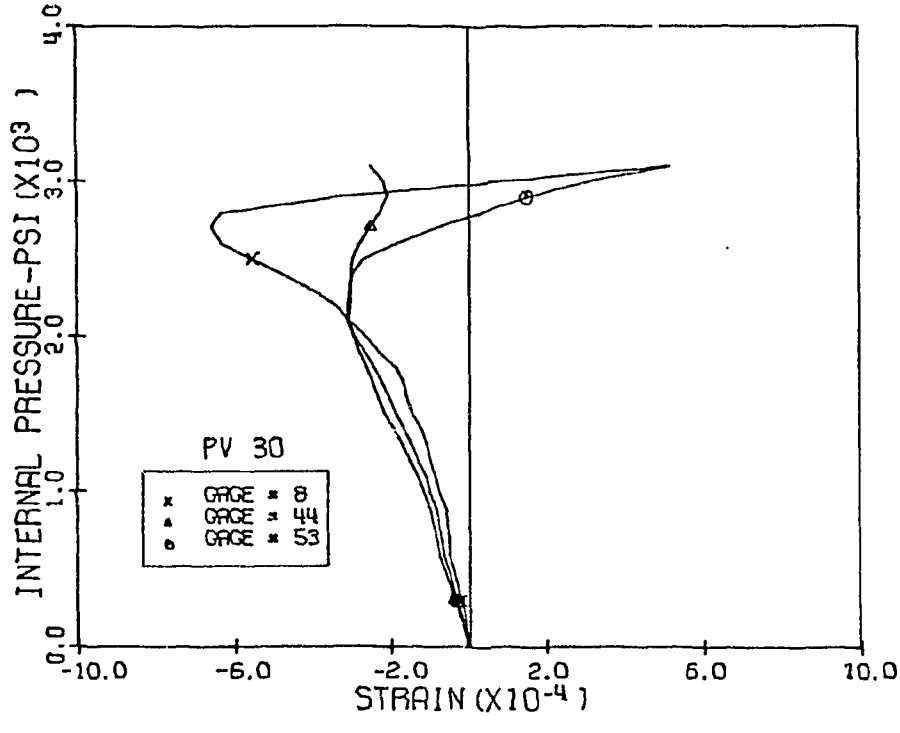

Fig. 5.11 Measured Horizontal Strains, Level 3 Penetrations 1 and 3, PV30

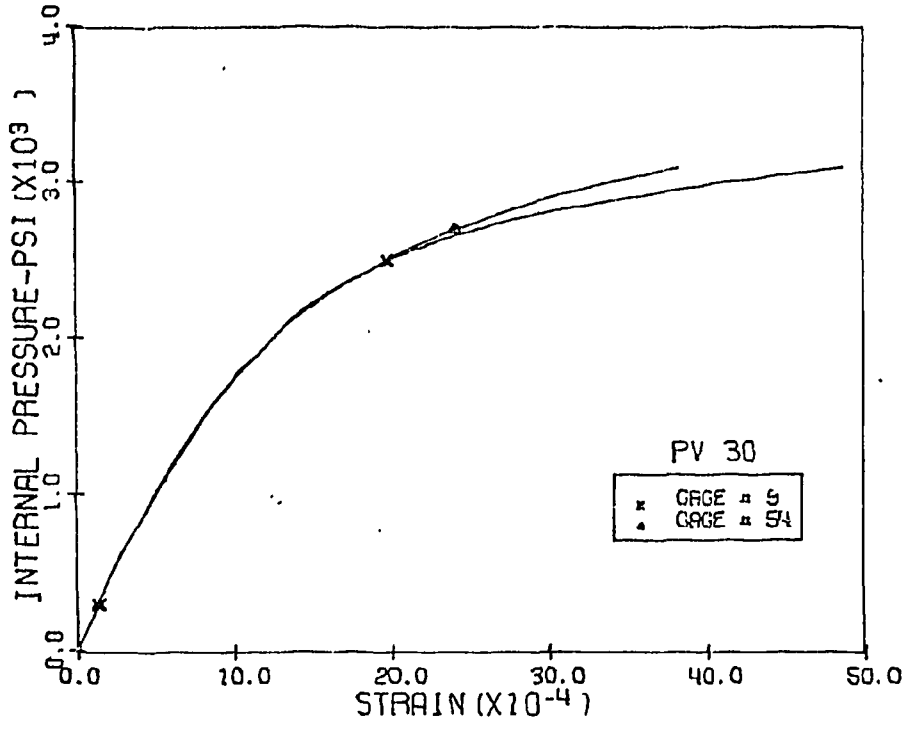

Fig. 5.12 Measured Compression Diagonal Strains, Level 3 Penetrations 1 and 3, PV30

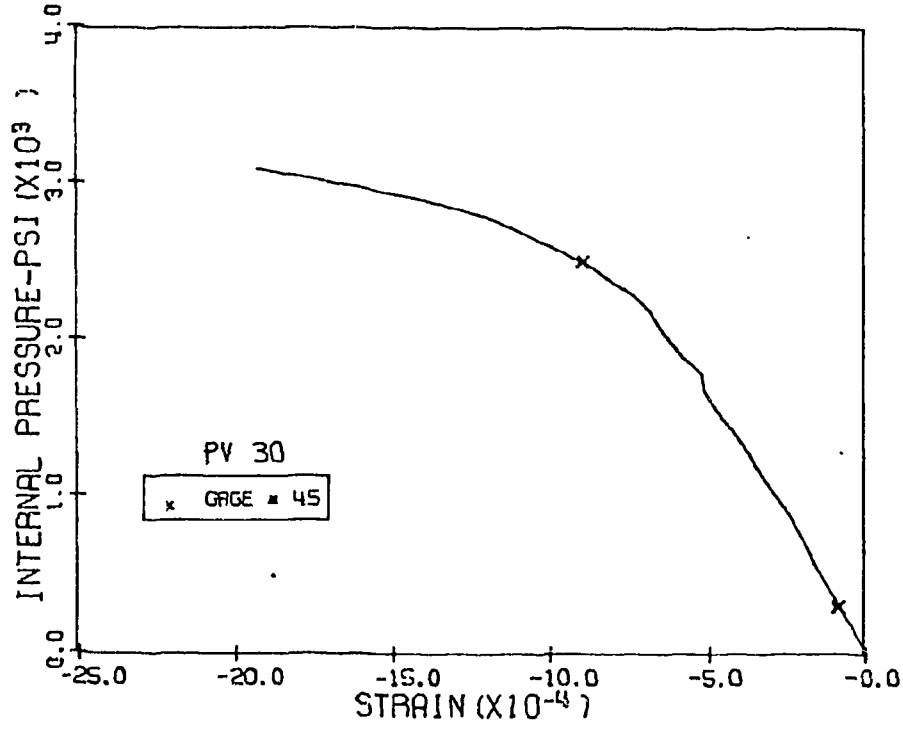

Fig. 5.13 Measured Tension Diagonal Strain, Level 3 Penetrations 1 and 3, PV30

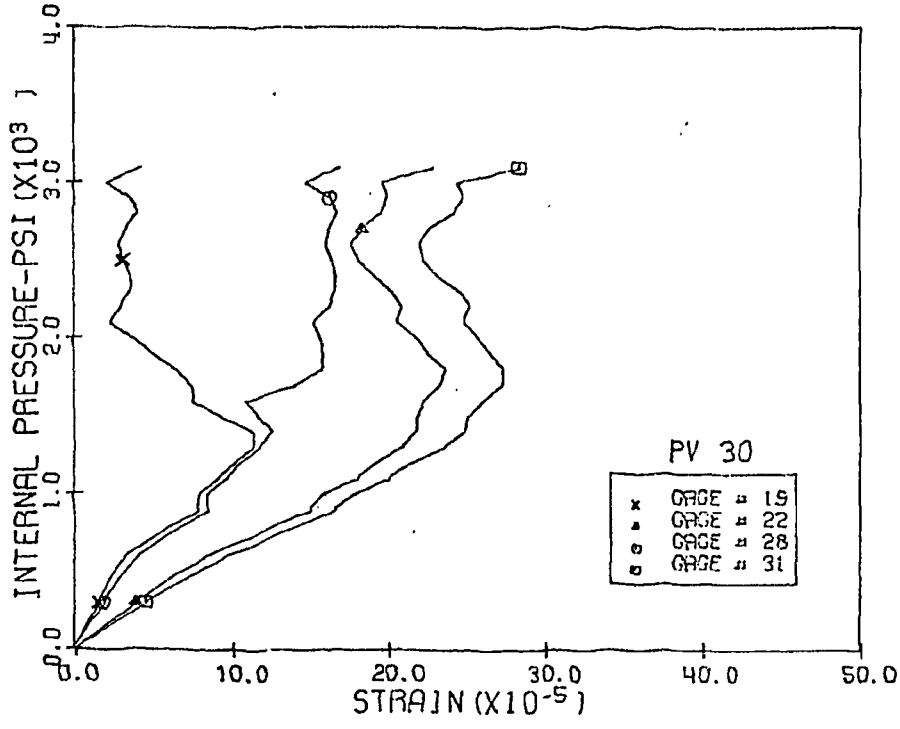

Fig. 5.14 Measured Vertical Strains, Levels 1 and 2 Penetration 2, PV30

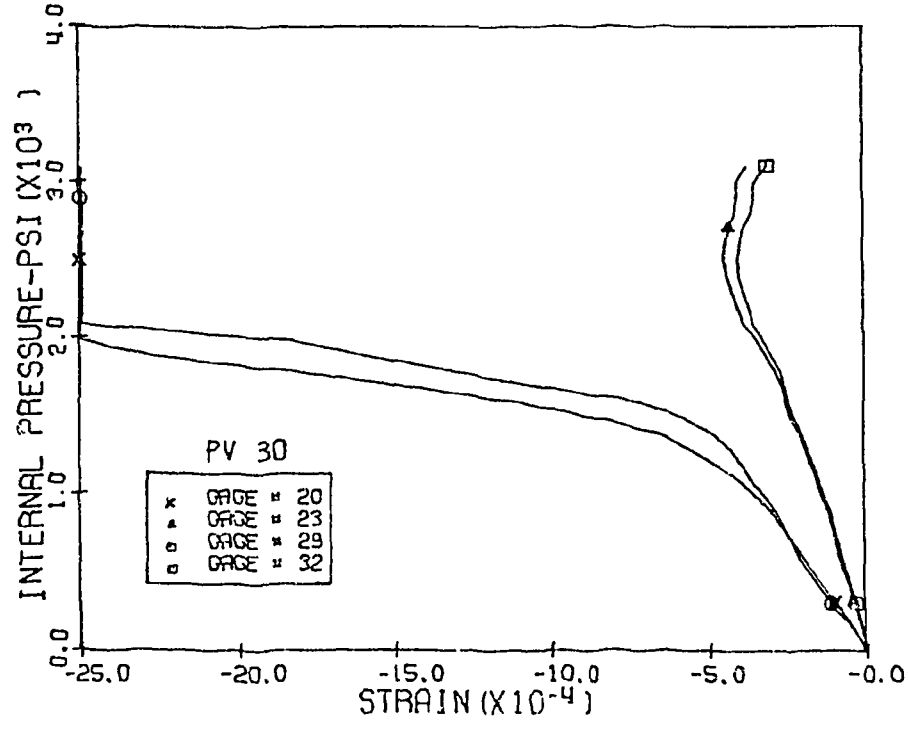

Fig. 5.15 Measured Horizontal Strains, Levels 1 and 2 Penetration 2, PV30

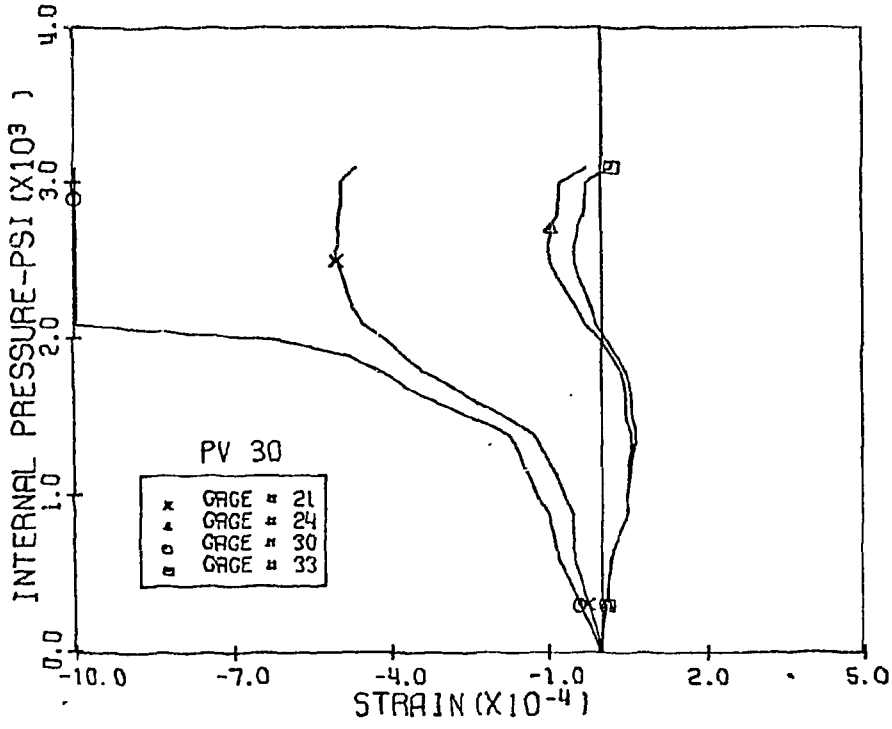

Fig. 5.16 Measured Diagonal Strains, Levels 1 and 2 Penetration 2, PV30

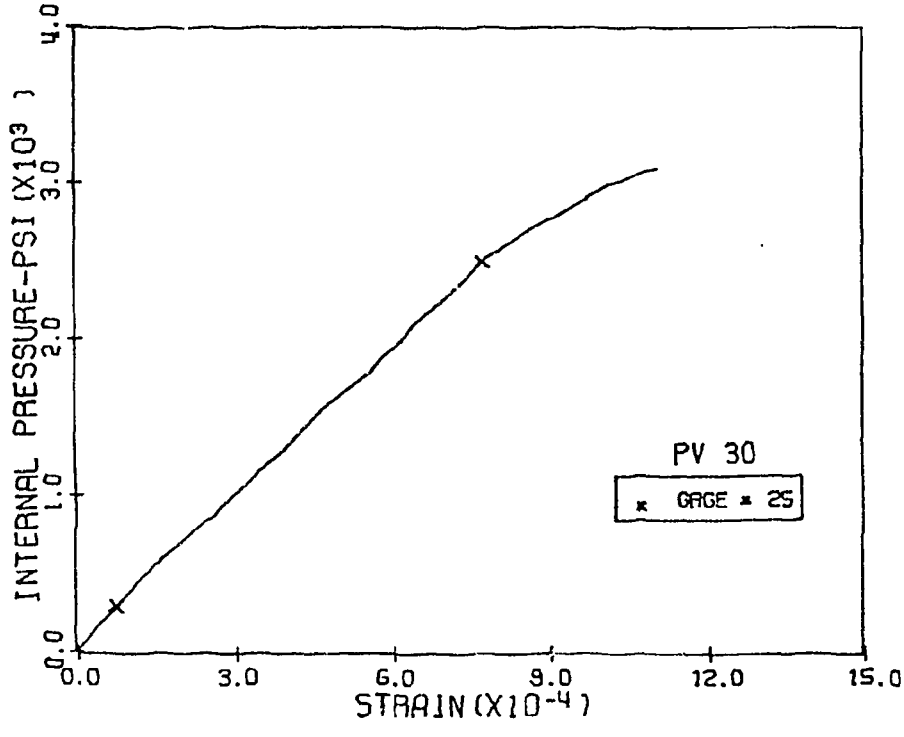

Fig. 5.17 Measured Vertical Strain, Level 3 Penetration 2, PV30

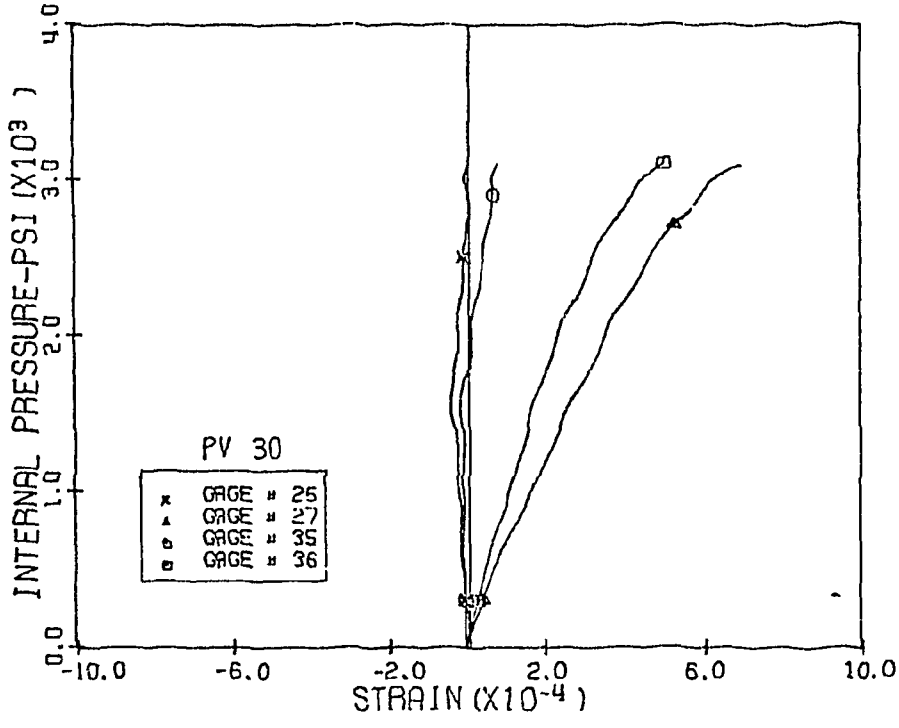

Fig. 5.18 Measured Horizontal and Diagonal Strains Level 3, Penetration 2, PV30

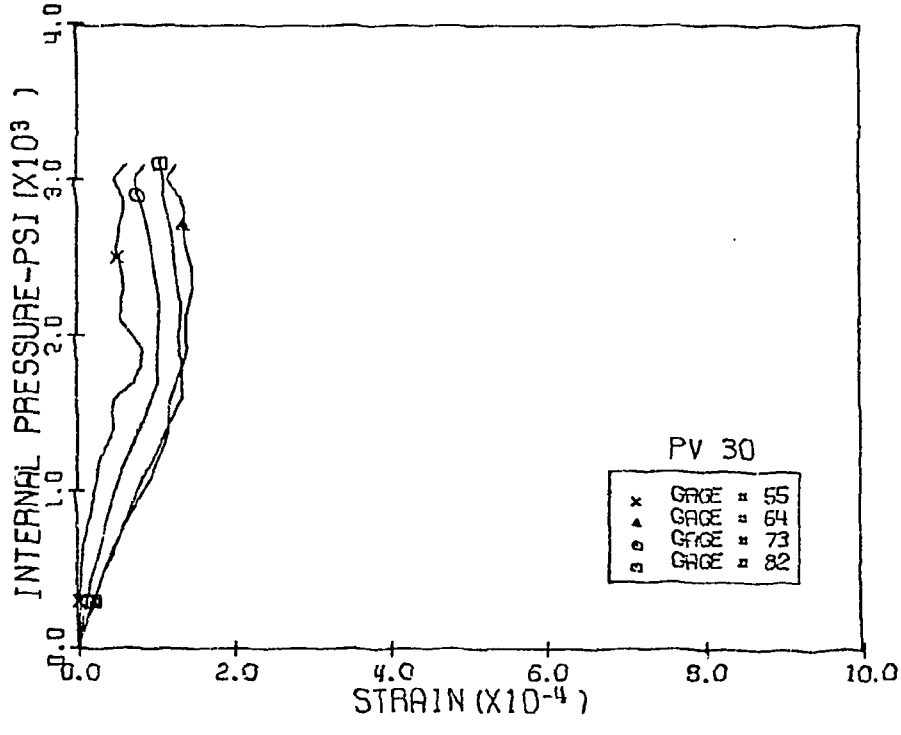

Fig. 5.19 Measured Vertical Strains, Level 1 Penetrations 4 and 5, PV30

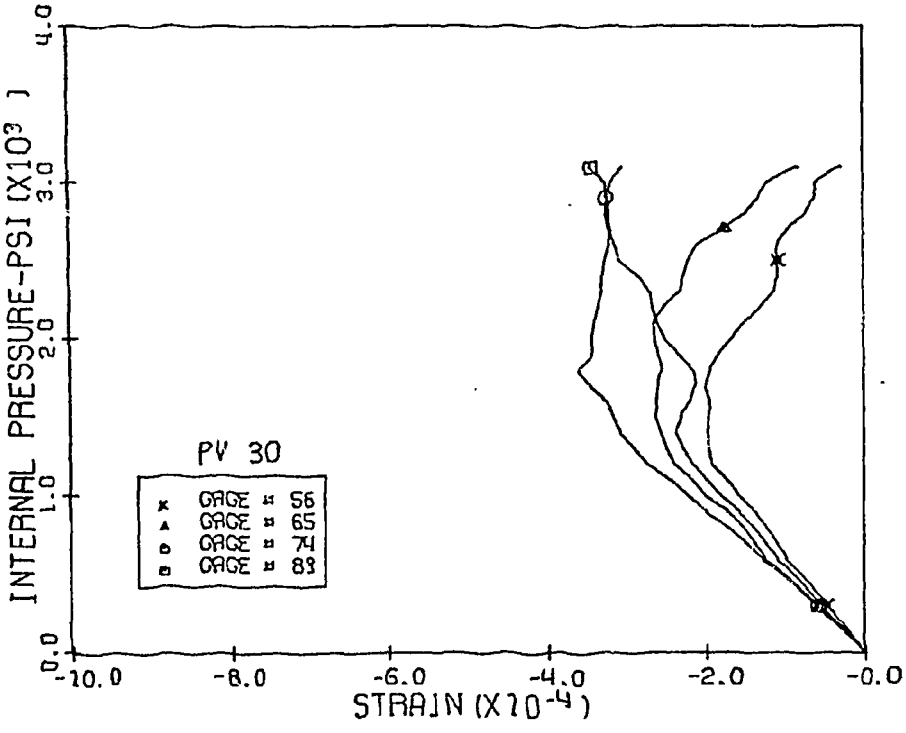

Fig. 5.20 Measured Horizontal Strains, Level 1 Penetrations 4 and 5, PV30

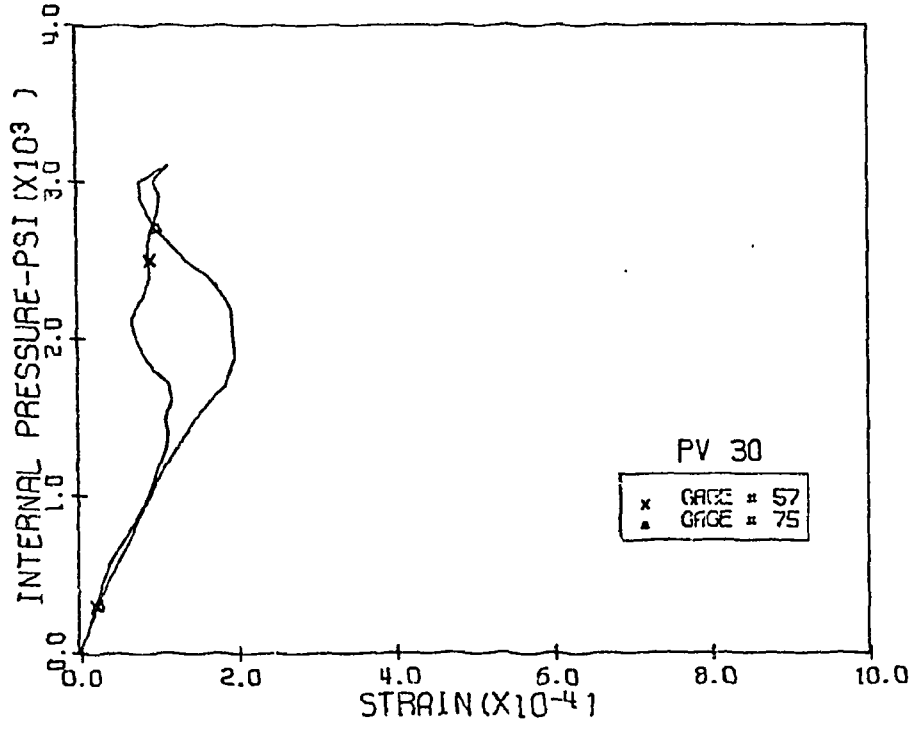

Fig. 5.21 Measured Compression Diagonal Strains, Level 1 Penetrations 4 and 5, PV30

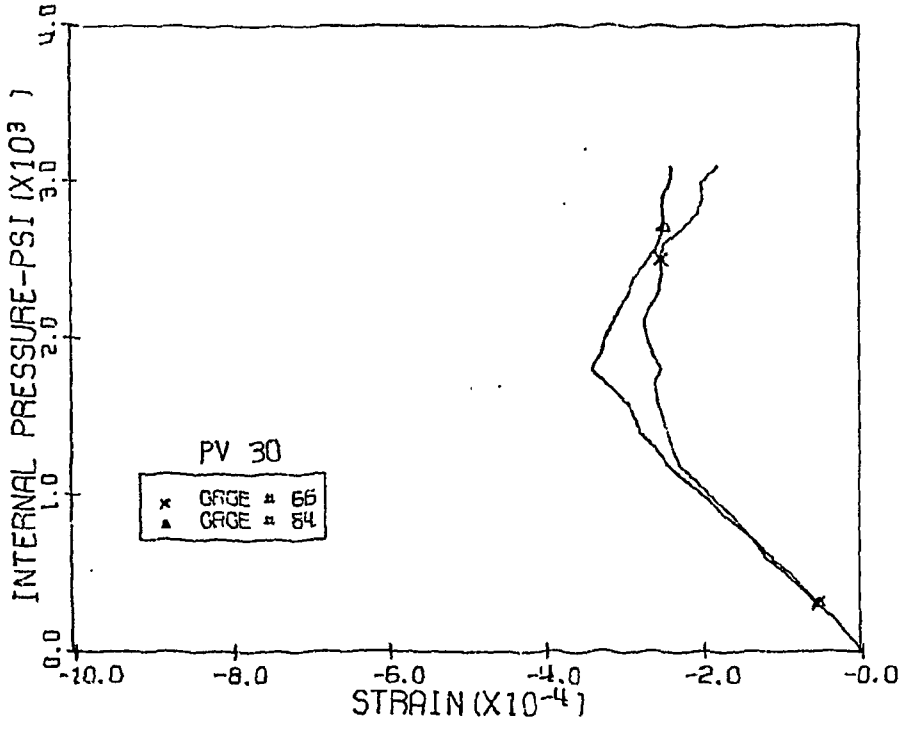

Fig. 5.22 Measured Tension Diagonal Strains, Level 1
Penetrations 4 and 5, PV30

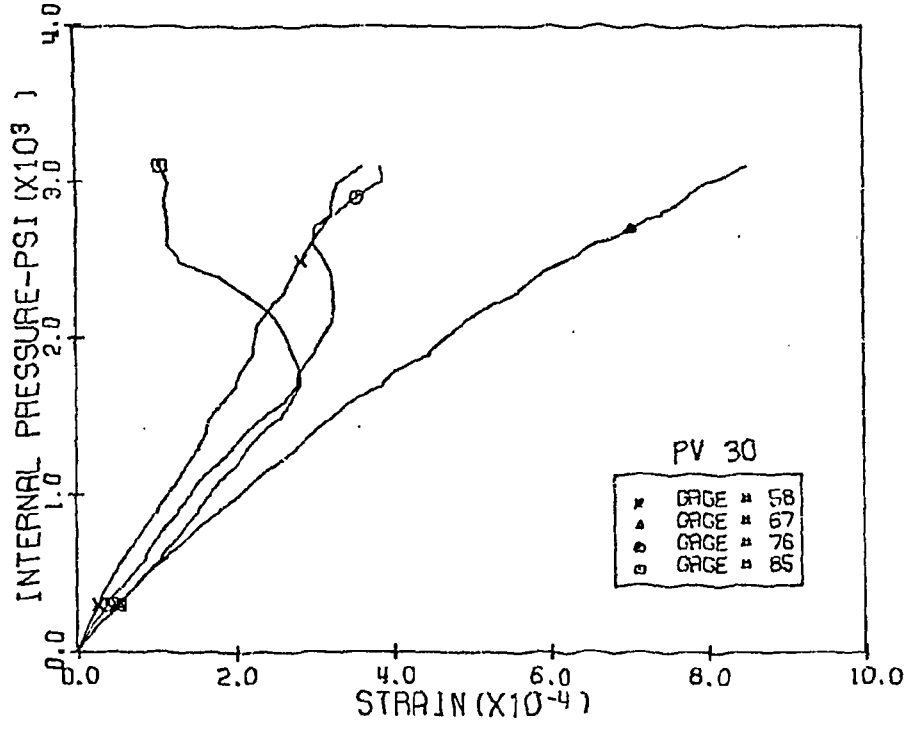

Fig. 5.23 Measured Vertical Strains, Level 2
Penetrations 4 and 5, PV30

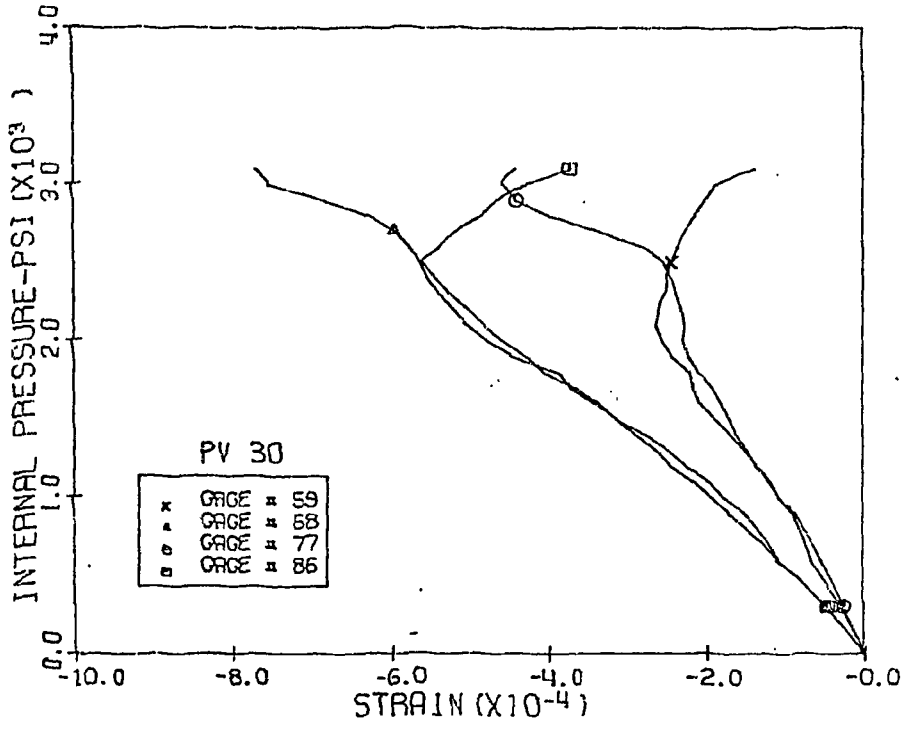

Fig. 5.24 Measured Horizontal Strains, Level 2 Penetrations 4 and 5, PV30

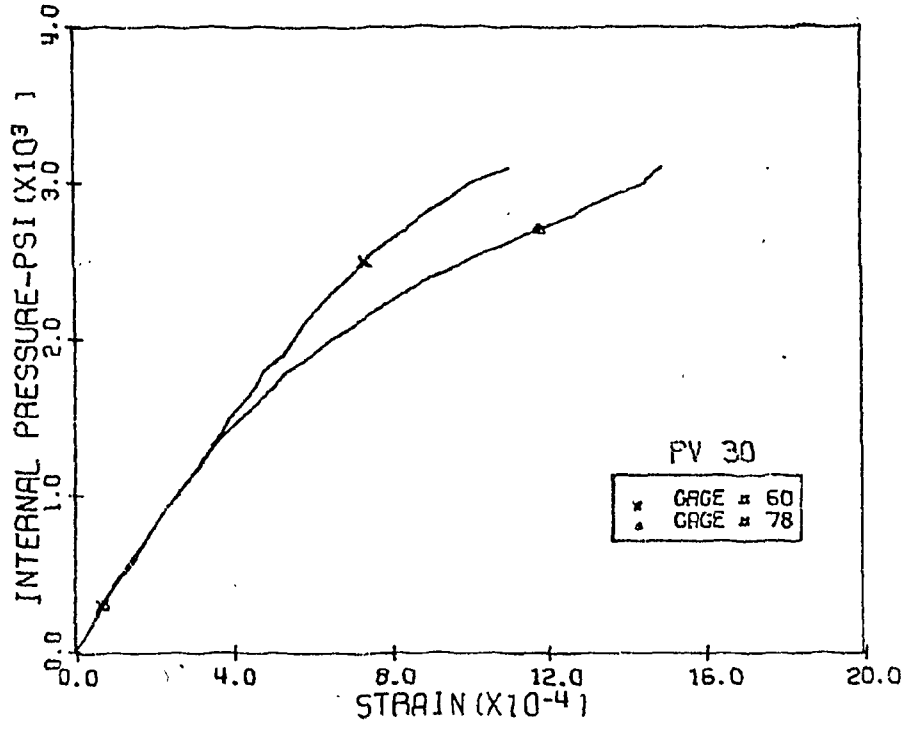

Fig. 5.25 Measured Compression Diagonal Strains, Level 2 Penetrations 4 and 5, PV30

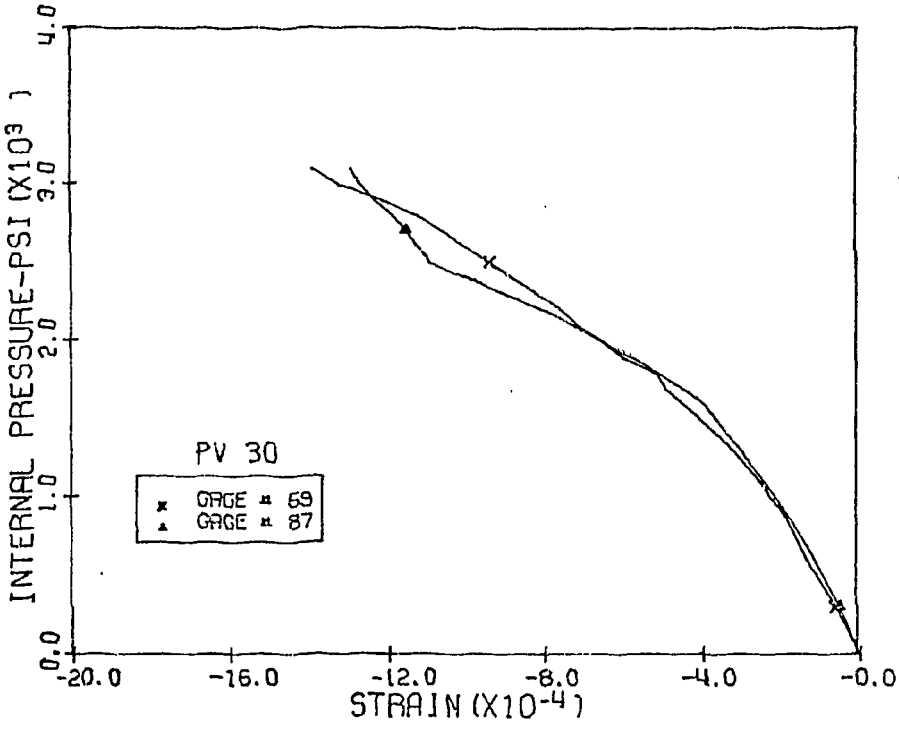

Fig. 5.26 Measured Tension Diagonal Strains, Level 2 Penetrations 4 and 5, PV30

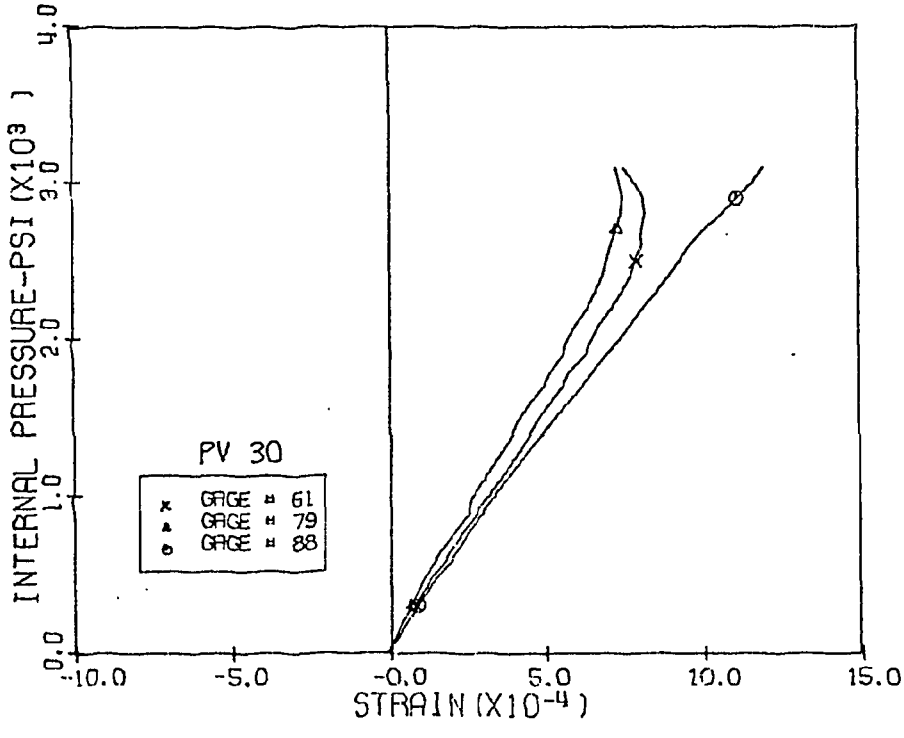

Fig. 5.27 Measured Vertical Strains, Level 3 Penetrations 4 and 5, PV30

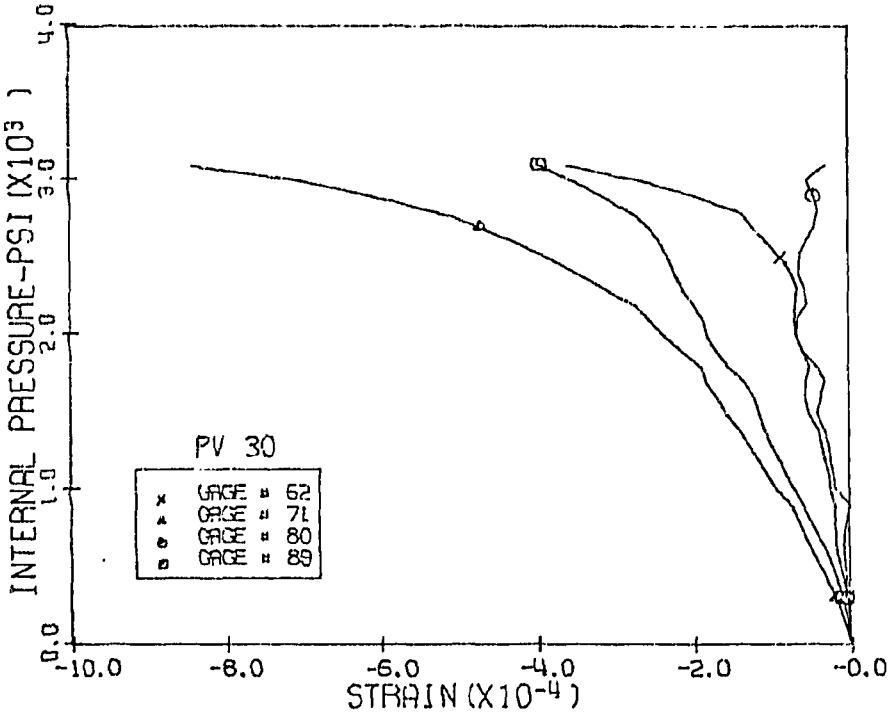

Fig. 5.28 Measured Horizontal Strains, Level 3 Penetrations 4 and 5, PV30

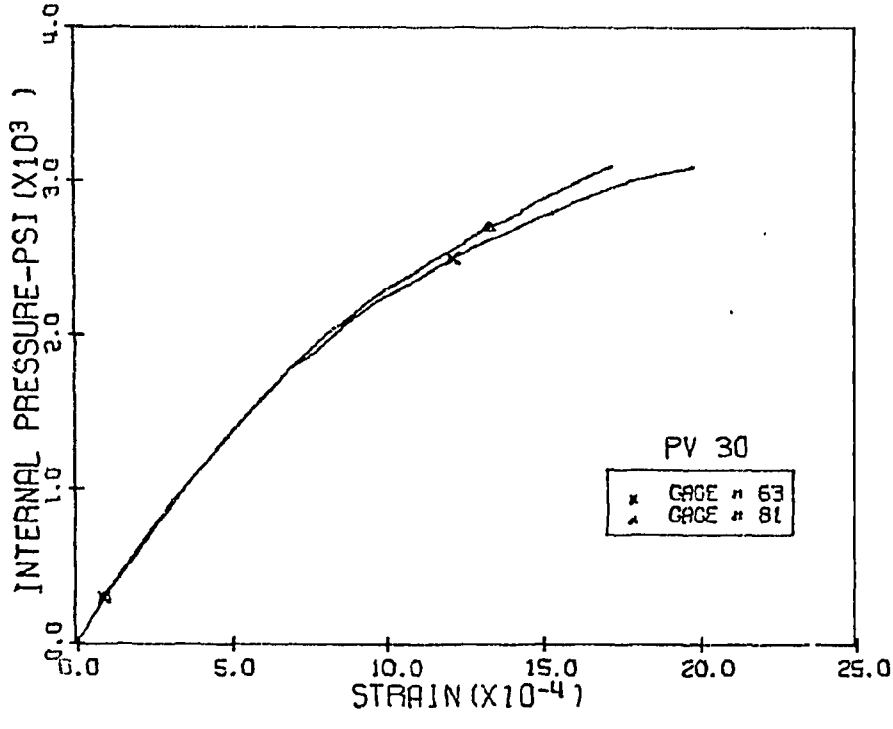

Fig. 5.29 Measured Compression Diagonal Strains, Level 3 Penetrations 4 and 5, PV30

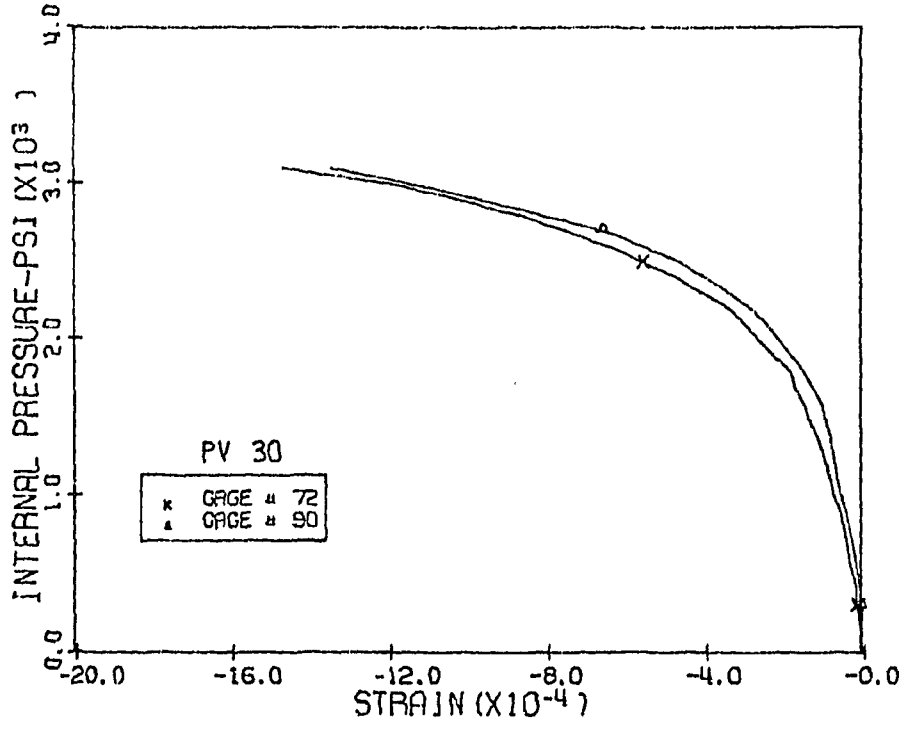

Fig. 5.30 Measured Tension Diagonal Strains, Level 3
Penetrations 4 and 5, PV30

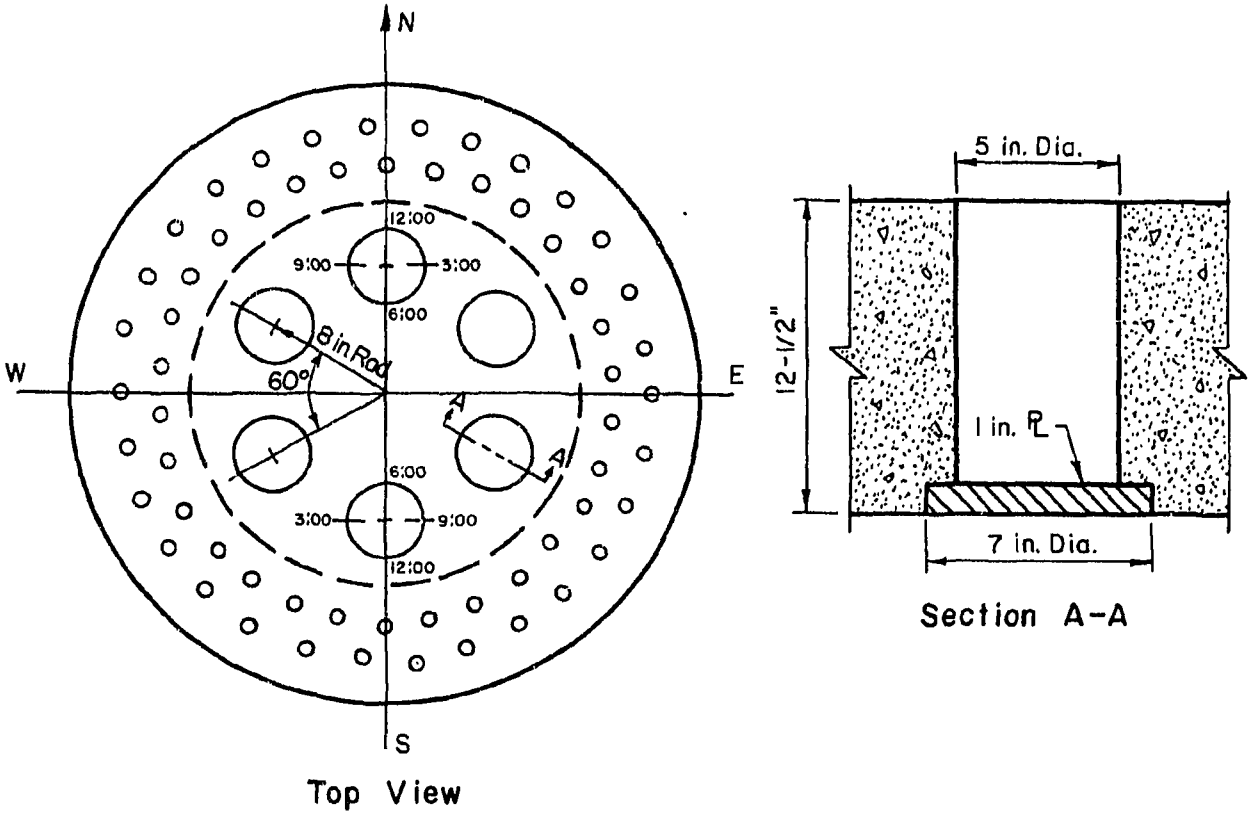

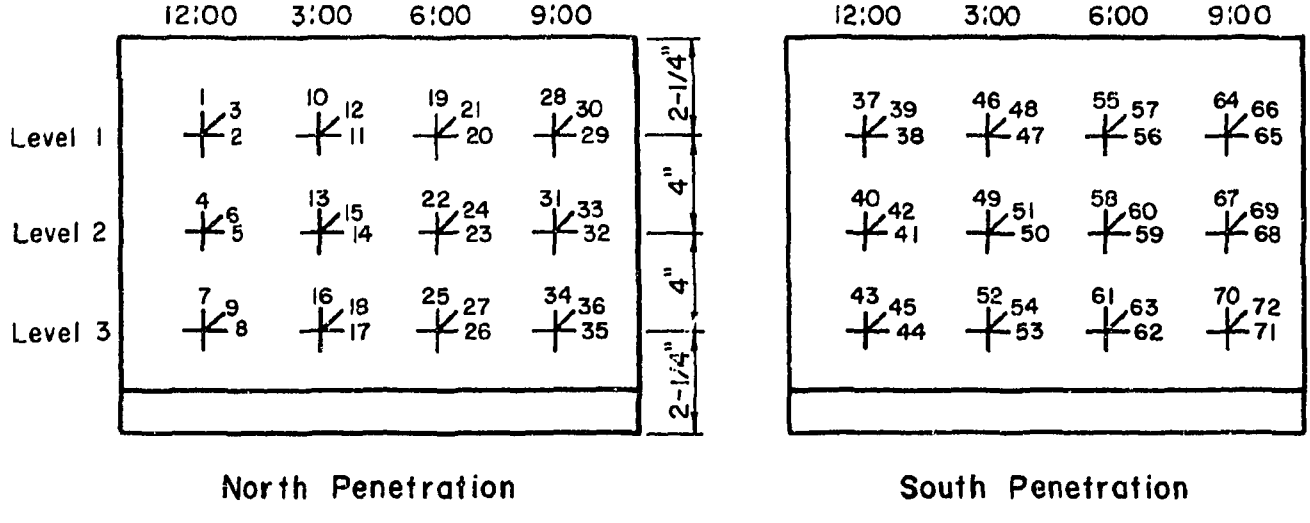

Fig. 5.31a Location of Strain Gages in End Slab with 5-in. Penetrations

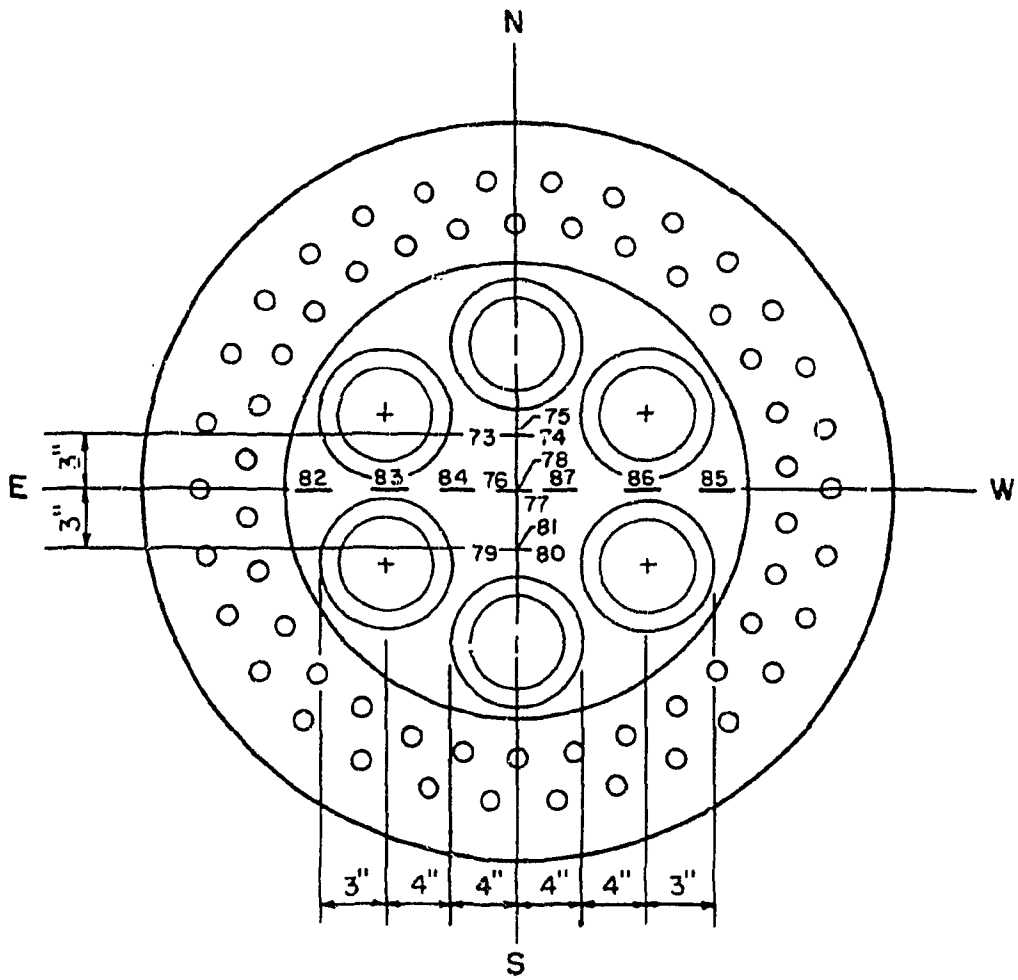

Fig. 5.31b Location of Strain Gages on Inside Face of End Slab with 5-in. Penetrations

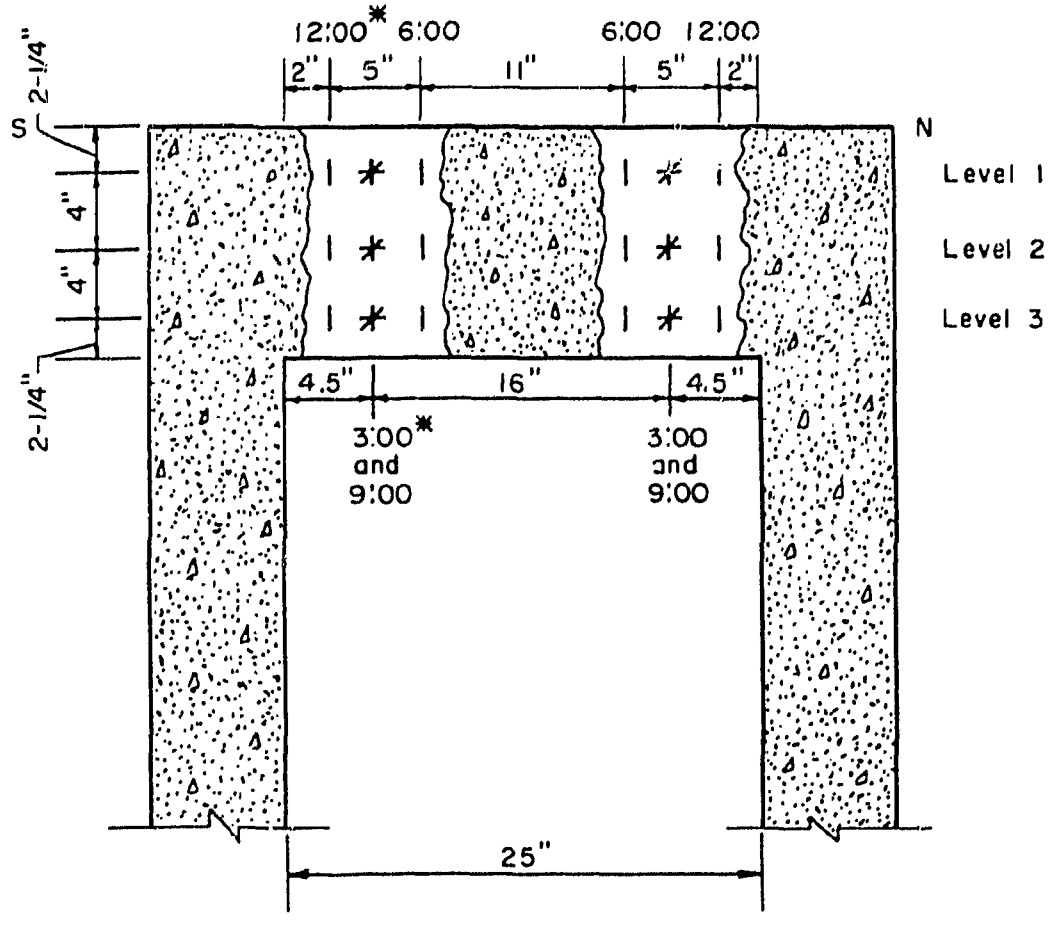

Fig. 5.31c Location of Strain Rosettes in the Vertical Plane (*Numerals designating location in plan. See Fig. 5.31a)

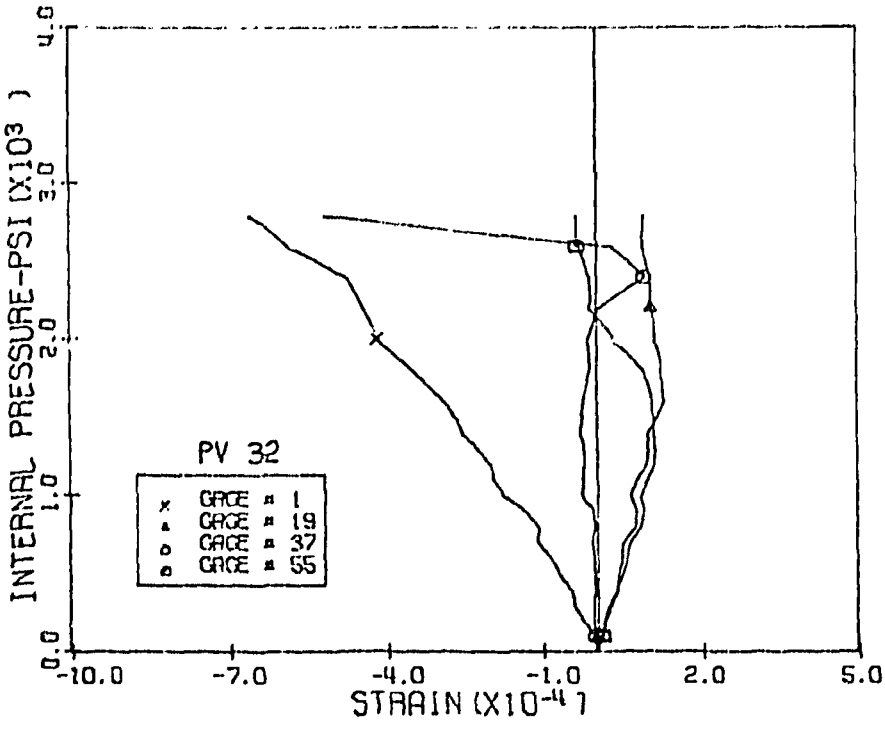

Fig. 5.32 Measured Vertical Strains, Level 1 12:00 and 6:00 Positions, PV32

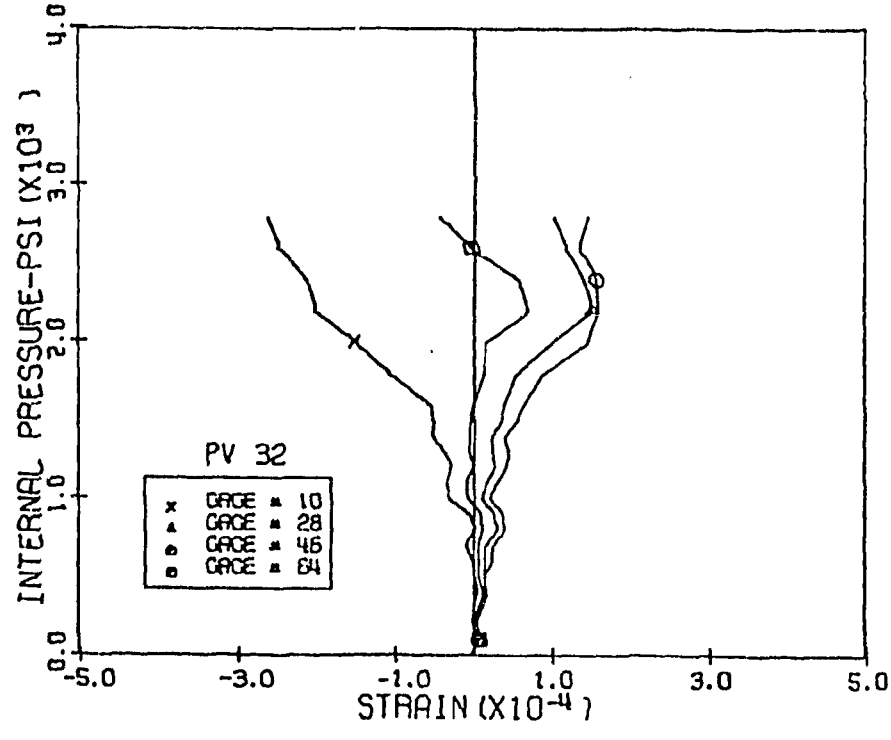

Fig. 5.33 Measured Vertical Strains, Level 1 3:00 and 9:00 Positions, PV32

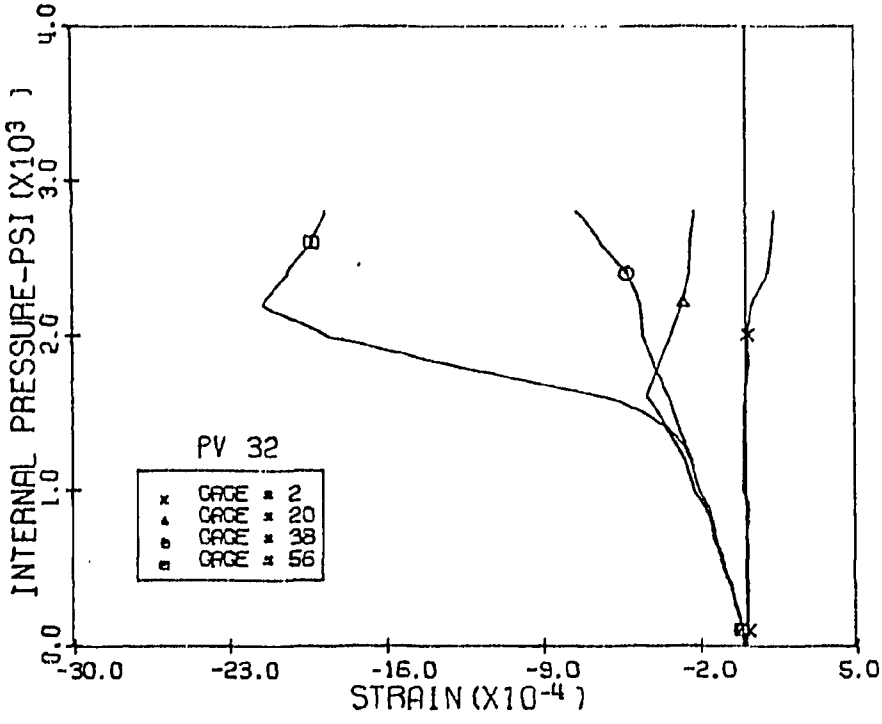

Fig. 5.34 Measured Horizontal Strains, Level 1 12:00 and 6:00 Positions, PV32

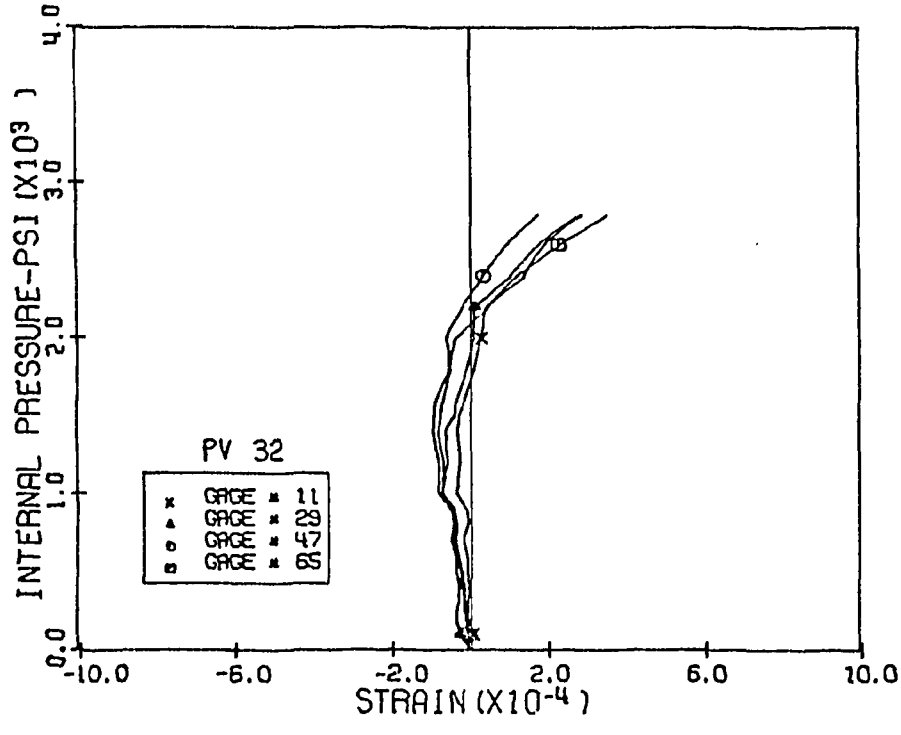

Fig. 5.35 Measured Horizontal Strains, Level 1 3:00 and 9:00 Positions, PV32

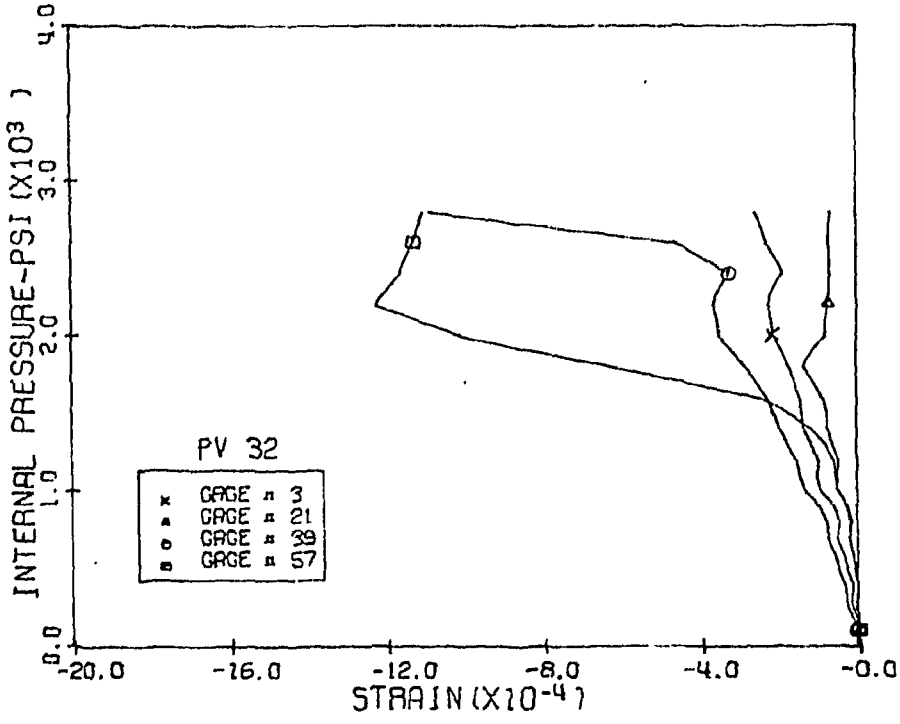

Fig. 5.36 Measured Diagonal Strains, Level 1 12:00 and 6:00 Positions, PV32.

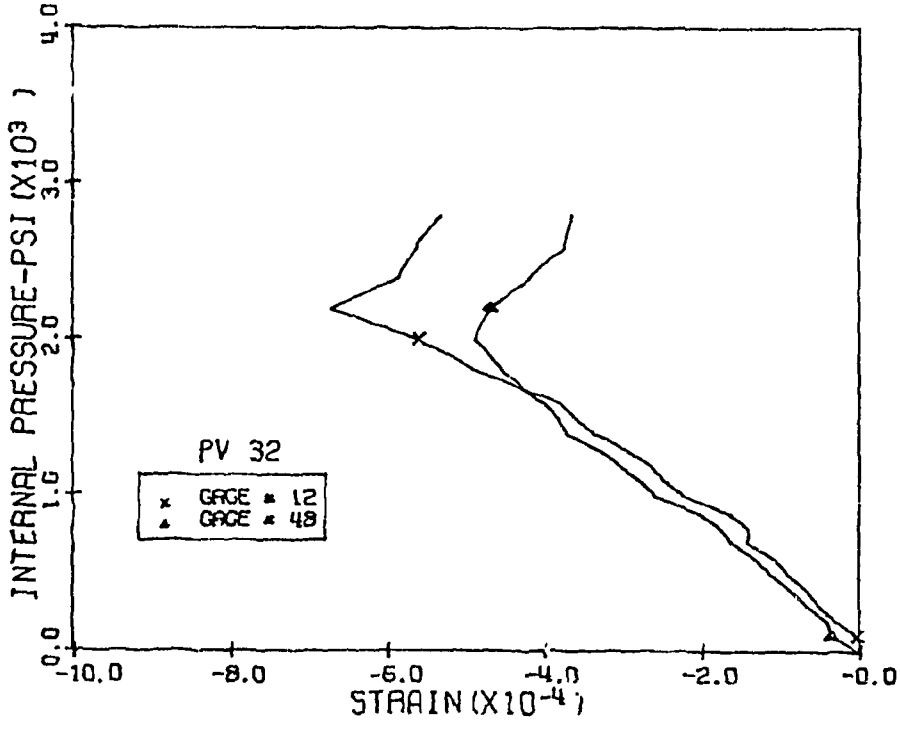

Fig. 5.37 Measured Tension Diagonal Strains, Level 1 3:00 Position, PV32

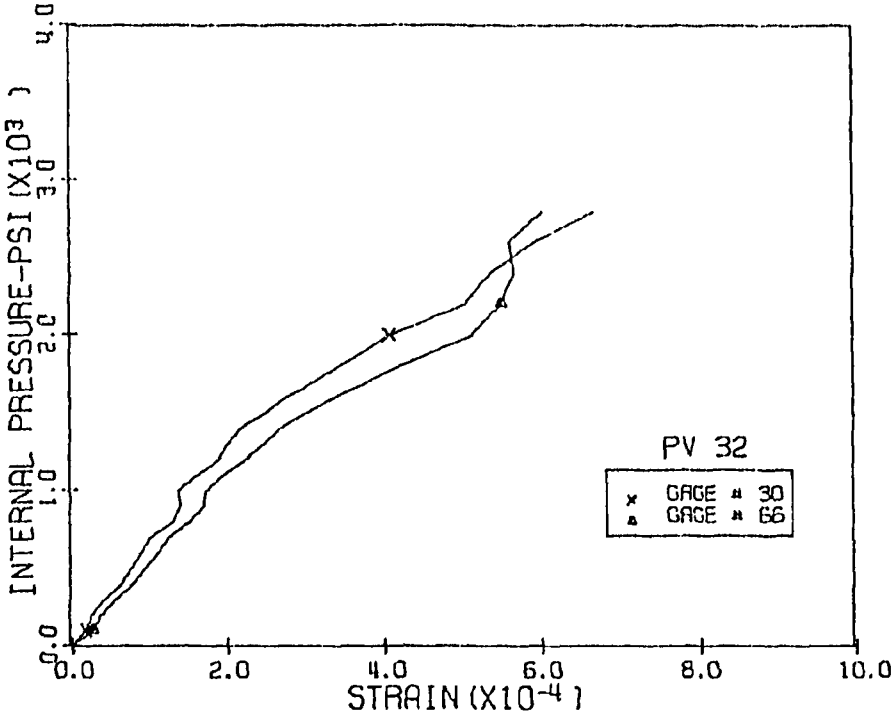

Fig. 5.38 Measured Compression Diagonal Strains, Level 1 9:00 Position, PV32

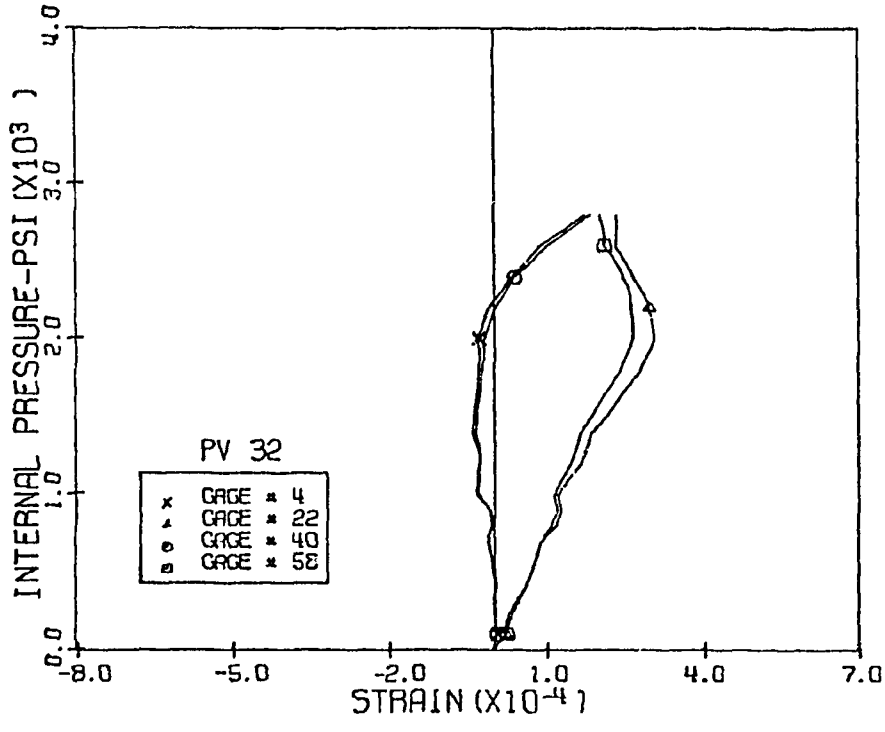

Fig. 5.39 Measured Vertical Strains, Level 2 12:00 and 6:00 Positions, PV32

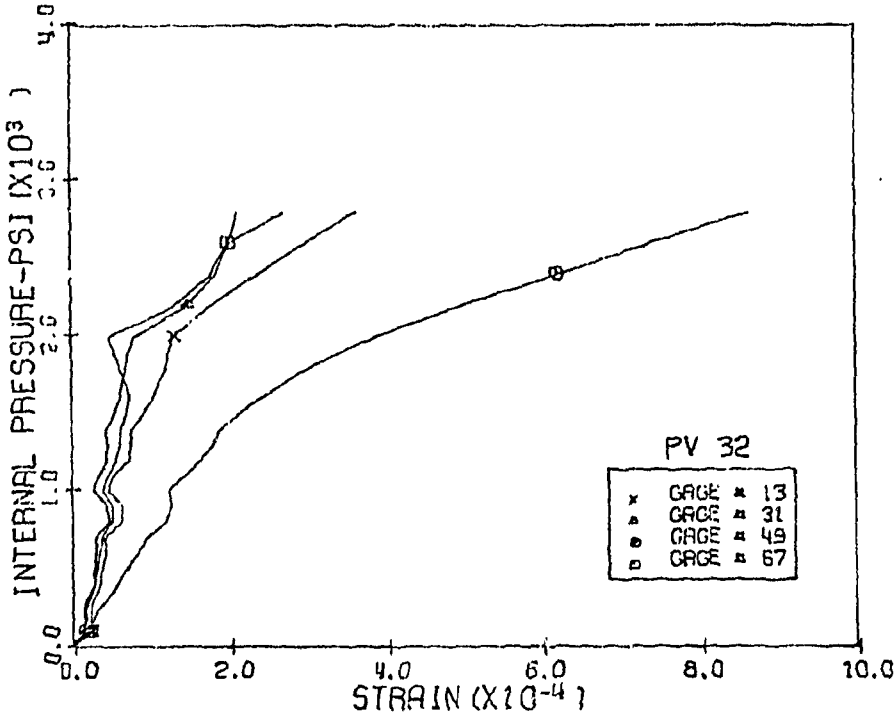

Fig. 5.40 Measured Vertical Strains, Level 2 3:00 and 9:00 Positions, PV32

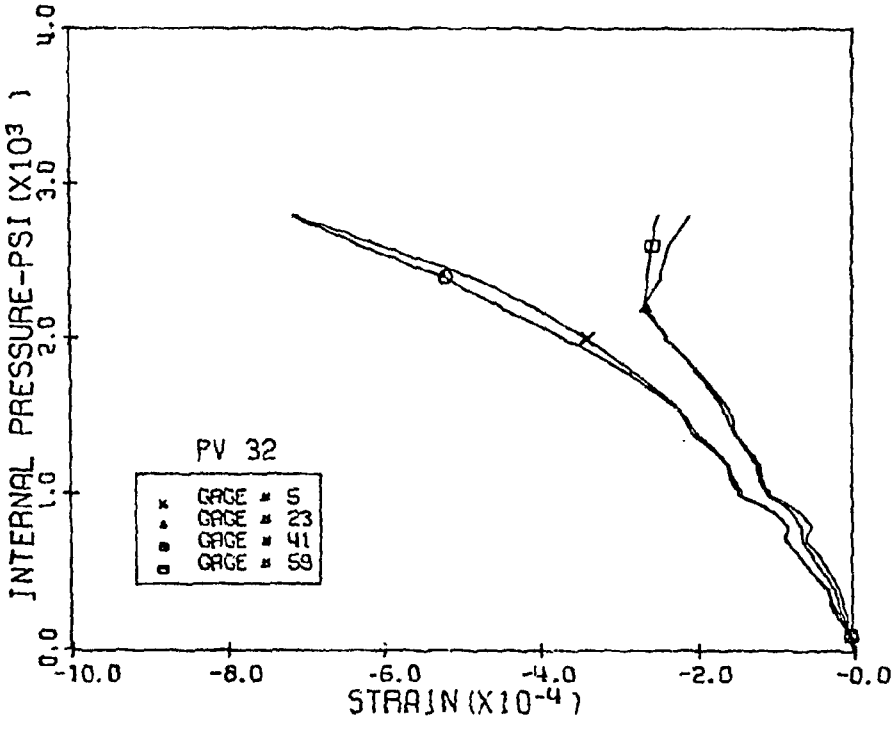

Fig. 5.41 Measured Horizontal Strains, Level 2 12:00 and 6:00 Positions, PV32

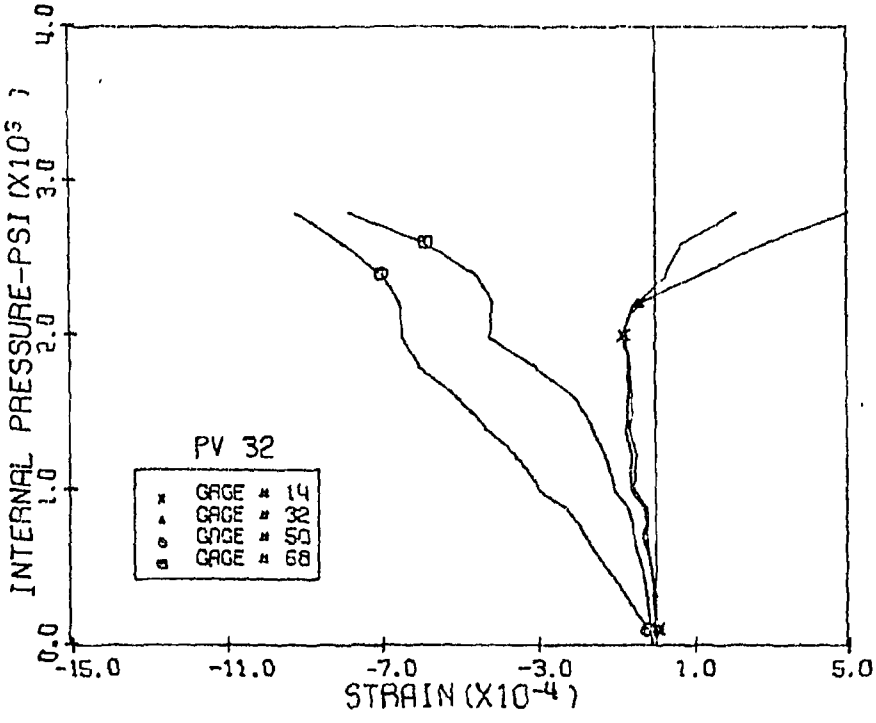

Fig. 5.42 Measured Horizontal Strains, Level 2 3:00 and 9:00 Positions, PV32

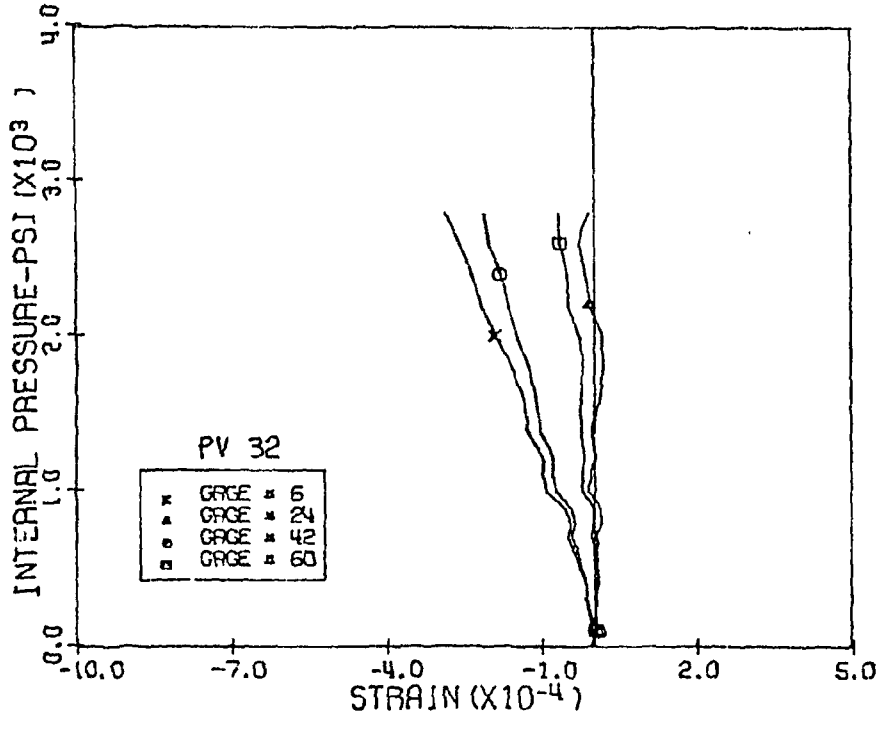

Fig. 5.43 Measured Diagonal Strains, Level 2 12:00 and 6:00 Positions, PV32

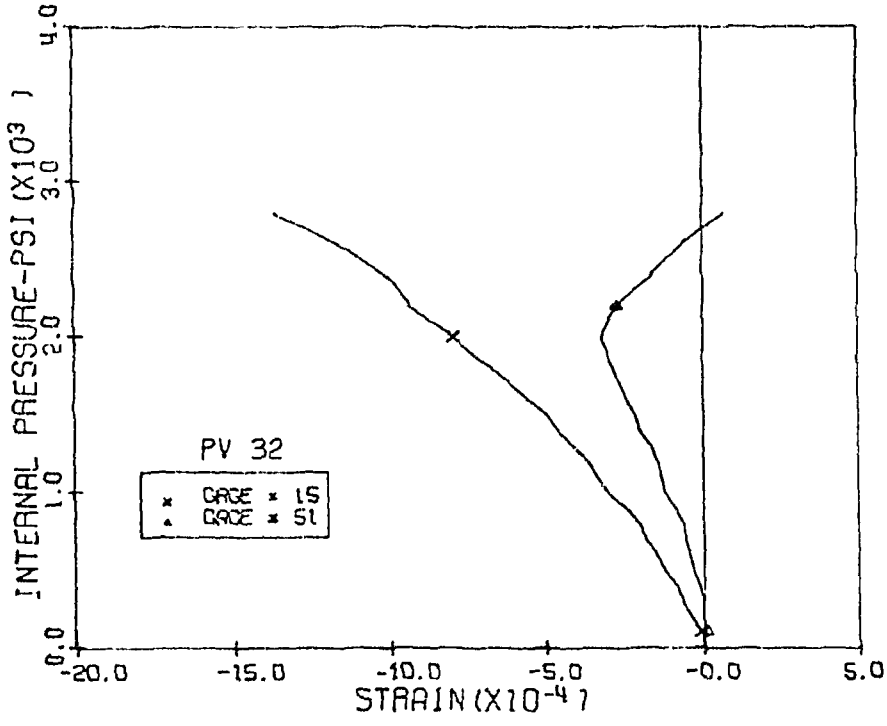

Fig. 5.44 Measured Tension Diagonal Strains, Level 2
3:00 Position, PV32

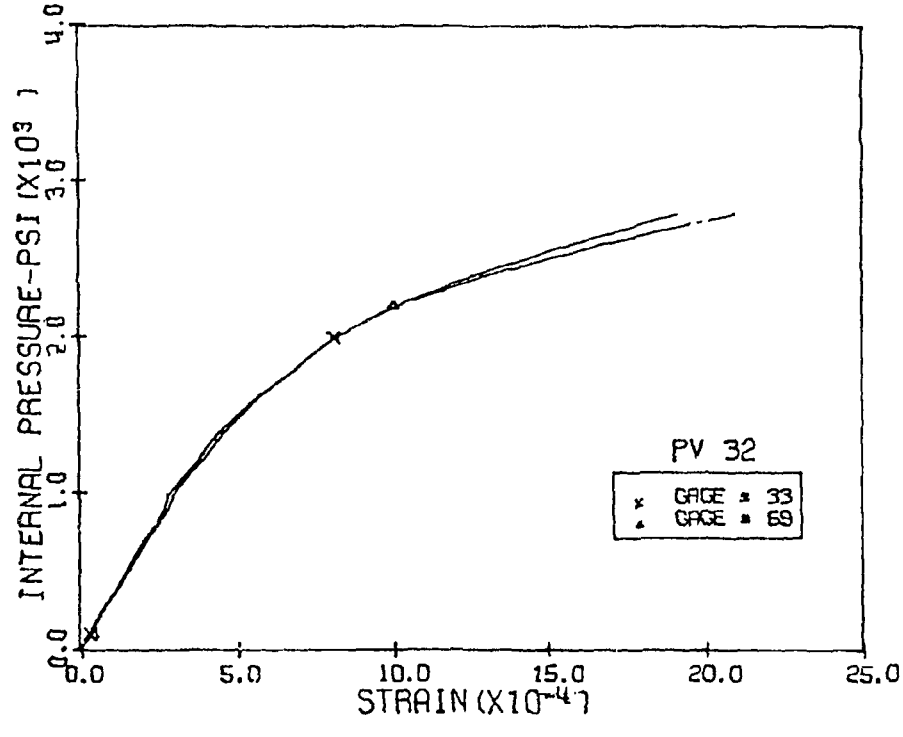

Fig. 5.45 Measured Compression Diagonal Strains, Level 2
9:00 Position, PV32

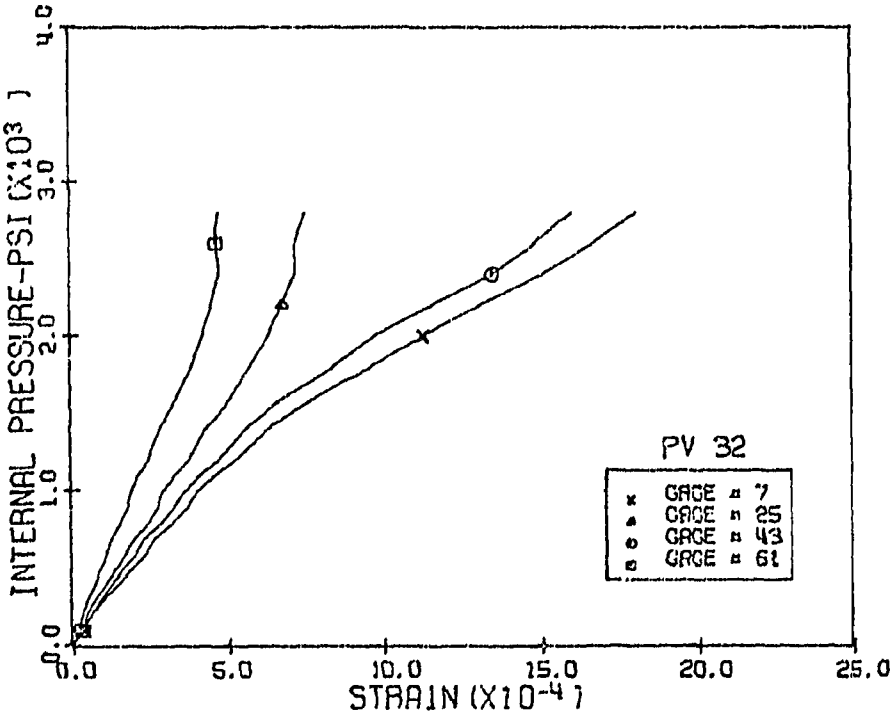

Fig. 5.46 Measured Vertical Strains, Level 3 12:00 and 6:00 Positions, PV32

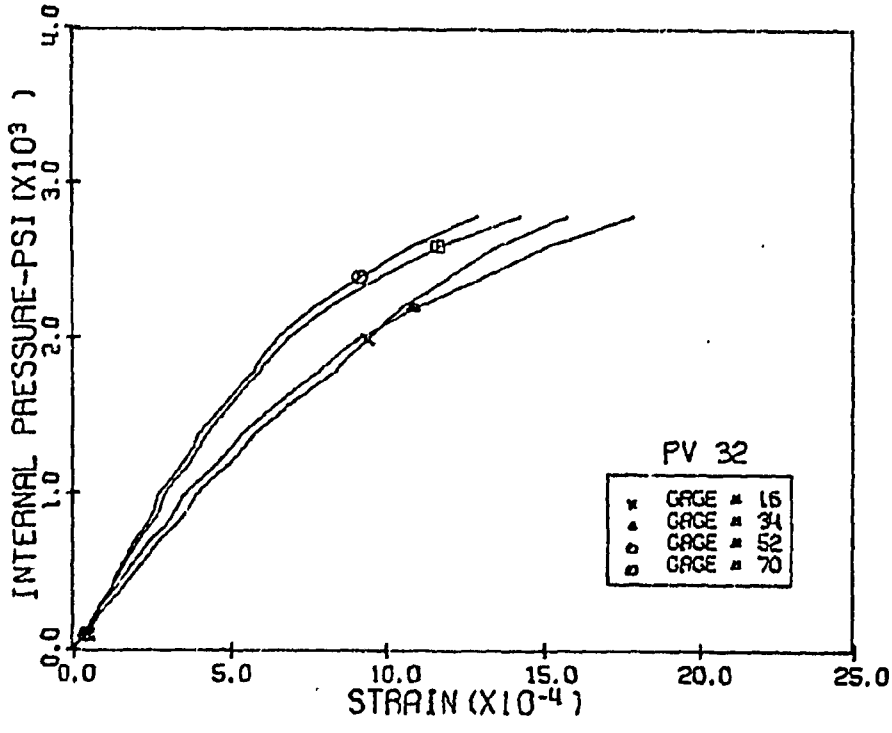

Fig. 5.47 Measured Vertical Strains, Level 3 3:00 and 9:00 Positions, PV32

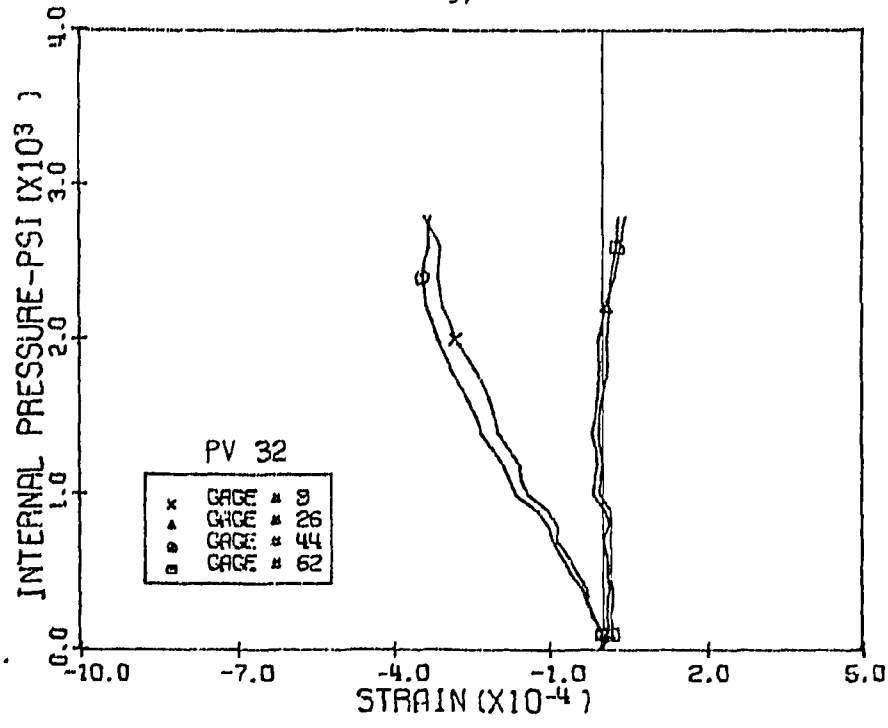

Fig. 5.48 Measured Horizontal Strains, Level 3 12:00 and 6:00 Positions, PV32

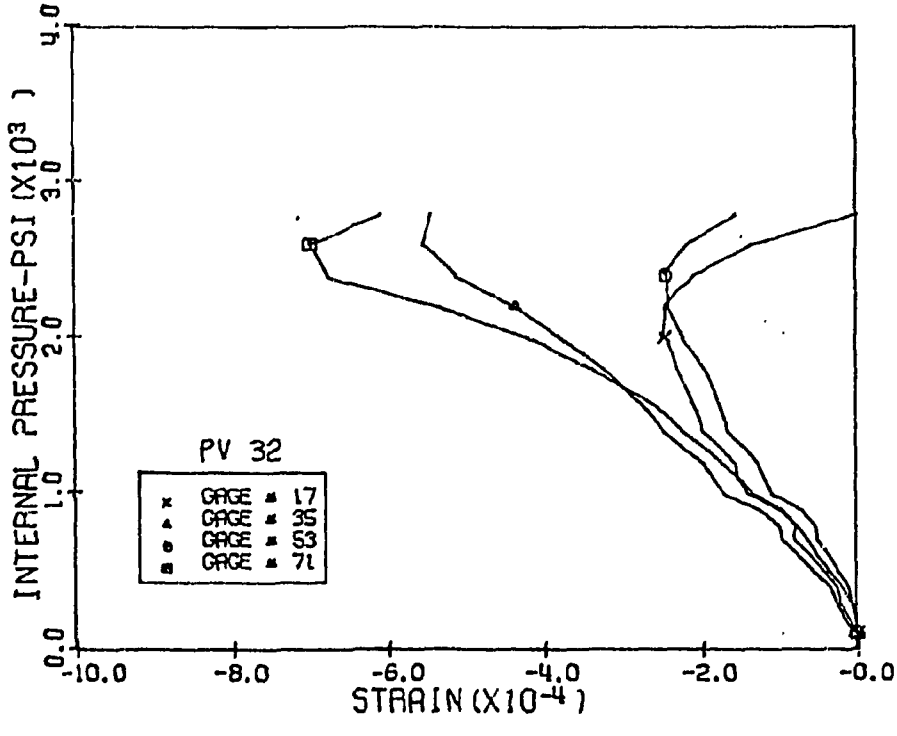

Fig. 5.49 Measured Horizontal Strains, Level 3 3:00 and 9:00 Positions, PV32

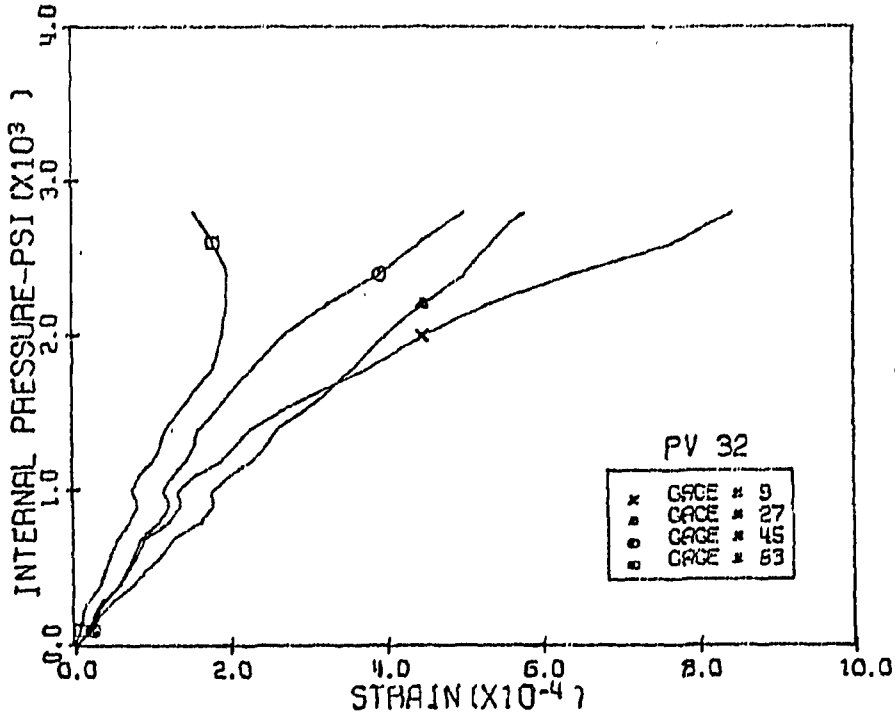

Fig. 5.50 Measured Diagonal Strains, Level 3 12:00 and 6:00 Positions, PV32

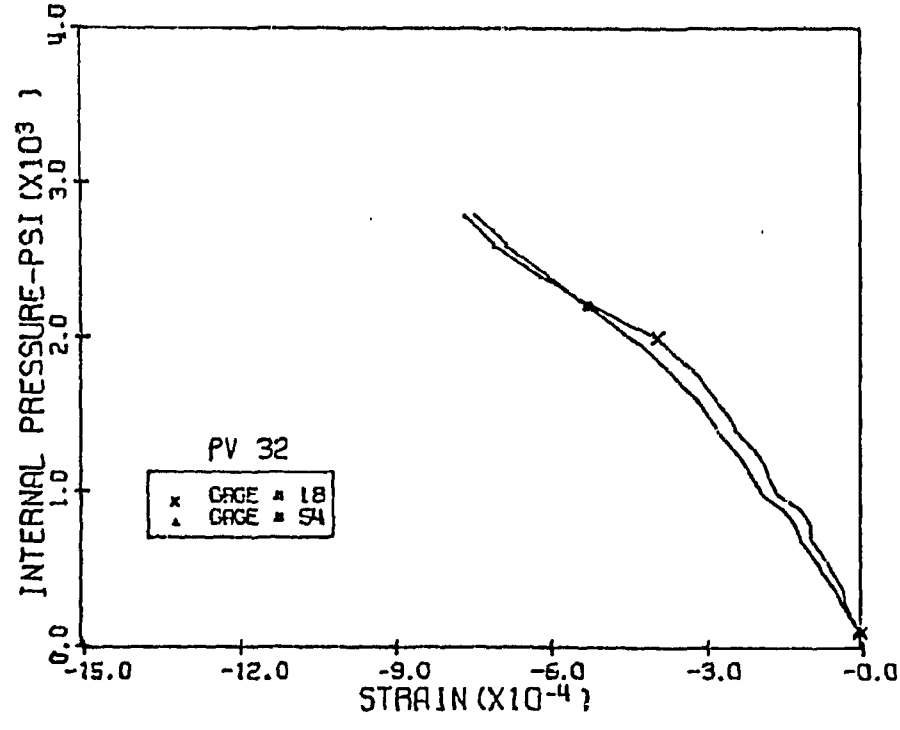

Fig. 5.51 Measured Tension Diagonal Strains, Level 3 3:00 Position, PV32

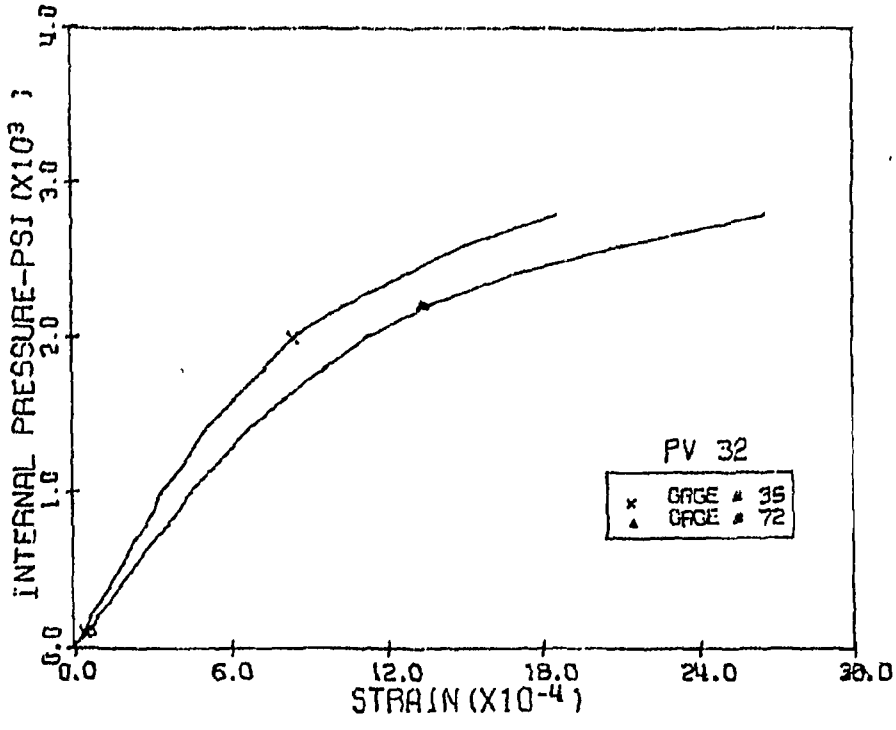

Fig. 5.52 Measured Compression Diagonal Strains, Level 3
9:00 Position, PV32

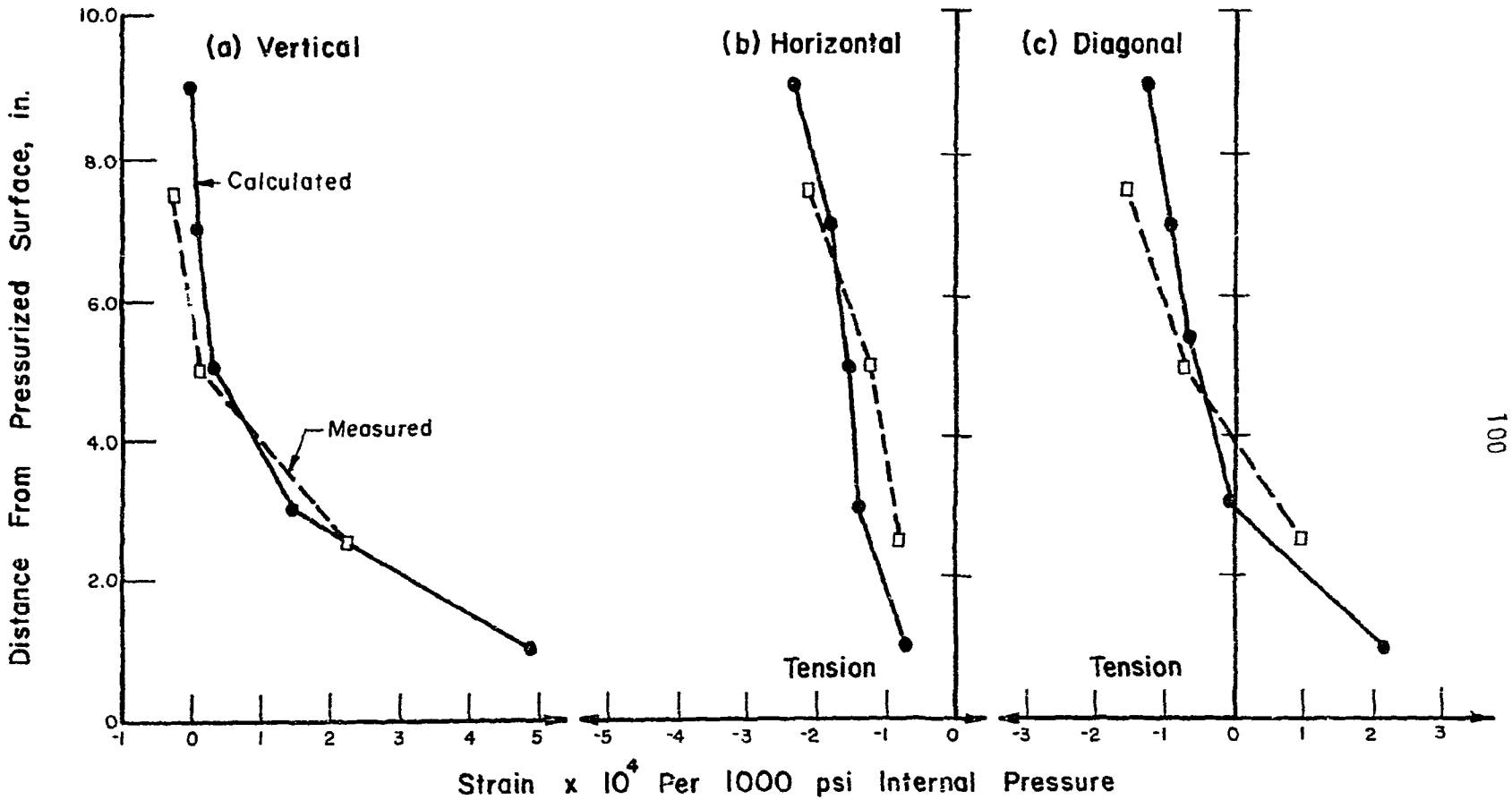

Fig. 5.53 Comparison of Measured and Calculated Strains at an Internal Pressure of 1000-psi for a 10.0-in. End Slab. Strains at 12:00 Position (See Fig. 5.31a)

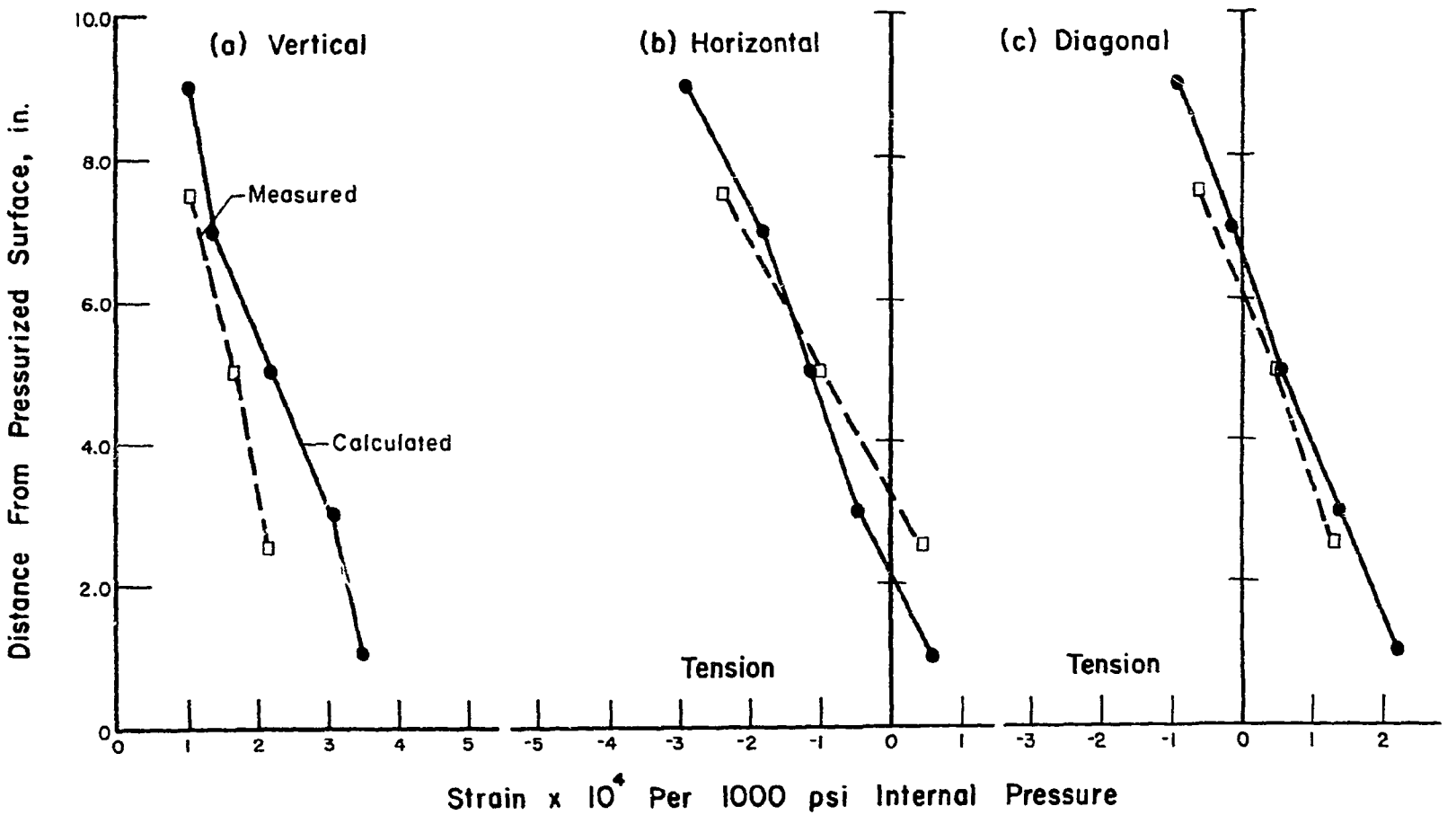

Fig. 5.54 Comparison of Measured and Calculated Strains at an Internal Pressure of 1000-psi for a 10.0-in. End Slab. Strains at 6:00 Position (See Fig. 5.31a)

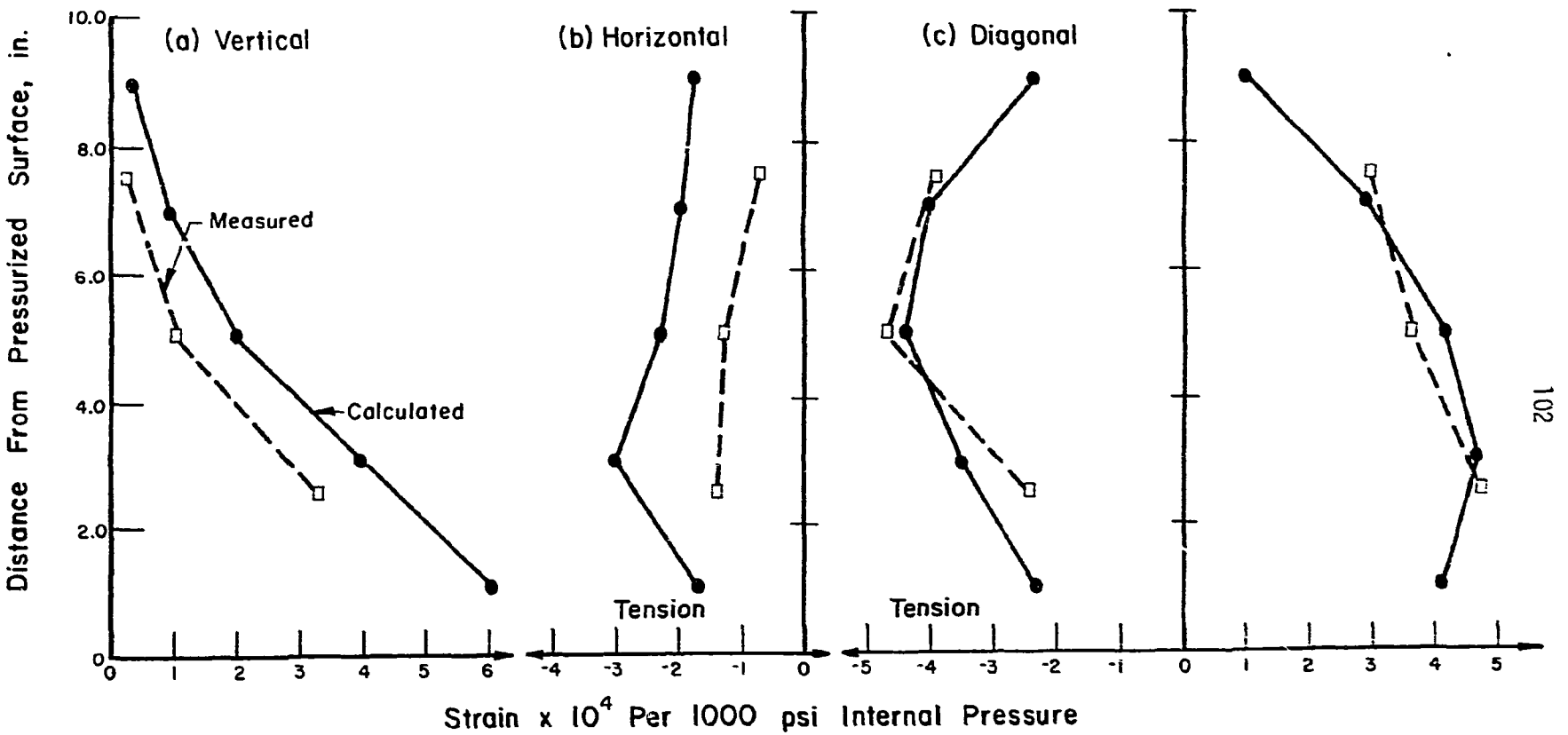

Fig. 5.55 Comparison of Measured and Calculated Strains at an Internal Pressure of 1000-psi for a 10.0-in. End Slab. Strains at 3:00 and 9:00 Positions (See Fig. 5.31a)

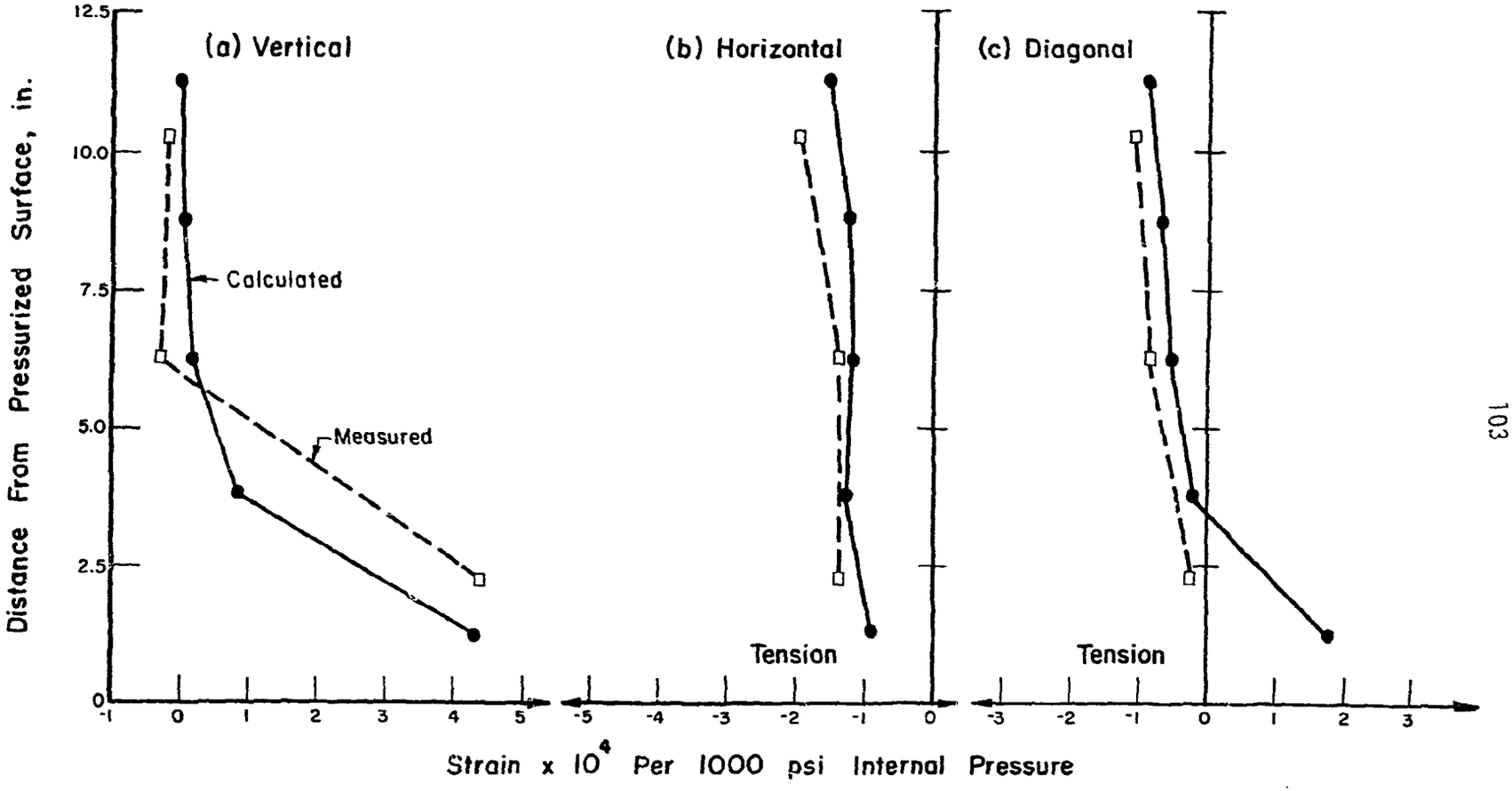

Fig. 5.56 Comparison of Measured and Calculated Strains at an Internal Pressure of 1000-psi for a 12.5-in. End Slab. Strains at 12:00 Position (See Fig. 5.31a)

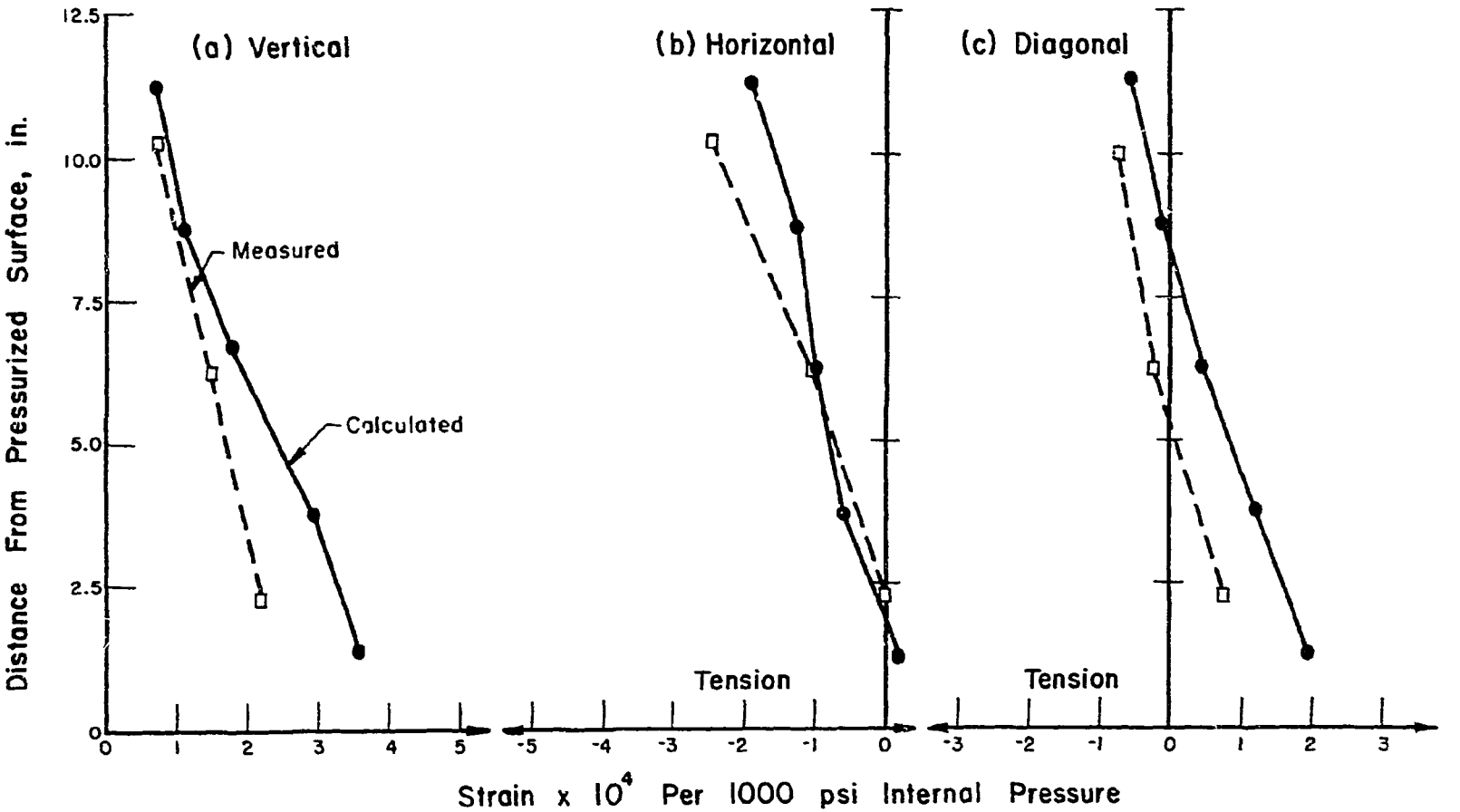

Fig. 5.57 Comparison of Measured and Calculated Strains at an Internal Pressure of 1000-psi for a 12.5-in. End Slab. Strains at 6:00 Position (See Fig. 5.31a)

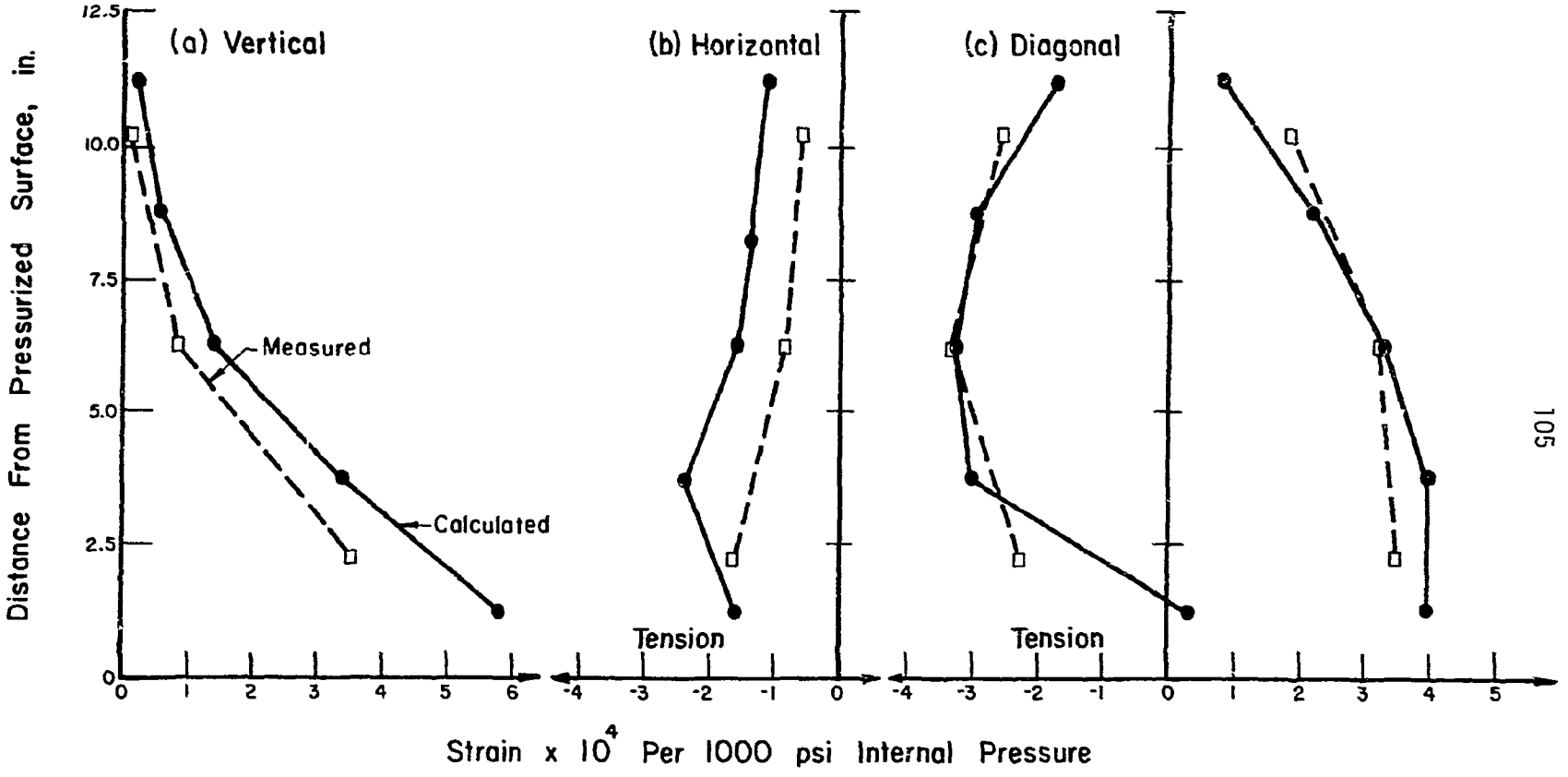

Fig. 5.58 Comparison of Measured and Calculated Strains at an Internal Pressure of 1000-psi for a 12.5-in. End Slab. Strains at 3:00 and 9:00 Positions (See Fig. 5.31a)

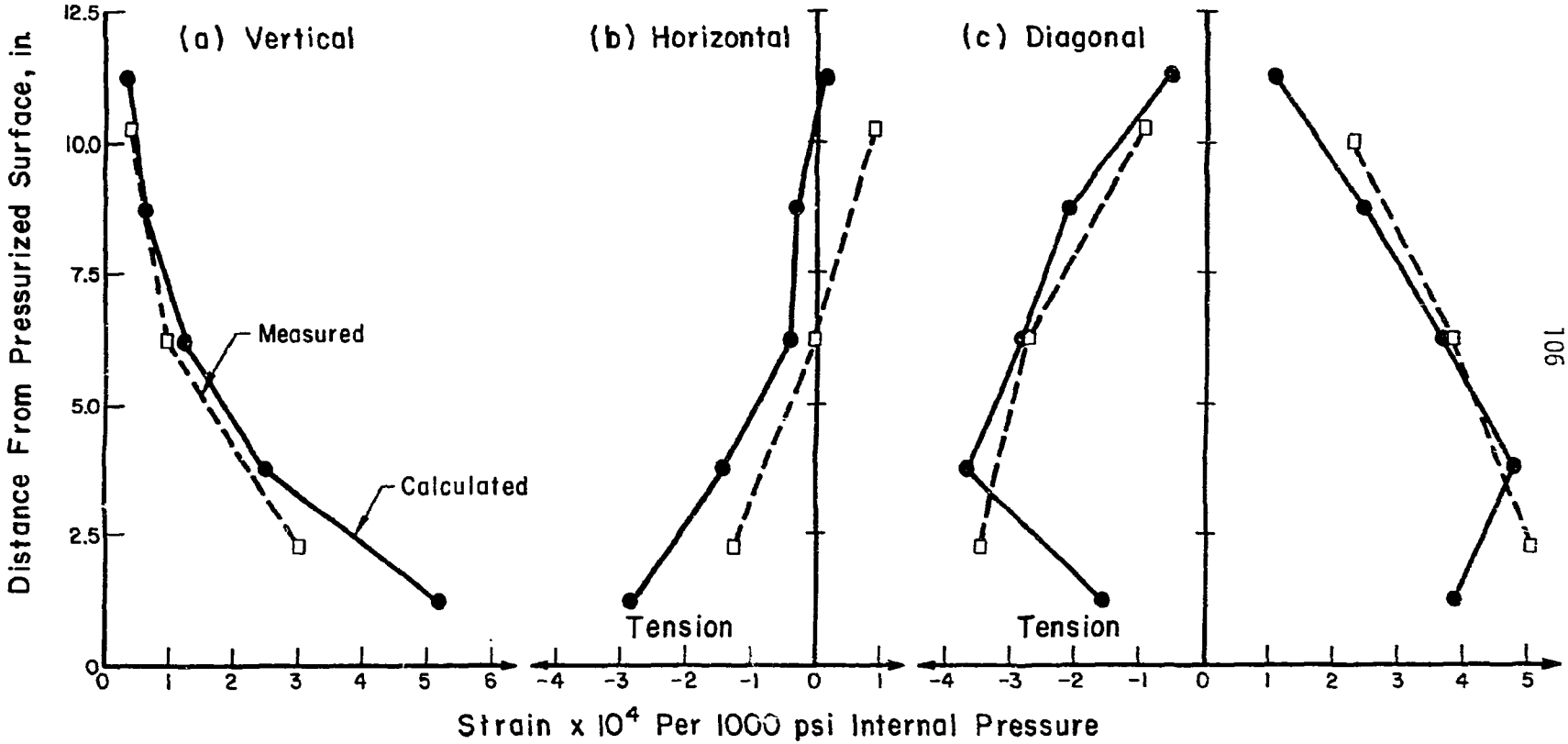

Fig. 5.59 Comparison of Measured and Calculated Strains at an Internal Pressure of 1000-psi for a 12.5-in. End Slab. Strains at Penetrations 1 and 3 (See Fig. 5.2)

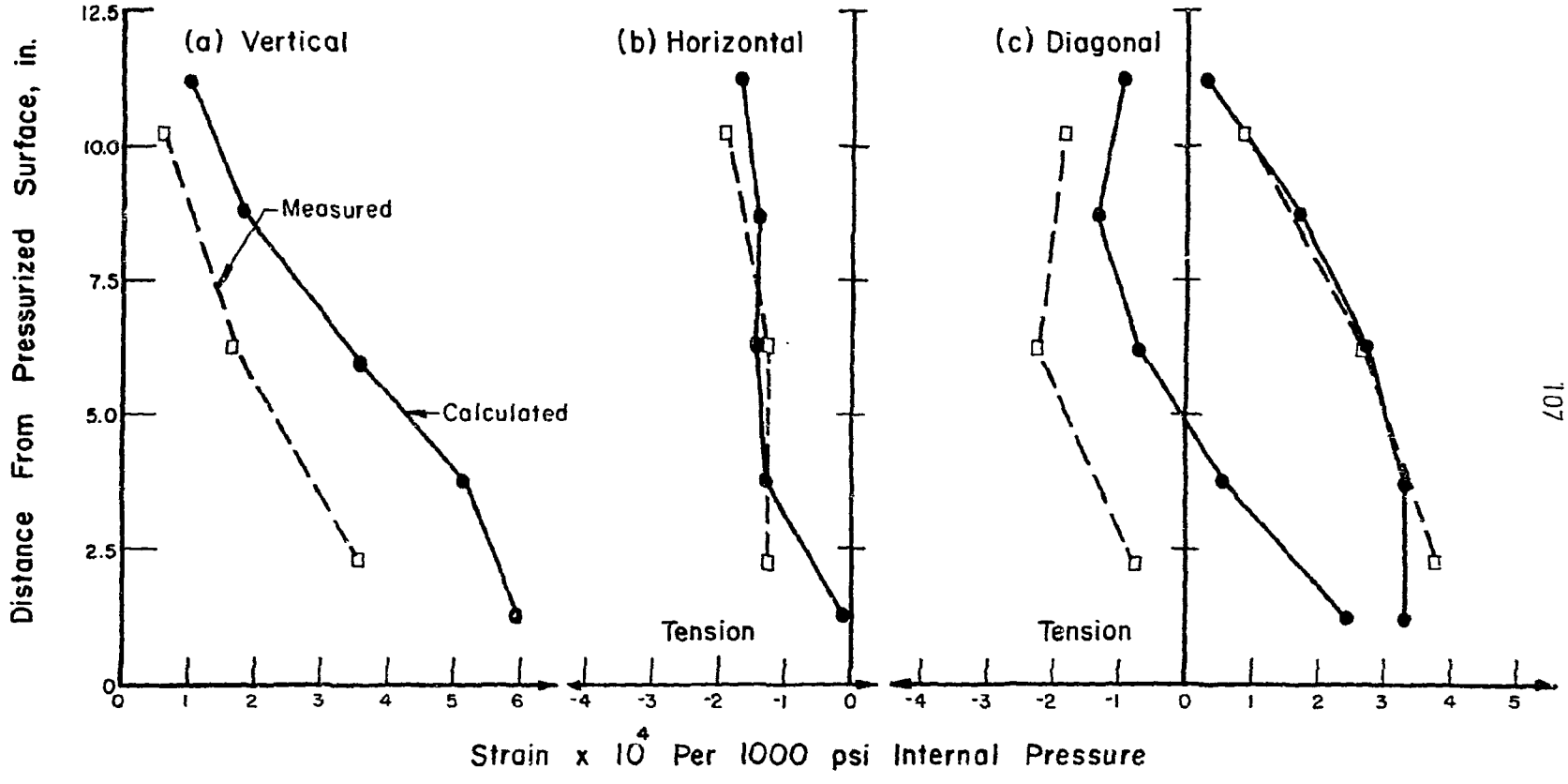

Fig. 5.60 Comparison of Measured and Calculated Strains at an Internal Pressure of 1000-psi for a 12.5-in. End Slab. Strains at Penetrations 4 and 5 (See Fig. 5.2)

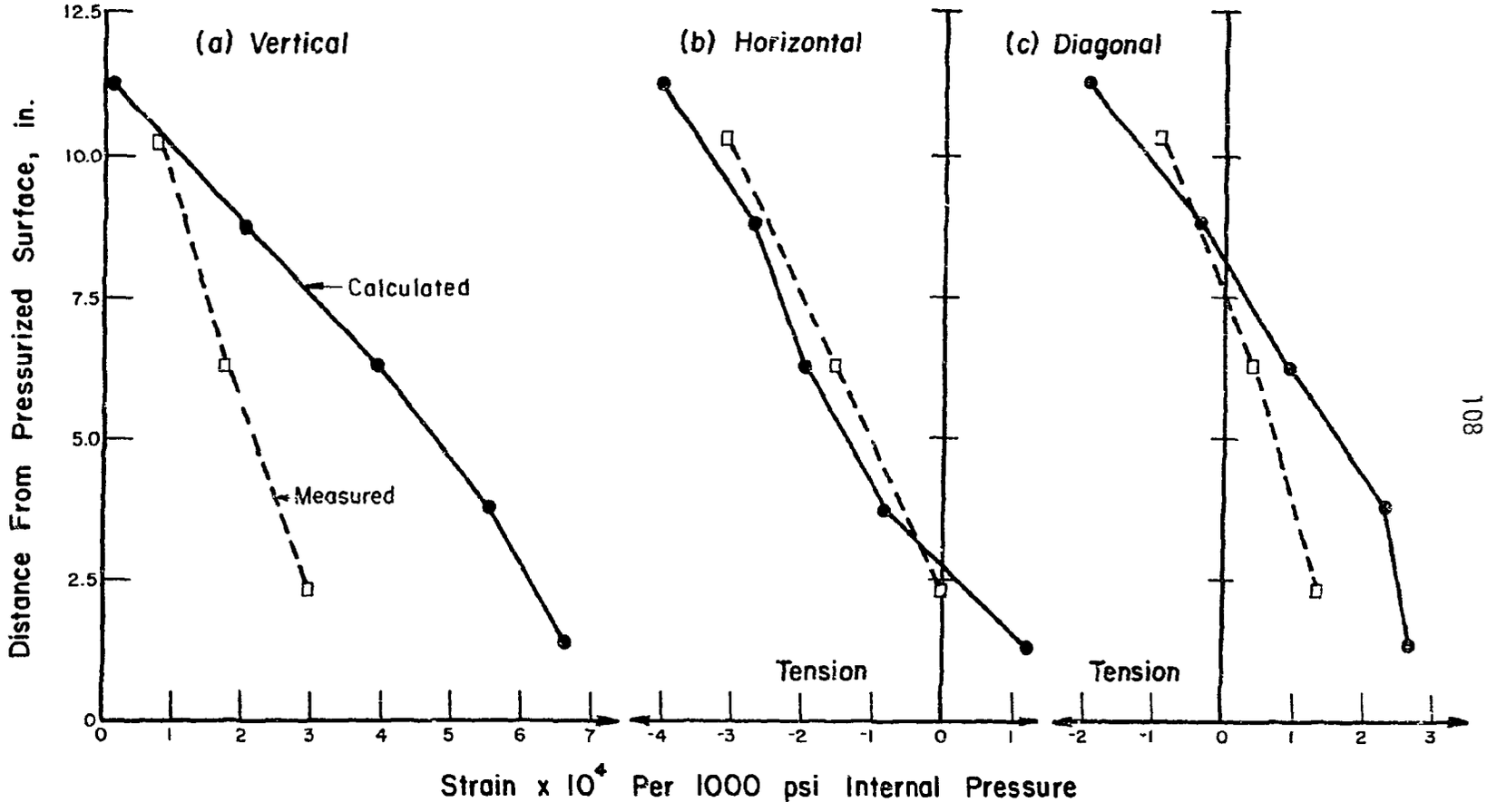

Fig. 5.61 Comparison of Measured and Calculated Strains at an Internal Pressure of 1000-psi for a 12.5-in. End Slab. Strains at Penetration 2 (See Fig. 5.2)

APPENDIX A

A1 MATERIALS

A1.1 Concrete

The vessels were cast from concrete mixed in the laboratory. Two different mixes were used, one for the cylindrical skirt and one for the end slab.

The first mix was used for the skirt up to a level of 2-in. below the reentrant corner. Two batches of concrete were required to cast the skirt. The concrete contained pea-gravel aggregate, sand and type III cement. The proportions by weight of cement: sand: gravel were 1.00: 2.77: 3.07 and the water cement ratio was 0.67.

The second mix was used for the slab and the top 2-in. of the skirt and was made in one batch. The concrete contained crushed limestone aggregate, sand and type III cement. The proportions by weight of cement: sand: gravel were 1.00: 3.51: 3.40. Type III cement was used with a water cement ratio of 0.80.

Five 6 x 12-in. cylinders were cast from each of the first two batches. Eight 6 x 12-in. cylinders and eight 6 x 6-in. cylinders were cast from the third batch used in the end slab of the vessles. The properties of the batches used in the end slabs of the vessels are shown in Table A.1.

A1.2 Longitudinal Reinforcement

PV 26 was prestressed with the rods from the previous series of tests, namely 0.775-in. diameter stressteel rods with an ultimate stress of

140 ksi. However, the threads on several of these rods stripped off during prestressing.

New rods and bolts were purchased and used in all of the subsequent tests. The results of a tensile test of a 30-in. stresssteel rod are plotted in Fig. A1. The strain was measured using an eight-in. extensometer. The ultimate stress in the rod, which had a measured cross-sectional area of 0.471 sq. in. was 140 ksi.

A1.3 Circumferential Reinforcement

The wire used to prestress the vessels circumferentially was obtained from ARMCO, Kansas City, Missouri. The wire was 0.08-in. diameter extra high strength high carbon rope. Two strain gages were attached on opposite sides of wire samples cut from the unstressed coils. These samples were subjected to tensile testing and the stress versus average strain was plotted. The Young's Modulus for the wire was found to be 30×10^6 psi. All of the samples failed at the grips of the testing machine. The failures occurred at an average load of 1400 lbs or approximately 280 ksi. Thus it can be assumed that the actual ultimate load is somewhat higher.

A1.4 Liner Materials

The neoprene used to seal the pressure vessels was purchased in 100-ft rolls. The sheets were 36-in. wide and 1/16-in. thick. It was specified as "60 Durameter Shore A Black Neoprene Sheeting, Type #260."

The O-ring material was obtained in 100-ft lengths. The diameters of the 3/16-in. and 3/4-in. O-ring stock were 0.210 ± 0.010 in. and 0.750 ± 0.010 in. respectively. The material was specified as "70 Durameter Buna-N O-ring Cord Stock."

The caulking used to seal and hold the neoprene intact was specified as "General Electric Construction Sealant, SE-1204 Neutral in 1/12 U.S. Gallon Paper Tubes."

Sheets of 0.104-in. thick steel and 16 oz. soft copper were used on the sides and end slabs of the vessels.

A2 FABRICATION

A2.1 Casting and Curing

All pressure vessels in the current series, PV 26 through PV 33, were cast in the same outer steel form. This form was rolled from 5/16-in. steel plate and reinforced with rolled 2 x 2 x 1/4-in. angles. The inner form was basically a closed steel cylinder. Its height could be adjusted by adding 2 1/2-in. steel bands around the bottom or open end of the cylinder. This made it possible to vary the thickness of the concrete vessel head. Both the inner and outer forms were bolted to a 1/2-in. thick base plate. Sixty holes were drilled 3/8 in. into the base plate to receive the 7/8-in. diameter aluminum rods which form the openings for the longitudinal prestress rods. The tops of the rods were secured by a template of 1/2-in. steel which was attached to the outer form by sections of 4-in. wide channel. The center of the template was cut out to allow easier access when casting and trowelling. For the vessels which had penetrations in the head, holes were drilled and tapped in the top or closed end of the inner form. Steel pipes having the desired length and diameter were then bolted to the form.

All vessels were cast in three batches. The first two batches containing pea gravel aggregate, were used for the skirt of the vessel up to a level approximately 2-in. below the top of the inner form. The third batch, which contained a limestone aggregate, was used to complete the remaining skirt and head slab. The concrete was vibrated internally with an electric vibrator during casting. The sidewalls of the vessels were reinforced with 40 No. 4 rebars, providing a reinforcement ratio of approximately

one percent. The bars were placed longitudinally around the outside of the skirt with about a 1/2-in. cover provided.

After the concrete had been placed and vibrated, the surface was trowelled until the concrete had begun to set up. The oiled aluminum rods and penetration pipes were periodically twisted during this time until the concrete was firm enough to allow the pulling of the rods and penetration pipes. This was accomplished by first removing the 1/2-in. steel template and then very carefully rotating and lifting the rods and penetrations out.

The vessel and cylinders were then covered with wet burlap and plastic. On the second day after casting, the forms were struck and a grinder was used to smooth out any rough spots on the surface of the vessel head. The cylinders were removed from their forms and placed around the vessel and again covered with wet burlap and plastic. The wet curing process continued until the seventh day after casting.

A2.2 Circumferential Prestressing

The pressure vessels were circumferentially prestressed in the Civil Engineering Machine Shop on a specially built prestressing rig. The 0.08-in. diameter wire was applied in a series of five "belts" as shown in Fig. A.2. Each of the five "belts" contained between 290 and 300 wraps of wire applied in six layers of about 50 turns each. The wires in each band were kept from slipping out of position by a series of steel plates bolted into coupling nuts cast into the concrete. The coupling nuts were cast into the vessel by drilling holes in the outer form and bolting them from the outside against the inside of the form. A 0.5-in. washer bolted to the coupling nut provided

bearing for anchorage. When the forms were struck, the bolts were unscrewed and the forms removed, leaving the openings of the nuts exposed. Screw-in clamps on each of the bands served as tie-offs for the beginning and end of each band of prestressing wire.

The prestressing operation was initiated by securing the wire in one of these clamps. The first wrap of prestress was applied at a reduced load to facilitate the proper alignment of the wire on the vessel. Subsequent wraps of the 0.08-in. diameter wire were applied at a tension of between 700 and 730 lbs. Ten steel rods were used to bolt the vessel securely on the lathe.

A schematic diagram of the prestressing apparatus is shown in Fig. A.3. The extra high strength wire was shipped in coils weighing around 500 lbs. It was necessary to rewind the coils of wire on a large spool to provide a more uniform rate of feed. The spool of wire was then mounted on a stand at the rear of the prestressing rig. A rope was wrapped around the spool axle and kept taut during the entire operation. This prevented the feed spool from gaining momentum and letting out more wire than was needed. The wire was first passed around a friction pulley a total of five times and then pulled over the first of the mounted pulleys. The wire was then passed under the pulley mounted on the 1500 lb. weight and back up and over the second mounted pulley. Finally, the wire was passed under a smaller pulley attached to a dynamometer and secured on the vessel (Fig. A.4).

Two automotive brakes were mounted on the axle of the friction pulley and they ultimately controlled the rate at which the wire was fed from the spool. It was the brakeman's function to control the rate of feed so that it equalled the rate at which the rotating lathe wrapped the wire onto the

vessel. The brakeman was able to gage this proper rate by watching the suspended 1500 lb weight and its relative motion. If the weight was rising, that indicated that the lathe was taking on wire faster than the spool was feeding it. Thus, the pressure on the brake had to be reduced. Conversely, if the weight was descending, the brake pressure had to be increased. Once the wrapping operation was begun, the weight was kept suspended at all times to maintain full tension in the wire. Approximately two hours was required to wrap one "belt" of 295 turns.

After all five bands had been applied, the vessel was unbolted from the turret lathe and inspected for cracks. In each case, a series of two or three circumferential cracks was found on the inside walls of the vessel at a spacing of approximately nine in. from the open end.

The dynamometer or load cell attached to the last pulley was connected to a strip chart and continuous strain readings were taken during prestressing. From these readings, a value for the average tension in the wire was obtained.

The effective prestress was determined with the help of information on shrinkage and creep characteristics of the concrete used (Reference, Vol. II, Fig. A.3). The "anchoring" stress for each wrap was measured. The instantaneous stress reduction on each wrap caused by subsequent wraps was calculated using a linear elastic model of the vessel. The following expressions, based on experimental data, were used for time-dependent strain changes in the concrete:

$$\varepsilon_c = \frac{10^{-3}}{1250 + \frac{30{,}000}{t_p}} \qquad (A.1)$$

$$\varepsilon_{sh} = \frac{1}{1700 + \frac{30,000}{t_c}} \qquad (A.2)$$

where ε_c = creep strain per psi

ε_{sh} = shrinkage strain

t_p = time after prestress, days

t_c = time after casting, days

Both expressions are intended to apply to the concrete used and for values of t less than 120 days. The rate-of-creep method was used to determine the effective prestress with an integration interval of one day. The calculated reduction in stress for the prestressing bands near the end slab ranged from approximately 15 to 20 percent (Table A.2).

A2.3 Longitudinal Prestressing

Sixty stressteel bolts were used to prestress all of the vessels. Strain gages were placed on 15 of the rods and were calibrated in the laboratory. Loading of the bolts was accomplished with a 30-ton Simplex jack with the scheme shown in Fig. A.5. A continuous steel plate 1 1/4-in. thick was used as a bearing plate. The fifteen gaged rods were pulled first, with strain readings taken before and after. The load in the bolts after the jack was released varied from 40 to 45 kips. After the rest of the bolts were prestressed the gaged bolts registered loads of less than 40 kips. This loss was attributed to the effects of creep and to the fact that the loading of a bolt adjacent to an already loaded bolt tended to reduce the force in the loaded bolt. To minimize this effect, the rods were pulled a second time in the

same manner. In this way, a force approaching 45 kips was attained in each of the rods. A final set of readings from the gaged bolts was taken immediately before the test so that the vertical prestressing force was known at the time of the test.

A2.4 Liner

A detail of the typical liner used for all the vessels is provided in Fig. A6. For the vessels having penetrations, steel plugs or plates were used to cover the holes on the inside of the vessel (Fig. A.7). A welded steel can, 0.104-in. thick, was then grouted into place with the use of an electric vibrator. The 16-oz. soft copper can was soldered in next with all copper to copper and copper to steel connections tinned and sweated. The vessels were then lightly prestressed longitudinally and pressurized to 50 psi gas pressure to check for leaks. A layer of 1/16-in. thick neoprene was placed over the copper and secured with rubber cement and General Electric Silicone Caulking. A 3/4-in. neoprene O-ring was also installed at the junction of the end slab and the sidewall. An aluminum expansion ring was used to hold the neoprene securely in place around the bottom of the sidewall. The seal between the steel base plate and the sealing ring was made by compressing a 0.210-in. O-ring into the groove in the base plate (Fig. A.8).

A3 TEST SETUP

All testing was conducted in the basement at the east end of the Civil Engineering Building. The vessels, having been lined and prestressed, were transported by crane and fork lift to the test room. On the day prior to testing, the vessels were filled with water to within approximately 1/2-in. of the end slab. An oil pump was used to pressurize the vessel to failure. This procedure greatly reduces the violent release of energy that occurs when using gas pressurization. However, it was still necessary to contain the explosion by the use of steel channels bolted across the top of the prestress rods in a criss-cross pattern (Fig. A.9).

During the tests, the door to the test room was barricaded and warning signs were posted in all adjacent corridors. All operations were conducted remotely in an area at the east end of the Crane Bay, directly above the test room located in the basement. Here strain measurements were taken and recorded on a teletype equipped with a paper tape, deflection readings were taken from the two television monitors, and the internal pressure of the vessel was monitored and controlled by the test personnel.

A4 INSTRUMENTATION AND TEST PROCEDURE

In general, the instrumentation of the vessels consisted of deflection dials across one diameter of the head and down the side on a line at one end of this diameter, strain gages on the inside surface of the head and the surfaces of the penetration walls and load cells on the fifteen prestressing rods.

Deflections across the head of the specimen and on the side wall were measured with 0.0005-in. Brown and Sharpe Dial Indicators. For PV 26 the dial gages were connected to push rod extensions in direct contact with the surface but due to the explosion at failure, all of the dials on top were destroyed. For PV 27, push rods were again used for the sidewall gages. However, the head dial gages were connected to piano wires which were strung over ball bearing pulleys and attached to metal tabs glued to the specimen. Tension springs connected to the back end of the dial gage plunger kept the piano wires taut. This system proved unsatisfactory due to the great amount of internal friction which markedly reduced the sensitivity of the gages. Thus, for PV 28, the head gages were mounted directly above the specimen and connected to piano wires running vertically down to the vessel head and attached to the metal tabs glued to the surface (Fig. A.10). The gages were protected from damage by a series of steel channels bolted over the head. This method proved satisfactory and was adopted for all subsequent tests. The dial gages were read with a closed circuit television hookup with the monitors situated on the first floor at the east end of the Crane Bay. Two television cameras equipped with telephoto lenses were used to read the deflection gages (Fig. A.11).

Strain gages were used on the inside surface of the concrete and in the penetrations were limited to two types: the BLH type A12 which has a one-in. gage length and 3/32-in. gage width, and the BLH type AR-2-S6 which is a rosette having a gage length of 3/4-in. and gage width of 9/64-in. Careful steps were taken to ensure a smooth surface and good bonding for all gages. The concrete surface was first sanded to a smooth finish. A hydrocal paste was then applied over the surface to fill in any holes or indentations. The surface was again sanded down and a layer of cement glue was placed on the concrete and allowed to set to a smooth, hard finish. The gages were then attached to this prepared surface with Eastman 910 cement (Fig. A.12). In addition, a soft rubbery protective coating was placed over all strain gages on the inside surface of the vessel. The wires from the inside gages were run down the inside wall of the vessel and out between the concrete skirt and the one-in. steel ring. Channels 1 in. wide by 1/8-in. deep were cast into the concrete to accommodate the gage wires.

Load cells were used to measure the changes in force in the prestress bolts. Four strain gages were cemented to the outside of these bolts and wired into a full bridge. Before they were used, the load cells were calibrated in a testing machine.

Strains were read by a Pivan switching strain indicator located at the east end of the Crane Bay in the Civil Engineering Building, directly over the testing room one floor below. The load cells were calibrated with a 10k ohm resistor while all others required a 60k ohm resistor.

Pressure was applied to the inside of the specimen by a high-pressure hydraulic pump with a maximum capacity of 10,000 psi. During a test the

gas pressure was increased in increments and once the pressure was set and became stable all measurements were taken. Approximately 3 to 4 minutes were usually required for each set of readings. The size of the pressure increments varied among the tests.

TABLE A.1

Concrete Properties

Mark	Age @ Test Days	Slump in.	Modulus of Elasticity psi x 10^6	Splitting Strength psi	Compressive Strength		
					Batch 1 psi	Batch 2 psi	Batch 3 (End Slab) psi
PV26	98	3 1/2	3.9	445	7320	7910	6710
PV27	102	4	3.8	460	7620	7610	6845
PV29	52	3/4	3.8	450	5760	6660	5480
PV28	117	2	3.9	440	7620	8120	6420
PV30	93	2 3/4	3.7	495	6350	5890	6300
PV31	85	2 1/2	3.7	380	4910	5890	4970
PV32	114	2 1/2	3.8	450	4940	5560	5720
PV33	95	1 1/2	3.7	375	5030	5670	4875

TABLE A.2

Longitudinal and Circumferential Prestress

Mark	Longitudinal Prestressing			Circumferential Prestress			
					Mean Force in Bands 1 & 2[b]		
	Age Days	Force per rod kips	Index[a] psi	Age days	Initial kips	Final kips	Final Index[c] psi
PV26.1	56	40.0	4890	19	199	159	1590
PV26.2	93	41.0	5010	--	199	155	1560
PV27	126	43.7	5340	27	194	156	1560
PV29	45	43.6	5330	29	199	171	1710
PV28.1	83	44.1	5390	56	203	175	1760
PV28.2	111	47.1	5760	--	203	170	1700
PV30	85	43.7	5340	30	206	169	1690
PV31.1	64	43.8	5350	30	201	171	1710
PV31.2	80	45.0	5500	--	201	168	1680
PV32	112	45.3	5540	83	203	178	1780
PV33.1	76	44.4	5430	34	205	173	1730
PV33.2	84	44.2	5400	--	205	170	1700

[a]Total force divided by horizontal cross-sectional area of cavity

[b]Mean force in bands 1 and 2 around end slab at time of prestressing

[c]Mean effective prestress in bands 1 and 2 around end slab at time of test

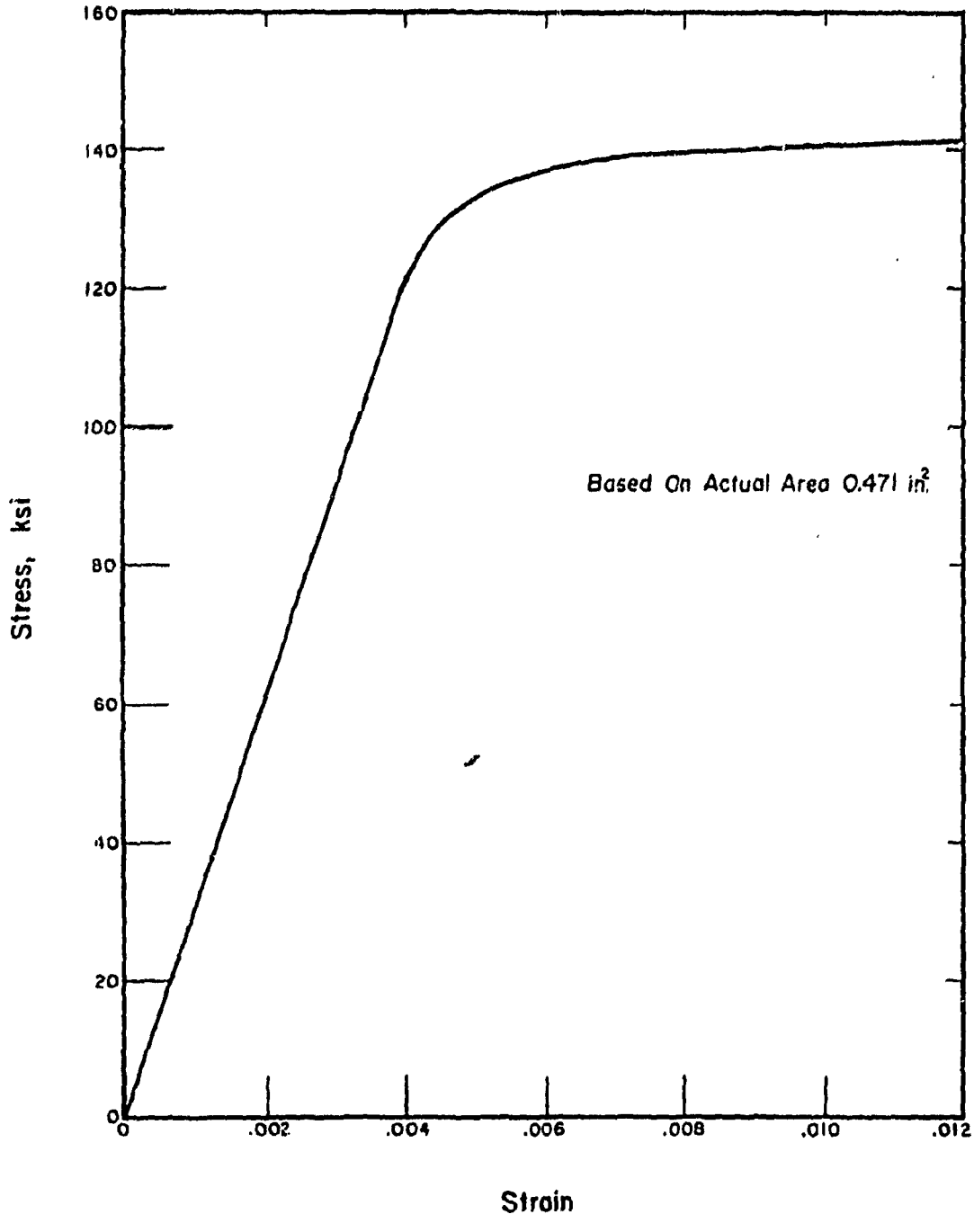

Fig. A.1 Stress-Strain Curve for Stressteel Rods

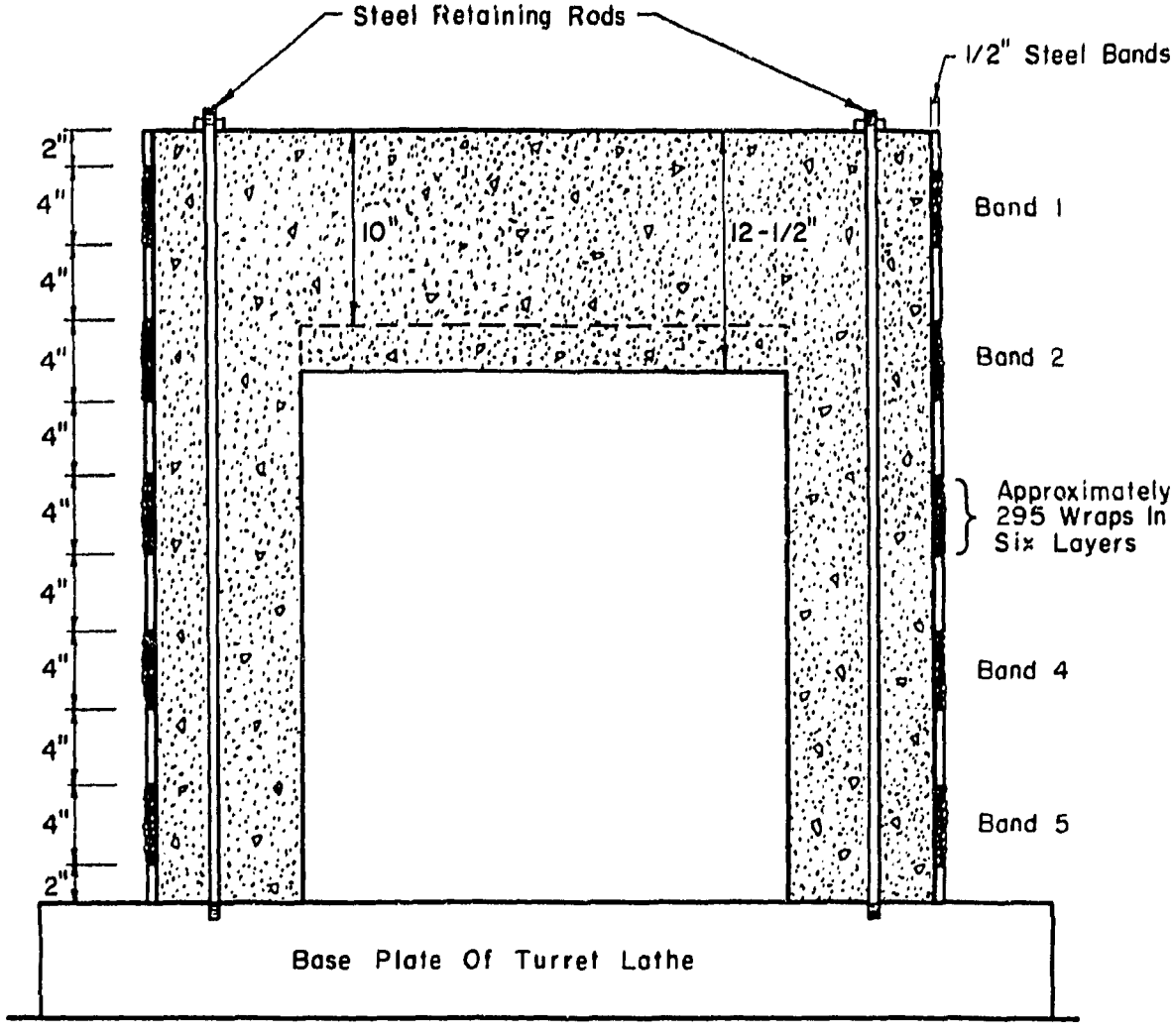

Fig. A.2 Locations of Bands of 0.08-in. Wire Used

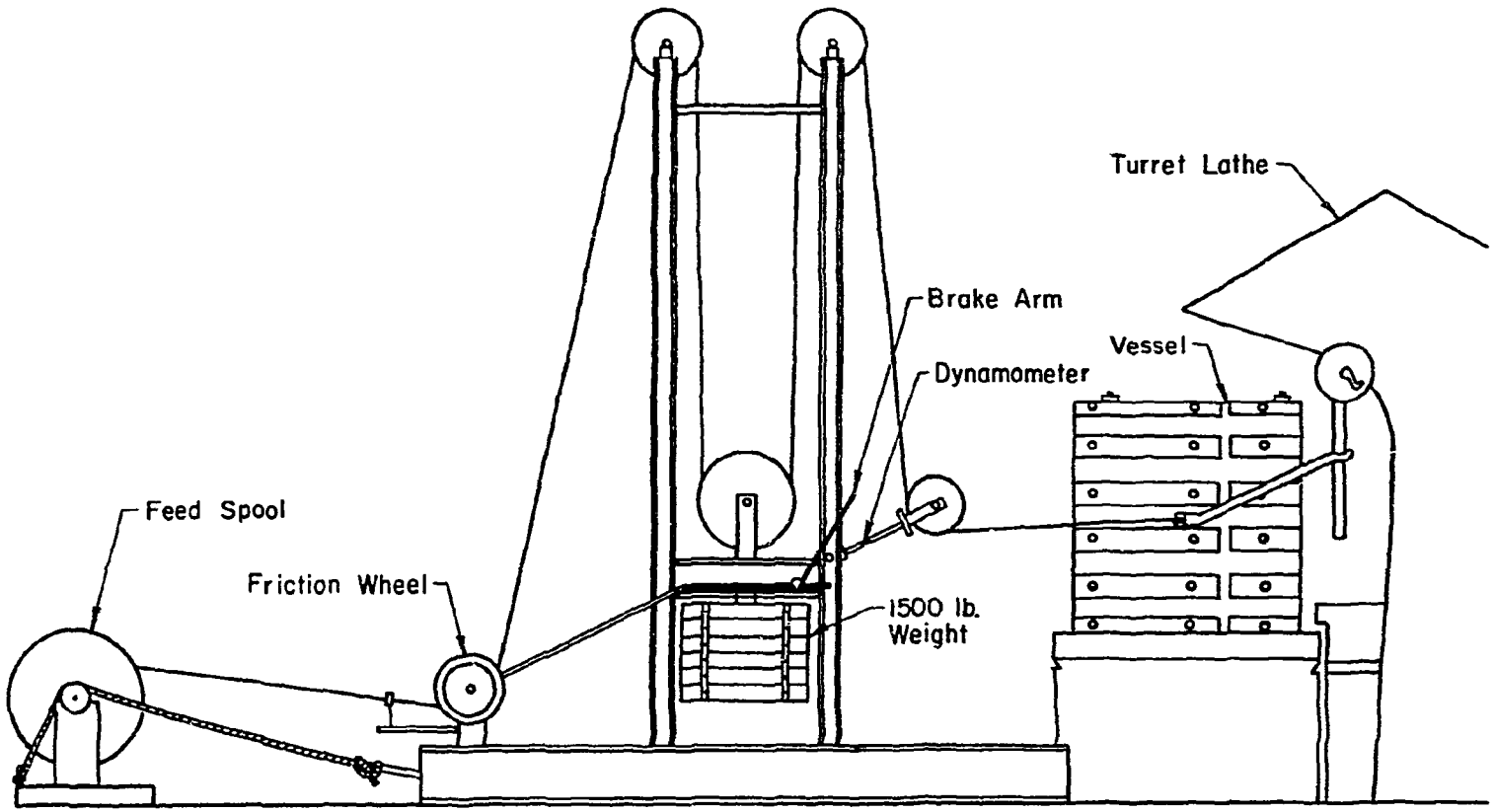

Fig. A.3 Schematic View of Circumferential Prestressing Rig

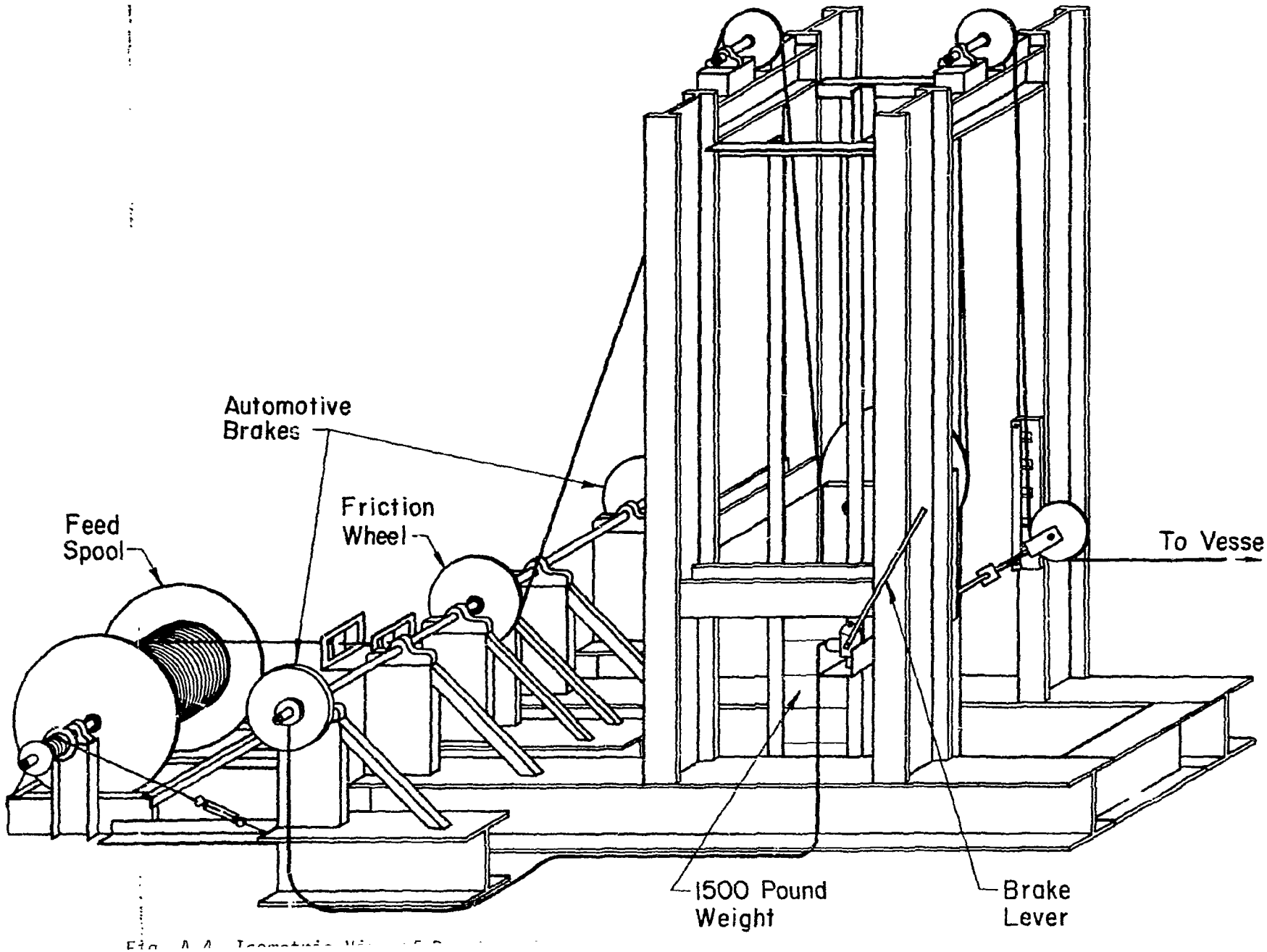

Fig. A-4. Isometric View of Payout

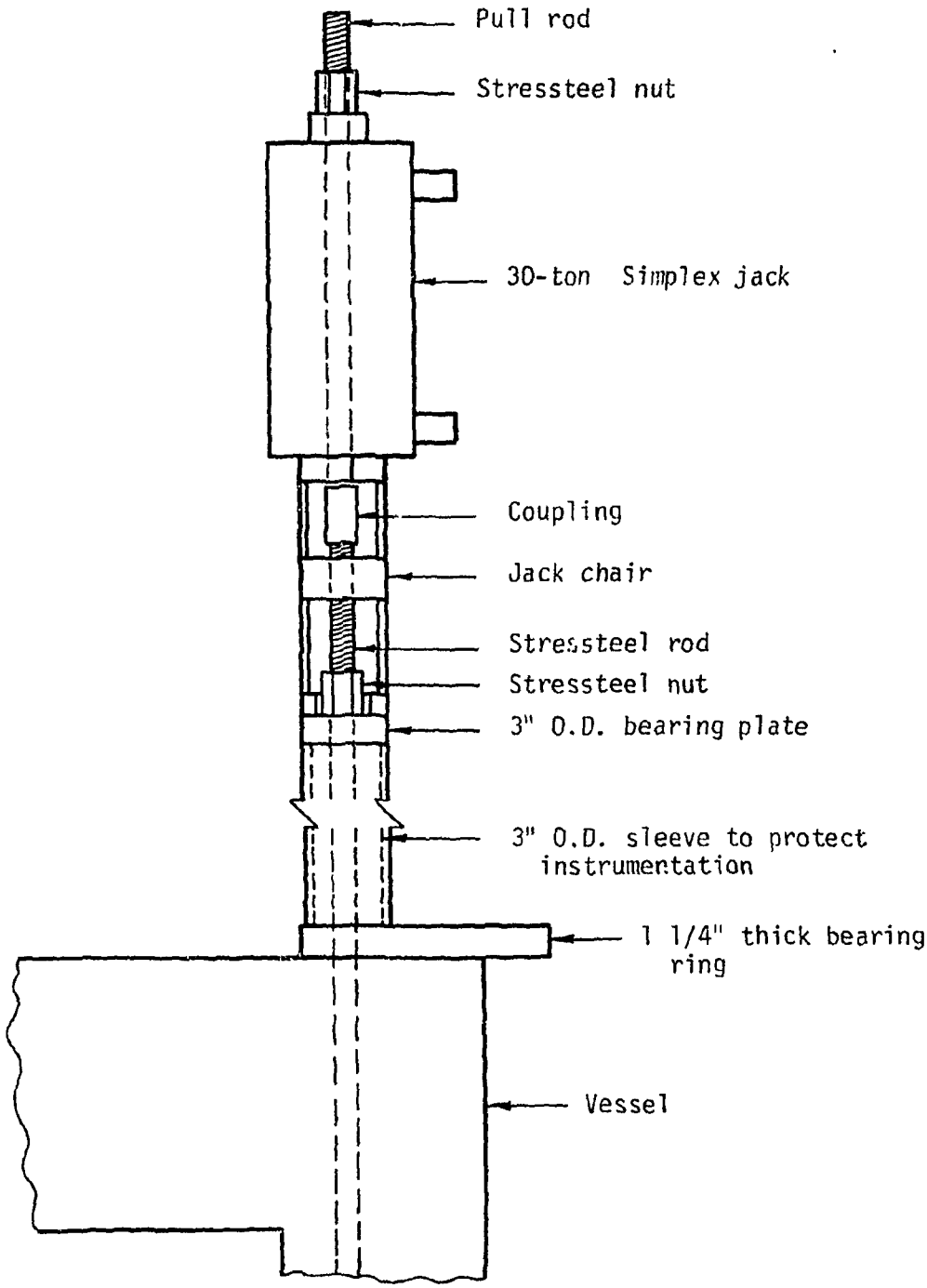

Fig. A.5 Apparatus Used for Longitudinal Prestressing

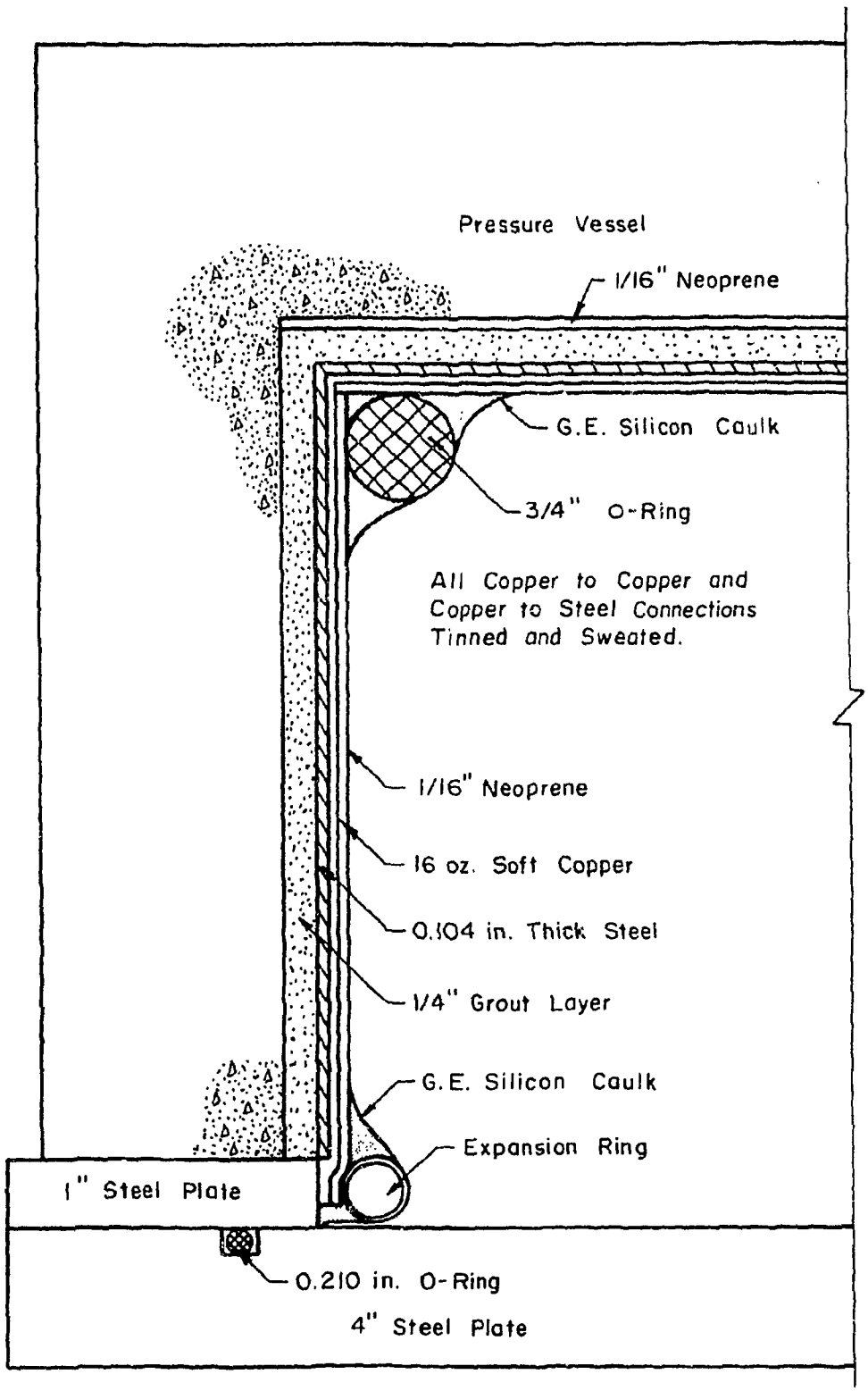

Fig. A.6 Typical Liner Details (not to scale)

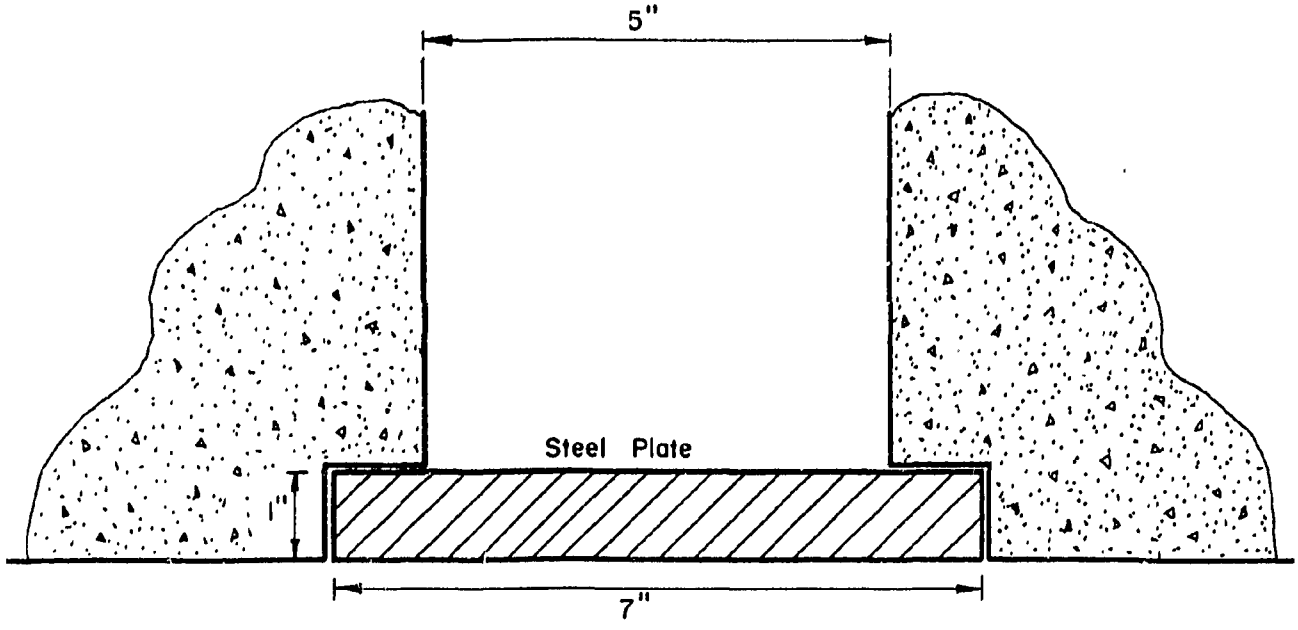

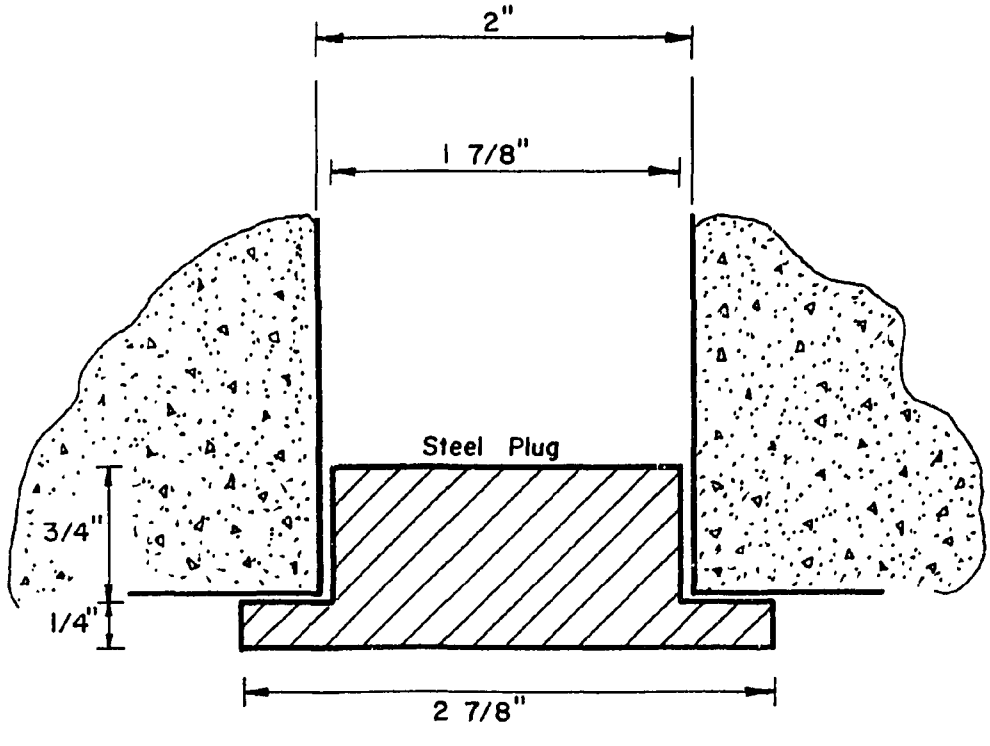

Fig. A.7 Steel Closure Plates

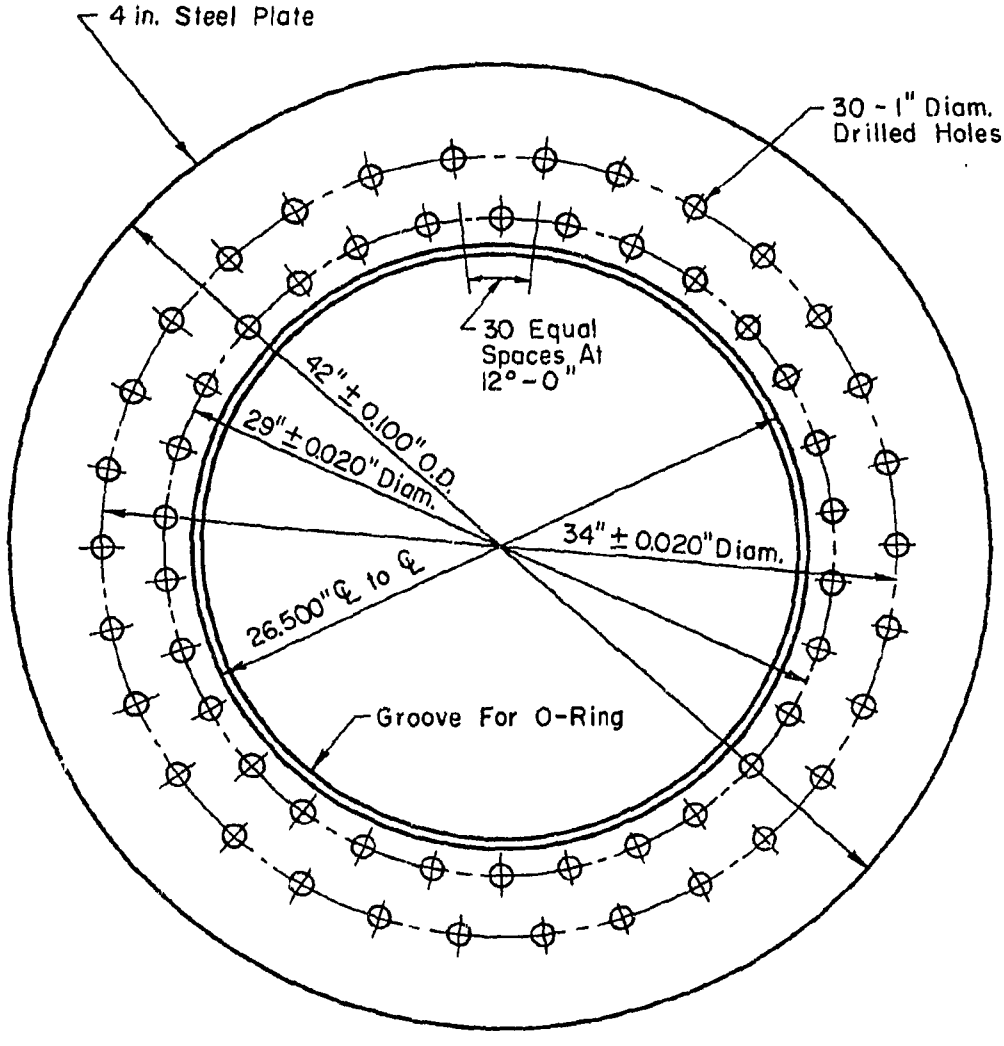

Base Plate

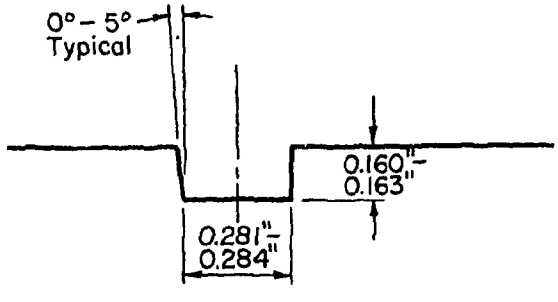

Detail Of Groove

Fig. A.8 Steel Base Plate

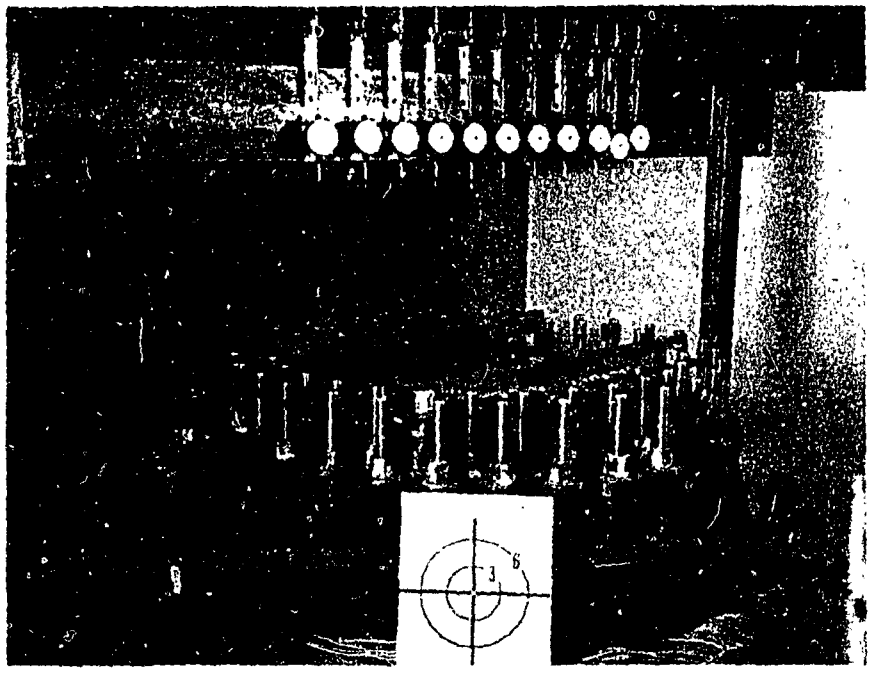

Fig. A.9 Protective Steel Channels Across Top of Vessel

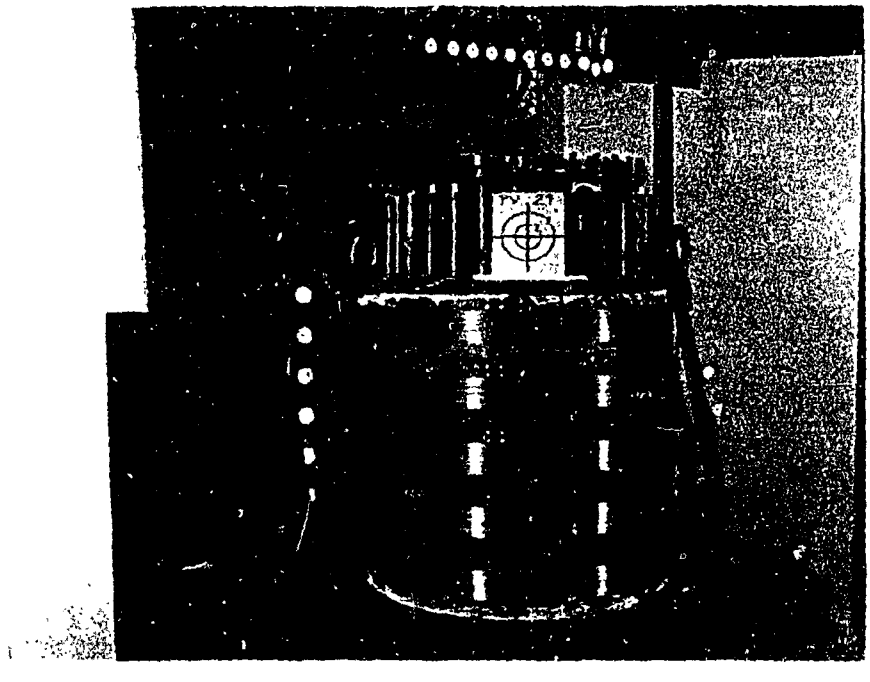

Fig. A.10 Dial Gages Measuring End-Slab Deflections

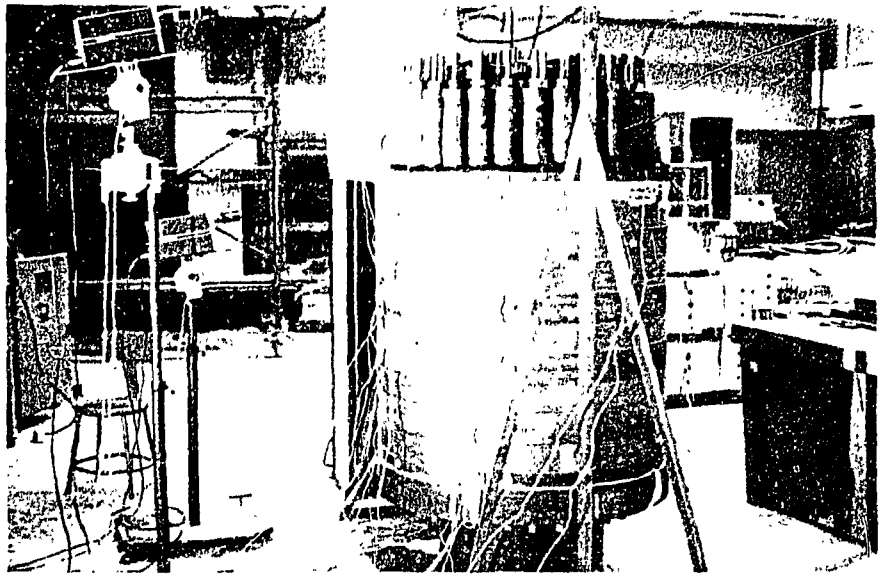

Fig. A.11 Closed-Circuit TV Cameras to Read Dial Gages

Fig. A.12 Strain Rosettes

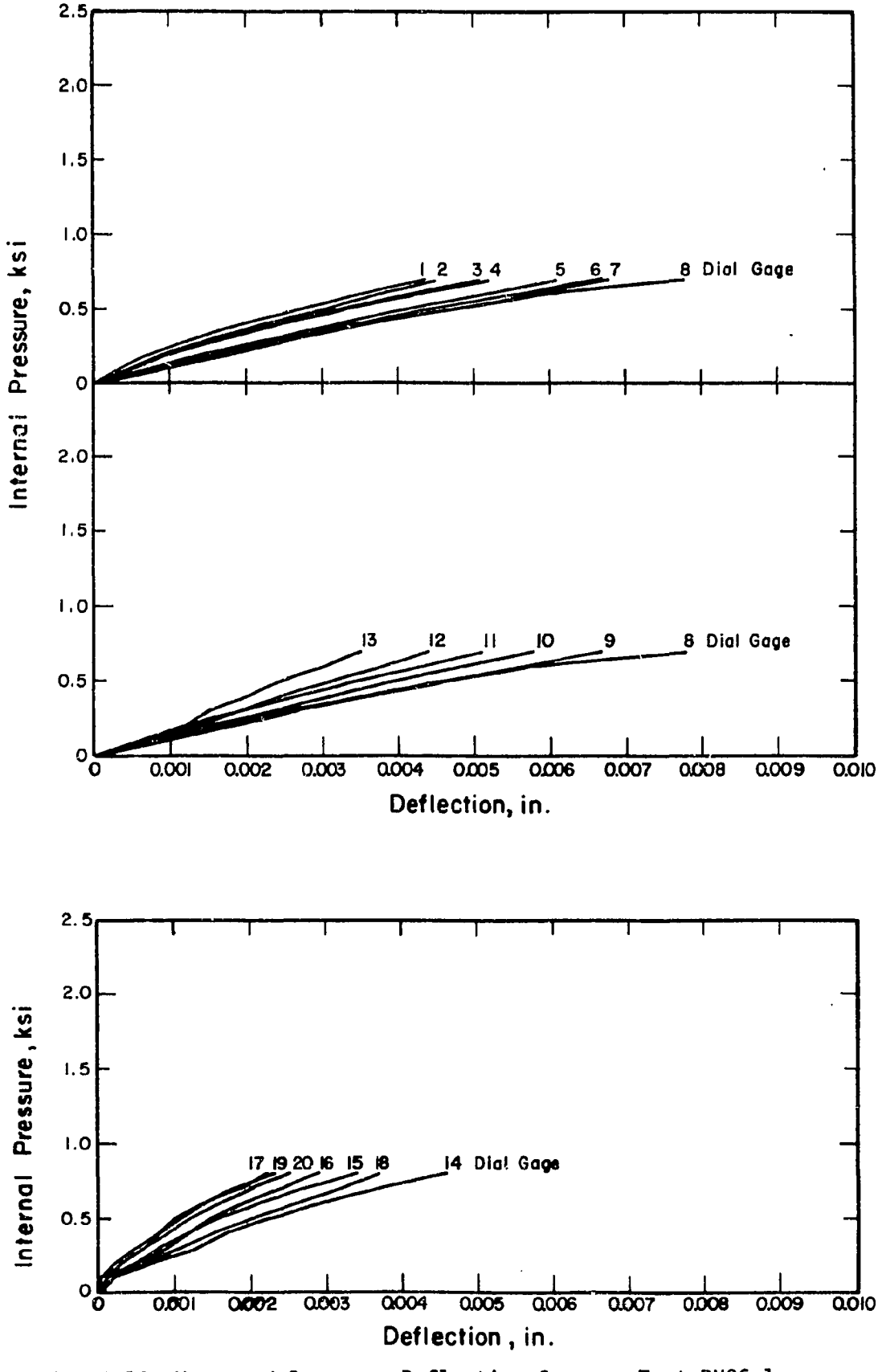

Fig. A.13 Measured Pressure-Deflection Curves, Test PV26.1

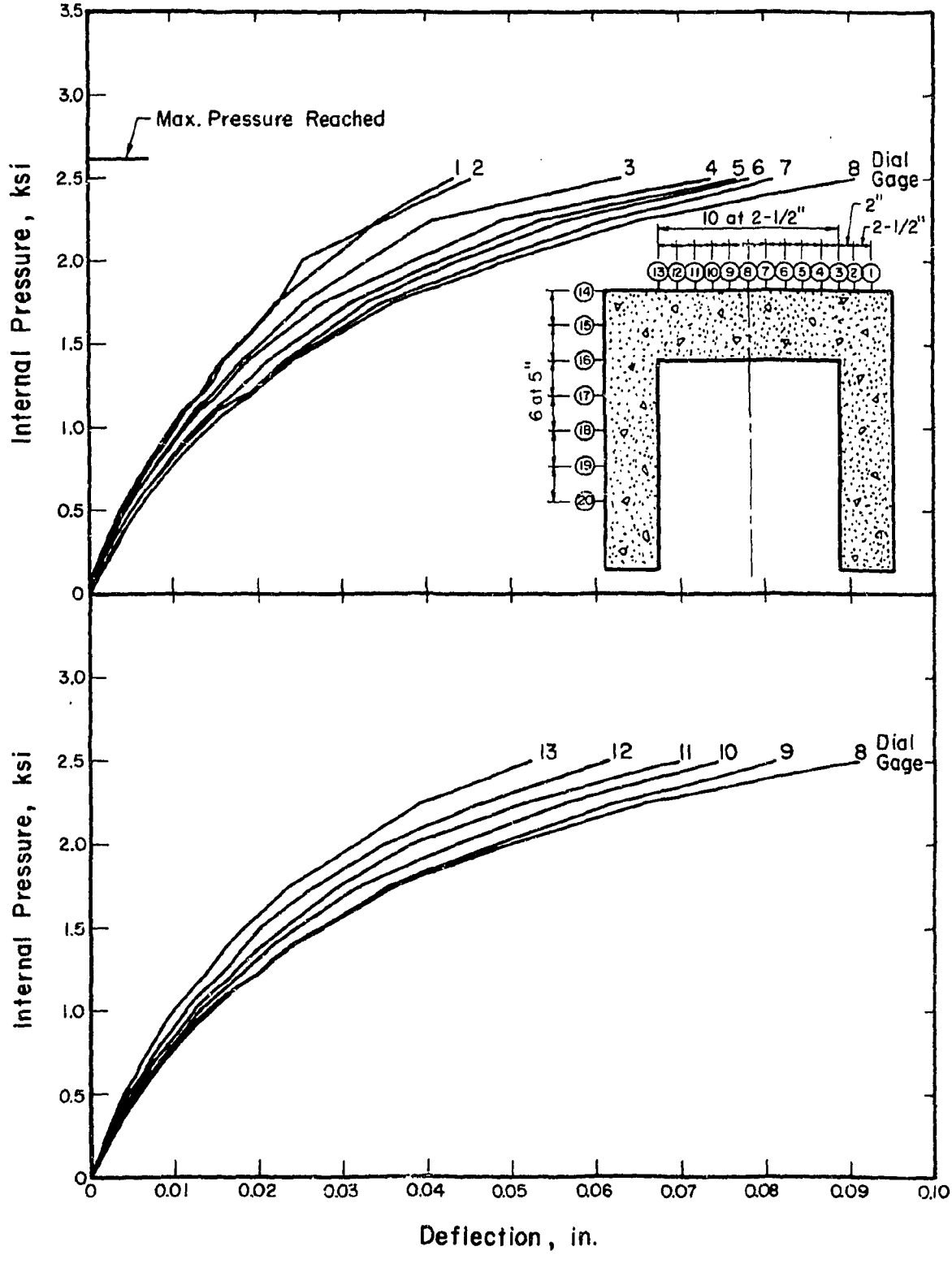

Fig. A.14 Measured Pressure-Deflection Curves End Slab, Test PV26.2

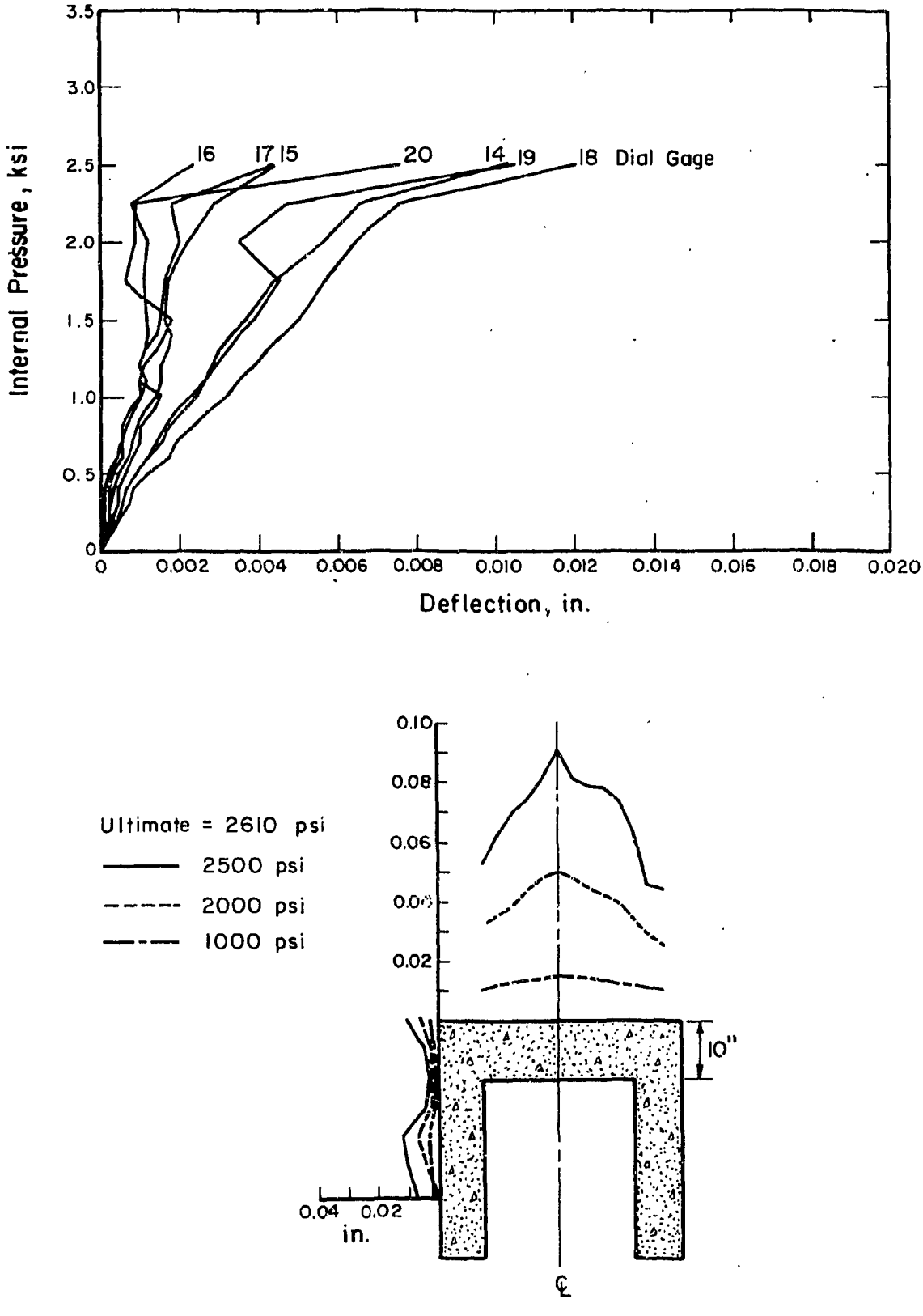

Fig. A.15 Measured Pressure-Deflection Curves Side Wall, Test PV26.2

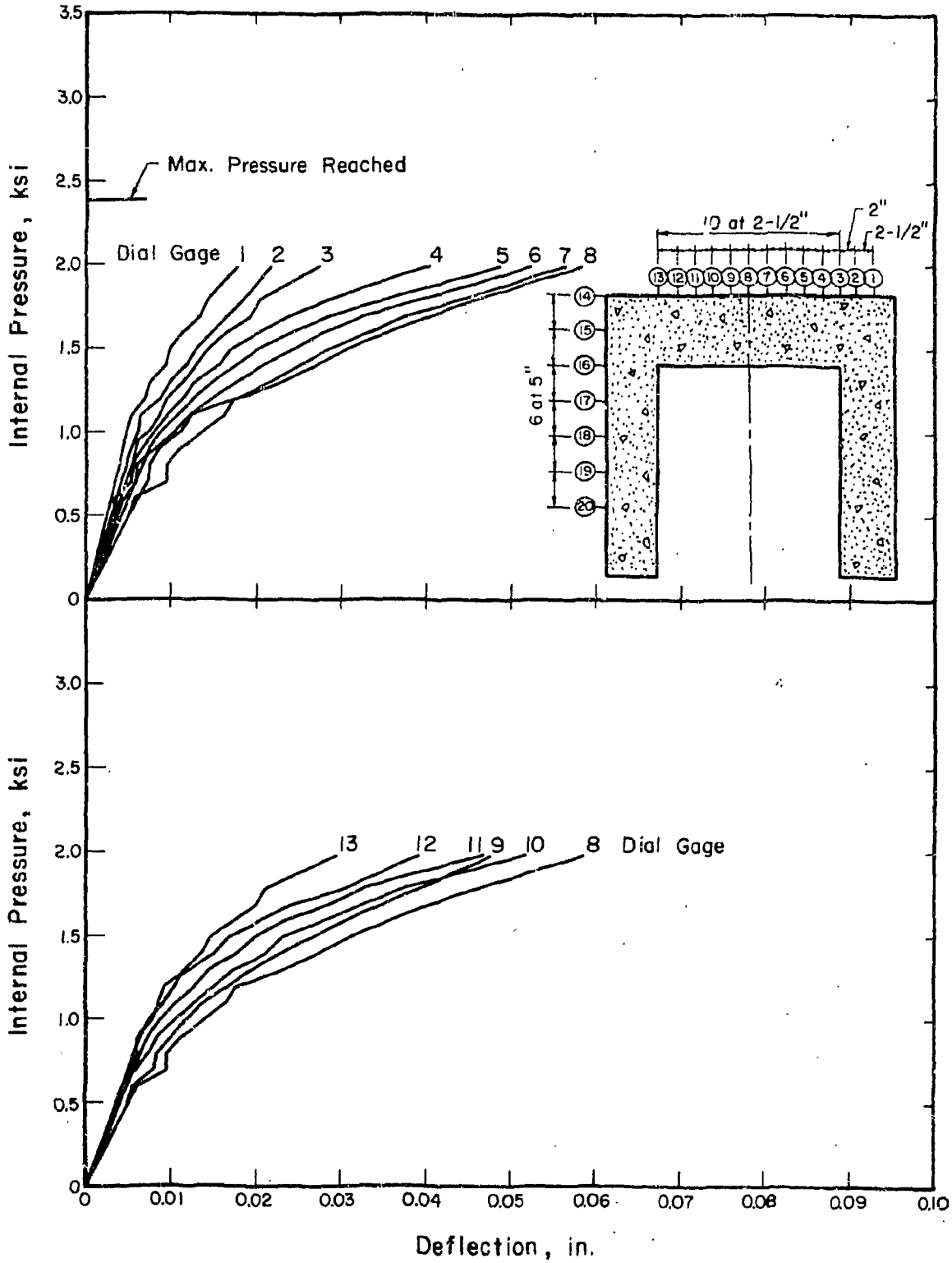

Fig. A.16 Measured Pressure-Deflection Curves End Slab, Test PV27

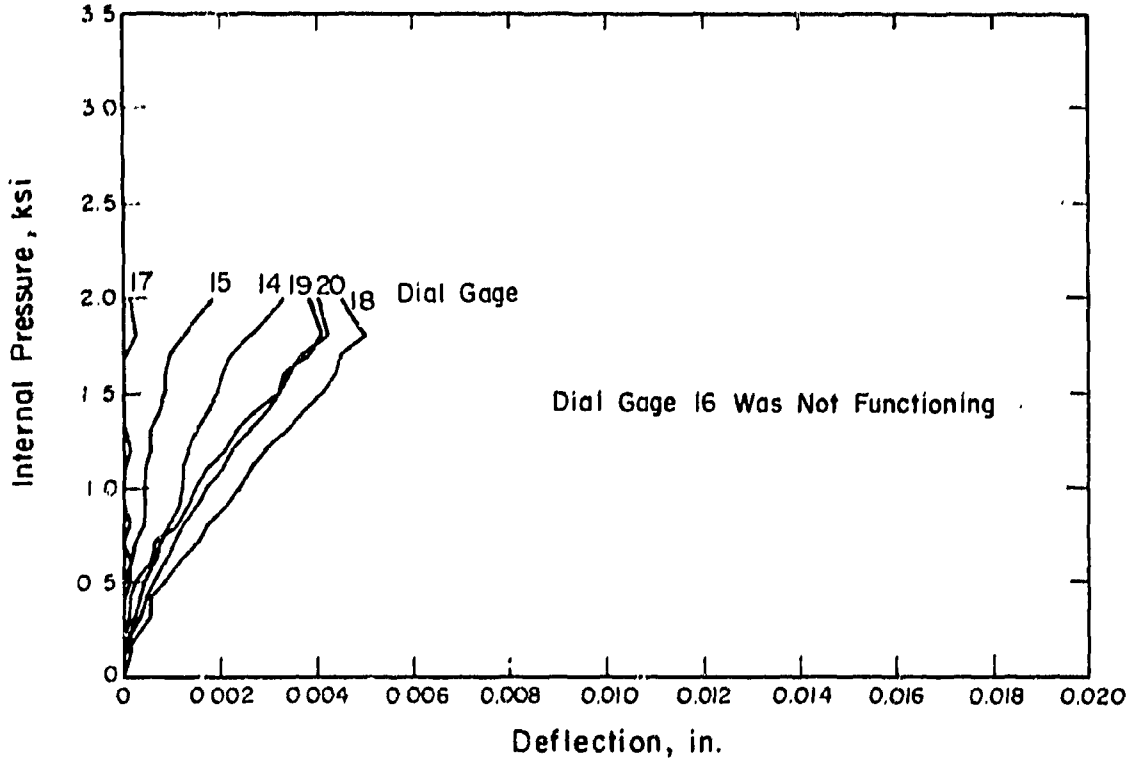

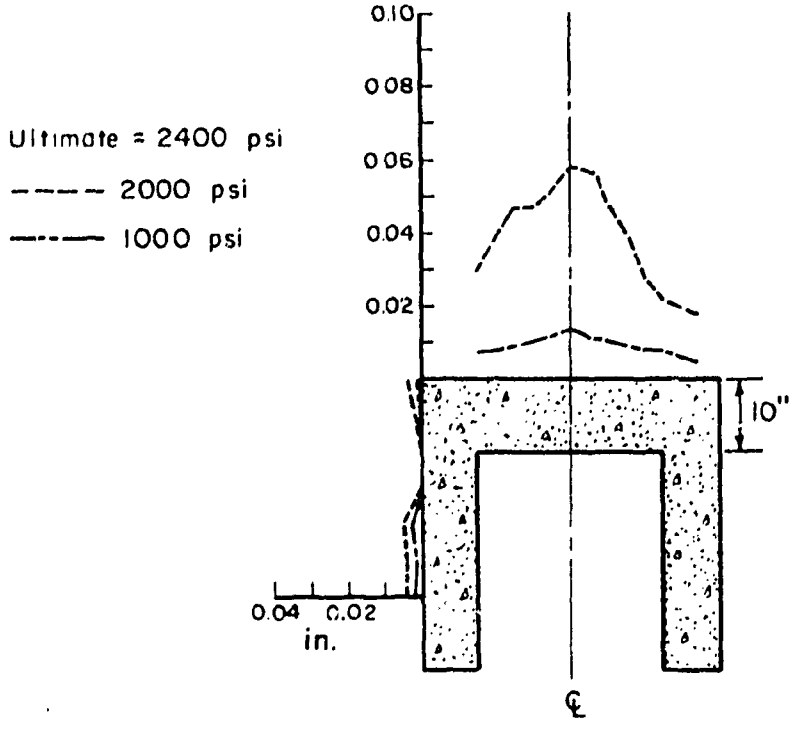

Fig. A.17 Measured Pressure-Deflection Curves Side Wall, Test PV27

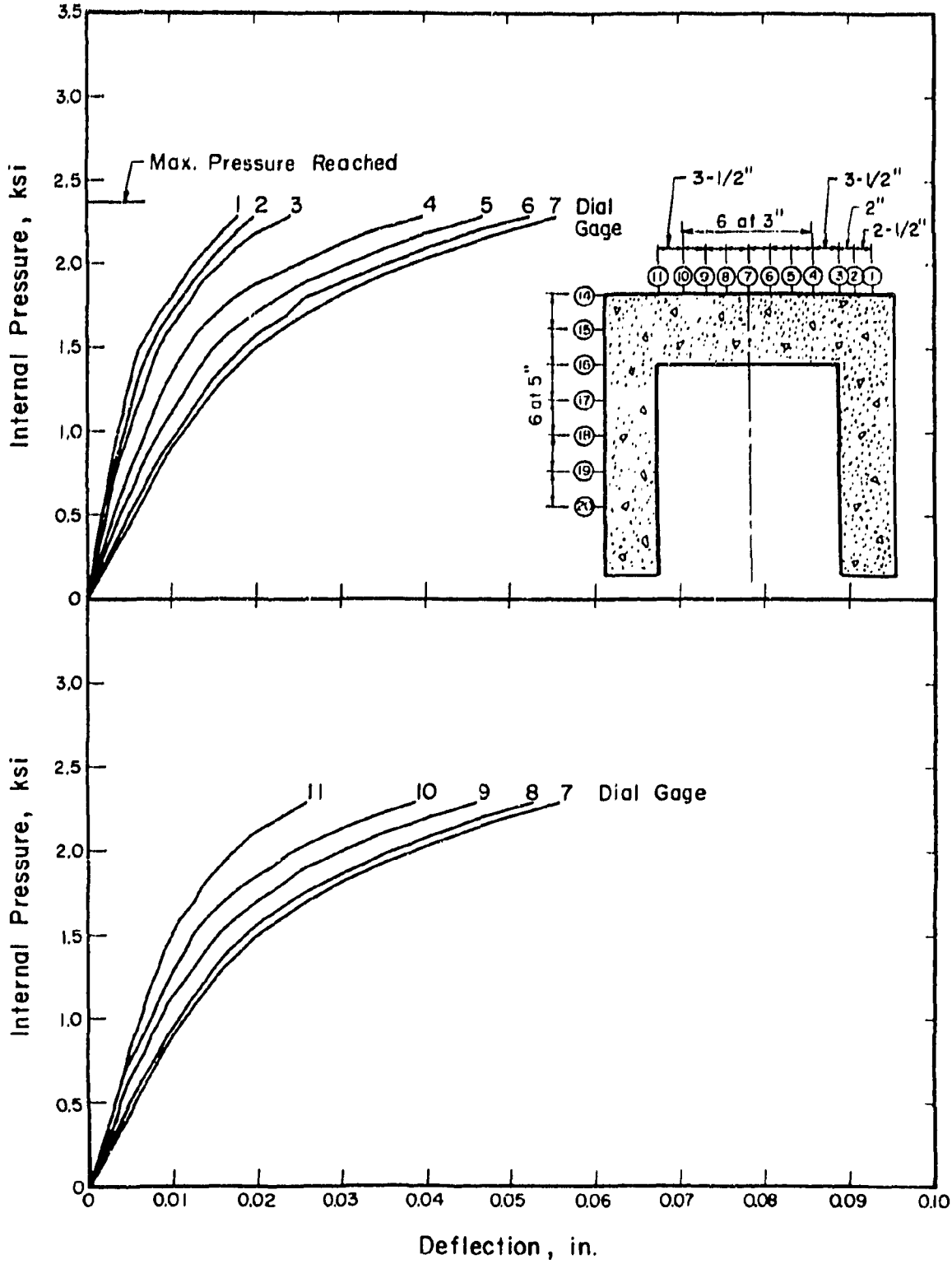

Fig. A.18 Measured Pressure-Deflection Curves End Slab, Test PV29

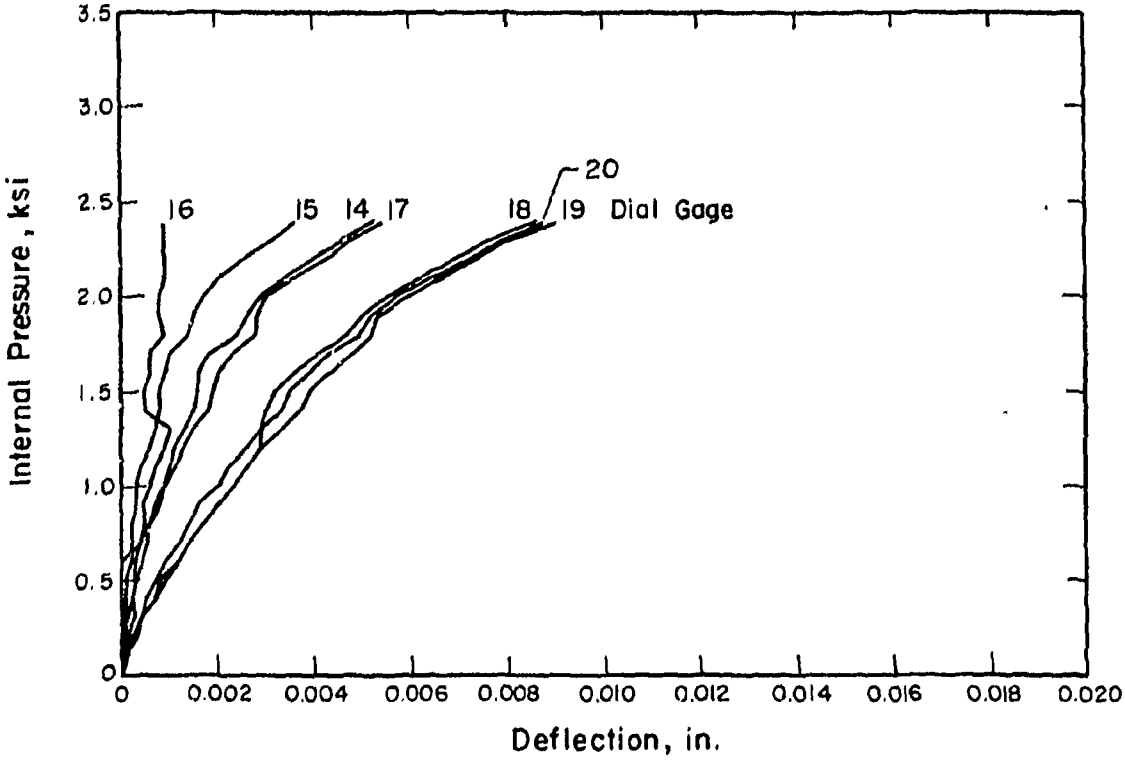

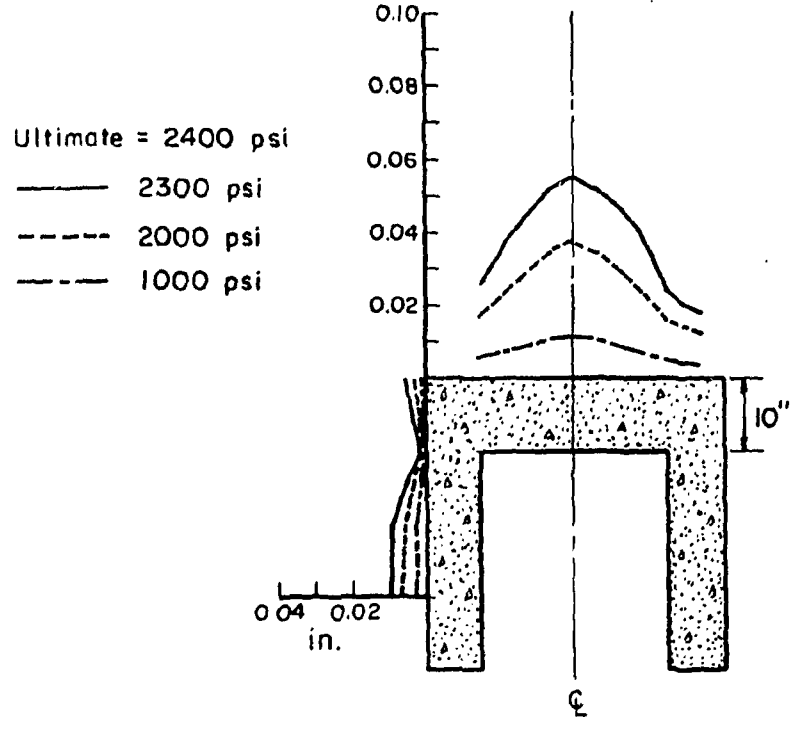

Fig. A.19 Measured Pressure-Deflection Curves Side Wall, Test PV29

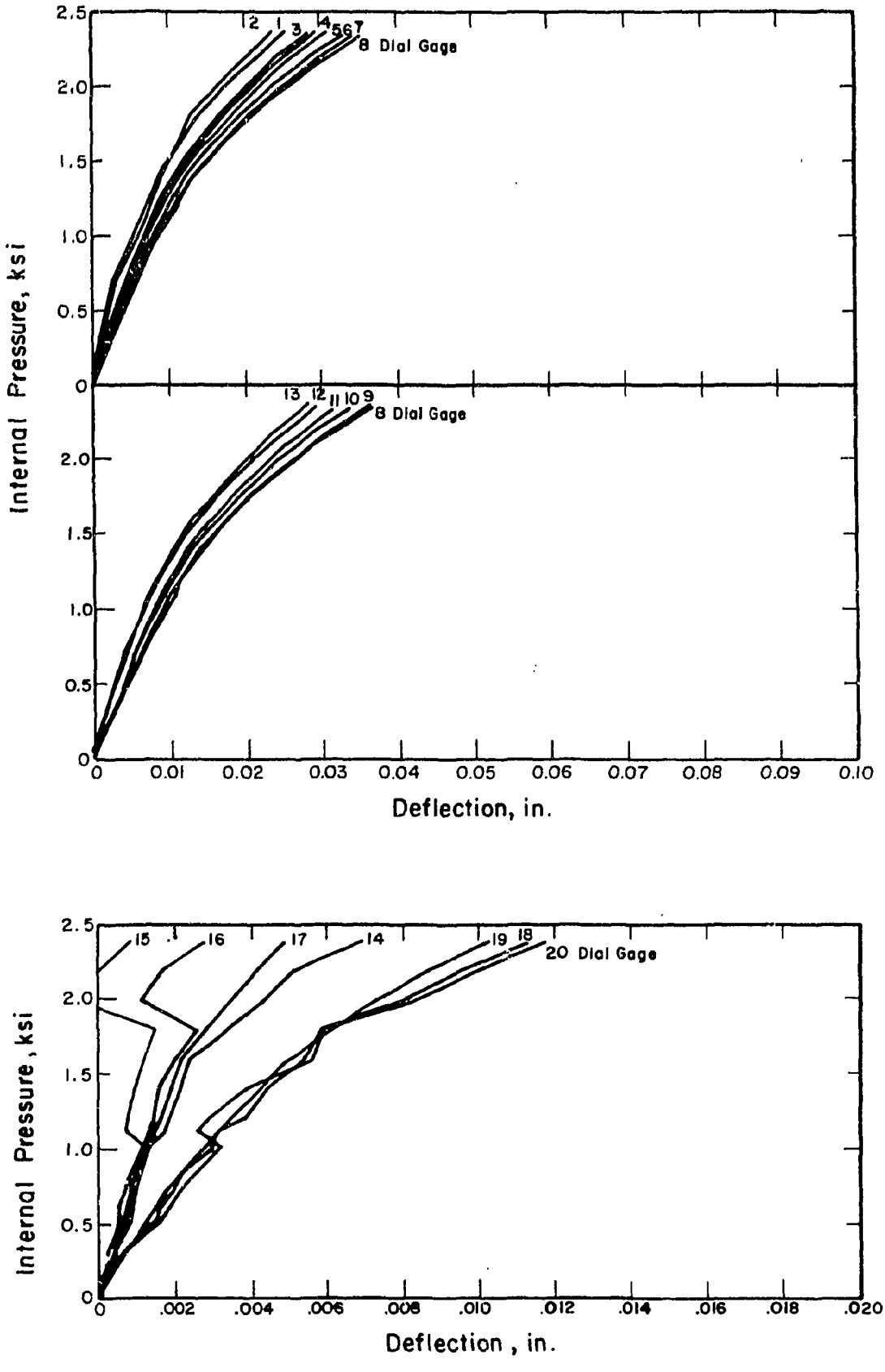

Fig. A.20 Measured Pressure-Deflection Curves, Test PV28.1

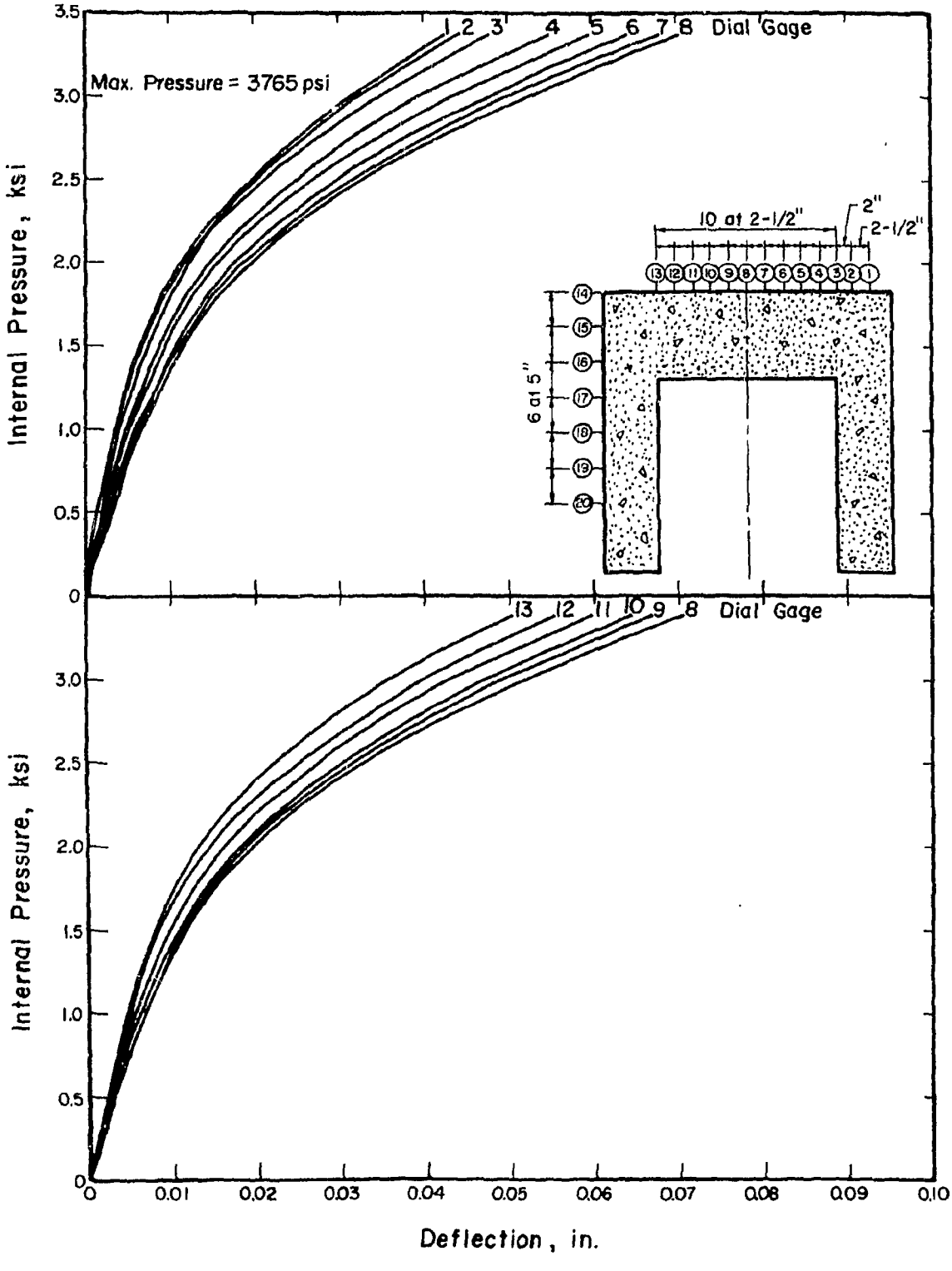

Fig. A.21 Measured Pressure-Deflection Curves End Slab, Test PV28.2

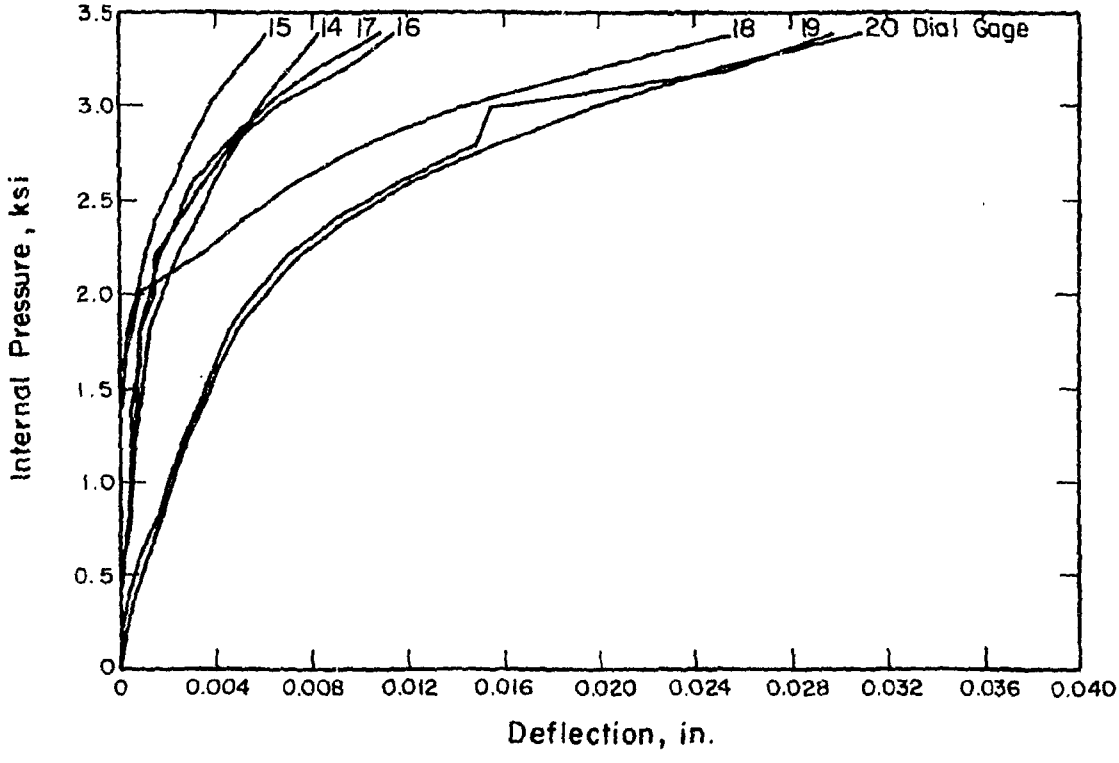

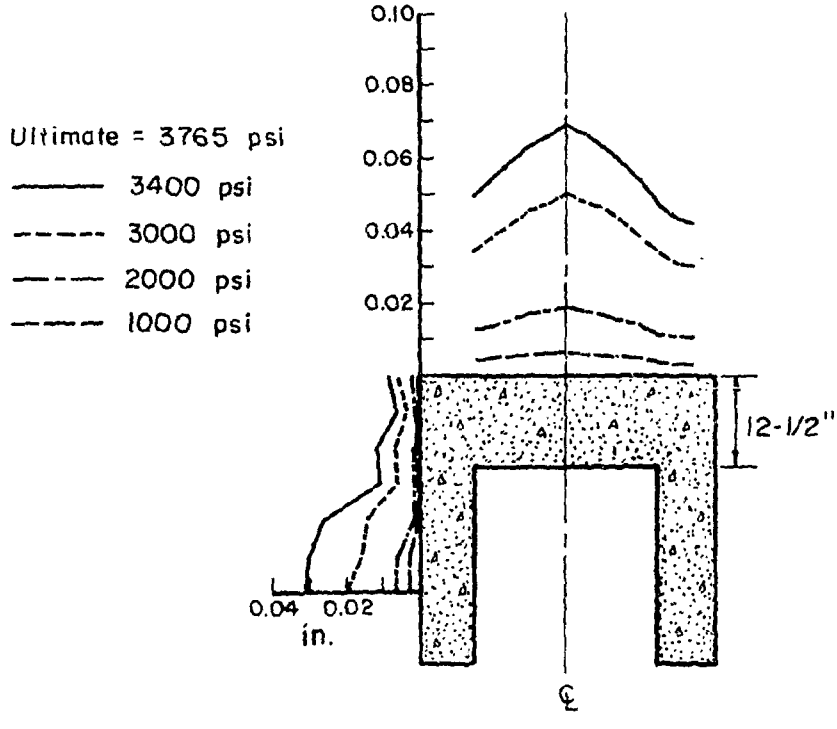

Fig. A.22 Measured Pressure-Deflection Curves Side Wall, Test PV28.2

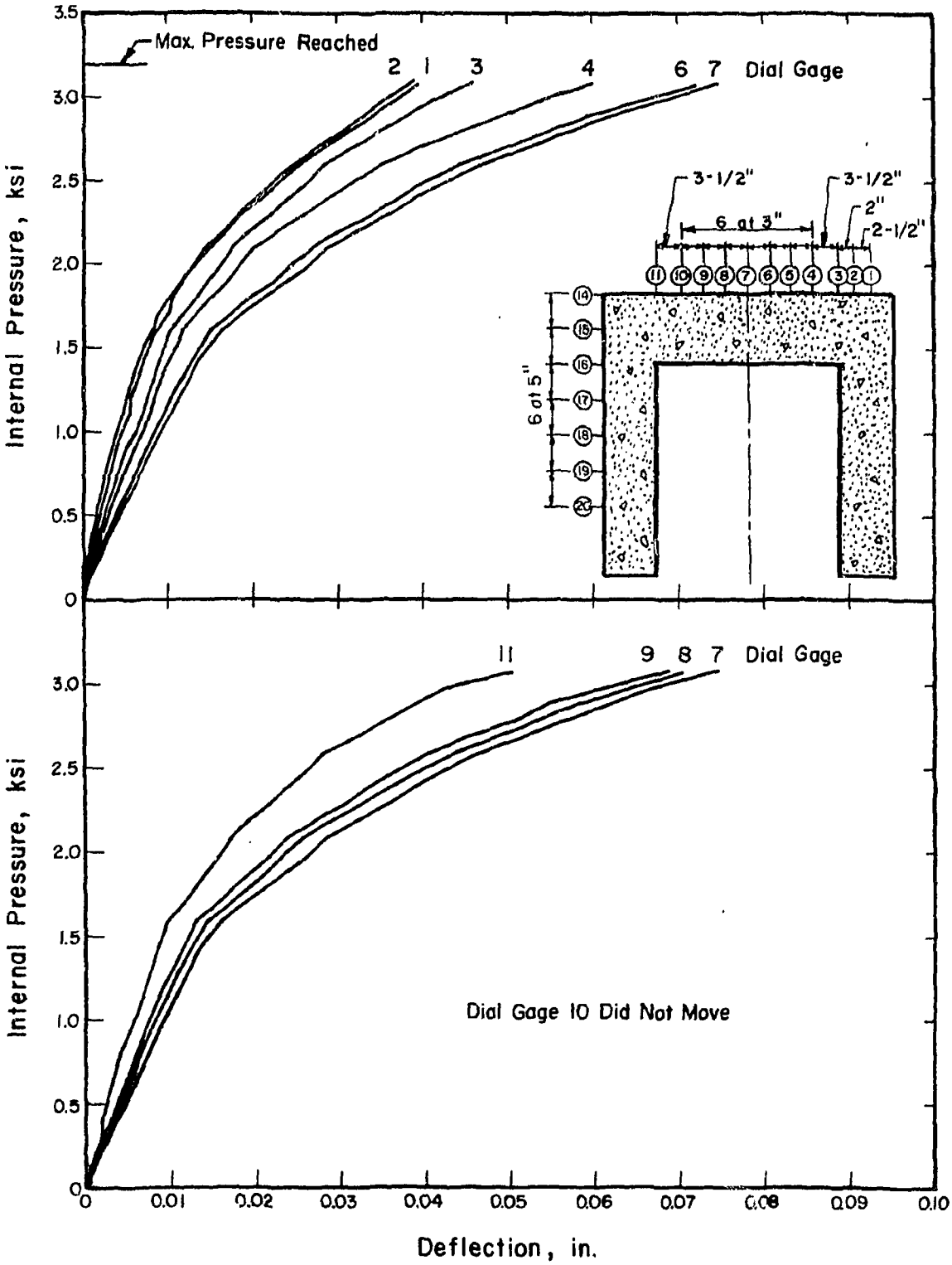

Fig. A.23 Measured Pressure-Deflection Curves End Slab, Test PV30

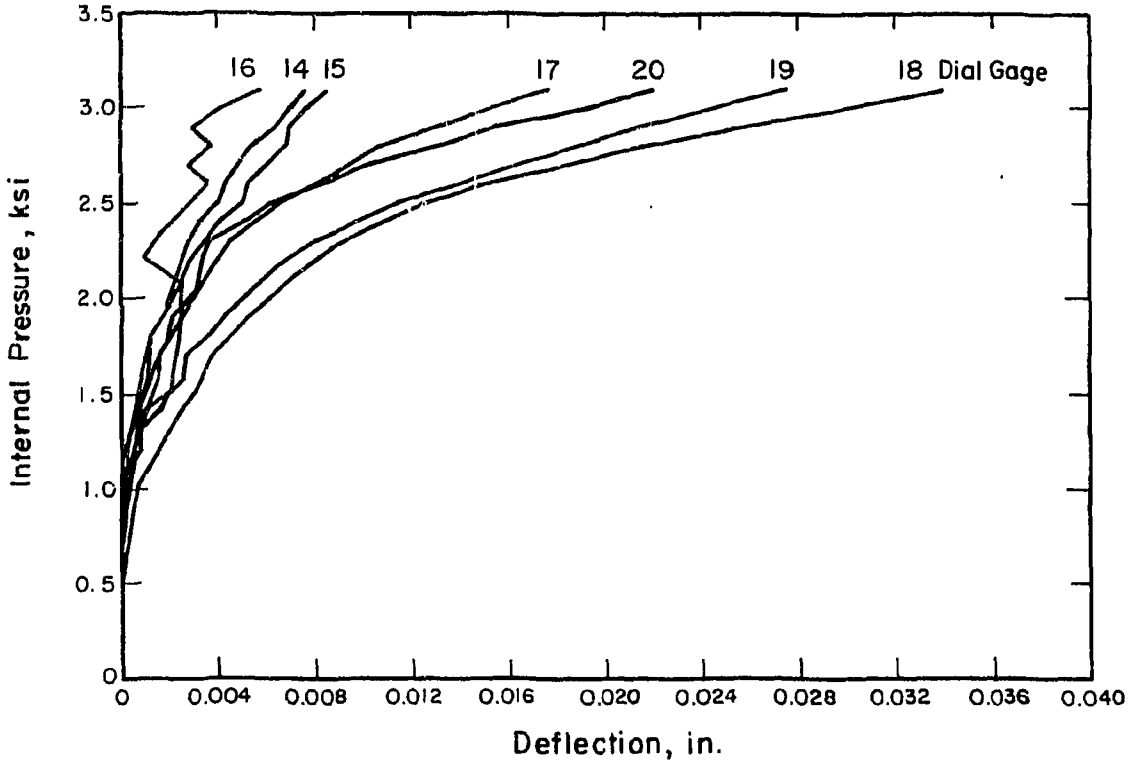

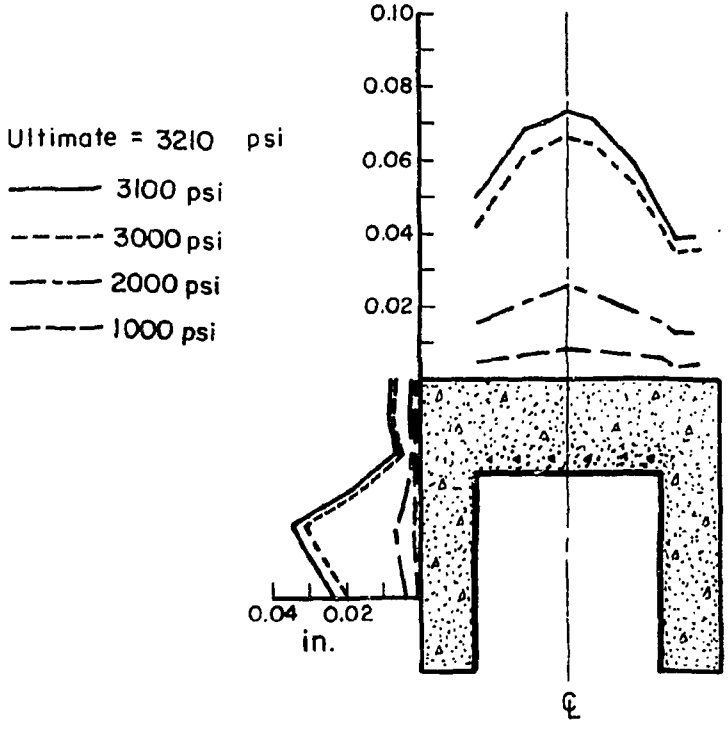

Fig. A.24 Measured Pressure-Deflection Curves Side Wall, Test PV30

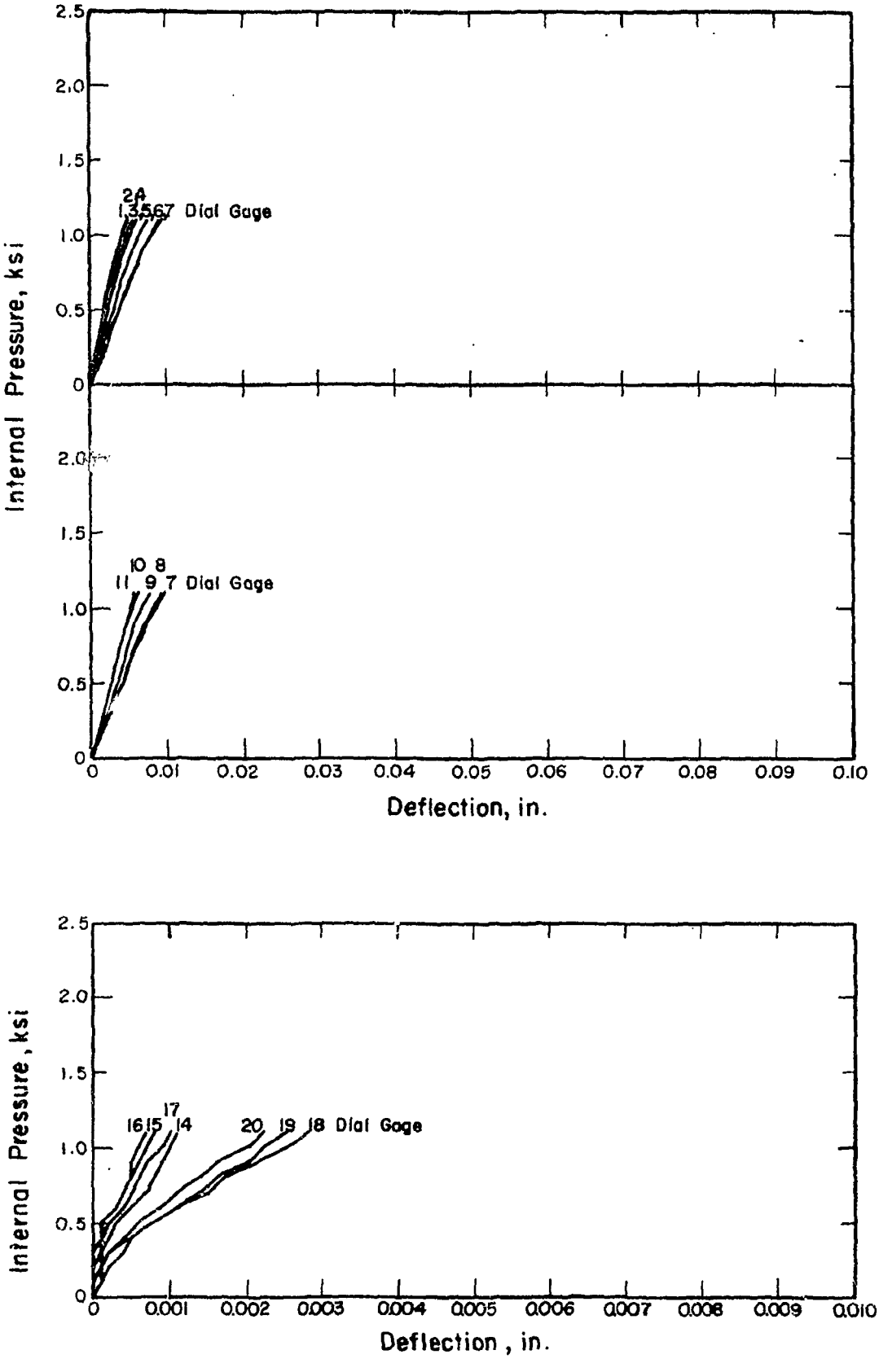

Fig. A.25 Measured Pressure-Deflection Curves, Test PV31.1

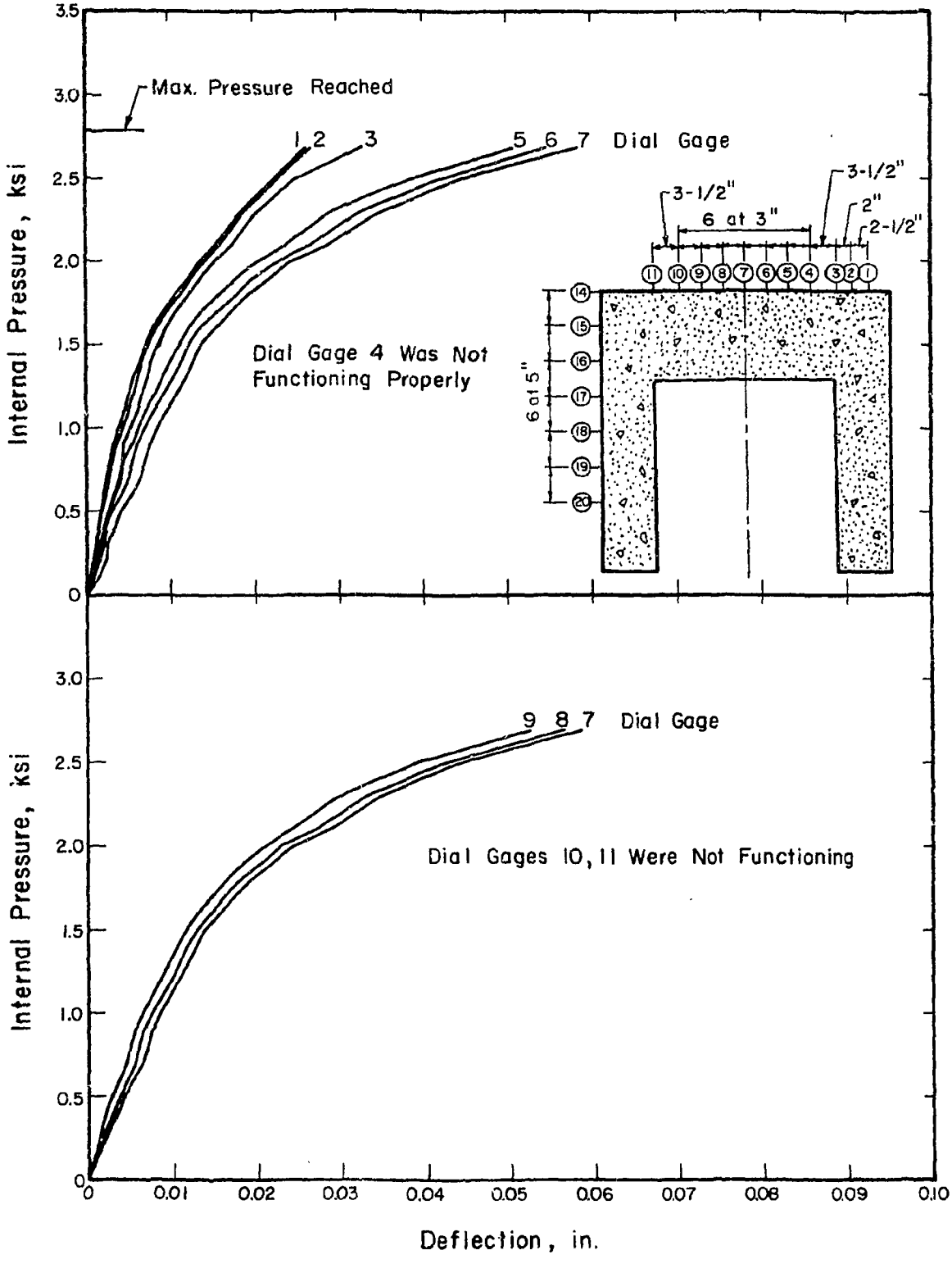

Fig. A.26 Measured Pressure-Deflection Curves End Slab, Test PV31.2

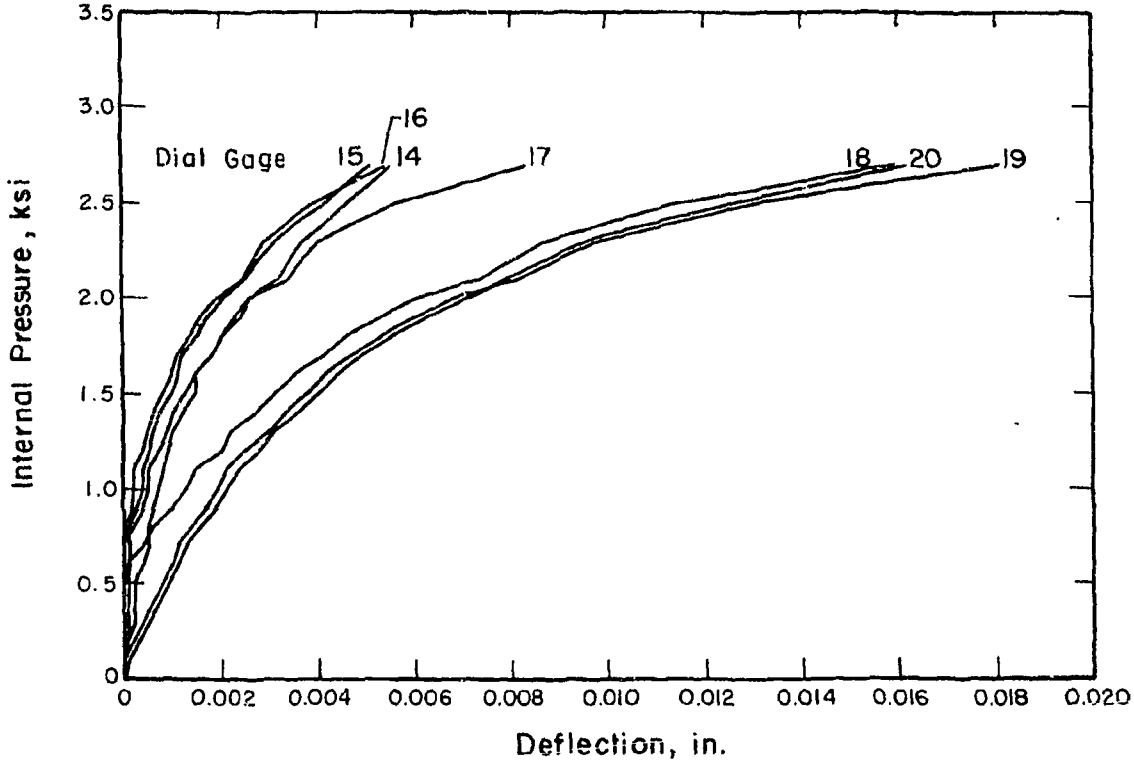

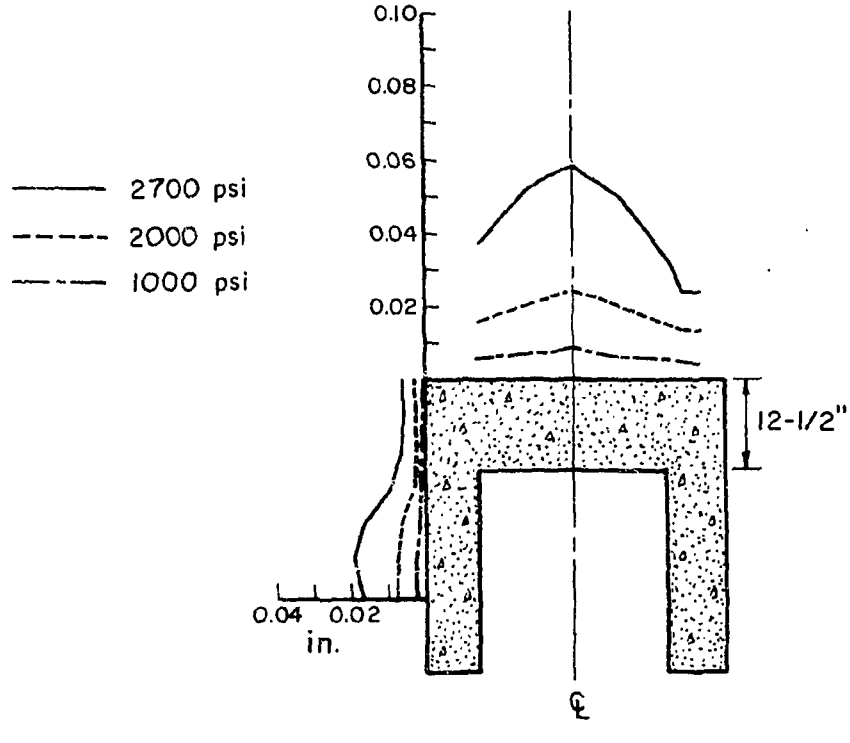

Fig. A.27 Measured Pressure-Deflection Curves Side Wall, Test PV31.2

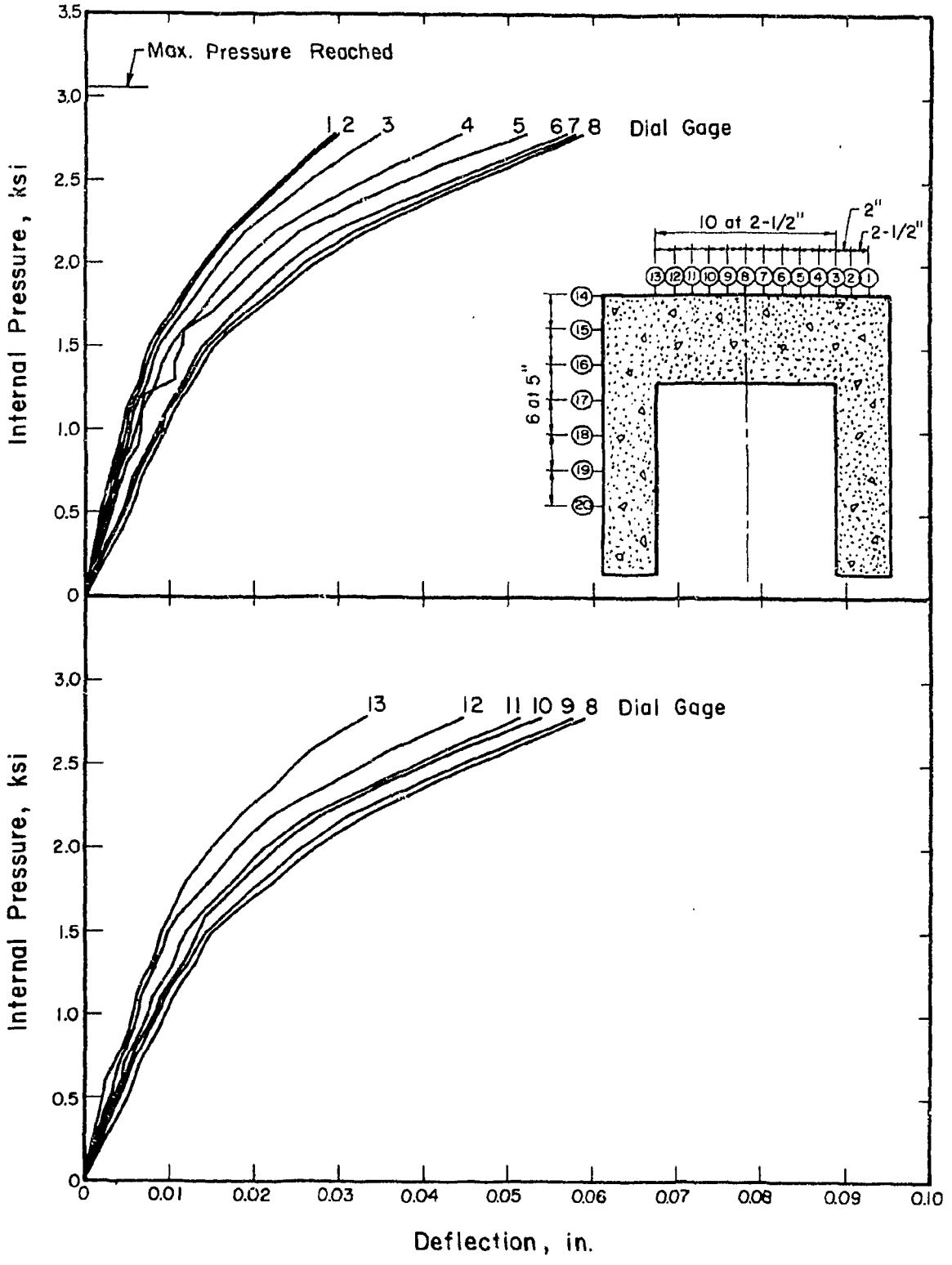

Fig. A.28 Measured Pressure-Deflection Curves End Slab, Test PV32

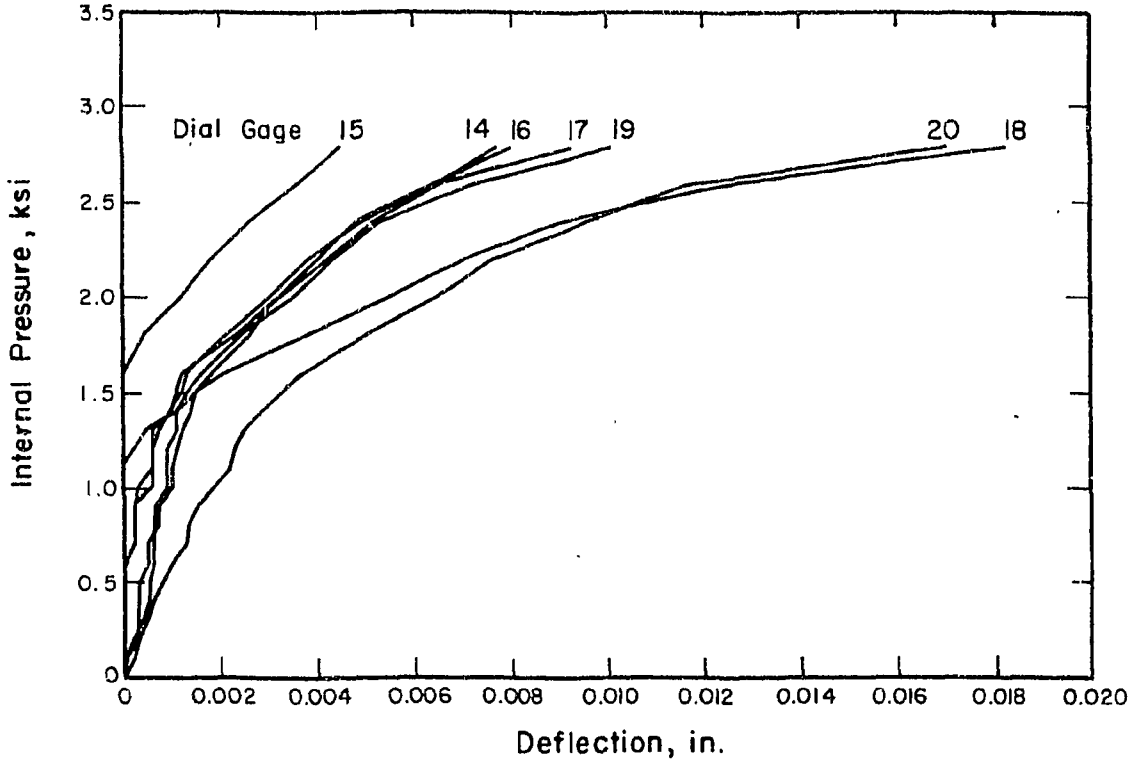

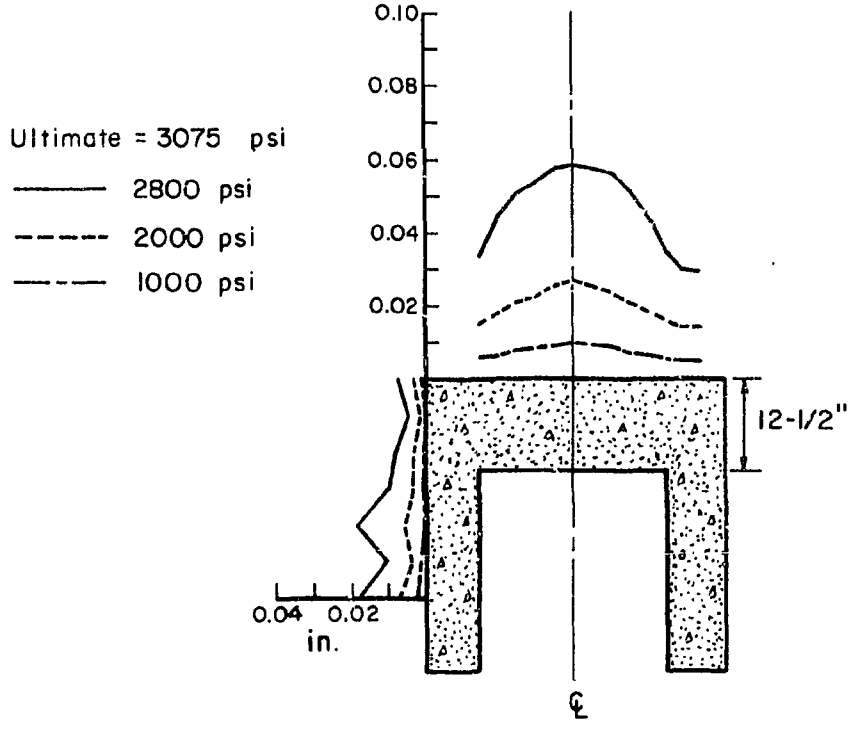

Fig. A.29 Measured Pressure-Deflection Curves Side Wall, Test PV32

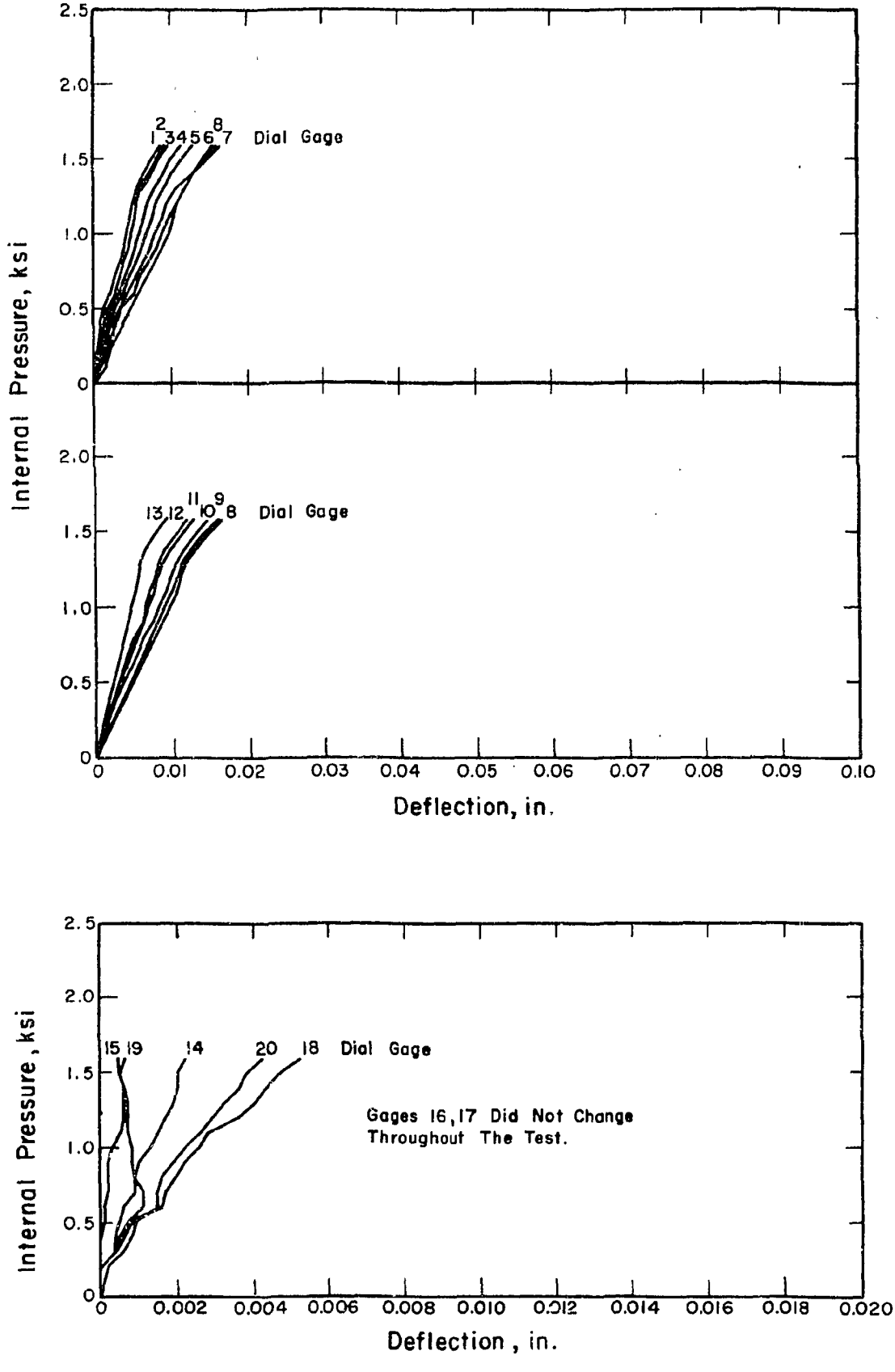

Fig. A.30 Measured Pressure-Deflection Curves, Test PV33.1

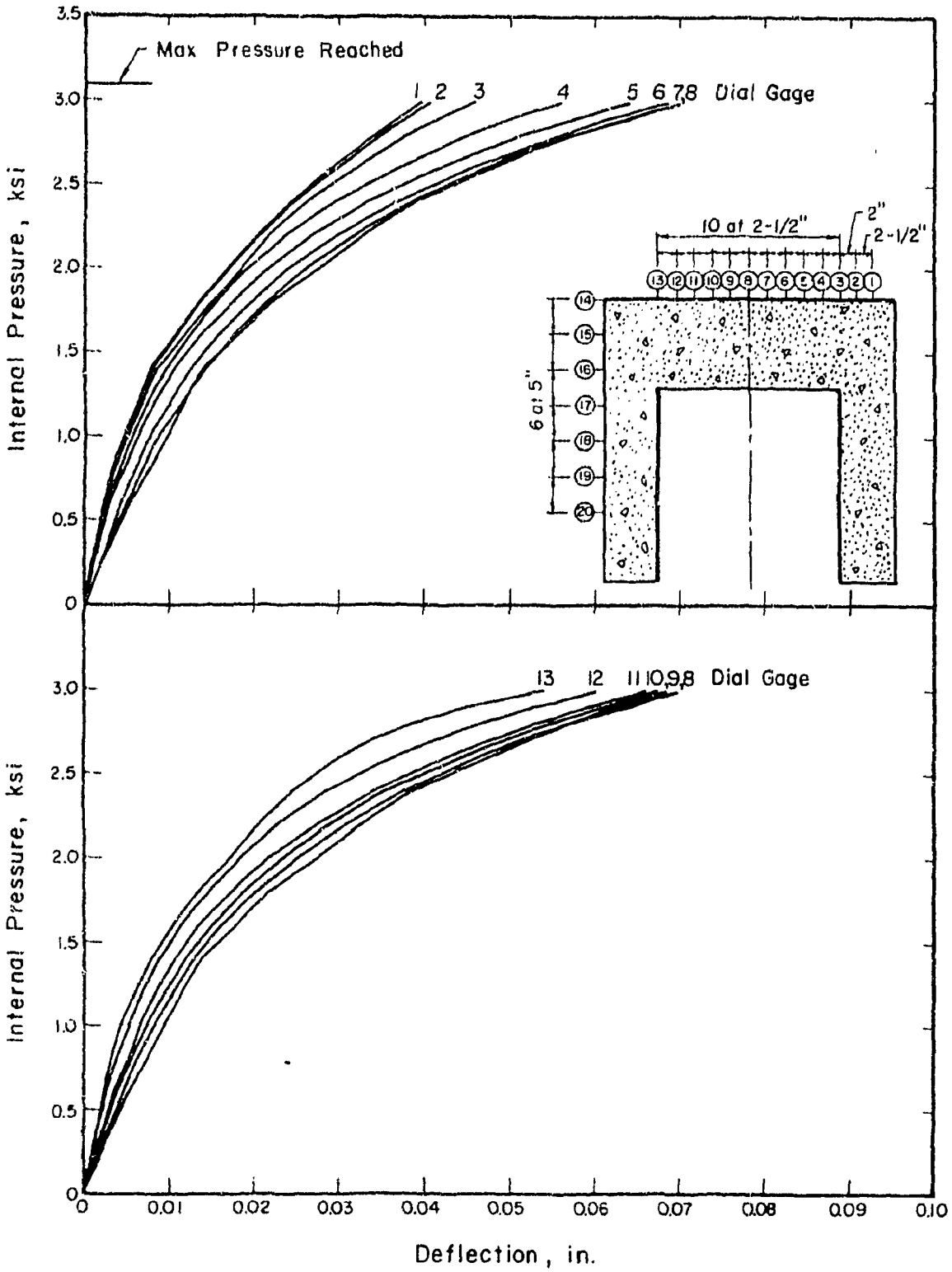

Fig. A.31 Measured Pressure-Deflection Curves End Slab, Test PV33.2

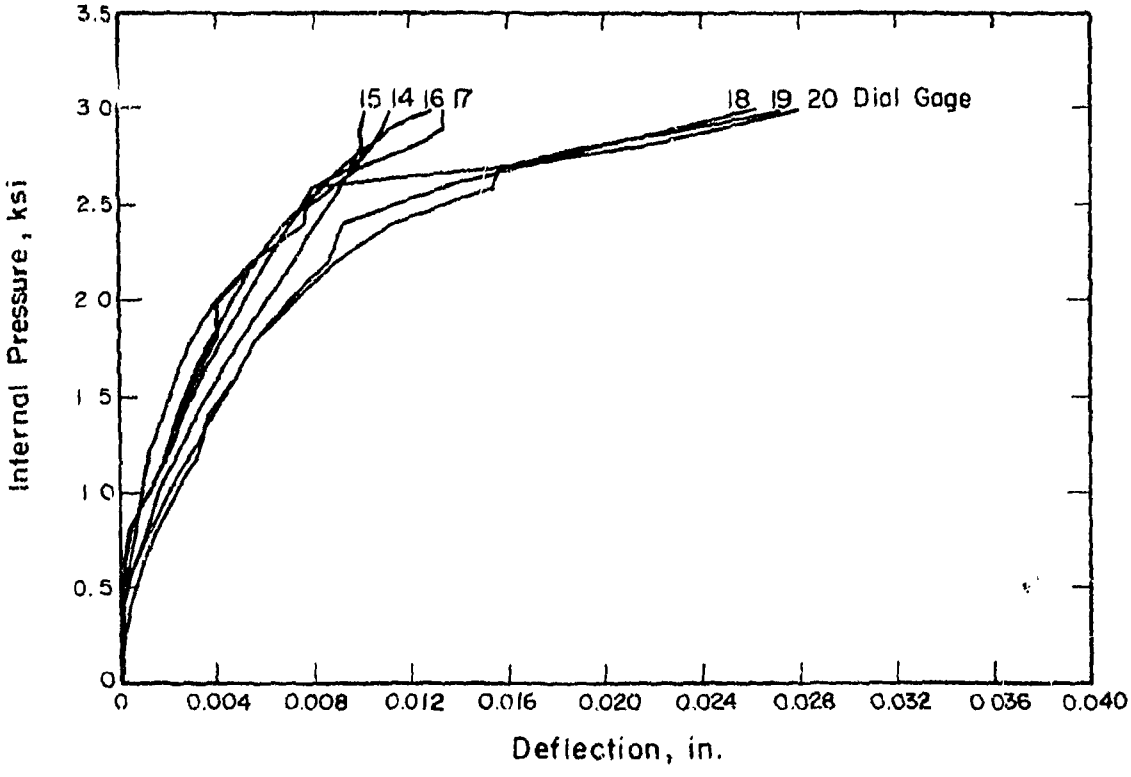

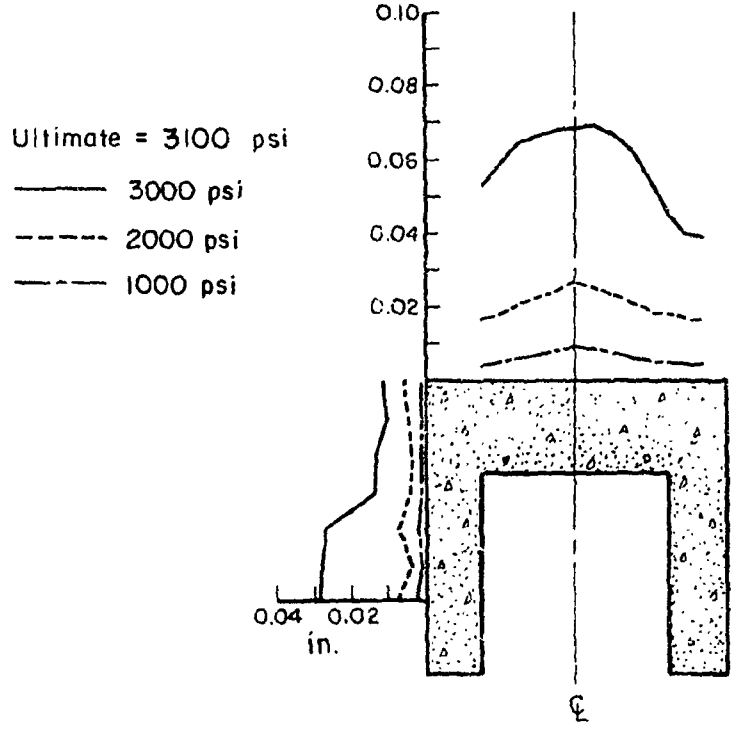

Fig. A.32 Measured Pressure-Deflection Curves Side Wall, Test PV33.2

APPENDIX B

TEST DATA

INTRODUCTION

Eight vessels were tested in the current phase of the investigation. This appendix contains specific information on the different characteristics of each vessel. The dates of casting, prestressing, and testing of each specimen are recorded in Table B.1.

A brief description of each vessel is provided in this section. Since the basic materials and procedures used for each specimen were detailed in Appendix A, they will not be repeated in each vessel description. The graphs of pressure-deflection readings for each test are included at the end of Appendix A.

B.1. Test Vessel PV26 (Solid, 10-in. head)

Since PV26 was the first vessel tested in the current series it had many unique features which were later modified or eliminated from the other vessels. It was circumferentially prestressed going from the bottom to the top, an operation which resulted in radial cracks in the end slab after the bottom four bands were completely prestressed. These cracks closed upon prestressing the last band located around the slab.

PV26 was also the only vessel that was longitudinally prestressed using the rods from the previous series. The vessel was originally lined with only a welded steel can grouted into place. However, the first test of the vessel had to be aborted after reaching 800 psi due

to leaks through the welds of the steel can. The specimen was lined with copper and neoprene over the steel as described in Appendix A. This served as the liner for all subsequent tests with only minor changes. The second test proved successful with an ultimate pressure of 2610 psi obtained. The deflection readings of the head surface were obtained using push rod extension gages in direct contact with the concrete. The readings taken in the two tests were quite good using this setup. However the explosive manner of failure destroyed all of the head deflection gages and thus a new method had to be used for later vessels.

B.2 Test Vessel PV27 (six 5-in. penetrations, 10-in. head)

PV27 and all subsequent vessels were circumferentially prestressed going from top to bottom. In addition, new stressteel rods were purchased for the longitudinal prestressing. The vessel was tested successfully on the first attempt, reaching an ultimate pressure of 2400 psi. A new deflection gage system was designed for this vessel. The head dial gages were mounted to the side of the vessel out of the direct line of the explosive failure path. Metal tabs were glued to the specimen and piano wire was threaded into these tabs and tied off. The wire was then strung over ball bearing pulleys and across the head to the spring loaded gages on the side. This system was effective in protecting the gages from damage but the readings taken from these gages indicated a great amount of friction was present in the system. Thus, a new system was adopted for the next vessel.

B.3 Test Vessel PV28 (Solid, 12½-in. head)

The deflection gage system used for all remaining vessels was first used for PV28. The gages were mounted over the vessel, directly above the metal tabs glued to the surface. Piano wire was tied to the tab, stretched taut and attached to the spring loaded gages. Steel channels were run across the top of the vessel between the piano wires and bolted to the prestress rods. This system gave good readings and at the same time contained the explosion and protected the gages. An internal pressure of 3170 psi was reached during the first test of PV28 before the leaks in the vessel could not be outrun by the pump. The vessel was relined and tested successfully three weeks later to an ultimate pressure of 3765 psi.

B.4 Test Vessel PV29 (Thirty-seven 2-in. penetrations, 10-in. head)

Fabrication and testing procedures had become well established with the successful testing of three vessels. No major changes were made for PV29. It was cast and tested to failure in a relatively short period of time. No concrete strain gages were applied to the vessel.

B.5 Test Vessels PV30, PV31 (Thirty-seven 2-in. penetrations, 12½-in. head)

PV30 and PV31 were nominally the same in size and penetration pattern. However, there were several important differences in their physical properties and behaviors. The actual head thickness of PV30 was found to be 12.22-in. while PV31 had a thickness of 12.02-in. The compressive strength of the concrete head was 6350 psi for PV30 and 4950 psi for PV31. PV30 failed on the first attempt at 3210 psi in a

symmetric manner. PV31 developed a leak in the liner on the first test and reached an internal pressure of only 1200 psi. Upon retest PV31 failed at 2800 psi in a somewhat unsymmetric shear failure.

B.6 Test Vessels PV32, PV33 (Six 5-in. penetrations, 12½-in. head)

PV32 and PV33 were also designed and tested as a check against each other. Their properties were in closer agreement than were PV30 and PV31 and the results reflect this similarity. PV32 and PV33 had concrete compressive strengths of 5720 psi and 4875 psi respectively. The average head thickness of PV33 was 12.45-in. as compared to 12.30-in. for PV32. These two factors of concrete strength and slab thickness appear to have offset one another. PV32 failed at 3075 psi while PV33, after an aborted first test due to leakage, failed at 3100 psi. After PV33 developed a leak in its first test at 1700 psi, a new type of copper liner was used for the second test. A copper can was fabricated to fit into the steel liner grouted into the vessel. The use of a copper can provided a better fit in the reentrant corners and thus reduced the amount of expansion that high pressures would produce. PV33 was retested with this new liner and was pressurized to failure without a single leak.

TABLE B.1

Chronology

Mark	Casting	Circumferential Prestressing	Longitudinal Prestressing	Testing
PV26.1	1-29-75	2-17-75	3-26-75	4-16-75
PV26.2	--	--	5-2-75	5-8-75
PV27	3-13-75	4-9-75	7-17-75	7-25-75
PV28.1	6-5-75	7-31-75	8-27-75	9-4-75
PV28.2	--	--	9-24-75	9-30-75
PV29	9-15-75	10-14-75	10-30-75	11-6-75
PV30	10-20-75	11-19-75	1-13-76	1-21-76
PV31.1	12-9-75	1-8-76	2-11-76	2-17-76
PV31.2	--	--	2-27-76	3-2-76
PV32	12-17-75	3-9-76	4-7-76	4-9-76
PV33.1	2-20-76	3-25-76	5-6-76	5-11-76
PV33.2	--	--	5-20-76	5-25-76